

The Journal of the Indian Association of Sedimentologists



The Indian Association of Sedimentologists

Volume 41

No. 1

Jan - June, 2024



Fieldwork in sedimentary basins during the Training-cum-Field Workshop on February 21-22, 2024

Copyright © 2024 by the Indian Association of Sedimentologists

All rights reserved. No part of this publication may be reproduced, distributed, or transmitted in any form or by any means, including photocopying, recording, or other electronic or mechanical methods, without the prior written permission of the publisher, except in the case of brief quotations embodied in critical reviews and certain other non-commercial uses permitted by copyright law. For permission requests, write to the Managing Editor/s.

Editor-in-Chief

John S. Armstrong-Altrin, National Autonomous University, Mexico

Managing Editors

Bashir Ahmed Lone, University of Jammu, India

Mateen Hafiz, Jammu, Higher Education Department, J&K, India

Production Editor

Yudhbir Singh, University of Jammu, India

Associate Editors

Ananya Mukhopadhyay, Kolkata, India

Avinash Kumar, National Centre for Polar and Ocean Research, Goa, India

A. V. Joshi, M.S. University, Baroda, India

Aymon Baud, Lausanne University, Switzerland

Erfan Mondal, AMU, Aligarh, India

G.M. Bhat, Jammu/Srinagar, India

G.N. Nayak, Goa, India

G. Shanmugam, Arlington Texas, USA

Guido Meinhold, Keel University, UK

Mayla A. Ramos-Vázquez, Inst. Potosino de Invest. Científica y Tecnológica, Mexico

M.E. Brookfield, University of Massachusetts at Boston, USA

Najmeh Etemad-Saeed, Inst. for Adv. Studies in Basic Sciences, Zanjan, Iran

Neha Aggarwal, BSIP, Lucknow, India

Prabhakar Sangurmath, Bengaluru, India

Rajeev Saraswat, National Institute of Oceanography, Goa, India

R. Nagendra, Bengaluru, India

Seema Singh, Panjab University, Chandigarh, India

S. K. Pandita, Jammu University, Jammu, India

S. M. Hussain, Madras University, Chennai, India

Uma Kant Shukhla, BHU, Varanasi, India

Yamuna Singh, Hyderabad, India

The journal of the Indian Association of Sedimentologists

DOI:

<https://doi.org/10.51710/jias.v4i1>

Managing Editors:

Bashir Ahmad Lone

Mateen Hafiz

The Journal of the Indian Association of Sedimentologists (IAS) is both an international open access online and print journal and is leader in its field and publishes ground-breaking research from across the spectrum of sedimentology, sedimentary geology, sedimentary geochemistry, experimental and theoretical sediment transport, mass movement fluxes, modern and ancient sedimentary environments, sequence – cyclo – chrono – and chemostratigraphy, sediment – biological interaction, palaeosols, diagenesis, stable isotope geochemistry, environmental sedimentology, neo-tectonics, geo-hazards, stratigraphy, palynology, sedimentary mineral resources and hydrocarbons, and allied branches of sedimentary - stratigraphic research. It also publishes review articles, editorials, conference reports, tributes, announcements, advertisements, etc. It is currently distributed to universities and research laboratories in India and abroad. Access is open to complete electronic journal archive. Subscribers also have the option to buy the printed journal at subsidized cost.

Indian
Association of
Sedimentologists



TABLE OF CONTENTS

ARTICLES	AUTHOR	PAGE NO
<i>Editorial</i>	<i>G M Bhat</i>	<i>1 – 2</i>
<i>Geochemistry of Neoproterozoic arenites from the Murwara area, Katni District, Madhya Pradesh: Implications for provenance, weathering and Tectonic Setting</i>	<i>Priyanka Onker, H.U. Usmani and R.S. Raghuwanshi</i>	<i>3 – 12</i>
<i>Textural characteristics of fluvial sediments in the Kosi River Basin, Bihar, India</i>	<i>Saba Imam and Atul Aditya Pandey</i>	<i>13 – 21</i>
<i>Constraining provenance and age of the siliciclastic rocks from the south-western Bundelkhand Craton, Central India</i>	<i>M.E.A. Mondal, Kamaal Parvez, Iftikhar Ahmad and Wamiq Mohammed Khan</i>	<i>22 – 30</i>
<i>Landslide susceptibility mapping using frequency ratio method along the Bholderwah-Bani Road, Jammu and Kashmir, India</i>	<i>Yudhbir Singh, Mehreen Liaqat, Sumit Johar, Shifali Chib, and Gaurav Singh Parihar</i>	<i>31 – 38</i>
<i>Heavy metal toxicity and its human health assessment: A preliminary study from the Perumal Lake sediments, Tamil Nadu, India</i>	<i>Baranidharan Sathyanarayanan and Vasudevan Sivaprakasam</i>	<i>39 – 54</i>
<i>Provenance of sediments and environmental risk assessment of heavy metals in the “Mis Amores” beach, Veracruz, Gulf of Mexico, Mexico</i>	<i>Mayla A. Ramos-Vázquez, John S. Armstrong-Altrin, Gloria D. Fernández-Guevara, Jayagopal Madhavaraju, Sanjeet K. Verma, and Rathinam Arthur James</i>	<i>55 – 67</i>
<i>Depositional sequences and sea level changes during Bathonian-Oxfordian, Kutch (Kachchh) Basin, Gujarat, India</i>	<i>Diwakar Mishra</i>	<i>68 – 79</i>
<i>Stability assessment and mitigation of vulnerable slopes utilizing kinematic analysis and slope mass rating approach along Basohli-Bani Road, Kathua District, Jammu and Kashmir</i>	<i>Shifali Chib and Yudhbir Singh</i>	<i>80 – 92</i>
<i>A Report on 39th Convention of Indian Association of Sedimentologists and International Conference on “Voyage of Sedimentology from the Mountains to the Oceans: An Innovative Trajectory”</i>	<i>Dr. S Vasudevan</i>	<i>93 – 108</i>
<i>A report of Training-cum-Field Workshop on "Decoding Clastic Sedimentary Systems"</i>	<i>Iftikhar Ahmad, M.E.A. Mondal, Kr. Farahim Khan and P.P. Chakraborty</i>	<i>109 – 115</i>

Editorial

Combating Global Warming and Modern Wars is much about Sedimentology

The Paris Agreement on climate change came into force on 4 November 2016 which was adopted by 196 Parties at the UN Climate Change Conference (COP21) in Paris on 12 December 2015. Under this agreement, 175 countries are legally bound to commit themselves to limit the increase of global warming temperatures to under 2 °C above pre-industrial levels. To achieve this goal, mitigation and adaptation policies have been adopted at the national and international levels. Mitigation measures include decarbonisation policy, for example the large-scale development of low-carbon energies to replace fossil fuel energy in a sustainable way. At present, efforts are focussed on the energy transition from fossil fuel driven energy to low-carbon energy which is mineral intensive. Rare earth elements (REEs) are core components of clean energy technologies such as solar, wind turbines and electric vehicles in the process of energy transition. In the quest for slow down the global temperature rise, development of low-carbon energy to achieve carbon emission reduction goals, rare earth elements are the key components to the energy transition. The criticality of supply and demand of raw materials is the key issue in planning the sustainable transition from fossil fuel driven energy to green energy. Over the past few years many countries established critical raw materials lists, in which rare earth elements have been given most attention.

Many critical minerals extracted from sedimentary ore deposits contain critical chemical elements, rare earth elements (REEs), which are vital in transition from fossil fuel driven energy resources to green energy to combat the global warming at the one end. At the other end some of these critical elements are used in development of high-tech equipment and weapons including, guided missiles, drones and new generation satellites, lasers, magnets for motors, optical devices, etc. being used in modern warfare, e. g., Ukraine-Russia war. Some of the REEs are used in the production of the batteries with greater energy density, better discharge characteristics and fewer environmental problems upon disposal. Others, are used in the manufacture of miniaturized higher-strength magnets, and fibre-optic cables capable of transmitting signals over long distances, on account of their capacity to amplify signals to a comparatively greater magnitude.

This family of chemical elements are not relatively scarce in the Earth's crust but typically dispersed and sporadic in economically exploitable ore deposits. Rare earth elements constitute a family of 17 chemical elements, including 15 lanthanides (lanthanum, cerium, praseodymium, neodymium, promethium, samarium, europium, gadolinium, terbium, dysprosium, holmium, erbium, thulium, ytterbium and lutetium) and scandium and yttrium which have chemical properties similar to lanthanides and tend to occur in the same ore deposits as lanthanides. The rare earth elements have similar chemical properties and are divided into light rare earths (cerium, lanthanum, praseodymium, neodymium, promethium, europium, gadolinium and samarium), and heavy rare earths (dysprosium, yttrium, terbium, erbium, thulium, ytterbium, yttrium and lutetium). Rare

earth elements occur in various types of salt deposits, in placer deposits of marine sands, in volcano-sedimentary deposits and in seafloor sediments. Details on occurrence, distribution and geology of REEs is discussed in vast literature base (e. g., Gupta and Krishnamurthy, 1992; Ganguli and Cook, 2018; Balaram, 2019; Dushyantha et al., 2020 and reference therein). Despite their denomination REEs are not particularly rare in their crustal abundance concentration compared to regular metals such as zinc and copper (Gupta and Krishnamurthy, 1992). REEs show a great variation in their distribution and abundance in sediments and sedimentary rocks; the most abundant one is cerium and the least is thulium. The sparse distribution of REEs in Earth makes their processing and recovery a technological challenge which results in their disproportionate availability among the countries. Studies on REEs have revealed that these deposits are located in the interior and marginal regions of continents, for example, in the Inner Mongolia, East African rift zones, Northern Scandinavia-Kola peninsula, Eastern Canada, Southern Brazil and Southern China. Gupta and Krishnamurthy (1992) and Balram (2019) state that overall there are 250 minerals which contain REEs out of these only a dozen are commercially viable for extraction. The most common rare earth minerals and the principal economic source of REEs are Monazite, Bastnaesite, Xenotime and Ion-adsorption clay. Others include Euxenite, Apatite, Gadolinite, Laporite, Uraninite, Brannerite, Doverite, Pyrochlore, Allanite, Perovskite and Zircon.

Figure 1 represents the World wise REEs distribution and, deposits in production and exploration



Fig. 1: Global REEs distribution including deposits in production and exploration targets.(after Depraeter and Stephane, 2023), Sources: GEUS, USGS, Canadian Government, TMR

targets. Among these the three major deposits are 1) Bayan Obo (China), Mountain Pass (USA) and Mount Weld (Australia). Bayan Obo deposit is located northwest of Baotou, a northern China industrial region, 2) The Mountain Pass deposit is located in the Mojave Desert of California (the second largest deposit in the world and the only REEs-mine in the United States), 3) Mount Weld comprises four deposits with monazite as the main REEs mineral. This deposit is enriched in heavy rare earths, and it is the only heavy rare earths mine outside China.

Another important resource of REEs is the ion adsorption clay deposit which occur along seven provinces in southern China. This deposit of rare earths comprises of heavy rare earths which is more economically viable compared to others. Rare earth elements have been extracted from the surface clay in China which accounted for 26% of the China's REEs production from 1988 – 2008.

Initially, the United States was the world's first supplier of REEs starting in 1950s with production of REEs from the Mountain Pass deposit. The USA was also the leader in rare earths applications and innovation. China's interest in rare earths emerged in the 1960s when it developed the mining of non-ferrous metals in the Baotou region. They set up the Baotou as the industrial region for large factories to process coal, steel, and rare earth metals (Klinger, 2017). According to the Center, N.M.I.U.S. Geological Survey Mineral Commodity Summaries (2022), the global reserves of rare earth elements are estimated at 120 million metric tons. China possess the largest reserve with 44 million metric tons, followed by Vietnam (22 million metric tons), then Russia and Brazil with 21 million metric tons. India, Australia, the United States and Greenland's individual reserves exceed 1 million metric tons. The current legal annual global production of rare earths is estimated at 280 thousand tons, of which China produces 60%, USA 16%, Myanmar 9%, Australia 8% and 3% Thailand. India is a country rich in mineral resources, especially rare earth minerals, and owns the fifth-largest reserves of rare earth minerals in the world, and produces about 2.5% of the global output. The important rare earth element bearing minerals found in India include Monazite. Zircon. Ilmenite. Columbite-tantalite. Beryl. Apatite and Sillimanite. Recently, in February 2023 with the speculated discovery of massive lithium reserves at Reasi in Jammu and Kashmir, the estimated reserve of 5.9 billion tonnes (if proved) would make India one of the world's largest lithium producers.

As we know, the world nations are showing an increasing interest in rare earth elements due to their use in many advanced technologies, including low-carbon technology, mainly in wind turbine generators, solar energy and electric vehicle motors. India is among the nations who is at the forefront of implementing the Paris Agreement to reduce global temperature by shifting to low carbon energy resources which require rare earth element resources. REEs are principally produced in China, and its political management of the resource, China has maintained monopoly in REEs production, supply, innovation and application. In addition, studies have drawn attention to the availability risks of main REEs used for wind turbines and electric vehicles, and more generally, the challenges surrounding rare earth elements supply (Wang et al., 2020). Few articles focus on the challenges of rare earths in the energy transition concerning disparity in supply and demand. Evidently the energy transition is putting pressure on the extraction of critical minerals required in low-carbon technologies. Rare earths used in wind turbines and electric vehicles are in more and more demand, whereas the supply is controlled by production concentration in China and it's protective resource policy. This current situation raises several issues regarding the availability of the resource for

the development of renewable energy resources and electric mobility. As we know, neodymium, praseodymium, dysprosium, terbium and lithium are the main rare earth elements critical to the energy transition through their application in wind turbine generators and electric vehicle motors. The demand for these minerals is likely to grow substantially over the next decade, and so is the critical mineral supply.

The natural resources and materials needed to meet the needs of the transition from fossil fuel energy to green energy are required to be explored, mined in sustainable manner and develop technology to increase production to meet the demand. Strong actions are needed to be taken to innovation and recycling, make production rapidly enough to meet the demand growth to make the large investments and strong policy support are needed to ensure that the demand - supply gap is reduced of key REEs minerals arising from energy transition or other sectors. However, even with these actions, it is being projected that there could be significant supply gaps for six key energy transition materials: lithium, nickel, graphite, cobalt, neodymium and copper by 2030. The most vital solution is to explore for more and more REEs and technology development for their production in the country. Contribute your bit in this quest as Sedimentologists.

REFERENCES:

- Balaram, V. Rare earth elements: A review of applications, occurrence, exploration, analysis, recycling, and environmental impact. *Geoscience Frontiers* 10, 4 (July 2019), 1285–1303.
- Depraeter, Lisa and Goutte, Stephane, *The Role and Challenges of Rare Earths in the Energy Transition* (June 13, 2023). Available at SSRN: <https://ssrn.com/abstract=4477111> or <http://dx.doi.org/10.2139/ssrn.4477111>
- Ganguli, R., and Cook, D. R. Rare earths: A review of the landscape. *MRS Energy & Sustainability* 5, 1 (May 2018), 6.
- Gupta, C. K., and Krishnamurthy, N. Extractive metallurgy of rare earths. *International Materials Reviews* 37, 1 (Jan. 1992), 197–248.
- Dushyantha, N., Batapola, N., Ilankoon, I., Rohitha, S., Premasiri, R., Abeyasinghe, B., Ratnayake, N., and Dissanayake, K. The story of rare earth elements (REEs): Occurrences, global distribution, genesis, geology, mineralogy and global production. *Ore Geology Reviews* 122 (July 2020), 103521.
- Klinger, J. M. *Placing China in the World History of Discovery, Production and Use*. In *Rare Earth Frontiers: From Terrestrial Subsoils to Lunar Landscapes*. Cornell University Press, Ithaca, 2017, pp. 67–102.
- Wang, J., Guo, M., Liu, M., and Wei, X. Long-term outlook for global rare earth production. *Resources Policy* 65 (2020), 101569.

G. M. Bhat

University of Jammu, Jammu
bhatgm@jugaa.com

Geochemistry of Neoproterozoic arenites from the Murwara area, Katni District, Madhya Pradesh: Implications for provenance, weathering and Tectonic Setting

Priyanka Onker, H.U. Usmani and R.S. Raghuvanshi

Department of Geology, Government Motilal Vigyan Mahavidyalaya, Bhopal, Madhya Pradesh, India 462008

E-mail Address: chourey.priyanka9@gmail.com

ABSTRACT

Geochemical analysis in terms of major, trace and rare earth elements of the Neoproterozoic arenites of Rewa and Bhandar Groups of the Vindhyan Supergroup from Murwara, Katni district, M.P., has been carried out to determine the provenance, weathering and tectonic setting. The arenites are rich in SiO₂ content but less in Na₂O, K₂O and CaO contents, suggesting the dominance of quartz and less amount of feldspars and rock fragments. Geochemically, these rocks are classified as quartz arenites to sub litharenite to sub-arkose. The CIA (75-98) and PIA values for these arenites and A-CN-K diagram indicates a high intensity of weathering in the source area. High LREE/HREE ratios, negative Eu anomaly and La/Sc, Th/Sc, Th/Co and Cr/Th ratio values suggest felsic source of these arenites. The discriminant diagram for these arenites indicates a quartzose sedimentary provenance. Ni vs TiO₂ and Th/Sc vs Sc bivariate plots indicate that the felsic rocks have been the source rock for these arenites. The discrimination diagrams based on log (K₂O+Na₂O) vs SiO₂ and Fe₂O₃+MgO vs TiO₂ contents show a passive margin setting. Whereas the results of new discriminant function multi-dimensional diagram for the high silica arenites reveals a change from collision to continental rift setting.

Keywords: Geochemistry, Arenites, Vindhyan Supergroup, Neoproterozoic, Katni

INTRODUCTION

Sedimentary rocks are the most useful rock type in deciphering the past conditions of the Earth surface. Clastic rocks are the important source of information because they are the residue left over, after a long and continued process of erosion and provide the valuable clues about their sources. Geochemistry of sedimentary rocks may be an addition to petrographic data when petrography does not provide any significant clue. Geochemistry becomes important tool in delineating the source of sediments, weathering, transportation, sorting and diagenesis (Bhatia, 1983; Cox and Lowe, 1995; Ramos-Vázquez et al., 2017). The use of geochemical data of sedimentary rocks to understand the sedimentary processes is increasing as the geochemistry and especially the trace element concentration is becoming a sensitive tool (Graver et al., 1996; Tawfik et al., 2017, 2018). Several REE's like La, Nd, Ce, Gd and trace elements such as Y, Th, Zr, Hf and Sc are being used as a tool to decipher the processes like provenance and tectonic setting because these elements are relatively less mobile during the process of erosion and transportation (Armstrong-Altrin et al., 2021, 2022; Sopic et al., 2023). Hence, these elements concentrate into the clastic residue and provide the clue regarding their parent material, tectonic setting and nature of source rocks (Bhatia and Crook, 1986; Condie, 1993; Yadav et al., 2022).

Additionally, the geochemical features of the clastic rocks also reflect the chemistry of authigenic minerals formed by the diagenetic changes. In this study, we made an attempt to delineate the provenance, weathering condition of source rocks

and tectonic environment based on the geochemical composition of the Neoproterozoic arenites in the Murwara area, Katni district, eastern part of M.P. The objective of this study is to infer the provenance of arenites based on the geochemical composition.

GEOLOGY OF THE AREA

Murwara area, Katni district, Madhya Pradesh is bounded between latitude 23°45' N to 24°0' N and longitude 80°24' E to 80°30' E and falls in SOI Toposheet 64A/5 and aerially extended over 320 km² (Fig.1).

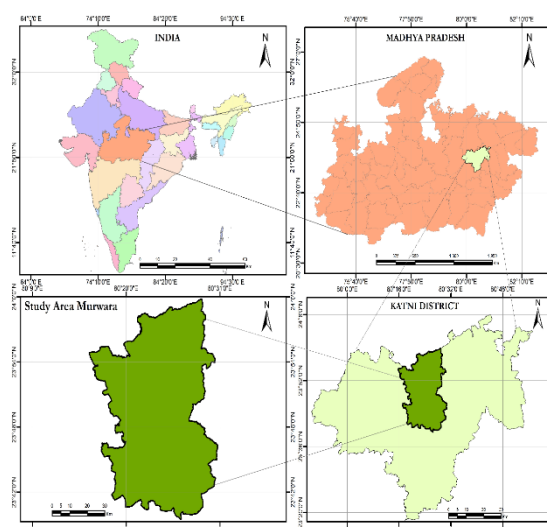


Fig. 1 Location map of the study area

The rocks belong to the Lower Vindhyan of Semri Group, Upper Vindhyan of Kaimur, Rewa and Bhandar Groups, laterite and alluvium of the Quaternary age. More than half of the area is occupied by the laterite and alluvium, among the Vindhyan, the Upper Vindhyan occupy the larger part of the study area (Fig. 2), and are seen on the eastern side, whereas the Lower Vindhyan are present on either side of the faults, which are extending from north to south.

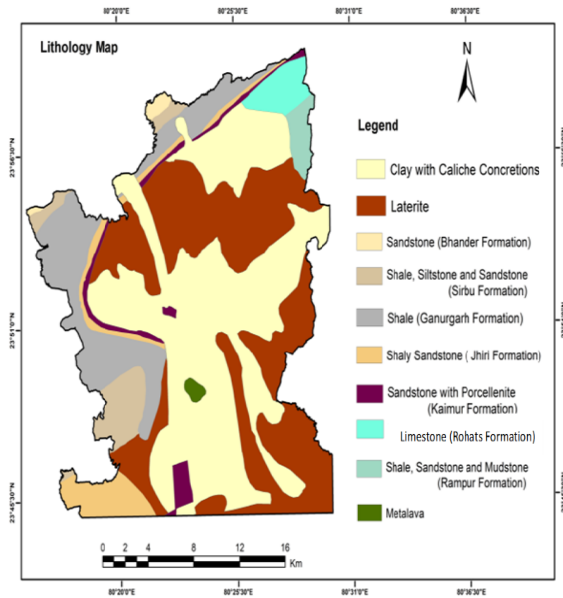


Figure 2 Geological Map of the Study Area (Interpreted from Remotely Sensed image and District resource Map, GSI).

The oldest rocks of Semri Group unconformably rest over the granite and metamorphics of the Bundelkhand and Mahakoshal Groups. These rocks of Semri Group include shale, sandstone and mudstones of the Rampura Formation. The shales are overlain the limestones. The limestones are thick to thinly bedded and also folded. Whereas the Upper Vindhyan observed in the area are sandstones with porcellanite of Kaimur shale and sandstone of Rewa Group, which are overlain by the Gunargarh shale and Sirbu sandstone and shale of the Bhandar Group. Kaimur sandstone with porcellanite and sandstone of the Rewa Group are the dominant rock

types in the study area. These sandstones are thickly bedded, hard and compact mostly gently dipping but along fault planes these beds are more inclined, highly fractured and shared. Sandstones are with variety of primary sedimentary structures including wavy and current ripples, tabular and planar, cross-bedding, parting lineation and flute casts along with load and ball and pillow structures. Two almost parallel, N-S trending fault also present, the sandstone with porcellanite seems the most effected bed dislocated by these faults. Vindhyan

rocks are overlain by the Laterite and Alluvium of Quaternary age.

METHODOLOGY

80 rock samples were collected during field visit, 12 sandstone samples were selected from the exposed rock surfaces along the stream, road and railway cuttings for chemical analysis. These samples were cleaned by washing with distilled water to avoid any contamination and then dried. These dried samples were powdered to -200 mesh size and sent for geochemical analysis. The major oxides, trace elements have been analyzed using HR-ICP-MS technique at the Geochemical Laboratory, National Geographic Research Institute (NGRI), Hyderabad. The instrument used is the AttoM HR-ICP-MS, a double focusing single collector instrument with forward Nier-Johnson analyzer geometry (Nu instrument, UK). For dissolution savillex pressure decomposition vessels (60ml.) (Savillex Corporation, Minnoetonka, Mn, USA) were used. Electronic grade Hydrofluoric Acid, AR grade HClO₄, distilled HNO₃ and HCl and lithium metaborate were used for the preparation of samples. For fusion a muffle furnace provided with silicon carbide tiles Kanthal heating elements with digital temperature controller (Max. temperature 1150°C) was used. The standard reference material used for analyzing the rock samples are JG1a, JA1, JB2, BHUO1, UBN, SY3, JBD2, NOD-M, SARM-64 and PTC1A. Prior to analysis, the instrument was purged with a 2% HNO₃ (V/V) solution for about an hour. The trace and REE data obtained by analyzing acidic (JG1a, JG1) and basic (JB2, BHOV1) reference materials through the HR-ICP-MS and the results of analysis are given in Tables 1, 2 and 3.

RESULTS AND DISCUSSION

Major elements

The major elements concentration in terms of wt.% of oxides of the arenites are listed in Table 1. On the Fe₂O₃/K₂O vs SiO₂/Al₂O₃ plot the samples are classified as quartz arenite to sub-arkosic arenites (Fig. 3a, after Herron, 1988). Similarly, based on the Pettijohn's (1972) diagram these arenites are classified as quartzose to sub-arkose type, which may be due to their relatively higher Al₂O₃ concentration (Fig. 3b).

The average SiO₂ content (wt.%) in the quartz arenites is 91% with a maximum value of 96% and a minimum of 78.8%, the arenite with 78.81% of SiO₂ shows an abnormally high wt.% of Fe₂O₃ (i.e., 5.95). Average Al₂O₃ is 4.17%, with an exception of higher content of Al₂O₃ in two arenite samples that is, 9.68 and 8.39 which may be attributed to the K-feldspar present in these rocks. Less Na₂O wt.%. (average < 0.1) can be attributed to relatively small amount of sodic plagioclase in these

Table 1. The Major oxides and ratios calculated for the arenites in the Murwara area (wt. %)

Rock Type	Arenites									
Samples	L1C	L3A	L3B	L4C	L5	L6	L7A	L8	L-11	L-12C
SiO ₂	84.34	92.94	96.42	78.81	92.96	95.21	95.08	92.76	85.91	95.54
Al ₂ O ₃	9.68	2.98	2.10	8.39	3.04	1.75	2.69	2.76	7.74	2.08
Fe ₂ O ₃	2.25	2.44	1.00	5.95	2.45	1.72	0.55	3.01	1.95	1.40
MnO	0.02	0.01	0.01	0.00	0.01	0.01	0.00	0.01	0.07	0.06
MgO	0.15	0.00	0.00	0.40	0.00	0.01	0.06	0.01	0.86	0.12
CaO	0.05	0.01	0.01	0.07	0.01	0.01	0.01	0.02	0.58	0.07
Na ₂ O	0.01	0.01	0.01	0.03	0.01	0.01	0.01	0.01	0.10	0.02
K ₂ O	0.66	0.03	0.03	1.30	0.04	0.01	0.11	0.05	2.37	0.45
TiO ₂	0.19	0.07	0.06	0.28	0.20	0.10	0.06	0.36	0.20	0.11
P ₂ O ₅	0.09	0.03	0.03	0.05	0.04	0.03	0.03	0.02	0.04	0.04
CIA	95.9	98.6	98.2	86.4	98.4	98.7	95.7	97.9	75.8	81.6
ICV	0.34	0.86	0.53	0.96	0.89	1.06	0.30	1.25	0.79	1.07
SiO ₂ /Al ₂ O ₃	8.71	31.22	45.89	9.39	30.54	54.28	35.39	33.61	1.16	1.05
K ₂ O/Na ₂ O	132.8	3.2	2.9	49.8	3.8	1.3	11.0	5.0	0.18	0.25
MgO/K ₂ O	0.23	0.13	0.10	0.31	0.05	0.77	0.54	0.12	0.66	3.35
Na ₂ O/K ₂ O	0.01	0.31	2.9	0.02	0.26	0.77	0.09	0.20	5.64	4.07
K ₂ O/Al ₂ O ₃	0.07	0.01	0.01	0.15	0.01	0.01	0.04	5.0	0.31	0.22
Fe ₂ O ₃ /K ₂ O	3.39	76.09	34.55	4.59	64.37	132.46	4.97	60.20	75.74	115
Al ₂ O ₃ /TiO ₂	50.4	40.2	36.2	29.9	15.1	17.7	46.3	7.7	36.2	211

arenites. Average K₂O wt.% is up to 0.3, whereas this K₂O content is higher in the rocks with more Al₂O₃, which also indicates more amount of K-feldspars. Generally, Fe₂O₃ and TiO₂ contents reflect low Fe, Ti bearing heavy minerals in these arenites. This classification is consistent with the petrographic study (Fig. 4) as the petrographic study shows the dominance of quartz in these arenites and in a few rock sections feldspar of fresh as well as altered types are observed.

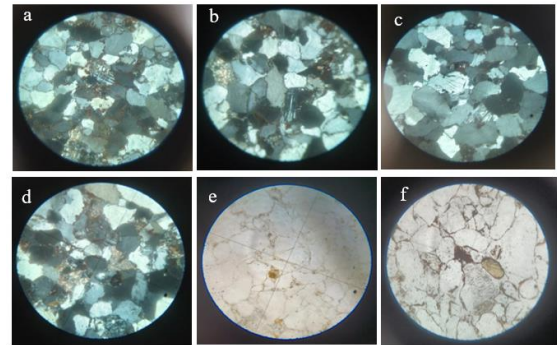


Figure 4. Photomicrographs of arenites of the Murwara area under crossed Nicol's (a, b, c, d) and plane polarized light (e, f) (10x)

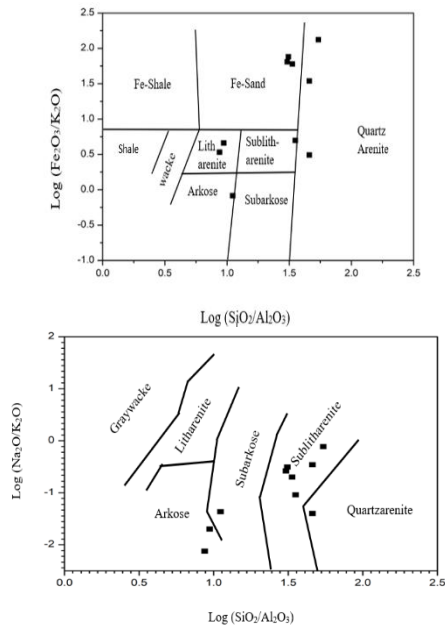


Fig. (3a). Log (Fe₂O₃/K₂O) vs Log (SiO₂/Al₂O₃) plot for the arenites (after Herron, 1988). (3b) Log (Na₂O/K₂O) vs Log (SiO₂/Al₂O₃) plot for the arenites (after Pettijohn, 1972).

Trace Element concentrations

The trace element contents of the arenites of Murwara area are listed in Table 2. Compared with that of the average upper continental crust (UCC) values the concentration of most of the trace elements is low. The average concentrations of trace elements lie between 0.1 and 1 (Fig. 5). Similarly, few elements like Rb, Ni, Cr, and Co are less

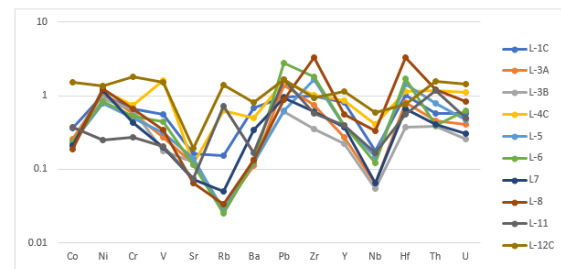


Fig 5. Spider plot for the trace elements of arenites from the Murwara area, normalized against UCC (Taylor and McLennan, 1995)

abundant, whereas concentrations of Zr and Ba are higher relative to UCC.

Rare Earth Element concentrations

Analysed values of REE (Table 3) and the chondrite normalised pattern is shown in Fig. 6. The Σ REE for the arenites varies between 62.72 to 176 (Table 3). The REE contents in the arenites are less than the average values for sandstones. The slightly higher LREE and the negative Eu show that the rocks contain less amount of Calcium in these arenites as these rocks do not contain much calcic plagioclase.

PROVENANCE

Provenance defines the origin of sediments and the composition of source rocks dominantly controls the composition of sediments derived from them (Taylor and McLennan, 1985; Bessa et al., 2021; Madhavaraju et al., 2021). Geochemistry of the sedimentary rocks is a valuable tool for the delineation of provenance (Bhatia, 1983; Gotze, 1998; Yang et al., 2004; Kettanah et al., 2021). Feng and Kerrich (1990) proposed the HFSE (High Field Strength Elements) such as Zr, Hf, Nb, Y, Th and U enriched in felsic rocks as they preferentially partitioned into the melts during crystallization and due to their highly immobile nature they remain in rocks and reflect the provenance. However, processes like weathering, transportation, diagenesis, etc. can affect the chemical composition (Cullers et al., 1987; Wang et al., 2018; Bela et al., 2023).

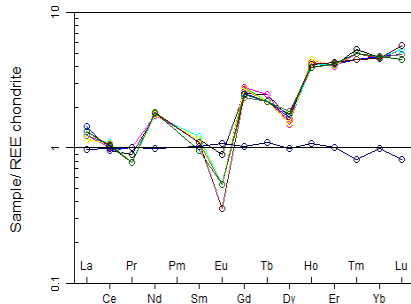


Fig 6. Chondrite normalized REE Spider plot for the arenites of Murwara area (After Anders and Grevesse, 1989).

REE, Th and Sc are widely used to infer the composition of crustal rocks as the distribution of these elements is least affected by physical process like diagenesis and metamorphism and by the heavy mineral fractionation than that of elements like Zr, Hf and Sn (Bhatia and Crook, 1986). Different igneous source rocks and their weathering products show different concentrations of trace and REE. REE and Th show higher abundance in felsic source whereas Co, Cr and Cs concentrated in mafic igneous source and in their weathered products. Ratios such as La/Sc, Th/Sc, Th/Co and Cr/Th are different in felsic and mafic source rocks and may

provide information about the provenance of sedimentary rocks (Wronkiewicz and Condie, 1989; Ramos-Vázquez et al., 2022). In the present study these ratios are calculated and compared with the values for sediments derived from felsic and mafic sources and UCC values (Table 4), suggesting that these arenites were probably derived from a felsic source. LREE /HREE ratios and Eu anomaly are also widely used to infer the source of sedimentary rocks and provenance (Cullers and Graf, 1984; Banerji et al., 2022; Nayak and Singh, 2022). In the present study, higher LREE/HREE ratio (21.11) and negative Eu anomaly indicate a possible felsic source rock.

A discriminant function diagram (Roser and Korsch, 1988) also allows to discriminate the

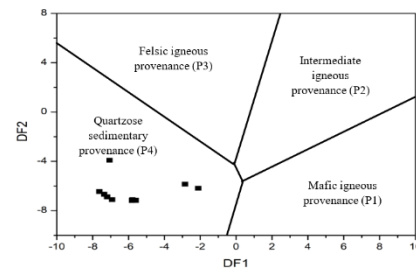


Figure 7. Provenance discriminant function plot for the arenites of Murwara area (After Roser and Korsch 1988). F1 and F2 refer to $-1.773\text{TiO}_2 + 0.067\text{Al}_2\text{O}_3 + 0.76\text{FeO}^* - 1.5\text{MgO} + 0.616\text{CaO} + 0.509\text{Na}_2\text{O} - 1.224\text{K}_2\text{O} - 9.09$ and $0.0445\text{TiO}_2 + 0.07\text{Al}_2\text{O}_3 - 0.25\text{FeO}^* - 1.142\text{MgO} + 0.438\text{CaO} + 1.475\text{Na}_2\text{O} + 1.426\text{K}_2\text{O} - 6.861$, respectively

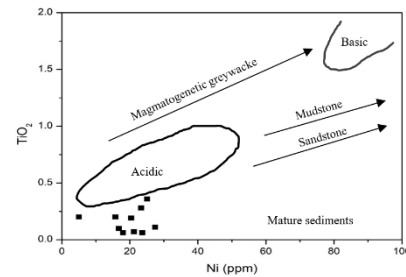


Figure 8. TiO₂ vs Ni bivariate plot for the arenites of Murwara area (after Floyd et al., 1989)

provenance into major groups viz. mafic igneous, intermediate igneous, felsic igneous and quartzose sedimentary provenance (Fig. 7). In this diagram the arenites are plotting in the quartzose sedimentary provenance.

To delineate the possible source of the arenites of Murwara area binary diagram between TiO₂ (wt.%) and Ni is plotted as Fig. 8 (after Floyd et al., 1989) which reveals that arenites are falling close to acidic source field. Among the ferromagnesian suite of trace elements Cr, Ni, Co and V show similar behaviour in magmatic process and their abundance indicate the mafic source rock (Armstrong- Altrin, 2004). In the studied arenites the concentration of Cr, Ni, Co and V elements (Table 2;) is low suggesting felsic rocks as source of these rocks.

Table 2. Trace element concentrations in arenites from the Murwara area (in ppm)										
Arenites										
Elements	L1C	L3A	L3B	L4C	L5	L6	L7A	L8	L-11	L-12C
Sc	3.52	1.39	1.15	7.70	1.98	3.30	2.10	3.13	2.93	15.91
V	33.80	16.21	10.47	97.44	18.82	26.19	11.94	20.39	12.33	90.28
Cr	22.84	20.07	22.20	25.80	17.46	18.57	14.83	23.05	9.41	63.82
Co	3.62	2.57	2.31	2.08	2.30	2.35	2.08	1.85	3.74	15.02
Ni	20.34	21.19	17.98	23.30	15.76	16.76	23.61	25.06	5.02	27.41
Cu	17.73	18.23	20.89	40.90	15.62	21.80	16.70	23.10	8.53	30.68
Zn	37.20	40.45	53.45	43.00	29.80	25.77	36.60	28.45	19.22	79.04
Ga	5.51	2.63	1.86	9.89	2.57	2.19	2.51	2.53	5.37	19.13
Rb	17.16	3.24	3.11	70.75	3.10	2.83	5.58	3.77	79.57	157
Sr	56.43	41.16	44.41	41.83	49.64	40.54	25.29	22.61	26.26	67.98
Y	17.82	6.01	4.86	18.69	8.38	8.58	8.22	12.08	8.62	24.81
Zr	185.88	141.78	67.69	194.2	318.10	337.9	115	616.6	109.9	176.82
Nb	4.45	1.58	1.36	10.01	3.71	3.05	1.61	8.18	4.13	14.67
Cs	0.90	0.27	0.27	3.88	0.23	0.24	0.50	0.26	-	-
Ba	375	61.88	75.25	273	67.09	69.61	186.1	72.50	91.7	442.2
Hf	5.96	4.62	2.16	6.65	8.25	9.88	3.78	19.05	3.25	4.48
Ta	0.76	0.16	0.12	0.79	0.32	0.30	0.35	0.89	19.85	38.72
Pb	19.02	27.76	12.05	31.65	12.62	55.03	18.39	17.55	32.59	33.09
Th	6.05	4.92	4.07	12.57	8.33	4.23	4.38	12.80	12.60	16.67
U	1.58	1.14	0.71	3.12	1.30	1.74	0.85	2.30	1.39	4.02
Th/Sc	1.72	3.52	3.54	1.63	4.20	1.28	2.08	4.09	4.29	4.15
Th/U	3.83	4.32	5.70	4.02	6.38	2.43	5.16	5.56	9.04	1.11
Th/Co	1.67	1.91	1.76	6.03	3.62	1.79	2.11	6.89	3.37	1.11
La/Sc	5.51	10.20	10.21	2.50	7.87	5.46	7.22	5.24	10.04	0.07
La/Co	5.36	5.55	5.08	9.24	6.78	7.66	7.31	8.84	7.87	0.07
Cr/Th	3.77	4.08	5.45	2.05	2.09	4.39	3.38	1.80	0.75	2.33
Cr/Ni	1.12	0.95	1.24	1.11	1.11	1.11	0.63	0.92	1.88	2.33

Th/Sc vs Sc bivariate plot also provides information about the source of terrigenous sedimentary rocks (McLennan and Taylor, 1991; Cullers, 2002). The ratios Th/Sc and the elemental concentration of Sc are plotted in Fig. 9 to decipher the source rock. For comparison these values (Th/Sc

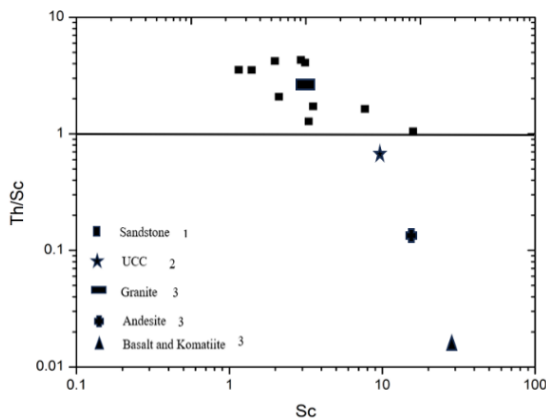


Fig 9. Th/Sc-Sc bivariate plot for the arenites of the Murwara area. ¹study area, ²upper continental crust (UCC; McLennan, 2001) and ³Condie (1993).

vs Sc) of the studied arenites are plotted together with UCC (McLennan, 2001) values, Archaean granite, Andesite, Basalt + Komatiite (Condie, 1993), which confirms that the source of arenites is a felsic rock.

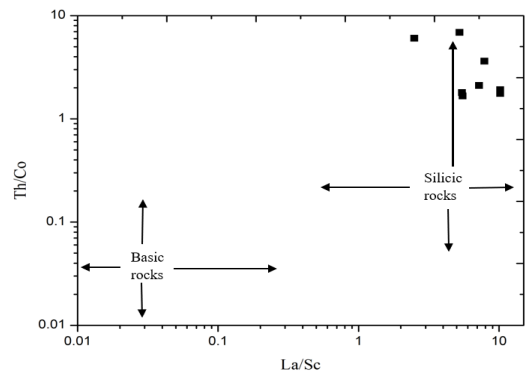


Figure 10. Th/Co vs La/Sc bivariate plot for the arenites of Murwara area (after Culler, 2002)

Th/Co vs La/Sc bivariate plot proposed by Cullers (2002) also reaffirm the silicic source of these rocks (Fig. 10).

WEATHERING OF SOURCE ROCKS

The duration and intensity of weathering in sedimentary rocks can be evaluated by examining the relationship between alkali and alkaline earth elements (Nesbitt and Young, 1982, Nesbitt et al., 1996). Feldspars are the most dominant phase actively participate in weathering, during weathering calcium, sodium and potassium atoms largely remove from feldspars (Nesbitt et al., 1980). To assess the degree of weathering most effective measures are chemical index of alteration (CIA

Nesbitt and Young, 1982) and plagioclase index of alteration (PIA; Fedo et al., 1995) CIA is calculated

using the formula: $CIA = [Al_2O_3 / (Al_2O_3 + CaO^* + Na_2O + K_2O)] \times 100$ where, concentrations are in

Table 3. Rare Earth Elements concentration in arenites of the Murwara area

Elements	L1C	L3A	L3B	L4C	L5	L6	L7A	L8	L-11	L-12C
La	19.44	14.27	11.75	19.26	15.60	18.06	15.21	16.41	19.85	38.72
Ce	33.9	34.5	28.3	33.1	37.7	37.7	36.3	36.4	40.4	77.1
Pr	4.68	3.86	3.19	5.07	4.21	5.7	4.2	4.2	4.3	8.7
Nd	17.2	14.3	11.8	20.3	15.9	22.9	16.6	15.2	14.8	29.7
Sm	3.83	2.71	2.35	4.56	3.56	5.00	3.52	3.00	2.82	5.17
Eu	1.02	0.43	0.40	0.84	0.62	1.01	0.68	0.54	0.36	0.97
Gd	4.60	1.80	1.64	4.24	2.64	3.85	2.85	2.43	2.01	4.37
Tb	0.78	0.26	0.25	0.69	0.40	0.64	0.43	0.45	0.34	0.67
Dy	3.79	1.30	1.11	3.49	1.82	2.56	1.94	2.40	1.78	3.86
Ho	0.67	0.23	0.19	0.67	0.31	0.35	0.32	0.46	0.36	0.82
Er	1.84	0.65	0.50	1.99	0.87	0.91	0.87	1.37	1.06	2.52
Tm	0.29	0.11	0.09	0.33	0.15	0.15	0.14	0.25	0.14	0.44
Yb	1.80	0.74	0.56	2.26	0.97	1.03	0.87	1.65	0.94	2.85
Lu	0.27	0.12	0.08	0.36	0.16	0.17	0.13	0.27	0.17	0.41
LREE/HREE	251.9	178.5	152.2	257.3	204.5	254.6	204.9	207.5	212.6	413.3
ΣREE	0.09	0.20	0.23	0.10	0.15	0.10	0.14	0.16	0.21	0.08

Table 4. Range of elemental ratios of arenites of this study compared to the ratios from felsic rocks, mafic rocks and average UCC (Taylor and McLennan, 1985)

Elemental ratios	Range of arenites of this study	Range of sediments from felsic sources	Range of sediments from mafic sources	UCC
Th/Sc	0.66-4.20	0.84-20.54	0.50-0.22	0.79
La/Sc	2.50-10.21	2.50-16.3	0.43-0.86	2.21
Th/Co	1.67-6.89	0.67-19.4	0.04-0.40	0.63
Cr/Th	1.80-5.44	4.00-15.0	25-500	7.76

*Culler (1994, 1998, 2000); Cullers and Podkovyrov (2000)
 ** McLennan (2001); Taylor and McLennan (1985).

molecular proportion and CaO* is the amount of CaO incorporated in the silicate fraction of rock.

The CIA values calculated for the arenites of the present area (Table 1) vary from 75 to 98 and values of $Al_2O_3 - (CaO^* + Na_2O) - K_2O$ plotted in the A-CN-K triangular diagram (Fig. 11).

In this diagram, the arenite samples plot close to the Al_2O_3 rich in kaolinite, illite field suggesting a high degree of chemical weathering in the source area. A high degree of chemical weathering in the source region may be inferred from the petrographic observations. The arenites are composed of quartz as a mineral present up to 90%, high % of quartz is attributed to high intensity of

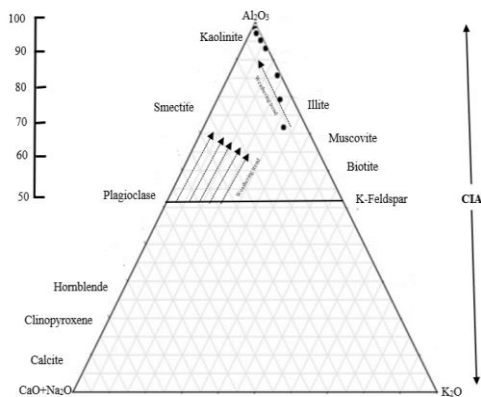


Figure 11. A-CN-K diagram for the arenites of Murwara area (Nesbitt and Young, 1982)

weathering. The values of PIA calculated (Table 1) also, high and consistent with the values of CIA.

The ratio Th/U in sedimentary rocks is also important because weathering, recycling and removal of U during weathering by the oxidation results an increase in this ratio (Armstrong- Altrin et al., 2004; Chougong et al., 2021). This high ratio between 3.8 to 6 is attributed to removal of U during weathering and suggesting a high degree of weathering.

Intense chemical weathering is the result of humid climate. A bivariate plot between SiO_2 vs $(Al_2O_3 + K_2O + Na_2O)$ proposed by Suttner and Dutta (1986), was plotted for the present area (Fig.

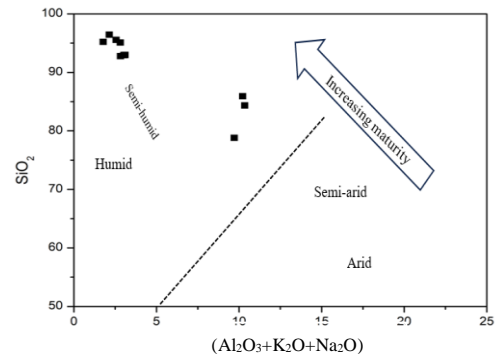


Figure 12. Bivariate plot of SiO_2 vs $(Al_2O_3 + K_2O + Na_2O)$ for the arenites of Murwara area. (Suttner and Dutta, 1986).

12) reveals the humid conditions in the area which also favours intense chemical weathering.

TECTONIC SETTING

A discrimination diagram proposed by Roser and Korsch (1986) to delineate the tectonic setting of clastic sedimentary rocks, the diagram is plotted using log (K₂O /Na₂O) vs SiO₂. Here, in this diagram the parameters used have been recalculated to 100%, on the CaO and LOI free basis, before plotting. This diagram (Fig. 13) clearly indicates a passive-margin setting of the arenites. The results show that these arenites were deposited at a passive-margin tectonic setting.

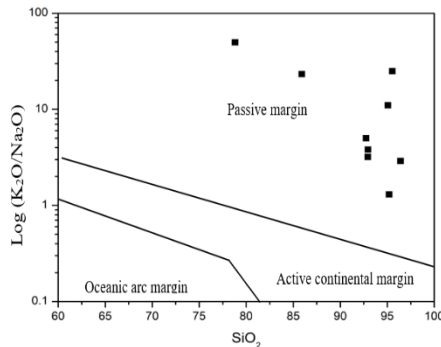


Figure 13. Tectonic discrimination diagram SiO₂ vs Log (K₂O/Na₂O) for the arenites of Murwara area (after Roser and Korsch, 1986)

Another multi-dimensional diagram for tectonic discrimination of siliciclastic sediments for high silica rocks (Verma and Armstrong-Altrin, 2013) have been plotted for the present arenites (Fig.14) the diagram is plotted between DF1 and DF2 functions calculated for the respective equations for high [(SiO₂)adj =>>63%-<=95%].

$$DF1(\text{Arc-Rift-Col})m1 = (-0.263 \times \ln(\text{TiO}_2/\text{SiO}_2)_{\text{adj}}) + (0.604 \times \ln(\text{Al}_2\text{O}_3/\text{SiO}_2)_{\text{adj}}) + (-1.725 \times \ln(\text{Fe}_2\text{O}_3/\text{SiO}_2)_{\text{adj}}) + (0.660 \times \ln(\text{MnO}/\text{SiO}_2)_{\text{adj}}) + (2.191 \times \ln(\text{MgO}/\text{SiO}_2)_{\text{adj}}) + (0.144 \times \ln(\text{CaO}/\text{SiO}_2)_{\text{adj}}) + (-1.304 \times \ln(\text{Na}_2\text{O}/\text{SiO}_2)_{\text{adj}}) + (0.054 \times \ln(\text{K}_2\text{O}/\text{SiO}_2)_{\text{adj}}) + (-0.330 \times \ln(\text{P}_2\text{O}_5/\text{SiO}_2)_{\text{adj}}) + 1.588$$

$$DF2(\text{Arc-Rift-Col})m1 = (-1.196 \times \ln(\text{TiO}_2/\text{SiO}_2)_{\text{adj}}) + (1.604 \times \ln(\text{Al}_2\text{O}_3/\text{SiO}_2)_{\text{adj}}) + (0.303 \times \ln(\text{Fe}_2\text{O}_3/\text{SiO}_2)_{\text{adj}}) + (0.436 \times \ln(\text{MnO}/\text{SiO}_2)_{\text{adj}}) + (0.838 \times \ln(\text{MgO}/\text{SiO}_2)_{\text{adj}}) + (-0.407 \times \ln(\text{CaO}/\text{SiO}_2)_{\text{adj}}) + (1.021 \times \ln(\text{Na}_2\text{O}/\text{SiO}_2)_{\text{adj}}) + (-1.706 \times \ln(\text{K}_2\text{O}/\text{SiO}_2)_{\text{adj}}) + (-0.126 \times \ln(\text{P}_2\text{O}_5/\text{SiO}_2)_{\text{adj}}) - 1.068$$

Data used has been adjusted to 100% on an anhydrous basis and Fe is taken as Total Fe₂O₃. This plotting reveals the present studied arenites plot in the collision and continental rift tectonic setting.

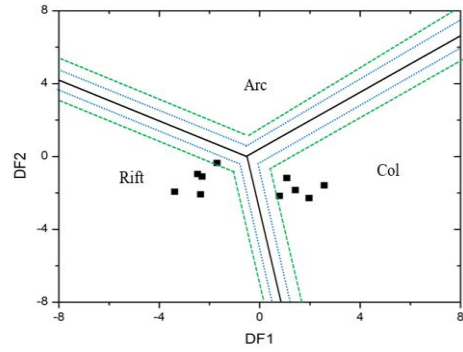


Figure 14. New discriminant-function multi-dimensional diagram for high silica arenites of the Murwara area (After Verma and Armstrong-Altrin, 2013).

CONCLUSIONS

The arenites of the Kaimur, Rewa and Bhandar Groups belonging to Vindhyan Supergroup in the Murwara area have been assessed for the first time in terms of geochemistry. The major element analysis reveals the dominance of silica and less concentration of K₂O, Na₂O contents indicate that these rocks vary between quartz arenites and sub-lithic, with dominance of K-feldspar over plagioclase. Some samples are classified as sub-arkosic. The high CIA values reflect the extensive weathering in the source region and PIA values also confirm the high weathering conditions. REE pattern, high LREE / HREE ratios and less concentrations of trace elements like Ni, Cr, Co and V reflect the felsic source for these arenites. Discriminant function diagram shows quartzose sedimentary provenance and the bivariate plots between Ni vs TiO₂, Sc vs Th/Sc and La/Sc vs Th/Co also suggest silicic source for these Neo-Proterozoic arenites of the Vindhyan Supergroup. The DF1-DF2 multi-dimensional tectonic discrimination diagram shows the continental collision to continental rift settings. Based on the results of this study it can be concluded that the arenites of the area might have been derived by the granitic rocks of the Bundelkhand Massif.

ACKNOWLEDGEMENT

The authors are thankful to Director, NGRI, Director IIT Kanpur and Director, Roorkee for according necessary permission to analyse the sample and also grateful to Dr. Ram Mohan, Mr. Manavalan Satyanarayana, Dr. Prince Tiwari and Dr. Indra Shekhar Sen for providing the details of analytical procedures. The authors also thankful to the anonymous reviewers for their critical review and providing the most beneficial comments and suggestions to improve the manuscript.

REFERENCES

- Armstrong-Altrin, J.S., Lee, Y. I., Verma, P.S. and Ramasamy S. (2004). Geochemistry of Sandstone from the Upper Miocene Kudankulam Formation, Southern India: Implication for Provenance, Weathering and Tectonic Setting. *Journal of Sedimentary Research*, v.74, pp. 285–297.
- Armstrong-Altrin, J.S., Madhavaraju, J., Vega-Bautista, F., Ramos-Vázquez, M.A., Pérez-Alvarado, B.Y., Kasper-Zubillaga, J.J. and Eko Bessa, A.Z. (2021). Mineralogy and geochemistry of Tecolutla and Coatzacoalcos beach sediments, SW Gulf of Mexico. *Applied Geochemistry*, v. 134, no. 105103.
- Armstrong-Altrin, J.S., Ramos-Vázquez, M.A., Madhavaraju, J., Marca-Castillo, M.E., Machain-Castillo, M.L. and Márquez-García, A.Z. (2022). Geochemistry of marine sediments adjacent to the Los Tuxtlas Volcanic Complex, Gulf of Mexico: Constraints on weathering and provenance. *Applied Geochemistry*, v. 141, no. 105321.
- Anders, E. and Grevesse, N. (1989). The abundance of the elements: Meteorite and Solar. *Geochimica et Cosmochimica Acta*, v. 53, pp. 197-214.
- Banerji, U.S., Dubey, C.P., Goswami, V. and Joshi, K.B. (2022). Geochemical indicators in provenance Estimation. In: Armstrong-Altrin JA, Pandarinath K, Verma S. (Eds.), *Geochemical Treasures and Petrogenetic Processes*. P. 95-121.
- Bela, V.A., Bessa, A.Z.E., Armstrong-Altrin, J.S., Kamani, F.A., Nya, E.D.B. and Ngueutchoua, G. (2023). Provenance of clastic sediments: A case study from Cameroon, Central Africa. *Solid Earth Sciences*, v. 8(2), pp. 105-122.
- Bessa, E. A. Z., Paul-Désiré, N., Fuh, G.C., Armstrong-Altrin, J.S. and Betsi, T.B. (2021). Mineralogy and geochemistry of the Ossa lake Complex sediments, Southern Cameroon: Implications for paleoweathering and provenance. *Arabian Journal of Geosciences*, v. 14, Article no. 322
- Bhatia, M.R. and Crook, K.W. (1986). Trace element characteristics of greywackes and tectonic setting discrimination of sedimentary basins. *Contributions to Mineralogy and Petrology*, v. 92, pp. 181–193.
- Bhatia, M.R. (1983). Plate tectonics and geochemical composition of sandstone. *The journal of Geology*, v. 91, pp. 611-627.
- Chanda, S.K. (1967). Petrogenesis of the calcareous constituents of the Lameta Group around Jabalpur, M.P., India. *Jour. Sediment. Petrol*; v.37, pp. 425-437.
- Chougong, D.T., Bessa, A.Z.E., Ngueutchoua G., Yongue, R.F., Ntyam, S.C. and Armstrong-Altrin, J.S. (2021). Mineralogy and geochemistry of Lobé River sediments, SW Cameroon: Implications for provenance and weathering. *Journal of African Earth Sciences*, v. 183, pp. 1-19.
- Condie, K.C. (1993). Chemical composition and evolution of the upper continental crust; contrasting results from surface samples and shales. *Chemical Geology*, v. 104, pp. 1-37.
- Cox, R. and Lowe, D.R. (1995). A conceptual review of regional scale control on the composition of clastic sediments and the co-evolution of continental blocks and their sedimentary cover. *Journal of Sedimentary Research*, v. A65, No.1, pp.1-12.
- Cullers, R.L. (1994). The control on major and trace elements variation of shale, siltstone and sandstone on Pennsylvanian-Permian age, from uplifted continental blocks in Colorado to platform sediments in Kansas, USA. *Geochimica Cosmochimica Acta*, v. 58, pp. 4955-4972.
- Cullers, R.L. (1998). Mineralogical and chemical changes of soil and stream sediments formed by intense weathering of the Danberg granite, Georgia, USA. *Lithos*, v. 21, pp. 301-314.
- Cullers, R.L. (2000). The geochemistry of shales, siltstones and sandstones of Pennsylvanian-Permian Age, Colorado, USA: Implication for Provenance and Metamorphic Studies. *Lithos*, v. 51, pp.181-203.
- Cullers, R.L. and Podkovyrov, V.N. (2000). Geochemistry of the Mesoproterozoic Lakhanda shale in southern Yakutia, Russia: Implication for mineralogy and provenance control and recycling. *Precambrian Research*, v. 104, pp. 77-93.
- Cullers, R.L. (2002). Implications of elemental concentration for provenance, redox conditions and metamorphic studies of shale and limestones near Pueblo, CO, USA. *Chemical Geology*, v.191, pp. 305-327.
- Cullers, R.L. and Graf, J.L. (1984). Rare Earth elements in igneous rocks of the Continental crust: Intermediate and Silicic rocks- Ore petrogenesis. In Henderson, P., *Rare Earth Elements Geochemistry*, Elsevier Amsterdam, pp. 275-316.
- Cullers, R.L., Barrett, T., Carlson, R. and Robinson, B. (1987). Rare earth elements and mineralogical changes in Holocene soil and stream sediments: a case study in the Wet Mountain Colorado, USA. *Chemical Geology*, v. 63, pp. 275-297.
- Feng, R. and Kerrich, R. (1990). Geochemistry of fine-grained clastic sediments in the Archean Abitibi Greenstone belt, Canada: Implication for provenance and tectonic Setting. *Geochimica et Cosmochimica Acta*, v. 54, pp. 1061-1081.
- Floyd, P.A., Winchester, J.A. and Park, R.G. (1989). Geochemistry and tectonic setting of Lewisian clastic metasediments from the Early Proterozoic Loch Maree group of Gairloch, NW Scotland. *Precambrian Research*, 45(1-3), pp. 203-214.
- Gao, S. and Wedepohl, K.H. (1995). The negative Eu anomaly in Archean sedimentary rocks: implications for decomposition, age and importance of their granitic sources. *Earth and Planetary Letters*, v. 133, pp. 81-94.
- Graver, J.I., Royce, P.R. and Smick, T.A. (1996). Chromium and Nickel in shale of the Taconic

- Foreland: A case study for the provenance of fine-grained sediments with an ultramafic source. *Journal of Sedimentary Research*, v. 66, pp.100-106.
- Götze, J. (1998). Geochemistry and provenance of the Altendorf feldspathic sandstone in the middle Bunter of the Thuringian basin (Germany). *Chemical Geology*, v. 150, issue 1-2, pp. 43-61.
- Herron, M.M. (1988). Geochemical classification of terrigenous sands and shales from core or log data. *Journal of Sedimentary Petrology*, v. 58, pp. 820-829.
- Huene, F.V. and Metley, C.A. (1933). The Cretaceous Saurischia and Ornithischia of the Central Province India. *Mem. Geol. Sur. India, Palaentology Indica*, v. 21, pp. 172.
- Kettanah, Y.A., Armstrong-Altrin, J.S. and Mohammad, F.A. (2021). Petrography and geochemistry of siliciclastic rocks of the Middle Eocene Gercus Formation, northern Iraq: Implications for provenance and tectonic setting. *Geological Journal*, v. 56, pp. 2528-2549.
- Khosla, A. and Sahni, A. (1995). Paratoxonomic classification of Late Cretaceous dinosaur eggshells. *Journal of the Palaeontological Society of India*, v. 40, pp. 87-102.
- Madhavaraju, J. Armstrong-Altrin, J.S., Pillai, R.B. and Pi-Puig, T. (2021). Geochemistry of sands from the Huatabampo and Altata beaches. *Gulf of California, Mexico. Geological Journal*, v. 56, pp. 2398-2417.
- McLennan, S.M. (2001). Relationship between the trace elements composition of sedimentary rocks and upper continental crust. *Geochemistry, Geophysics, Geosystems*, v. 2, issue 4.
- McLennan, S.M. and Taylor, S.R. (1991) Sedimentary rocks and crustal evolution: tectonic setting and secular trends. *Journal of Geology*, v. 99, pp. 1-21.
- Nayak, G.N. and Singh, K.T. (2022). Source, processes, and depositional environments of estuarine mudflat core sediments, central western coast of India. In: Armstrong-Altrin JA, Pandarinath K, Verma S. (Eds.), *Geochemical Treasures and Petrogenetic Processes*. P. 123-152.
- Nesbitt, H. W., Markovics, G and Proce, R.C. (1980). Chemical processes affecting alkalise and alkaline earths during continental weathering. *Geochimica et Cosmochimica Acta*, v. 44, p. 1659-1666.
- Nesbitt, H. W. and Young, G.M. (1982). Early Proterozoic climates and plate motions inferred from major elements chemistry of Lutites. *Nature*, v. 299, pp. 715-717.
- Nesbitt, H.W., Young, H.W., McLennan, S.M. and Keays, R.R., (1996). Effects of Chemical Weathering and Sorting on the Petrogenesis of Siliciclastic Sediments, with Implications for Provenance Studies. *The Journal of Geology*, v. 104, pp.525-542.
- Pettijohn, F.J., Potter, P.E. and Siever, R. (1972). *Sand and Sandstone*. Springer-Verlag, Berlin.
- Ramos-Vázquez, M.A., Armstrong-Altrin, J.S., Madhavaraju, J., Gracia, A. and Salas-de-León, D.A. (2022). Mineralogy and geochemistry of marine sediments in the Northeastern Gulf of Mexico. In: Armstrong-Altrin JA, Pandarinath K, Verma S. (Eds.), *Geochemical Treasures and Petrogenetic Processes*. P. 153-183.
- Ramos-Vázquez, M., Armstrong-Altrin, J.S., Rosales-Hoz, L., Machain-Castillo, M.L. and Carranza-Edwards, A. (2017). Geochemistry of deep-sea sediments in two cores retrieved at the mouth of the Coatzacoalcos river delta, Western Gulf of Mexico, Mexico. *Arabian Journal of Geosciences*, v. 10 (6), p. 148.
- Rao, G.V. (1947-48). Report (unpublished) Field Session 1947-48, *Geol. Sur. India*.
- Rao, G.V. (1947-48). *Mem. Geol. Sur. Ind.*, v. 7, I, 1969.
- Roser, B.P. and Korsch, R.J. (1986). Determination of tectonic setting of sandstones-mudstone suites using SiO₂ content and K₂O/Na₂O ratio. *The Journal of Geology*, 94, pp. 635-650.
- Roser, B.P. and Korsch, R.J. (1988). Provenance signatures of sandstone mudstone suites determined using discrimination function analysis of major element data. *Chemical Geology*, v.67, pp. 119-139.
- Sopie, F.T., Ngueutchoua, G., Armstrong-Altrin, J.S., Njanko, T., Sonfack, A.N., Sonfack, A.N., Ngagoum, Y.S.K., Fossa, D. and Tembu, L.T. (2023). Provenance, weathering, and tectonic setting of the Yoyo, Kribi, and Campo beach sediments in the southern Gulf of Guinea, SW Cameroon. *Journal of Earth System Science*, 132, article no. 92.
- Suttner, L.J. and Dutta, P.K. (1986). Alluvial sandstone composition and paleoclimate framework mineralogy. *Journal of sedimentary petrology*, v. 56, pp. 329-345.
- Taylor, S.R. and McLennan, S.M. (1995). The geochemical evolution of the continental crust. *Reviews of Geophysics*, v. 33, issue 2, pp. 241-265.
- Taylor, S.R. and McLennan, S.M. (1985). The continental crust: its composition and evolution. Blackwell, Oxford, pp. 1-312.
- Taylor, S.R. and McLennan, S.M. (1991). Sedimentary rocks and crustal evolution: Tectonic setting and Secular trends. *Journal of Geology*, v. 99, pp.1-21.
- Tawfik, H.A., Ghandour, I.M., Maejima, W., Armstrong-Altrin, J.S. and Abdel-Hameed, A-M.T. (2017). Petrography and geochemistry of the siliciclastic Araba Formation (Cambrian), east Sinai, Egypt: Implications for provenance, tectonic setting and source weathering. *Geological Magazine*, vol. 154 (1), pp. 1-23.
- Tawfik, H.A., Salah, M.K., Maejima, W., Armstrong-Altrin, J.S., Abdel-Hameed, A-M.T. and

- Ghandour M.M.E. (2018). Petrography and geochemistry of the Lower Miocene Moghra sandstones, Qattara Depression, north Western Desert, Egypt. *Geological Journal*, v. 53, pp. 1938-1953.
- Verma, P.S. and Armstrong-Altrin, J.S. (2013). New multidimensional diagram for tectonic discrimination of siliciclastic sediments and their application to Precambrian basin. *Chemical Geology*, 355(2013), pp. 117-133.
- Wang, Z., Wang, J., Fu, X., Zhan, W., Armstrong-Altrin, J.S., Yu, F., Feng, X., Song, C. and Zeng, S. (2018). Geochemistry of the Upper Triassic black mudstones in the Qiangtang Basin, Tibet: Implications for paleoenvironment, provenance, and tectonic setting. *Journal of Asian Earth Sciences*, v. 160, pp. 118-135.
- Wronkiewicz, D.J. and Condie, K.C. (1989). Geochemistry and provenance of sediments from the Pongola Supergroup, South Africa: evidence for 3.0 Ga old continental craton. *Geochimica et Cosmochimica Acta*, v. 53, pp. 1537-1549.
- Yadav, P.K., Das, M. and Ray, S. (2022). Geology, petrology and geochemistry of the Mesoproterozoic Kaimur group of rocks of the Vindhyan Supergroup, Eastern India: implication for depositional environment and sequence stratigraphy. *Journal of Sedimentary Environment*, v.7, pp. 443-469.

Textural characteristics of fluvial sediments in the Kosi River Basin, Bihar, India

Saba Imam* and Atul Aditya Pandey

Department of Geology, Patna University, Patna

*E-mail address: sabaimam82@gmail.com

ABSTRACT

The fluvial sediment samples collected from the Kosi River Basin, Bihar were subjected to textural analysis. The textural parameters were computed using the appropriate phi values. Statistical metrics including mean, standard deviation, skewness, and kurtosis were estimated. From the findings, the mean size of river sand has been observed from medium to fine-grained nature (between 0.97 Φ and 2.72 Φ). Within the range of 0.50 Φ to 0.77 Φ , the standard deviation denotes a moderately well-sorted to moderately sorted nature. The sediment samples exhibit skewness values ranging from -0.344 Φ to 0.267 Φ . The Kurtosis varies between 0.86 Φ and 1.9 Φ , indicating a leptokurtic to mesokurtic nature. Thus, the statistical measures have revealed that sediments are dominant in the medium sand category, moderately well sorted, finely skewed, and fall under leptokurtic character. The bivariate plots constructed between the statistical metrics indicate the unimodal nature of sediments.

Keywords: Textural analysis, Statistical Parameters, Bivariate plots, CM pattern, Kurtosis

INTRODUCTION

River basins are indispensable ecosystems, providing vital water resources crucial for human survival, agricultural irrigation, and environmental decontamination (Siderius et al., 2022; Zhao et al., 2021; Ramos-Vázquez et al., 2022). Nevertheless, the escalating significance of environmental issues, such as the diminishing self-purification ability of river basins and the deterioration of ecological functions, can be attributed to the devastation of ecological habitats caused by human activities and the excessive exploitation of natural resources (Zhu et al., 2021; Dai et al., 2022). It is generally recognized that sediment grain-size distribution can be utilized to address changes in material sources, transit modes, and other sedimentation processes (Folk and Ward, 1957; Liu et al., 2016; Chougong et al., 2021). Reconstructing the hydro dynamics that were linked with the climatic conditions and environment has been done extensively through the use of various grain size statistics, such as mean size (Mz), standard deviation (σ_1), skewness (Sk1) and kurtosis (KG) (Xiao et al., 2009; Wang et al., 2009; Anaya-Gregorio et al., 2018; Madhavaraju et al., 2021).

Numerous researches have been done to use granulometric components to differentiate various environments of the formation of sediments (Krumbein, 1963; Keller, 1949; Folk & Ward, 1957; Friedman, 1961; Wang, 2009; Kanhaiya and Singh, 2014; Venkatesan et al., 2021; Yadav, 2023). Analyzing the grain size is crucial to identifying the transportation history and depositional environment (Folk and Ward, 1957; Friedman, 1979; Bui et al. 1989, Ganesh et al. 2013; Liu, 2017). Understanding the textural characteristics of sediments is vital for achieving a higher degree of success in determining

their depositional environments (Pettijohn, 1984; Balamurugan, 2014). The characteristics of grain size distribution within sediments depend upon source materials, weathering process, and sorting during sediment transport and deposition (Irfan, 2022). Analyzing the textural studies of frequency curves comprised of mean, standard deviation, skewness, kurtosis and to facilitated the interpretation of sediment deposition of the prevailing environment (Venkatesan and Singarasubramanian, 2016).

However, there exists a notable gap in the literature concerning the nature of the sediments carried by the river. Sediment transport plays a crucial role in interpreting river processes as it is the group of mechanisms that link the running water and the channel boundary. The present work aims to understand the transport mechanism of river sediments based on textural parameters.

STUDY AREA

The Kosi River is the most prominent left-bank tributary of the Ganga River in northern Bihar. The study area forms part of the Saharsa and Supaul districts. The area falls between latitudes N 25° 16' 18.5" to N 29° 7' 30.4" and longitude E 83° 59' 22.5" to E 88° 57' 53.3" in the survey of India toposheet no 72J/8, 72J/12, 72K/5, 72K/9, 72K/10, 72K/14 (Scale 1:50,000) (Fig. 1). The Kosi River has its source in the Himalayas at an elevation of 7000 meters above the sea level. Also, it is a significant transboundary river that serves as one of the primary left-bank tributaries of the Ganga River system (Rai, 2018). The geology of the megafan consists of

unconsolidated sediments of Quaternary age. The geological characteristics of the Kosi watershed render it inherently unstable, making it prone to substantial erosion and sediment accumulation, ultimately resulting in an elevated sediment load within the flowing river (Agarwal, 1992, Sinha et al., 2008). The escalating sediment load in the Kosi River significantly disrupts its natural flow dynamics, leading to alterations in its course over time (Wells and Dorr, 1987; Gole and Chitale, 1966, Shrestha et al., 2010; Sinha et al., 2019).

METHODOLOGY

Sediment samples were obtained from specific locations in the Northwestern section of the Kosi River Basin (Fig. 2). The samples were gathered and placed in dry, clean polythene bags for further laboratory analysis.

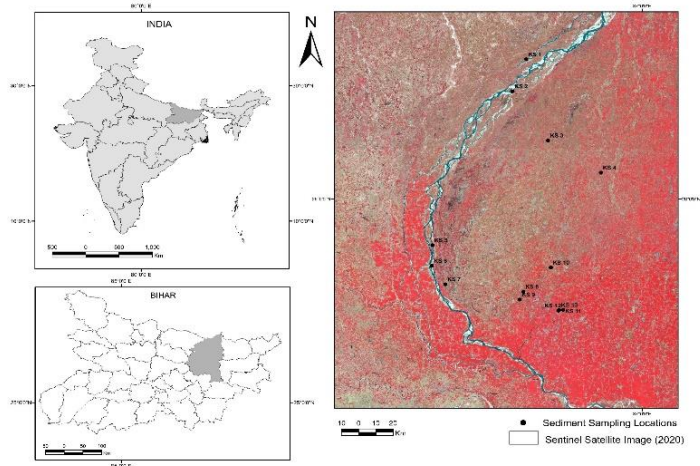


Fig. 1. Map showing sampling locations in the Kosi River Basin

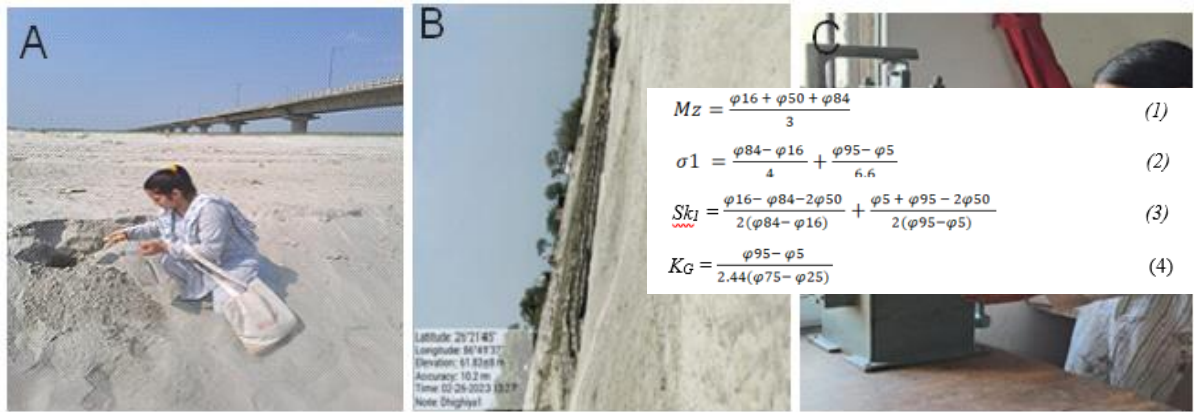


Fig. 2. A and B showing the collection of sediment samples from the Megafan area, and C) grain size analysis at the laboratory

Totally, 13 surface sediment samples of about 1 kg each from Megafan were collected in precise positions using a Global Positioning System (GPS) receiver. The samples were frequently washed, dried, and consistently mixed. In order to obtain the desired 100-gram weight of sediments, consecutive coning and quartering were performed. The dried samples were kept in topmost ASTM sieve and placed in a set of assembled sieves starting from 38 mesh (5Φ), 63 mesh (4Φ), 125 mesh (3Φ), 250 mesh (2Φ), and 500 (1Φ) mesh. The sieving of the sediments samples was done for 15 min in Rotop mechanical sieve shaker.

Following the sieve analysis, the sediments from each sieve were weighed with a digital balance. The weight percentage and cumulative weight percentage were recorded manually. Analytical data have been applied to generate cumulative frequency curves and calculate statistical parameters using standard techniques of Folk and Ward (1957). The formulae established by Folk and Ward (1957) were used to interpret the grain-size parameters. The grain

size was computed using phi (φ) units (φ = -log₂d, where d is size of grain in millimeters), and measured by applying domains like mean size (Mz), standard deviation (σ₁), skewness (Sk₁) and kurtosis (KG), as determined by the following formulae,

The evaluation of granulometric characteristics were done by using G-Stat software, it includes frequency curves, scatter plots, triangle diagrams, and CM patterns (Venkatesan et al., 2017).

RESULTS

FREQUENCY CURVES

The distribution of sediments grain size in the Kosi river basin has been plotted in the form of frequency distribution curves (Fig. 3). A Frequency distribution curve serves as a visual illustration of the weight percentages of different fractions of sediment and is used to outline the characteristic of

sediments (Arun, 2019). The frequency curves of the sediment sample exhibit distinct unimodal behavior. The chief modes are located within the size range of

1Φ to 2.5Φ which indicates that the majority of sediments fall in the medium to fine class. There is one subsidiary mode in the finer class i.e. KS12.

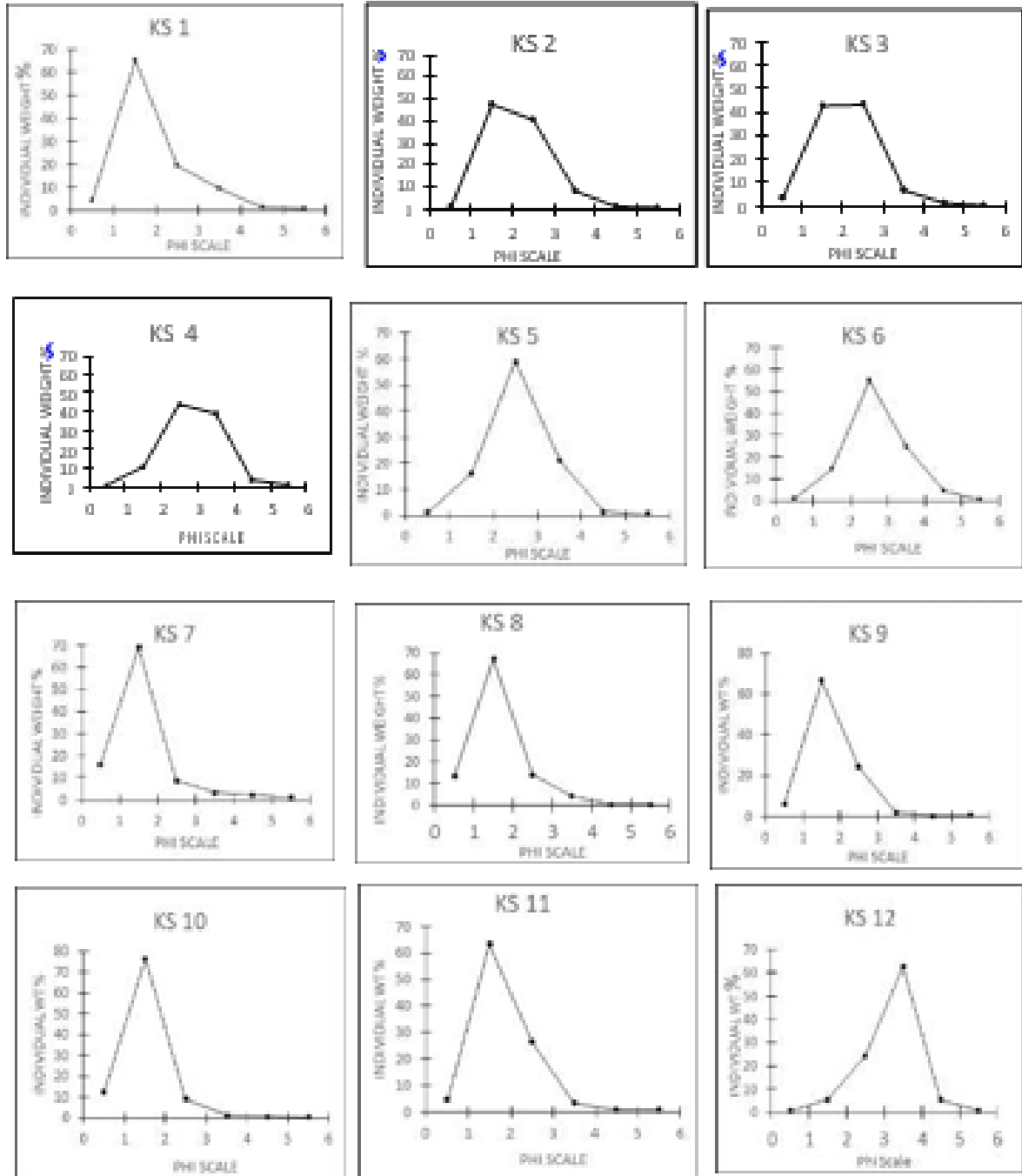


Fig. 3. Showing frequency distribution curves of sediments in different locations of the Kosi River basin.

CUMULATIVE CURVE

The cumulative curves are integral of frequency polygons. The pattern of the cumulative curves of the Kosi River basin is given in Figure 4. The curves of the sample i.e. KS4, KS5, KS6, and KS12 start with the range of $0-1\Phi$ with the initial low

slope, it maintains a rising trend up to 2.5Φ , and then it becomes steep and attains maximum at 5.5Φ . Rest all the samples are straight in the size range of 0.5Φ to 1.5Φ , then it became steep and attain maximum at 5.5Φ . From the cumulative curve, it is indicated that the sediments are moderately

well sorted to moderately sorted in nature.

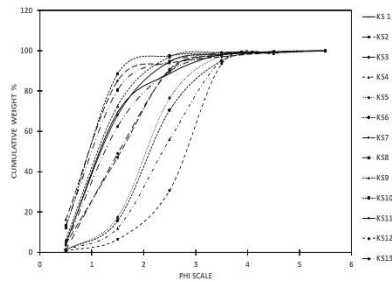


Fig. 4. Cumulative curves showing the grain size trends of sediment samples.

GRAIN SIZE PARAMETERS

Granulometric analysis is the most adopted methodology to reveal the sedimentation process like transportation, deposition, and energy level. The hydrodynamic factors that were formed at the time of the sedimentation process in a basin were determined using textural parameters like mean, standard deviation, skewness, and kurtosis. (Folk and Ward, 1957; Friedman, 1979; Passega, 1964). Various authors adopted different statistical approaches by using various formulas (Friedman, 1961; Passega, 1964; Sahu, 1964). The formulas provided by Folk and Ward (1957) are thought to be the most common and are used to compute the textural parameters of the sediments (Table 1 and Table 2).

MEAN GRAIN SIZE (MZ)

The transporting agents, energy level of deposition and the source of sediments are the prominent factors that influence the mean grain size (Folk and Ward, 1957). The mean size value range from 0.967Φ to 2.716Φ , with an average value of 1.622Φ (Fig. 5a). The majority of samples, 53.84%, are classified as medium sand, while 30.76% fall into the coarse sand category, and 15.38% fall into the fine sand category (Table 1). The average sediment size is determined by the sediment source, the mode of transportation, and the depositing medium's energy conditions (Ventakesan, 2016; Durai, 2017). Variation of mean size from the medium to coarse pinpoints the high-energy conditions during its deposition (Ganesh et al., 2013).

SEDIMENT SORTING (σ_1)

The variation in the velocity of the depositing medium and its kinetic energy was specified by the degree of sorting of the sediments. The degree of sorting could be determined by measuring the Standard deviation of the sediments (Sahu, 1964). Sorting and standard deviation have an inverse relationship. Sorting and standard deviation have an inverse relationship. Standard deviation measures the difference in kinetic energy

that corresponds to the depositing agent. Standard deviation measures the difference in kinetic energy corresponds with the mode of deposition. The standard deviation of the samples ranges between 0.5Φ to 0.766Φ , with an average of 0.673Φ (Fig. 5b). About 53.84% of samples were well sorted, 46.15% were moderately well sorted in nature. In the study area, sediment characteristics ranging from moderately well-sorted to well-sorted indicate a quick smack or back-and-forth action by the depositing agent. The dominant characteristics of moderately well-sorted and moderately sorted sediments suggest the impact of strong energy conditions in the basin (Rita Chauhan et al., 2014). The tough energy conditions of depositing agents or the predominance of strong energy conditions in the basin are indicated by the predominant well-sorted and moderately well-sorted results.

SEDIMENT SKEWNESS (Sk1)

Skewness is a statistical measure that indicates the degree of asymmetry in a frequency distribution. Duane (1964) ascertained that the positively skewness deposition area has changed to negative skewness due to the cyclic current pattern. This pattern is pointing to the high-energy environment that abound in the area. In the River Kosi, minimum and maximum skewness values are -0.344Φ and 0.44Φ respectively with an average value of 0.104Φ (Fig. 5c). However, a positively skewed category is dominant in the samples of the Kosi River. Among the total volume, 53.84% in positively skewed, 30.76% near symmetrical nature. 7.69% of the samples fall in very positively skewed and very negatively skewed (Table 1). In the depositional environment, an excess of coarser particles in the sediment distribution or the tailing of coarser fractions is indicated by a preponderance of positive skewness values.

Near symmetrical nature of sediments indicates the mixing of bimodal sources. Sediments veiled in the low-energy environments show positive skewness, while those deposited in high-energy environments exhibit negative skewness. The change in the skewness values in the region indicates the differential energy condition in their sector. Near symmetrical nature of sediments indicates the mixing of bimodal sources (Venkatesan et al., 2017). The change in the skewness values in the region indicates the differential energy condition in their sector.

SEDIMENT KURTOSIS (KG)

The sediment kurtosis is defined as the peak of grain size distribution based on the mode of environment. It also depicts the level of sorting in the tail and central regions (Folk and Ward, 1957). The mesokurtic condition is observed when the tail and center are equally sorted (Parthasarathy et al.,

Sample No.	Φ95	Φ84	Φ75	Φ50	Φ25	Φ16	Φ5	Φ1	C in micron	M in micron
KS1	3.1	2.15	1.7	1.15	0.8	0.7	0.5	0	1000	450
KS2	2.9	2.3	2.1	1.5	1	0.8	0.6	0.5	700	350
KS3	2.8	2.3	2.1	1.5	1	0.8	0.5	0	1000	350
KS4	3.5	3.15	2.9	2.3	1.9	1.6	1	0.5	700	200
KS5	3.3	2.7	2.5	2.1	1.7	1.5	0.8	0.5	700	230
KS6	3.5	2.9	2.6	2.1	1.7	1.6	0.9	0.5	700	230
KS7	2.7	1.5	1.3	0.9	0.6	0.5	0	0	1000	530
KS8	2.5	1.6	1.4	1	0.7	0.5	0	0	1000	500
KS9	2.4	2.8	1.5	1.1	0.7	0.7	0	0	1000	470
KS 10	1.9	1.4	1.3	0.9	0.7	0.5	0	0	1000	540
KS 11	2.5	2.0	1.7	1.2	0.8	0.7	0.5	0	700	430
KS 12	3.5	3.3	3.1	2.85	2.35	2	1.4	0.5	700	140
KS 13	2.9	2.2	1.9	1.3	0.85	0.7	0.5	0	1000	400

Sample No	Mean	Standard deviation	Skewness	Kurtosis	Remark			
					Ms	MS	VPS	LK
KS1	1.333	0.756	0.44	1.183	Ms	MS	VPS	LK
KS2	1.533	0.723	0.142	0.856	Ms	MS	PS	PK
KS3	1.55	0.723	0.043	0.856	Ms	MS	NLS	PK
KS4	2.366	0.766	-0.024	1.024	Fs	MS	NLS	PK
KS5	2.1	0.678	-0.15	1.281	Fs	MWS	NS	LK
KS6	2.166	0.743	0.186	0.665	Fs	MS	PS	VPK
KS7	0.967	0.659	0.267	1.580	Cs	MWS	PS	VLK
KS8	1.05	0.641	0.171	1.463	Ms	MWS	PS	LK
KS9	1.2	0.639	0.178	1.229	Ms	MWS	PS	LK
KS10	0.967	0.500	0.03	1.297	Cs	WS	NLS	LK
KS11	1.3	0.628	0.265	0.910	Ms	MWS	PS	MK
KS12	2.716	0.643	-0.344	1.075	Fs	MWS	VNS	MK
KS13	1.4	0.738	0.267	0.937	Ms	MS	PS	MK
Minimum	0.967	0.500	-0.344	0.856	Cs	WS	VNS	PK
Maximum	2.716	0.766	0.44	1.580	Fs	MS	VPS	VLK
Average	1.588	0.679	0.113	1.104	Ms	MWS	PS	MK

Fs – fine sand, **Ms** – medium sand, **Cs**- coarse sand; **MS** – moderately sorted, **MWS** – moderately well sorted, **WS** – well sorted; **VPS** – very positively skewed, **PS**- positively skewed, **NLS** – nearly symmetrical, **NS** – negatively skewed, **VNS** – very negatively skewed; **VLK** – very leptokurtic, **LK**- leptokurtic, **MK** – mesokurtic, **PK** – platykurtic

2016). The graphic kurtosis values obtained range from 0.67 Φ to 1.58 Φ, with an average of 1.106 Φ (Fig. 5d). Leptokurtic character (38.46%) is dominant among all, 23.07% of the samples fall in mesokurtic character and platykurtic 7.69% of the samples fall in very platykurtic and very leptokurtic (Table 1). The variability in kurtosis values reflects the flow features of the depositing agents (Seralthan and Padmalal, 1994; Baruah et al., 1997). The various sediment deposition processes are implied by the leptokurtic and mesokurtic characters (Solai et al., 2013; Rumuri, et al., 2021). Based on all statistical parameters, the sediments were most likely deposited during a high-energy period, such as the monsoon season.

BIVARIATE PLOTS

Bivariate plots between the textural parameters provide information about sedimentation environments and delineate overlapping zones of closely related environments. Inman (1952), Folk and Ward (1957), Friedman (1961) and (1979) successfully used the scatter plots to understand the geological significance of the four size parameters. Scatter plots between mean versus standard deviation, mean versus skewness, mean versus kurtosis, standard deviation versus skewness, standard deviation versus kurtosis, and skewness versus kurtosis were drawn to understand the interrelationship between different parameters.

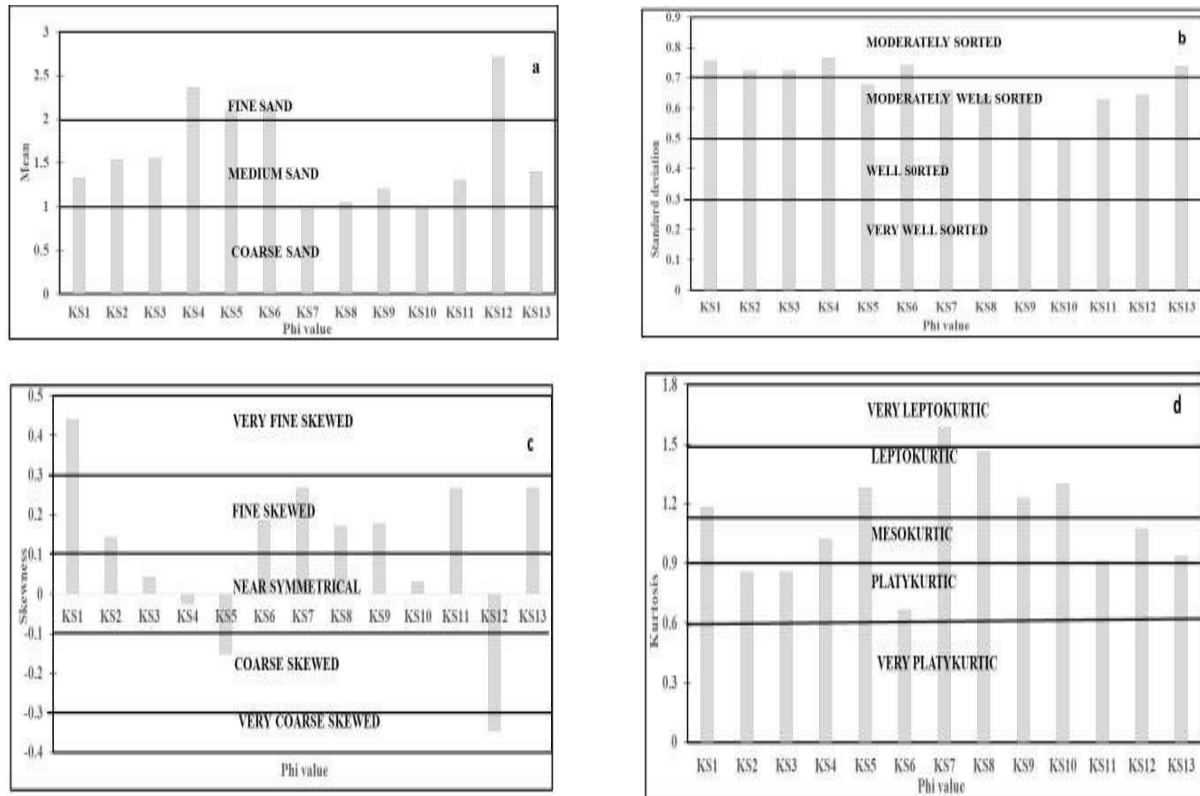


Fig. 5. Comparative histograms of all samples showing variation of a) mean, b) standard deviation, c) skewness, and d) kurtosis

MEAN SIZE VERSUS STANDARD DEVIATION

The scatter plot between the mean size and standard deviation of the Kosi sediments has been shown (Fig. 6a). Most of the sediments fall between 1Φ to 2.5Φ mean size value and indicate moderately well-sorted to moderately sorted nature of the medium to fine-grained sand.

MEAN SIZE VERSUS SKEWNESS

The scatter plot of the mean size versus skewness indicates scattering of medium sands in the positively skewed portion, above the normal curve (Fig. 6b). Below the normal curve, scattering is nearly symmetrical skewed, and only the scatter plot of the mean size against skewness shows dispersion of medium sands in the positively skewed area above the normal curve and only one sample falls in negatively and very negatively skewed i.e. KS5 and KS 12 respectively. The characteristic feature of the river sands is that they exhibit positive skewness (Friedman, 1961) and the same is true for the Kosi river sediments.

MEAN SIZE VERSUS KURTOSIS

In the mean size versus kurtosis plot, the medium-grained river sands are clustering around mesokurtic to leptokurtic values, about the normal curve (Fig. 6c). (Folk and Ward, 1957).

STANDARD DEVIATION VERSUS SKEWNESS

The relationship between standard deviation and skewness reveals that the moderately well-sorted to moderately sorted river sands are mostly positively skewed and few samples exhibit range from very negatively to very positively skewed in nature (Fig. 6d). Typically, as the standard deviation increases, the skewness value also tends to rise in sedimentology. Higher skewness values are indicative of poorer sediment sorting (Friedman, 1961).

STANDARD DEVIATION VERSUS KURTOSIS

The scatter plot of standard deviation versus kurtosis indicates that the moderately well-sorted to moderately sorted river sands are mostly leptokurtic to mesokurtic in nature. Only two samples KS2 and KS3 are moderately sorted and platykurtic (Fig. 6e).

SKEWNESS VERSUS KURTOSIS

As the modes are separated and the depositional environment is sorted, there is a large range of skewness and kurtosis values (Folk and Ward, 1957). The bivalent plot of skewness versus kurtosis corresponds to river sand (Friedman, 1961) as greater amount of the sands are mesokurtic to leptokurtic with positive skewness (Fig. 6f).

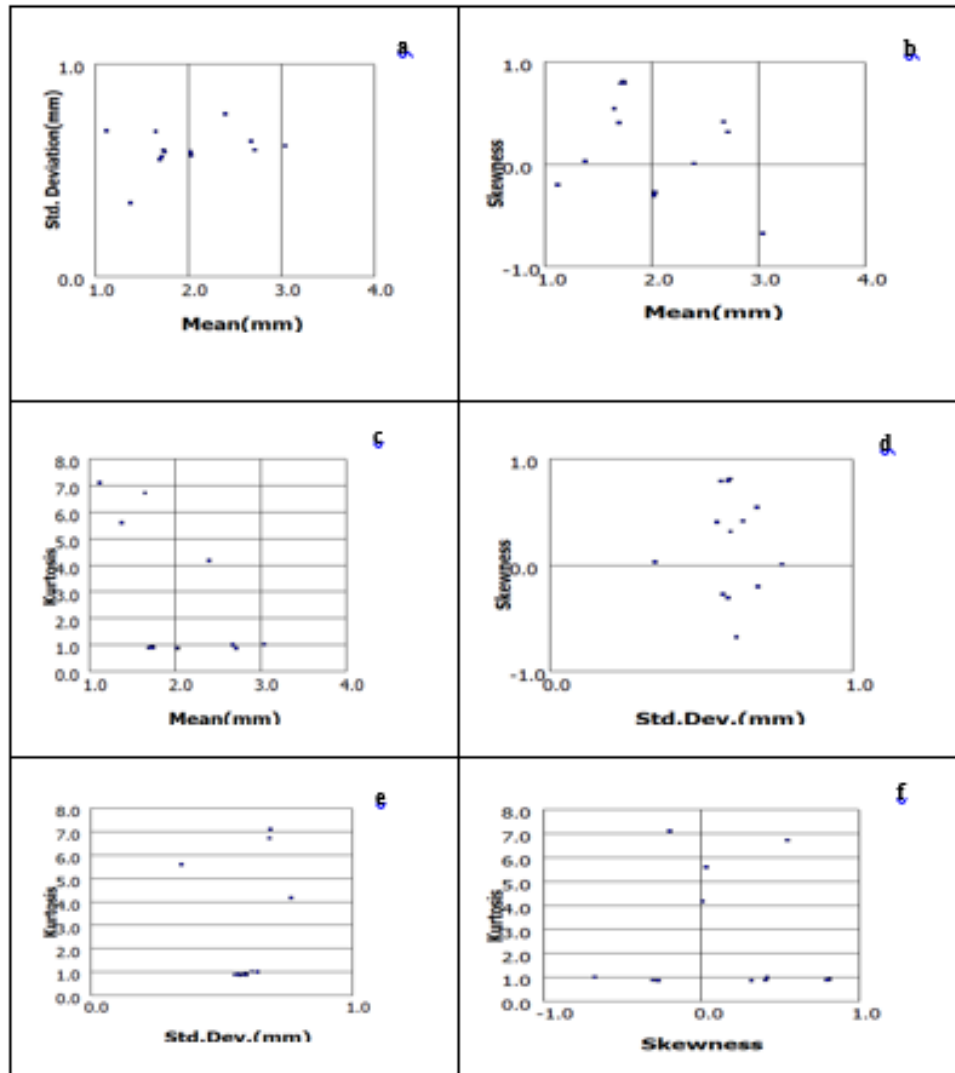


Figure 6. Scatter plots showing the model plot as proposed by Folk and Ward (1957). (a) mean vs standard deviation, (b) mean vs skewness, (c) mean vs kurtosis, (d) skewness vs standard deviation, (e) standard deviation vs kurtosis and (f) skewness vs kurtosis.

CM DIAGRAM

This research aims to determine the depositional mechanism of sediments in the Kosi River Basin through using the technique of CM pattern analysis. By using the corresponding micron values obtained from cumulative curves, the graph was made for the Phi values of parameters C and M, whereas C represents the one percentile of the grain size distribution and M represents the Median. The C and M is categorized based on the nature of bottom turbulence. There are five segments of CM patterns such as rolling (NO), bottom suspension and rolling (OPQ), graded suspension with no rolling (QR), uniform suspension (RS), and pelagic suspension (S) (Fig. 7). Exceeding the amount of sediment samples -from the Kosi River Basin fall into the OP sector, which indicates bottom suspension and rolling mode of deposition, while a few falls into the PQ sector, which indicates undegraded suspension and no rolling mode of deposition.

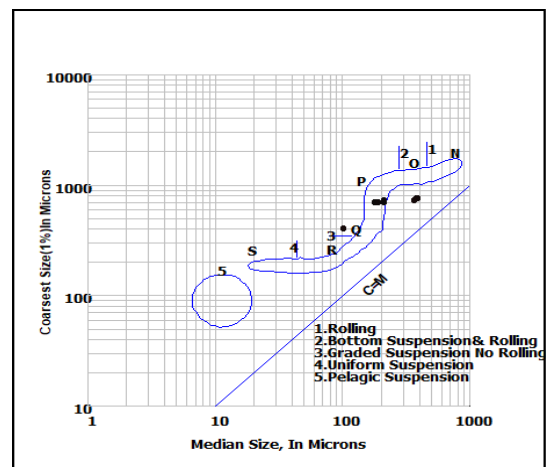


Fig. 7. CM diagram for the Kosi River sediments

CONCLUSIONS

This study aimed to assess the grain size distribution characteristics in sediment samples collected from diverse locations within the Kosi River basin. Parameters for textural characteristics such as mean size, standard deviation, skewness, and kurtosis were estimated for the sediments collected in the study area. The resulting Frequency Distribution Curves intensify that the sediments were mainly composed of medium sand and primarily unimodal in nature. The mean size indicates that the fine sands were deposited with sparsely low energy level conditions. The moderately well-sorted character of sediments indicates that the basin is experiencing greater energy conditions. The sediments are mostly of positively skewed indication of fluvial nature. Kurtosis indicates a leptokurtic to mesokurtic nature. Mesokurtic and Leptokurtic sediments are produced by continuously adding finer and coarser sediments after winnowing and maintaining their original properties during deposition. The relationship plots between the statistical domains highlighted the unimodal sediment characteristics in which, the medium-grained sand is the dominant mode.

ACKNOWLEDGMENT

I would like to express my sincere gratitude to the Head, Department of Geology, Patna University, for allowing me to conduct the textural analysis of fluvial sediments in the Department Sedimentology Laboratory. I am thankful to the UGC JRF for the financial support. We thank the Editor of the Journal Indian Association of Sedimentologists, Dr. John S. Armstrong-Altrin and the two reviewers for providing useful comments and suggestions to improve the quality of our presentation.

REFERENCES

- Arun, T.J. and Srinivas, R. (2019). Studies on the Textural Characteristics of Sediments from Vaigai River Basin, Tamil Nadu, Southern India. *International Journal of Science and Technology Research*, (8).
- Agarwal, R.P. and Bhoj, R. (1992). Evolution of Kosi river fan, India: structural implications and geomorphic significance. *International Journal of Remote Sensing*, v. 13 (10), pp. 1891-1901.
- Anaya-Gregorio, A., Armstrong-Altrin, J.S., Machain-Castillo, M.L., Montiel-García, P.C. and Ramos-Vázquez, M.A. (2018). Textural and geochemical characteristics of late Pleistocene to Holocene fine-grained deep-sea sediment cores (GM6 and GM7), recovered from southwestern Gulf of Mexico. *Journal of Palaeogeography*, v. 7(3), pp. 253-271.
- Balamurugan, P., Vasudevan, S., Selvaganapathi, R., Nishikanth, C. (2014). Spatial distribution of grain size characteristics and its role in interpreting the sedimentary depositional environment, Kodaikanal Lake, Tamil Nadu, India. *Journal of Earth Science and Climate Change*, v. 5 (8), pp. 1-8.
- Baruah J, Kotoky, Sharma, J.N. (1997). Textural and geochemical study on river sediments: a case study on the Jhanji River, Assam. *Journal of the Indian Association of Sedimentologist*, v. 16, pp. 195-206.
- Bui E.N., Mazzullo J.M. and Wilding L.P. (1989). Using quartz grain size and shape analysis to distinguish between aeolian and fluvial deposits in the Dallol Bosso of Niger (West Africa). *Earth Surface Processes and Landforms*, v. 14(2), pp. 157-166.
- Chauhan, R. (2014). Patterns of seasonal variability in granulometric characteristics of Bhitarkanika Mangrove-estuarine complex, East coast of India. *Indian Journal of Geo- Marine Sciences*, pp. 1083-1090.
- Chougong, D.T., Bessa, A.Z.E., Ngueutchoua G., Yongue, R.F., Ntyam, S.C. and Armstrong-Altrin, J.S. (2021). Mineralogy and geochemistry of Lobé River sediments, SW Cameroon: Implications for provenance and weathering. *Journal of African Earth Sciences*, v. 183, pp. 1-19 No. 104320.
- Dai, D., Sun, M., Lv, X., Hu, J., Zhang, H., Xu, X. and Lei, K. (2022). Comprehensive assessment of the water environment carrying capacity based on the spatial system dynamics model, a case study of Yongding River Basin in North China. *Journal of Cleaner Production*, v. 344, pp. 131-137.
- Duane, D.B. (1964). Significance of Skewness in Recent Sediments, Western Pamlico Sound, North Carolina. *Journal of Sedimentary Petrology*, v. 34, pp. 864-874.
- Durai A.C. (2017). A study on textural characteristics of the Palar River sediments, Sadurangapattinam to Mamandur, Kanchipuram District, Tamil Nadu, India. *International Research Journal of Earth Sciences*, v. 11, pp. 24-33.
- Folk, R.L. and Ward, W.C. (1957). Brazos River bar: a study in the significance of grain size parameters. *Journal of Sedimentary Petrology*, v. 27, pp. 3-26.
- Friedman, G.M. (1961). Distinction between dune, beach, and river sands from their textural characteristics. *Journal of Sedimentary Petrology*, v. 31(4), pp. 514-529.
- Friedman, G.M. (1979). Differences in size distributions of populations of particles among sands of various origins. *Sedimentology*, v. 26, pp. 3-32.
- Ganesh, B., Naidu, A.G.S.S., Jaganandha, M., Rao, T., Karuna, K. and Avatharam, P. (2013). Studies on textural characteristics of sediments from Gosthani River Estuary-Bheemunipatnam, A.P., East Coast of India. *Journal of the Indian Geophysical Union*, v. 17(2), pp. 139-151.
- Gole, C.V. and Chitale, S.V. (1966). Inland delta building activity of Kosi River. *Journal of the Hydraulics Division*, v. 92(2), pp. 111-126.
- Irfan, M., Singh, B.P., Kanhaiya, S. (2022). Textural behavior, facies, and depositional environments of the Middle Siwalik Subgroup of the Jammu area, Jammu & Kashmir State, NW Himalaya. *Journal of Palaeontological Society of India*, v. 67 (1), pp. 85-92.
- Kanhaiya, S. and Singh, B.P. (2014). Spatial Variation of Textural Parameters in a Small River: An Example from Khurar River, Khajuraho, Chhaterpur District, Madhya Pradesh, India. *Global Journal of Earth Science and Engineering*, v. (1), pp. 34-42.
- Keller, W.D. (1949). Size distribution of sand in some dunes, beach sand sandstones. *American Association of Petroleum Geology Bulletin*, v. 29, pp. 215-221.
- Krumbein, W.C. and Sloss, L.L. (1963). Properties of sedimentary rocks. *Stratigraphy and Sedimentation*, pp. 106-113.

- Liu, X., Vandenberghe, J., An, Z., Li, Y., Jin, Z., Dong, J. and Sun, Y. (2016). Grain size of Lake Qinghai sediments: Implications for riverine input and Holocene monsoon variability. *Palaeogeography Palaeoclimatology and Palaeoecology*, v. 449, pp. 41-51.
- Madhavaraju, J., Armstrong-Altrin, J.S., Pillai, R.B. and Pi-Puig, T. (2021). Geochemistry of sands from the Huatabampo and Altata beaches. Gulf of California, Mexico. *Geological Journal*, v. 56, pp. 2398-2417.
- Parthasarathy, P., Ramesh, G., Ramasamy, S. Arumugam, T., Govindaraj, P., Narayanan, S. and Jeyagopal, G. (2016). Sediment dynamics and depositional environment of Coleroon river sediments, Tamil Nadu, Southeast coast of India. *Journal of Coastal Science*, v. 3, pp. 1-7.
- Passega, R. (1964). Grain size representation by CM patterns as a geological tool. *Journal of Sedimentary Geology*, v. 34(4), pp. 830-847.
- Pettijohn, F.J. (1984). *Sedimentary Rocks*. 3rd ed. CBS Publishers, New Delhi, p. 628.
- Rai, P.K., Chandel, R.S., Mishra, V. N. and Singh, P. (2018). Hydrological inferences through morphometric analysis of lower Kosi river basin of India for water resource management based on remote sensing data. *Applied Water Science*, v. 8, pp. 1-16.
- Ramos-Vázquez, M.A., Armstrong-Altrin, J.S., Madhavaraju, J., Gracia, A. and Salas-de-León, D.A. (2022). Mineralogy and geochemistry of marine sediments in the Northeastern Gulf of Mexico. In: Armstrong-Altrin JA, Pandarinath K, Verma S. (Eds.), *Geochemical Treasures and Petrogenetic Processes*. pp. 153-183 https://doi.org/10.1007/978-981-19-4782-7_7.
- Rumuri, R., Ramkumar, T., Vasudevan, S. and Gnanachandrasamy, G. (2021). Variation of sediment grain size parameters, fish diversity, and phytoplankton richness in relation to sand and silt fractions in estuaries. *Geology Ecology and Landscapes*, p. 1-15. <https://doi.org/10.1080/24749508.2021.2022834>.
- Sahu, B.K. (1964). Depositional mechanisms from the size analysis of classic sediments. *Journal of Sedimentary Petrology*, v. 34(1), pp. 73-83.
- Sinha, R., Bapalu, G.V., Singh, L.K., Rath, B. (2008). Flood Risk Analysis in the Kosi River Basin, North Bihar using Multi Parametric Approach of Analytical Hierarchy Process (AHP). *Journal of the Indian Society of Remote Sensing*, v. 36, pp. 335-349.
- Seralathan, P. (1994). Textural studies of surface sediments of Muvattupuzha River and central Vembanand estuary, Kerala. *Journal of the Geological Society of India*, v. 43(2), pp.179-190.
- Shrestha, R.K., Ahlers, R., Bakker, M. and Gupta, J. (2010). Institutional dysfunction and challenges in flood control: a case study of the Kosi flood 2008. *Economic and Political Weekly*, p. 45-53.
- Siderius, C., Biemans, H., Kashaigili, J. and Conway, D. (2022). Water conservation can reduce future water-energy-food-environment trade-offs in a medium-sized African river basin. *Agricultural Water Management*, v. 266.
- Solai, A., Suresh Gandhi, M., Kasilingam, K. and Sriraman, E. (2013). Heavy metal accumulation in the surface sediments off Pondicherry, Bay of Bengal, South East Coast of India. *International Journal of Innovative Research in Science, Engineering and Technology*, v. 2 (10), pp. 5741-5753.
- Sinha, R., Gupta, A., Mishra, k. and Tripathi, S. (2019). Basin-scale hydrology and sediments dynamics of the Kosi river in the Himalayan foreland. *Journal of Hydrology*, v. 570, pp. 156-166.
- Venkatesan, S. and Singarasubramanian, S.R. (2016). Textural analysis of surface sediments in Arasalar River, Tamil Nadu and Pondicherry Union Territory, India. *International Journal of Applied Research*, v. 2(12), pp. 164-171.
- Venkatesan, S., Singarasubramanian S.R. and Suganraj, K. (2017). Depositional mechanism of sediments through size analysis from the core of Arasalar river near Karaikkal, east coast of India. *Indian Journal of Geo Marine Sciences*, volume 46 (10), pp. 2122-2131.
- Wang, Z., Chen, Z., Li, M., Chen, J. and Zhao, Y. (2009). Variations in downstream grain- sizes to interpret sediment transport in the middle-lower Yangtze River, China: A pre-study of Three-Gorges Dam. *Geomorphology*, v. 213, pp. 217-229.
- Wells, N.A. and Dorr, Jr., J.A. (1987). Shifting of the Kosi River, northern India. *Geology*, v. 15(3), pp. 204-207.
- Wang, X., Yang, H., Lora Kitch, J., Liu, J. and Xue, B. (2021). Grain-size characteristics in lake Fuxian sediments: Implication for dry-humid transformation of Indian summer monsoon over the past 150 years. *Journal of Asian Earth Sciences*, v. 6, 100073.
- Xiao, J., Chang, Z., Si, B., Qin, X., Itoh, S., Lomtadze, Z. (2009). Partitioning of the grainsize components of Dali Lake core sediments: evidence for lake-level changes during the Holocene. *Journal of Paleolimnology*, v. 42 (2), pp. 249-260.
- Yadav, S.K., Kanhaiya, S., Singh, S., Quasim, M.A., S.K. Singh, Kumar, P. (2023). Facies architecture and textural attributes of the Late Quaternary cliff embankment sections of the Sai River, Central Ganga Plain, India. *Geosystems and Geoenvironment*, v. 2(4), 100216.
- Zhu, Q., Guo, J., Chen, L., Han, Y. and Liu, S. (2021). Relationship between ecological quality and ecosystem services in a red soil hilly watershed in southern China. *Ecological Indicators*, v. 121, 107119.
- Zhao, G., Liang, R., Li, K., Wang, Y. and Pu, X. (2021). Study on the coupling model of urbanization and water environment with basin as a unit: A study on the Hanjiang Basin in China. *Ecological Indicators*, v. 131, 108130.

Constraining provenance and age of the siliciclastic rocks from the southwestern Bundelkhand Craton, Central India

M.E.A. Mondal*, Kamaal Parvez, Iftikhar Ahmad and Wamiq Mohammed Khan

Department of Geology, Aligarh Muslim University, Aligarh 202002 (India)

*E-mail Address: meamondal.gl@amu.ac.in

ABSTRACT

The lithology of the Bundelkhand craton, central India, includes highly deformed tonalite, trondhjemite and granodiorite (TTG) gneisses (3.55–2.7 Ga), followed by volcano-sedimentary greenstone belts and a suite of undeformed granitoids ranging in age from 2.52 to 2.49 Ga. The granitoids, which are by far the most dominant lithology of the craton, have intruded into the TTG gneiss-greenstone assemblage. In addition to huge granitic bodies, rhyolitic rocks of 2.54 Ga have also been observed in the Bundelkhand craton. In this study, we report the first occurrence of a small isolated outcrop of siliciclastic sedimentary rocks within the Bundelkhand granitoid suites in and around the Panchwara village, in the southwestern part of the craton. These siliciclastic sedimentary rocks are intruded by the youngest granitic phase of the Bundelkhand granitoid suite, dated as 2.49 Ga old. Thus, their age is determined to be older than 2.49 Ga. Petrographic studies suggest that these rocks are arkose in nature and geochemical composition indicates that they were derived from the older gneiss-greenstone successions and the older granitic phase (2.52 Ga) of the Bundelkhand granitoid suite. The REE modelling suggests that the sediment contribution from different sources is: 50% greenstone belt (15% basalt + 35% sedimentary rocks), 35% gneisses and 15% older granitoids. Detrital zircons from these sedimentary rocks reveal two age populations: one group of zircons is clustering around 2.52 Ga and the other group is ranging from 3.0 to 3.3 Ga indicating at least two protoliths for these sediments. Our field, petrographical and geochemical data, coupled with previously studied zircon geochronological data, is best explained by a model involving deposition of sediments derived from TTG gneiss, greenstone belt and also from the older phase of the granitoid suite. It is interesting to note that the basin received sediments from the older granitic phase of 2.52 Ga age and was closed before the emplacement of the youngest granitic phase at 2.49 Ga. This study, thus, provides for the first time, conclusive evidence for the presence of a late Archean sedimentary basin within the Bundelkhand craton. It is proposed that the sediments were deposited penecontemporaneously with the pulses of the granitoid magmatism in the Bundelkhand Craton that took place ~2.5 Ga.

Keywords: Geochemistry, provenance, modal components, clastic rocks, mineralogy

INTRODUCTION

In most of the cratons, the Archean sedimentary rocks mainly occur as a constituent component of Archean greenstone sequences. However, a few Archean cratons preserve sedimentary rocks which are not a part of the greenstone sequence. The relatively small number of these sedimentary basins, mainly of late Archean age, may point to their low preservation potential. These late Archean sedimentary sequences are distinct in that they are relatively less deformed than their counterparts in the greenstones. The relatively less deformed nature of these sedimentary sequences may give a deceptive notion of the Proterozoic age. These sedimentary basins constitute an essential aspect of Precambrian crustal evolution with respect to provenance characterization and geodynamic setting during late Archean time. In this study, we report field occurrence, petrographical, geochemical data along with previously reported zircon

geochronological data of a relatively small outcrop of siliciclastic sedimentary rocks from the southwestern part of the Bundelkhand craton (Fig. 1). The objective of this study is to characterize their provenance, paleoweathering condition and to decipher their tectonic setting.

GEOLOGICAL SETTING

The Central Indian Tectonic Zone (CITZ), trending ENE-WSW, separates the Indian land mass into two parts, the northern and southern blocks. The northern block consists of Aravalli and Bundelkhand Cratons and the southern block consists of Singhbhum, Dharwar and Bastar Cratons (Acharyya, 2003; Radhakrishna and Naqvi, 1986). The Bundelkhand Craton is located in the north-central part of India, covering an area of approximately 26000 km². It comprises almost 90% of granitoids that are intruded into the older gneisses-greenstone belt. The oldest lithological unit

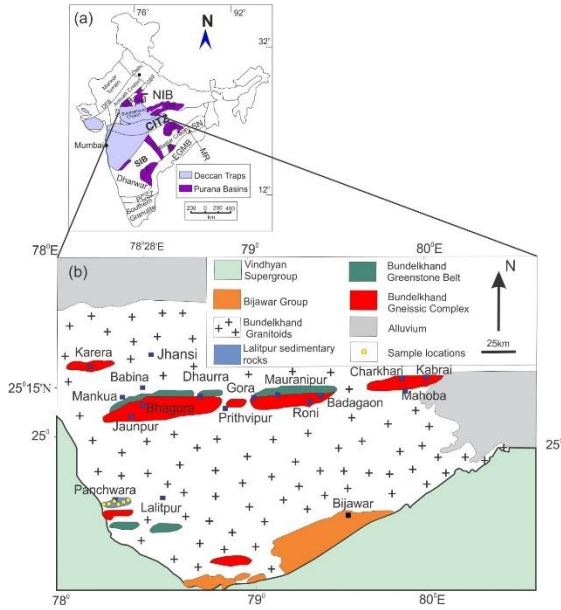


Fig. 1. (a) Map of India showing various major cratons (after Meert and Pandit, 2015). (b) Geological map of Bundelkhand Craton (after Basu, 1986) showing sample locations. ChB: Chhattisgarh Basin; CITZ: Central Indian Tectonic Zone; CuB: Cuddapah Basin; EGMB: Eastern Ghats Mobile Belt; GBF: Great Boundary Fault; IB: Indravati Basin; MB: Marwar Basin; MR: Mahanadi Rift; NIB: North Indian Block; SIB: South Indian Block; PCSZ: Palghat-Cauvery Shear Zone; PG: Pranhita-Godavari Basin; SN: Singhbhum Craton; and VB: Vindhyan Basin

of the Bundelkhand Craton is the tonalite-trondhjemite-granodiorite (TTG) gneisses, which have U-Pb zircon ages of 3.55-2.7 Ga (Mondal et al., 2002; Kaur et al., 2014, 2016). These granite gneisses are overlain by the volcano-sedimentary greenstone complexes. In the Bundelkhand Craton, two greenstone complexes are identified, out of which one is exposed near Girar and Baraitha at the southern edge of the craton known as southern Bundelkhand Greenstone Complex (SBGC) and the other one is exposed at the central part of the craton known as central Bundelkhand Greenstone Complex (CBGC) or Babina-Mauranipur greenstone belt (Malviya et al., 2006). The main litho-units of the SBGC are quartzite, ultramafics and Banded Iron Formation (BIF). The CBGC mainly consists of high-Mg metabasic rocks, ultramafics, BIF, and felsic volcanics. Three types of undeformed granitoids are present in the Bundelkhand Craton: (i) hornblende bearing granitoids (ii) biotite bearing granitoids and (iii) leucogranitoids. The hornblende bearing granitoids and biotite bearing granitoids are similar in age and have emplacement ages of 2516 ± 4 Ma and 2521 ± 7 Ma, respectively obtained by ion microprobe $^{207}\text{Pb}/^{206}\text{Pb}$ from zircon grains (Mondal et al., 2002). The leucogranitoid phase is slightly younger and has a crystallization age of 2492 ± 10 Ma (Mondal et al., 1998, 2002). These leucogranitoids are intrusive in the isolated small clastic sedimentary basin in and around Lalitpur (Fig. 1b, Fig. 2c). Numerous quartz veins trending NE-SW and NNE-

SSW and younger mafic dyke swarm trending NW-SE (~ 2.0 Ga; Pradhan et al., 2012) and ENE-WSW (~ 1.1 Ga; Pradhan et al., 2012) have been observed in the Bundelkhand Craton.

SAMPLING AND ANALYTICAL METHODS

Relatively six medium to coarse-grained sedimentary rocks were collected from small isolated outcrop in and around Panchwara village, Lalitpur of Bundelkhand Craton (Fig. 2). During sampling, weathered and jointed surfaces with quartz veins and other lithological contact surfaces were avoided. Thin sections were prepared and the petrographic study was carried out at the Department of Geology, Aligarh Muslim University (AMU), Aligarh using a petrological microscope (Olympus BX-51). The mineralogical composition of the arkose was determined by modal analysis using the Gazzi-Dickinson method (Gazzi 1966; Dickinson 1970). During the modal analysis, we counted more than 400 points and recalculated it on a matrix-free basis. This recalculated data is plotted in the Qt-F-L diagram given by Dickinson et al., (1983). Chips were made $\sim 2-3$ cm by using steel mortar and then pulverized up to ~ 200 mesh ($\sim 74 \mu\text{m}$) powder by using a tungsten carbide ball mill (FRITSCH pulverisette) in the Department of Geology, AMU. The major oxides have been measured by X-ray fluorescence (XRF; model: Panalytical Axios-mAX) by using pressed pellets at the CSIR-National Geophysical Research Institute (NGRI), Hyderabad with precision of $< 2\%$. Trace elements were determined by High-Resolution Inductively Coupled Plasma Mass Spectrometry (HR-ICP-MS; Model: Nu Instruments Attom, UK), CSIR-NGRI, Hyderabad with precision $< 10\%$.

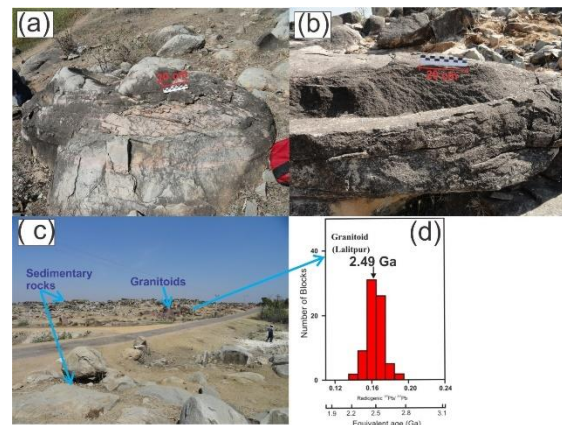


Fig. 2. Field photograph (a) showing a close-up view of the siliciclastic sedimentary rocks (arkose) exposed in the Panchwara village, Lalitpur, (b) showing cross-bedding at Panchwara village, Lalitpur, (c) showing intrusion of 2.49 Ga granitoid into the arkose at the Panchwara village, Lalitpur, (d) histogram of radiogenic $^{207}\text{Pb}/^{206}\text{Pb}$ block data of zircons from the intruding granitoids (Mondal et al., 1998, 2002).

PETROGRAPHY

The petrographic study suggests that these arkoses range in size from fine to medium-grained and mainly consist of polycrystalline quartz, monocrystalline quartz, plagioclase and microcline (Fig. 3). The polycrystalline quartz is a mosaic of quartz grains and suggests that they are derived from the deformed metamorphosed terrain. The monocrystalline quartz shows undulatory extinction. The quartz grains are angular to sub-rounded in nature and show undulatory extinction. The plagioclase grains are fresh, showing lamellar twinning and no alteration is observed. The microcline is identified by the cross-hatched twinning. The petrographic evidences suggest that they are dominant by first-cycle siliciclastic sediments. The petrography of the arkose rocks is examined in detail to delineate the provenance and tectonic setting. Petrography of the clastic sedimentary rock is important to identify the source and tectonic setting of the sediments (Dickinson et al., 1983). The studied samples are dominated by quartz (average 62%). Polycrystalline quartz is the dominant type (average 65%). Feldspar content in the studied rocks averages 37%. Based on the mineralogy a Q-F-R diagram (Folk, 1980) is constructed, on this plot the rocks are classified as arkose type (Fig. 4).

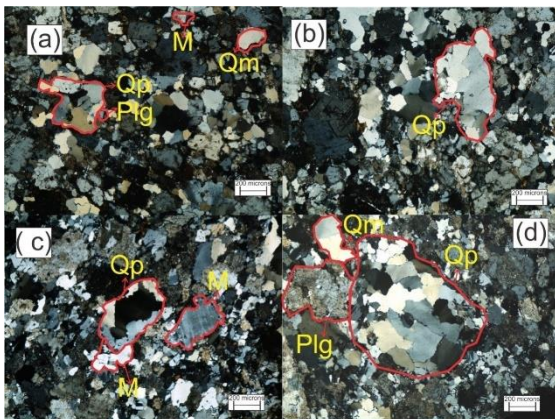


Fig. 3. Photomicrographs showing Lalitpur sedimentary rocks consisting of Qp - polycrystalline quartz; Qm - monocrystalline quartz; Plg - plagioclase; M - microcline

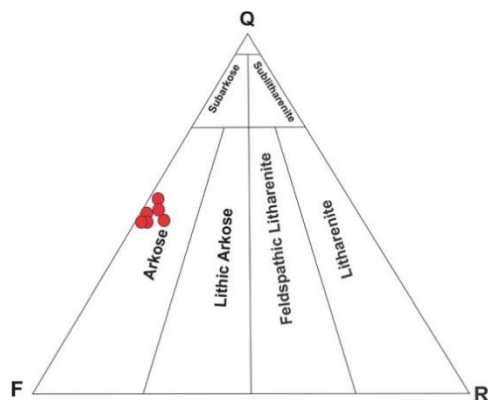


Fig. 4. Q-F-R ternary diagram for the arkoses (after Folk, 1980). Q - total quartz; F - total feldspar; R - total rock fragments including chert.

GEOCHEMICAL DATA

The geochemistry data of the six arkose samples are listed in Table 1. The SiO₂ content varies from 70.5 to 73.9 wt.% with an average of 72.2 wt.% and the Al₂O₃ has high values ranging from 14.0 to 15.6 wt.% (average = 14.8 wt.%). The concentration of Fe₂O₃^T is low ranging from 1.77 to 1.97 wt.% (average = 1.89 wt.%). The concentration of K₂O and Na₂O ranges from 3.01 to 5.99 wt.% (average = 4.05 wt.%) and 3.54 to 4.98 wt.% (average = 4.46 wt.%), respectively. The Na₂O/K₂O ratio values are ranging from 0.59 to 1.63 (average = 1.17). The SiO₂/Al₂O₃ ratio ranges from 4.52 to 5.19 (average = 4.90).

Trace element content is very important to understand the composition of the source rock and the weathering conditions of the clastic rocks, because they are not significantly affected during transportation and post-depositional processes such as diagenesis and metamorphism (Rollinson, 1993; Taylor and McLennan, 1985). The arkoses are characterized by medium to higher concentrations of large ion lithophile elements (LILE; Rb and Ba) with respect to Upper Archean Crust (UAC; Taylor and McLennan, 1985). Relative to UAC, the concentration of Rb varies from 75 to 217 ppm (avg. = 129 ppm; avg. UAC = 50ppm). The Ba concentrations are relatively very high, ranging from 562-694 ppm (average = 640 ppm; avg. UAC = 265ppm). In terms of high field strength elements (HFSE; Zr, Hf), the arkoses are characterized by moderate to high Zr ranging from 93 to 245 ppm (avg. = 148 ppm; avg. UAC = 125ppm) and slightly higher Hf ranging from 3 to 8 ppm (avg. = 4 ppm; avg. UAC = 3ppm). The transition trace elements (TTE) such as Sc, Ni and Cr are lower in the arkoses of this study when compare with UAC. The concentration of Sc, Ni and Cr ranges from 1.6 to 1.9 ppm (avg. = 1.7 ppm; avg. UAC = 14ppm), 3-6 ppm (avg. = 4 ppm; avg. UAC = 105ppm) and 3-5 ppm (avg. = 4 ppm; avg. UAC = 180ppm), respectively, are quite lower (Taylor and McLennan, 1985).

The chondrite normalized (McDonough and Sun, 1995) rare earth element (REE) patterns of

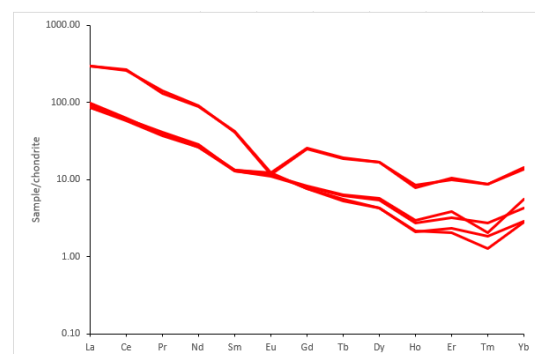


Fig. 5. Chondrite normalized rare earth elements (REE) pattern of the arkoses (after McDonough and Sun, 1995).

Table 1: Major, trace, and rare earth element concentrations for the Lalitpur arkose rocks						
Elements	LS101	LS139	LS102	LS104	LS140	LS137
SiO ₂ (wt. %)	70.97	70.46	73.87	72.67	73.16	72.26
TiO ₂	0.18	0.21	0.28	0.22	0.25	0.19
Al ₂ O ₃	14.89	15.6	14.67	14.01	14.37	14.99
Fe ₂ O ₃ ^T	1.86	1.96	1.85	1.97	1.94	1.77
MnO	0.06	0.03	0.05	0.02	0.04	0.03
MgO	0.62	0.45	0.54	0.51	0.24	0.41
CaO	1.85	1.95	0.97	2.13	0.69	2.3
Na ₂ O	4.98	4.71	3.86	4.78	3.54	4.9
K ₂ O	4.12	4.12	3.07	4.01	5.99	3.01
P ₂ O ₅	0.02	0.07	0.08	0.04	0.04	0.06
Sum	99.6	99.6	99.2	100.4	100.3	99.9
Sc (ppm)	1.89	1.61	1.87	1.56	1.66	1.59
V	6.10	8.69	7.90	8.01	5.25	7.56
Cr	3.90	4.23	4.98	3.21	3.69	4.35
Co	21.98	27.91	25.98	27.98	21.28	30.19
Ni	3.87	5.81	3.71	5.01	2.85	4.83
Cu	1.05	1.04	0.98	1.03	0.96	1.04
Zn	16.07	22.52	17.93	19.01	16.27	11.08
Ga	14.76	14.21	13.98	15.03	15.19	13.33
Rb	98.04	93.90	211.87	76.76	217.69	75.93
Sr	235.96	236.62	64.92	241.98	64.26	242.82
Y	5.92	5.81	22.89	7.88	23.59	7.81
Zr	102.89	103.35	244.78	96.78	245.32	93.30
Nb	4.76	4.47	17.98	5.43	17.04	5.22
Cs	1.31	1.35	1.71	1.73	1.72	1.71
Ba	692.91	693.76	662.19	615.17	562.27	614.85
La	23.12	21.93	70.21	20.09	70.42	20.54
Ce	37.94	37.59	160.23	36.85	162.59	35.78
Pr	3.61	3.55	13.01	3.78	12.22	3.44
Nd	12.09	12.52	41.01	12.94	40.48	12.10
Sm	1.96	1.95	6.01	1.89	6.21	1.91
Eu	0.68	0.70	0.65	0.64	0.69	0.62
Gd	1.52	1.52	5.01	1.62	5.04	1.58
Tb	0.20	0.19	0.67	0.23	0.68	0.22
Dy	1.05	1.06	4.11	1.40	4.13	1.33
Ho	0.12	0.12	0.43	0.16	0.46	0.15
Er	0.33	0.37	1.65	0.62	1.60	0.52
Tm	0.03	0.05	0.22	0.05	0.21	0.07
Yb	0.46	0.47	2.31	0.89	2.17	0.69
Lu	0.06	0.08	0.43	0.13	0.35	0.12
Hf	3.02	3.02	7.69	2.87	7.49	2.78
Ta	1.26	1.26	2.18	2.06	2.17	2.06
Pb	22.87	21.04	36.62	16.99	35.28	16.00
Th	4.75	4.45	26.89	4.89	27.12	4.84
U	1.05	1.05	4.86	3.87	4.84	1.86
Total REE	83.10	82.00	305.52	81.16	306.89	78.96
(La/Sm) _N	7.37	7.02	7.30	6.64	7.08	6.71
(La/Yb) _N	34.44	31.83	20.65	15.33	22.08	20.14
(Gd/Yb) _N	2.70	2.62	1.75	1.47	1.88	1.85
Eu/Eu*	1.20	1.24	0.36	1.12	0.37	1.09

REE – rare earth elements; Eu/Eu* = Eu_N/[(Sm_N)x (Gd_N)]^{1/2}; _N = chondrite-normalized value (after McDonough and Sun, 1995)

the arkoses are characterized by highly fractionated patterns (Fig. 5) with an average $(La/Yb)_N$ ratio of 24.1 (~ 15.3-34.4). The total REE abundance ranges from 79 to 306.9 ppm (avg. = 156.3 ppm). The light rare earth elements (LREE) are moderately enriched in the studied rocks and $(La/Sm)_N$ ratios range from 6.64 to 7.37 with an average value of 7.02. However, heavy rare earth elements (HREE) are relatively less enriched and the $(Gd/Yb)_N$ ratio varies from 1.47 to 2.70 with an average value of 2.05. The Eu anomaly of the is highly variable, ranging from 0.36 to 1.24.

DISCUSSION

PROVENANCE CHARACTERIZATION

The field relationship indicates that the arkoses are intruded by the granitoids, which yielded an age of 2.49 Ga (Mondal et al., 1998, 2002), suggesting that they are older than 2.49 Ga (Fig. 2a). So, these granitoids are not a plausible source for the Lalitpur sedimentary rocks. As documented by Mondal et al. (1998, 2002), based on the geochronology, arkose rocks consist of two age groups of zircon grains viz. one group is clustering around 3.3-3.0 Ga and the other group is clustering around 2.52 Ga. These reported ages are indicating that the possible source of these arkoses is Bundelkhand gneisses (~ 3.55 - 2.7 Ga), volcano-sedimentary greenstone sequence (~2.7-2.5 Ga) and older granitoids phase (~2.52 Ga; Mondal et al., 1998, 2002; Kaur et al., 2014; Singh and Slabunov, 2015).

The concentration of immobile or less mobile elements such as Al, Ti, Zr, Cr, Th, Sc, Co, and La during weathering processes can be used to identify the source rock of the clastic sediments (Cullers, 2002; McLennan and Taylor, 1991). The Al_2O_3 / TiO_2 ratio is used as an indicator of the source rock composition of the clastic sediments. The Al_2O_3/TiO_2 ratio in igneous rocks increases with increasing SiO_2 content (Hayashi et al., 1997; Sugitani, 1996). Generally, mafic rocks have Al_2O_3/TiO_2 ratio of <20, whereas that of felsic rocks range from 10 to 100 (occasionally even higher; Hayashi et al., 1997). The Al_2O_3/TiO_2 ratios of the arkose rocks vary from 52.39 to 82.72 (average = 68.24) indicating their felsic affinity. The higher concentration of trace elements such as Th, Zr and La are the indicators of a felsic source, whereas elements such as Co, Cr and Sc are the indicators of a mafic source. The ratios Th/Sc, La/Sc, Th/Co and Cr/Th are used as a powerful tool to delineate the provenance of the clastic sediments (Cullers, 1994; Wronkiewicz and Condie, 1990). The studied rocks have Th/Sc ratio ranging from 2.51 to 16.33 (average = 7.03; for coarse fraction, mafic source = 0.05-0.22, felsic source = 0.84-20.5; Cullers, 2000), La/Sc ratio varies from 12.2 to 42.4 (average = 21.9; for coarse fraction, mafic source = 0.43-0.86, felsic

source = 2.5-16.3; Cullers, 2000), Th/Co ratio ranges from 0.16 to 1.27 (average = 0.50; for coarse fraction, mafic source = 0.04-1.4, felsic source = 0.67-19.4; Cullers, 2000) and Th/Cr ratio from 1.05 to 7.35 (average = 2.94; for coarse fraction, mafic source = 0.018-0.046, felsic source = 0.13-2.7; Cullers, 2000). These elemental ratios indicate that sediments are derived from the heterogeneous source, dominantly from the felsic source but there must be some contribution of a mafic source. REE patterns of clastic rocks is a robust tool for deciphering the source rocks (Nesbitt, 1979; Taylor et al., 1986). The REE patterns of arkose have high $(La/Yb)_N$ ratios ranging from 15.33 to 34.4 indicating variable fractionation, supporting the heterogeneous source of the clastic sediments. However, these high values suggest that the contribution from the highly fractionated rocks is dominant. The higher values of Eu/Eu^* suggest that the contribution of sediments from the mafic source, whereas lower values of Eu/Eu^* suggest that sediments are derived from the felsic source (Cullers, 2000). The Eu/Eu^* values of the studied rocks range from 0.36 to 1.24, which may indicate the combination of mafic and felsic sources, thus supporting the heterogeneous source of the sediments.

The REE modelling is useful to determine the contribution of the probable sources. We have taken TTG, greenstone belt (basalt + sedimentary rocks) and older granite end members to ascertain their proportions in the arkose rocks. After performing the mixing calculations, it is observed that average sediments are derived from a provenance that consists of 35% TTG, 35% sedimentary rocks of the greenstone belt, 15% basalts of the greenstone belt and 15% of older granitoids (hornblende bearing granitoid and biotite bearing granitoids). These model values are

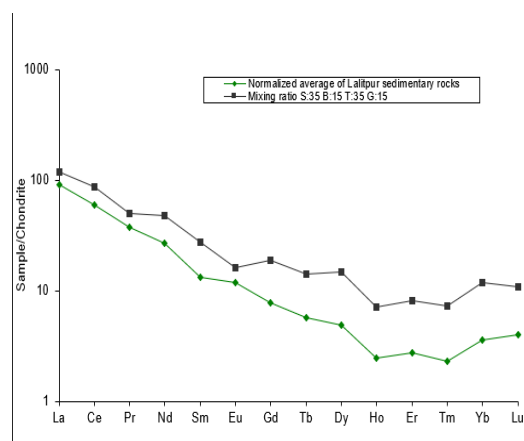


Fig. 6. REE modelling results for estimating the provenance of arkoses after mixing end members in the proportion of 35S:15B:35T:15G (S – sedimentary rocks from the greenstone belt; B – basalts from the greenstone belt; T – TTG gneisses; G – older granitoids).

approximately matched with that of the arkoses (Fig. 6).

PALEOWEATHERING AND PALEOCLIMATE

Several authors attempted to understand paleoweathering and paleoclimate by using different chemical parameters but the most widely used parameter to quantify the paleoweathering intensity is the chemical index of alteration (CIA), which indirectly leads to clues about paleoclimate conditions. Nesbitt and Young (1982) proposed the parameter CIA to evaluate the chemical weathering of the source rock based on the differential solubility of CaO, Na₂O, K₂O and Al₂O₃. CIA can be calculated by taking the molar proportion of the CaO, Na₂O, K₂O and Al₂O₃: $CIA = [Al_2O_3 / (Al_2O_3 + CaO^* + Na_2O + K_2O)] \times 100$, (molecular proportion), where CaO* represents the CaO derived from the silicate minerals only. The CIA values of the studied rocks vary from 47 to 56 (average = 50) indicating that they have not undergone significant weathering.

The arkoses are plotted in the A-CN-K diagram (Al₂O₃-CaO*+Na₂O-K₂O; Nesbitt and Young, 1984) to envisage the paleoweathering trend (Fig. 7). This diagram is helpful to understand the weathering trend because CaO and Na₂O bearing feldspar (plagioclase feldspar) are more easily leached out during chemical weathering than K-feldspar (Middelburg et al., 1988). Thus, the weathered samples give a parallel trend to A-CN

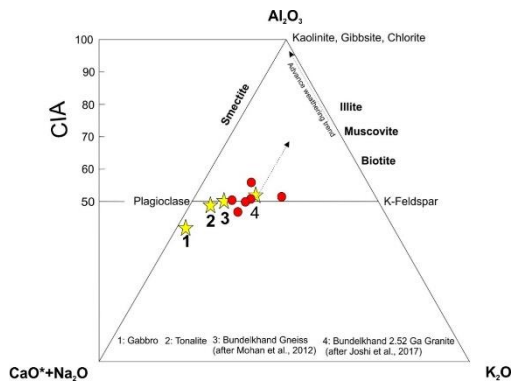


Fig. 7. A-CN-K (in molecular proportion) ternary plot (after Nesbitt and Young, 1984) gives a paleoweathering trend. Average composition is also plotted for comparison from 2.52 Ga Bundelkhand granite (after Joshi et al. 2017) and Bundelkhand gneiss (after Mohan et al. 2012).

axis. The studied samples fall on the tie line which joins the plagioclase feldspar and K-feldspar, indicating moderate weathering effect on the studied rocks. The Th/U ratio is considered a good indicator to assess the paleoweathering condition. U is soluble in water during the weathering and becomes mobile (U⁺⁴ converts into U⁺⁶). Due to the mobility of U, the Th/U ratio is elevated and becomes a good indicator of weathering. If the Th/U is greater than 4, it

stipulates that the rocks have gone through the weathering (McLennan and Taylor, 1991; McLennan et al., 1990). The average value of Th/U of the arkose is 3.96, further supporting the insignificant chemical weathering effect on the studied rocks. This may be due to the sedimentation occurring for a very short time period, as discussed earlier. So, mechanical weathering is dominant rather than the chemical weathering.

TECTONIC SETTING

The tectonic setting of the sedimentary basin can be identified by the geochemistry of the clastic rocks (Verma and Armstrong-Altrin, 2013, 2016). Based on Folk’s classification (1980) of sandstone, the studied sedimentary rocks are characterized as arkose (Fig.4). Pettijohn et al. (1987) suggested that arkose is formed at the high relief regions. This condition is generally found at continental rifts. Based on the major oxides chemistry (K₂O/Na₂O vs SiO₂), Roser and Korsch (1986) proposed a tectonic discriminant diagram to depict the tectonic environment from which sediments were derived. The Lalitpur arkoses are plotted in the passive margin field (Fig. 8). Bhatia and Crook (1986) give a tectonic discriminant diagram based on the trace elements Th, Sc and Zr. The trace elements are more trustworthy than the major oxides during post-depositional processes. The arkoses are plotted in the passive margin field in the Th-Sc-Zr/10 ternary diagram, endorsing the rift-related origin of the basin (Fig. 9). The passive margins were characterized by the separation of continents and rifting (Dickinson, 1981). Based on the mineralogy of the sandstone, Dickinson et al. (1983) proposed a Q_r-F-L diagram to discriminate the tectonic setting of the source region. The arkoses plot in the basement uplift field (Fig. 10), indicating that the sediments were derived from the greater relief, further supporting the rifting origin of the basin. Based on the preceding discussion, a plausible model has been proposed for the arkose rocks, which is shown in a schematic cartoon in Fig. 11.

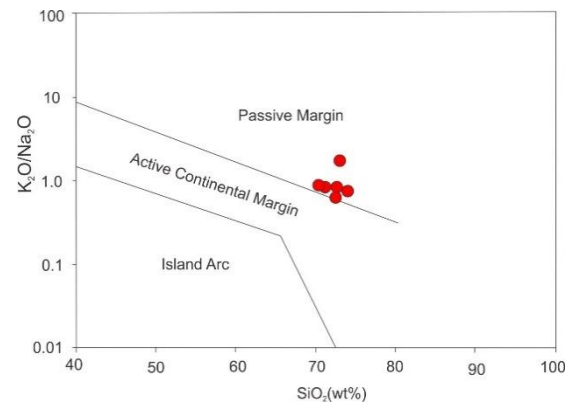


Fig. 8. SiO₂ vs. K₂O/Na₂O binary tectonic discriminant diagram for the arkoses (after Roser and Korsch, 1986).

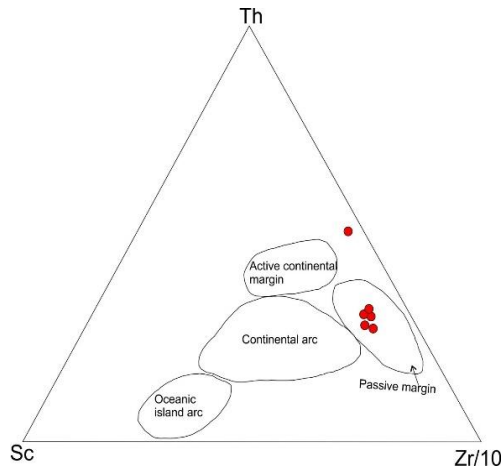


Fig. 9. Th-Sc-Zr/10 tectonic discrimination diagram for the arkoses (after Bhatia and Crook, 1986)

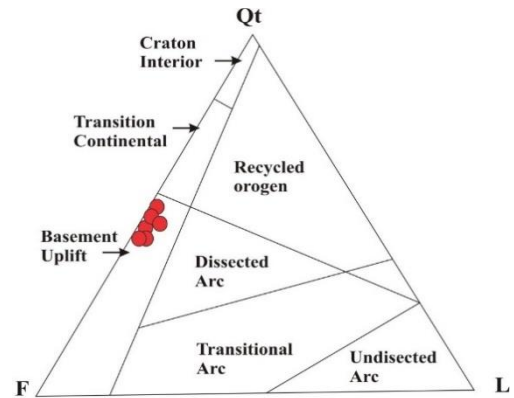


Fig. 10. Qt-F-L ternary diagram for the arkoses, fields are after Dickinson et al. (1983). Qt – total quartz (monocrystalline quartz + polycrystalline quartz); F – total feldspar; L – total lithic fragments

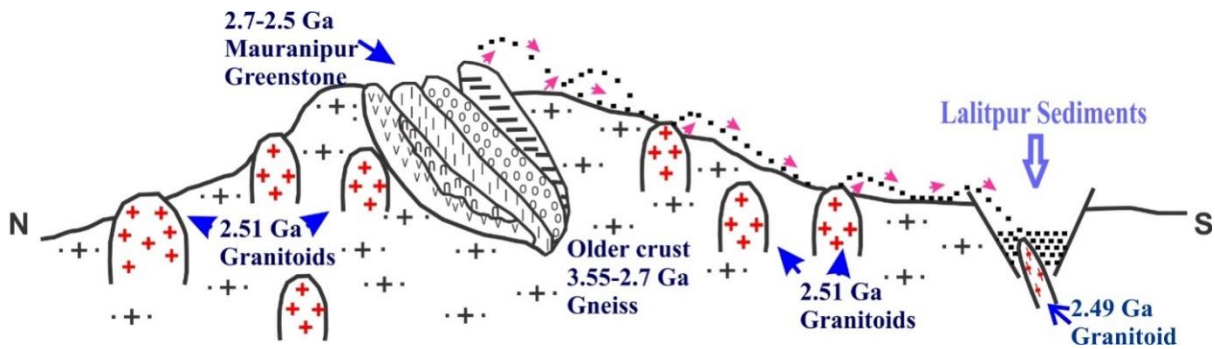


Fig. 11 Schematic diagram showing the contribution of the sediments from different sources (TTG, greenstone belt and granitoids).

CONCLUSION

1. The rocks are classified as arkose type.
2. These arkoses are derived from the TTG gneisses, volcano-sedimentary greenstone sequences and older undeformed granitoids.
3. Based on the REE modelling, the contribution of different sources is depicted as, i.e. 50% greenstone belt (15% basalt + 35% sedimentary rocks), 35% TTG and 15% older undeformed granitoids.
4. The arkoses show insignificant effect of chemical weathering.
5. The compiled data reveal that the Lalitpur basin was developed due to the continental rifting between 2.52 Ga and 2.49 Ga.

ACKNOWLEDGEMENTS

We are thankful to the Chairperson, Department of Geology, AMU, Aligarh and the Director, CSIR-NGRI, Hyderabad for providing facilities to carry out this work.

FUNDING

This work did not receive any external funding.

CONFLICT OF INTEREST

The authors declare no conflict of interest.

REFERENCES

- Acharyya, S.K. (2003). The nature of the mesoproterozoic Central Indian Tectonic Zone with exhumed and reworked older granites. *Gondwana Research*, v. 6, pp. 197-214.
- Basu, A.K. (1986). Geology of parts of Bundelkhand granite massif, central India. *Records of the Geological Survey, India*, v. 11/2, pp. 61-124.
- Bhatia, M.R. and Crook, K.A.W. (1986). Trace element characteristics of greywackes and tectonic discrimination of sedimentary basins. *Contribution to Mineralogy and Petrology*, v. 92, pp. 181-193.
- Cullers, R.L. (2000). The geochemistry of shales, siltstones and sandstones of Pennsylvanian-Permian age, Colorado, USA: Implications for

- provenance and metamorphic studies. *Lithos*, v. 51, pp. 181-203.
- Cullers, R.L. (1994). The controls on the major and trace element variation of shales, siltstones, and sandstones of Pennsylvanian-Permian age from uplifted continental blocks in Colorado to platform sediment in Kansas, USA. *Geochimica et Cosmochimica Acta*, v. 58, pp. 4955-4972.
- Cullers, R.L. (2002). Implications of elemental concentrations for provenance, redox conditions, and metamorphic studies of shales and limestones near Pueblo, CO, USA. *Chemical Geology*, v. 191, pp. 305-327.
- Dickinson, W.R. (1970). Interpreting detrital modes of graywacke and arkose: *Journal of Sedimentary Petrology*, v. 40, pp. 695-707.
- Dickinson, W.R. (1981). Plate tectonic evolution of the southern Cordillera. *Arizona Geological Society Digest*, v. 14, pp. 113-135.
- Dickinson, W.R., Beard, L.S., Brakenridge, G.R., Erjavec, J.L., Ferguson, R.C., Inman, K.F., Knepp, R.A., Lindberg, F.A. and Ryberg, P.T. (1983). Provenance of North Phanerozoic sandstones in relation to tectonic. *Geological Society of America Bulletin*, v. 94, pp. 222-235.
- Folk, R.L. (1980). *Petrology of sedimentary rocks*. Hemphill publishing company.
- Gazzi, P. (1966). Le arenarie del flysch sopracretaceo dell'Appennino modense: Correlazioni con il flysch di Monghidoro: *Mineralogica et Petrographica Acta*, v. 12, p. 69-97.
- Hayashi, K.I., Fujisawa, H., Holland, H.D. and Ohmoto, H. (1997). Geochemistry of ~1.9 Ga sedimentary rocks from northern Labrador Canada. *Geochimica et Cosmochimica Acta*, v. 61(19), pp. 4115-4137.
- Joshi, K.B., Bhattacharjee, J., Rai, G., Halla, J., Ahmad, T., Kurhila, M., Heilimo, E. and Choudhary, A.K. (2017). The diversification of granitoids and plate tectonic implications at the Archean-Proterozoic boundary in the Bundelkhand Craton, Central India. *Geological Society of London Special Publications*, v. 449, pp. 123-157.
- Kaur, P., Zeh, A. and Chaudhri, N. (2014). Characterization and U-Pb-Hf record of the 3.55 Ga felsic crust from the Bundelkhand Craton, northern India. *Precambrian Research*, v. 255, pp. 236-244.
- Kaur, P., Zeh, A., Chaudhri, N. and Elias, N. (2016). Unravelling the record of Archean crustal evolution of the Bundelkhand Craton, northern India using U-Pb zircon-monazite ages, Lu-Hf isotope systematics, and whole-rock geochemistry of granitoids. *Precambrian Research*, v. 281, pp. 384-413.
- Malviya, V.P., Arima, M., Pati, J.K. and Kaneko, Y. (2006). Petrology and geochemistry of metamorphosed basaltic pillow lava and basaltic komatiite in the Mauranipur area: Subduction related volcanism in the Archean Bundelkhand craton, central India. *Journal of Mineralogy and Petrology*, v. 101, pp. 199-217.
- McDonough, W.F. and Sun, S.S. (1995). The composition of the Earth. *Chemical Geology*, v. 120, pp. 223-253.
- McLennan, S.M., Taylor, S.R., McCulloch, M.T. and Maynard, J.B. (1990). Geochemical and Nd-Sr isotopic composition of deep sea turbidites: Crustal evolution and plate tectonic associations. *Geochimica et Cosmochimica Acta*, v. 54, pp. 2015-2050.
- McLennan, S.M. and Taylor, S.R. (1991). Sedimentary rocks and crustal evolution: tectonic setting and secular trends. *Journal of Geology*, v. 99, pp. 1-21.
- Meert, J.G. and Pandit, M.K. (2015). The Archean and Proterozoic history of Peninsular India: Tectonic framework for Precambrian sedimentary basins in India. *Geological Society of London, Memoirs*, v. 43, pp. 29-54.
- Middelburg, J., Vanderweijden, C. and Woittiez, J. (1988). Chemical processes affecting the mobility of major, minor and trace elements during weathering of granitic rocks. *Chemical Geology*, v. 68, pp. 253-273.
- Mohan, M.R., Singh, S.P., Santosh, M., Siddiqui, M.A. and Balam, V. (2012). TTG suite from the Bundelkhand Craton, Central India: geochemistry, petrogenesis and implications for Archean crustal evolution. *Journal of Asian Earth Sciences*, v. 58, pp. 38-50.
- Mondal, M.E.A., Sharma, K.K., Rahman, A. and Goswami, J.N. (1998). Ion microprobe $^{207}\text{Pb}/^{206}\text{Pb}$ zircon ages for the gneiss-granitoid rocks from Bundelkhand massif: evidence for the Archean components. *Current Science*, v. 74, pp. 70-75.
- Mondal, M.E.A., Goswami, J.N., Deomurari, M.P. and Sharma, K.K. (2002). Ion microprobe $^{207}\text{Pb}/^{206}\text{Pb}$ ages of zircons from the Bundelkhand massif, northern India: implications for crustal evolution of the Bundelkhand-Aravalli protocontinent. *Precambrian Research*, v. 117, pp. 85-100.
- Nesbitt, H.W. (1979). Mobility and fractionation of rare earth elements during weathering of a granodiorite. *Nature*, v. 279, pp. 206-210.
- Nesbitt, H.W. and Young, G.M. (1982). Early Proterozoic climates and plate motions inferred from major element chemistry of lutites. *Nature*, v. 299, pp. 715-717.
- Nesbitt, H.W. and Young, G.M. (1984). Prediction of some weathering trends of plutonic and volcanic rocks based on thermodynamic and kinetic considerations. *Geochimica et Cosmochimica Acta*, v. 48, pp. 1523-1534.
- Pettijohn, F.J., Potter, P.E. and Siever, R. (1987). *Sand and Sandstone*, 2nd ed. Springer, New York, pp. 553.
- Pradhan, V.R., Meert, J.G., Pandit, M., Kamenov, G. and Mondal, M.E.A. (2012). Paleomagnetic and geochronological studies of the mafic dyke swarms of Bundelkhand craton, central India:

- implications for the tectonic evolution and paleogeographic reconstructions. *Precambrian Research*, v. 198-199, pp. 51-76.
- Radhakrishna, B.P. and Naqvi, S.M. (1986). Precambrian continental crust of India and its evolution. *Journal of Geology*, v. 94, pp. 145-166.
- Rollinson, H.R. (1993). Using geochemical data: Evaluation, Presentation, Interpretation. Longman Singapore Publishers (Pte) Ltd. Singapore, pp 352.
- Roser, B.P. and Korsch, R.J. (1986). Determination of tectonic setting of sandstone-mudstone suites using SiO₂ content and K₂O/Na₂O ratio. *The Journal of Geology*, v. 94(5), pp. 635-650.
- Singh, V.K., and Slabunov, A. (2015). The Central Bundelkhand Archean greenstone complex, Bundelkhand craton, central India: geology, composition, and geochronology of supracrustal rocks. *International Geology Review*, v. 57, pp. 1349-1364.
- Sugitani, K. (1996). Anomalously low Al₂O₃/TiO₂ values for Archean cherts from the Pilbara Block, Western Australia-possible evidence for extensive chemical weathering on the early earth. *Precambrian Research*, v. 80, pp. 49-76.
- Taylor, S.R. and McLennan, S.M. (1985). The continental crust. Its Composition and Evolution. Blackwell, Oxford, UK. ISBN 0632011483.
- Taylor, S.R., Rudnick, R.L., McLennan, S.M. and Eriksson, K.A. (1986). Rare earth element patterns in Archean high-grade meta sediments and their tectonic significance. *Geochimica et Cosmochimica Acta*, v. 50, pp. 2267-2279.
- Verma, S.P. and Armstrong-Altrin, J.S. (2016). Geochemical discrimination of siliciclastic sediments from active and passive margin settings. *Sedimentary Geology*, v. 332, pp. 1-12.
- Verma, S.P. and Armstrong-Altrin, J.S. (2013). New multi-dimensional diagrams for tectonic discrimination of siliciclastic sediments and their application to Precambrian basins. *Chemical Geology*, v. 355, pp. 117-133.
- Wronkiewicz, D.J. and Condie, K.C. (1990). Geochemistry and mineralogy of sediments from the Ventersdorp and Transvaal Supergroups, South Africa: Cratonic evolution during the early Proterozoic. *Geochimica et Cosmochimica Acta*, 5v. 4, pp. 343-354.

Landslide susceptibility mapping using frequency ratio method along the Bhaderwah-Bani Road, Jammu and Kashmir, India

Yudhbir Singh¹, Mehreen Liaqat², Sumit Johar^{1*}, Shifali Chib¹, and Gaurav Singh Parihar¹

¹Department of Geology, University of Jammu, Jammu-180006, India

²Department of Geography, Jamia Millia Islamia, New Delhi-110025, India

*Email Address: sumitjohar1996@gmail.com

ABSTRACT

This study outlines a method for landslide susceptibility mapping utilizing remote sensing and geographic information systems (GIS). Since the terrain from Bhaderwah to Bani in J&K is prone to landslide threats, the study has been conducted there. The purpose of the current study is to determine and identify the significant terrain elements causing landslides. Nine contributing factors on landslides were taken into account throughout the analysis. Thematic data layers are created in the GIS domain based on local events. Topographic maps, satellite images, on-site observations and publicly available published maps are used to gather the landscape data. To determine the standardized scores of criteria expressing their factor of importance for a given decision problem in terms of thematic parameters, categories, and their normalized weights the Frequency ratio (FR) method is used to digitize these maps along with tabular data and to create a GIS database. A particular landslide susceptibility zonation (LSZ) map was created on a GIS platform by statistically combining weightages from several thematic maps. Using FR, the LSZ map was divided into five separate susceptibility zones. According to the study's finding, 8% of the area is in a very high susceptibility zone, with the remaining 12%, 15%, 23%, and 42% falling into high, moderate, low, and very low susceptibility zones, respectively. The outcomes of the current study might aid policy and decision makers in moving forward with regional development initiatives including land use planning.

Keywords: Landslide, Hazard zonation, NH-244, frequency ratio, Remote Sensing, GIS

INTRODUCTION

Landslide is one of the most common natural hazards that has caused massive damage to infrastructure and property as well as loss of lives around the world. India is prone to variety of natural and human induced disasters such as landslides, floods, earthquakes, fires, windstorms hailstorms. Among various natural hazards, landslide is very common in hilly region of India. Landslide is the most harmful geological hazard in India causing significant number of fatalities, economic losses and is one of the major restraints in development (Petley et al., 2008). Landslide appraisal and hazard zonation are necessary for systematic landslide mitigation and management. Numerous methods for landslide appraisal and zonation have been developed during the last few decades. The correct assessment of landslide hazard of an area involves both intrinsic and extrinsic factors (Siddle et al., 1991; Dai et al., 2001). Since most studies for the assessment of hazard of an area involves only intrinsic factors, because it is difficult to obtain the data on extrinsic factors. Therefore, assessment of an area in the context of landslide hazard where extrinsic factors are disregarded is termed as landslide susceptibility mapping (Dai et al., 2001; Guzzetti et al., 2005). The landslide study has taken a great stride in modern times due to advancement

and development of spatial information technology. The easy availability of high-resolution satellite imageries and application of geographic information system (GIS) has helped in managing and manipulating of the spatial data with suitable models for mapping landslide susceptibility for large areas (Carrara et al., 1991; Van Westen et al., 2006).

A number of schemes are in vogue in which GIS technique is used for landslide susceptibility zonation. The qualitative method normally incorporates landslide susceptibility based on professional acquaintance and is useful for regional assessment (Aleotti and Chowdhury, 1999). The quantitative analysis of landslide includes statistical methods and can be grouped into multivariate and bivariate methods. In the multivariate method, the relative contribution of each factor layer to the total landslide susceptibility map is considered, while in the bivariate method the contribution of each factor is compared with landslide inventory to find out the relative importance. The overall methodology used for landslide susceptibility mapping is generally based on the principle that future landslide will occur in areas of similar conditions where past landslides have occurred (Varnes, 1984; Guzzetti et al., 2003). In this study, bivariate statistical method was used to prepare the landslide susceptibility map. Frequency ratio is one of the bivariate statistical

approaches of landslide susceptibility assessment based on the relationship between instability factors and the past and present distribution of landslides (Lee, 2005). The frequency ratio approach is a simple probabilistic form based on the observed relationships between the causative factors and distribution of landslides. The ratio value greater than unity represents a strong correlation for landslide and ratio value less than unity represent the lesser chance of landslide from an influencing factor (Lee and Pradhan, 2006). This method has been successfully used by various workers for landslide susceptibility mapping (Lee and Talib, 2005; Lee and Pradhan, 2006, 2007). In the present study frequency ratio model in GIS environment was used in which six intrinsic causative factors i.e., aspect, relief, curvature, slope, hill shade, and geology were taken into account.

In Jammu region most of the landslide's studies took place along national highways, because road network is considered to be the index of the development of the country and keeping in view the importance of National Highways (NH-44) mostly studies are concentrated along the highways (Andrabi, 2002; Bhat et al., 2002; Singh, 2006; Singh and Bhat, 2010; 2011; Singh et al., 2012, 2014). In the history of Jammu region, one of the deadliest landslide events was observed in Sadal Village in Panchari area of Udhampur district during the year 2014. This landslide devastated the entire Saddal habitation in the early morning of September 6, 2014 in which all the residents except those who were not in the village died. This landslide destroyed 45 houses, killing 41 people and more than 500 domestic animals perished. Besides this, number of landslides took place in and around Jammu region. These events often initiate especially during the onset of rainy season. A detailed knowledge about the expected frequency, character, pattern and magnitude of slope failures in an area can lead to successful mitigation of landslide hazards. For conducting quicker and safer mitigation programs over a specific area identification of landslide-prone regions is essential.

STUDY AREA

The present study is confined between Bhaderwah (latitudes- N32°60' and longitudes-E75°40') and Bani (latitudes-N 32°40' and longitudes- E 75°60') sector of the National highway-244 (NH-244) which falls in the Lesser Himalayan tectonic zone of the northwestern Himalaya (Figs. 1 and 2). The prominent structural unit falling in the study area is the Panjal Thrust (Fuchs, 1975; Gansser, 1981; Thakur, 1981). The oldest rocks exposed along the highway in this area are represented by the Bhaderwah Group of Precambrian age composed of grey phyllitic slates, calcareous slates and talc bearing slates, overlain by the Dalhousie Formation (Salkhala Formation)

comprising of augen gneisses and banded gneisses (McMohan, 1885). The Dalhousie Formation is overlain by the Sincha Formation which consists of bluish-grey sandy dolomite and pinkish limestone. The youngest rocks exposed in the study area are intrusive granites (Kaplas Granite). Seismically the area has been classified as seismic zone-IV and V. The area, in general, enjoys temperate to sub-tropical type of climate.

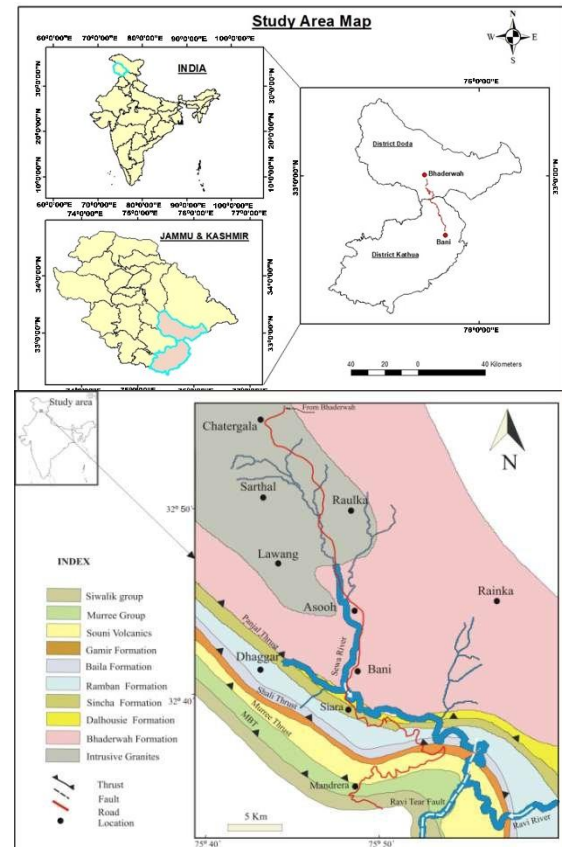


Fig. 2 Geological map of the study area (modified after Choudhary, 2006)

MATERIALS AND METHODS

The study is focused on different landslide causative factors, determination of their weights, preparation and analysis of the landslide susceptibility model while using Frequency ratio model and GIS-based statistical methods. Nine landslide conditioning characteristics, which are slope gradient, slope aspect, slope curvature, hill shade, relief, lithology, distance to road, distance to streams, and land use land cover (LULC) were taken into consideration for the study (Fig. 3). In the beginning, polygons are made to depict the sites of landslides in order to create a landslide inventory. Then, for each element taken into account in the research, thematic layers were produced, which were then resampled into raster format with uniform pixel size, categorized based on particular themes,

and classed appropriately. The landslide inventory is used to determine the importance of each element. The unique sequence of various spatial and statistical datasets was used to develop a susceptibility map which characterizes the whole study area into several susceptible classes such as: very high, high, moderate, low and very low (Soeters and van Westen, 1996; Brabb and Best, 1999).

LANDSLIDE SUSCEPTIBILITY ASSESSMENT USING FREQUENCY RATIO METHOD

From the correlation between places where landslides had not happened and the landslide-related variables, it was possible to infer the link between the landslide occurrence area and the landslide-related factors. One of the probability models, the frequency ratio, was utilized to quantify this distinction. The frequency ratio is the ratio of the likelihood that an event will occur to the likelihood that it won't happen given certain features (Bonham-Carter, 1994). The combination of multiple causal factors depending on their weight, which is estimated by various statistical methodologies, is the essential part of the assessment of landslide susceptibility. Due to its mathematical simplicity and relatively short evaluation time, frequency ratio (FR) was chosen for this study as the primary analysis for a preliminary probabilistic evaluation. When this ratio exceeds 1, there is a strong correlation between a landslide and the range or kind of the component. If the ratio is less than 1, there is a slight relationship between the range or type of the component and the likelihood of a landslide (Girma et al., 2015). The formula for calculating frequency ratios is as follows:

$$FR = \frac{Nlp / N}{Nlpi / Ni}$$

where,

Nlp = the number of pixels in each landslide conditioning factor class;

N = the total number of pixels in the research region;

Nl = total number of landslide pixels in the study region and

$Nlpi$ = number of landslide pixels in each landslide conditioning factor class.

LANDSLIDE INVENTORY

The landslide inventory provides information regarding the types of landslides, their failure processes, their locations, their triggers, as well as their frequency of occurrence, density, and damage (Fig. 4) (Van Westen et al., 2008). A few places were verified on the ground. For the purpose

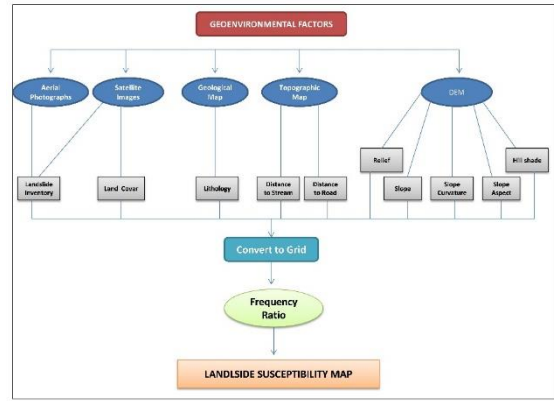


Fig. 3 Flowchart of the methodology used in the study

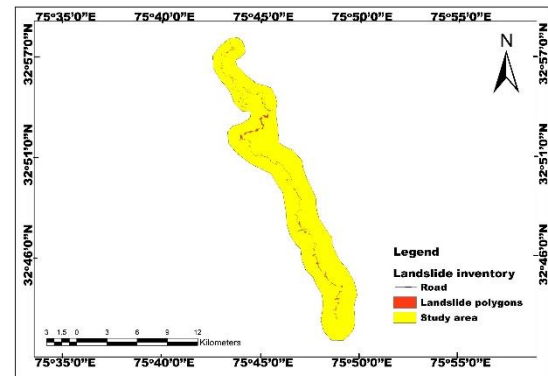


Fig. 4 Landslide inventory of the study area (Courtesy: Google earth pro).

of creating a landslide inventory map, 134 landslide locations were found and mapped overall in this study. Numerous studies have demonstrated that steeper slopes are more likely to have landslides (Poudel et al., 2016). Due to the varied wetness of the slope side, it is also one of the most important elements influencing the occurrences of landslides (Pham et al., 2018). Landslides may be influenced by aspect-related elements such as exposure to sunshine, drying winds, rainfall (degree of saturation), and discontinuities (Dai et al., 2001; Cevik and Topal, 2003). The acceleration or



Fig. 5 Field photographs showing the various types of slope failures in the study area.

slowdown of flow across a surface is influenced by curvature (Buckley, 2010). Some of the field photographs of the study area are shown in Figure 5. **RESULTS AND DISCUSSION**

Utilizing the frequency ratio approach, the frequency ratio values for the various conditioning factors is given in Table 1. The examination of the current study's findings provides crucial new information about how different elements affect landslides vulnerability. In terms of slope sub-categories, the range of 45°-55° shows the highest frequency ratio value (1.146), indicating the likelihood of landslides on these steep slopes. The slope sub-categories 20°-30°, 30°-45°, 55°-65°, also shows a frequency ratio greater than 1 (1.096, 1.105 and 1.086), which indicates a considerable probability of landslide happening in the areas with these slope sub categories. Furthermore, the frequency ratios for the slope sub-categories 0°-10°, 10°-20° and >65° are all less than 1 (0.531, 0.792 and 0.974), indicating minimal likelihood of landslides (Fig. 6a). The impact of aspect is higher in the northeast, northwest, north and east directions with FR values 1.269, 1.261, 1.196 and 1.095 (Fig. 6b). Areas with concave curvature are more susceptible to landslides with FR value of 1.306 (Fig. 6c). According to the hill shade results, the hill shade ranges (205-254, 117-161 and 0-69) have a stronger effect on the occurrence of landslides with FR of 1.102, 1.053 and 1.035 than the other hill shade ranges (Fig. 6d). According to the study's relief component, regions with high relief (2971-3415 m) have a bigger impact on the likelihood of landslides with a FR of 2.994. Areas with low relief, on the other hand, are less susceptible to landslides (Fig. 6e). Another affecting factor for landslides is the geological set-up of the area. The whole area is represented by three different rock formations. The effect of landslide is higher for the Salkhala Formation which has FR value of 1.15, followed by the Vaikrita Formation with FR value of 1.022 and lowest in the Kaplas Granite with FR value of 0.893 (Fig. 6f). Similarly, the study area's distance to stream map indicates that landslides are more common in the locations that are almost nearest to the river (100-200 m) with a FR of 5.333 (Fig. 6g). Landslides are more likely to occur in places covered by snow with a FR of 1.594, based on calculations from the land use and land cover map (Fig. 6h). According to the study area's distance to

road map, the closest distance from a road (0–150 m) with a frequency ratio value of 17.026 has the biggest influence on the likelihood of landslides (Fig. 6i). Anthropogenic activities and haphazard toe cutting are two possible causes of this, which result in further instability.

Using the data of Table 1, the values for each factor were used to prepare the Landslide susceptibility index (LSI) map using raster calculator. LSI is classified into specific classes

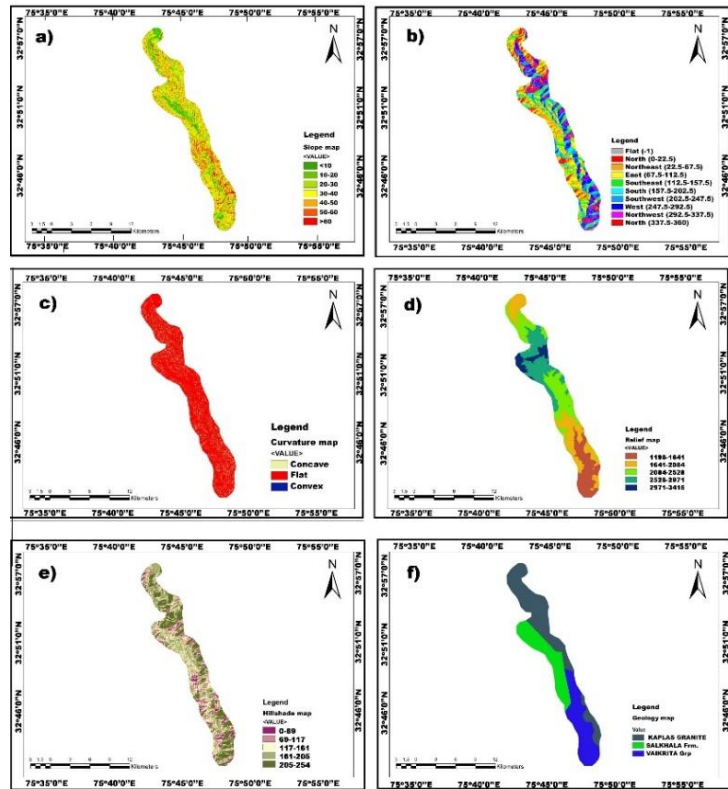


Fig. 6(a-f) Conditioning factors a) Slope map and b) Aspect map; c) Curvature map; d) Hill shade map; e) Relief map, and f) Lithology map

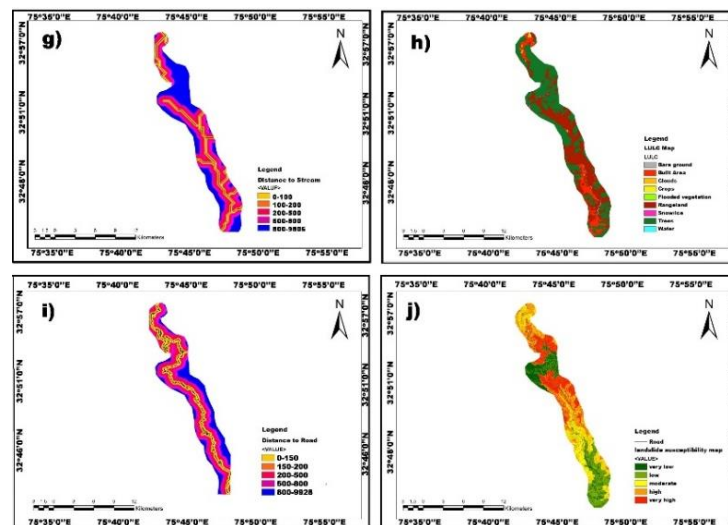


Fig. 6(g-j) Conditioning factors g) Distance to streams; h) LULC; i) Distance to road; and j) landslide susceptibility zonation map.

road map, the closest distance from a road (0–150 m) with a frequency ratio value of 17.026 has the biggest influence on the likelihood of landslides (Fig. 6i). Anthropogenic activities and haphazard toe cutting are two possible causes of this, which result in further instability.

defining susceptibility level to prepare the Landslide Susceptibility Map (Fig. 6j).

$$LSM_{FR} = \text{Total Sum of (weight* factor map)}$$

The LSM illustrates the landslide susceptible zones which are divided into five classes i.e., very low, low, moderate, high, and very high. The area covered by each class of landslide susceptibility map using FR method is shown as Table 2. It demonstrates that among total land sliding area of 103.41 sq. km, the landslide probable area under classification very high and high are 8.1 sq. km and 11.52 sq. km respectively. The comparison can be interpreted by change in area in different classes of landslide susceptible zone. The graph showing the ranking

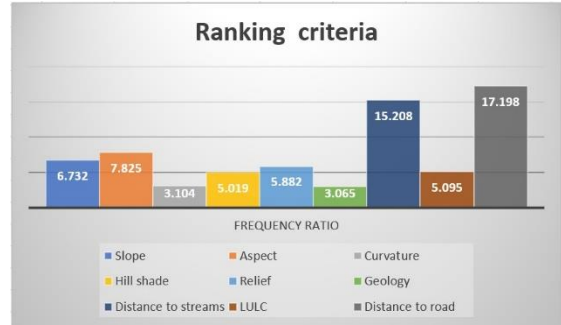


Fig. 7 Graph showing the ranking criteria and weightage to each factor

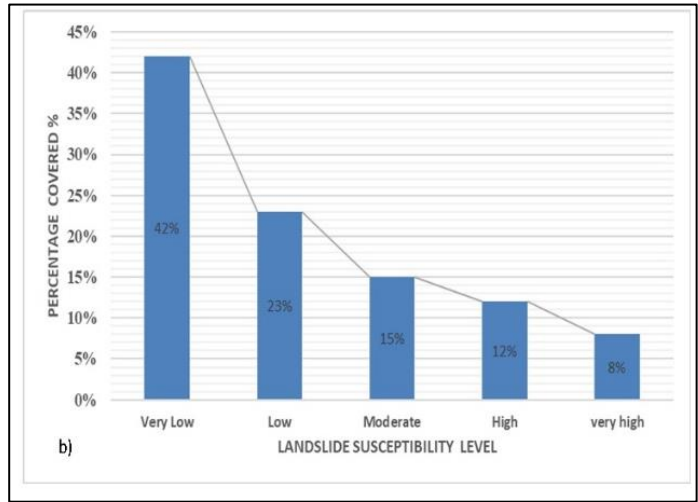
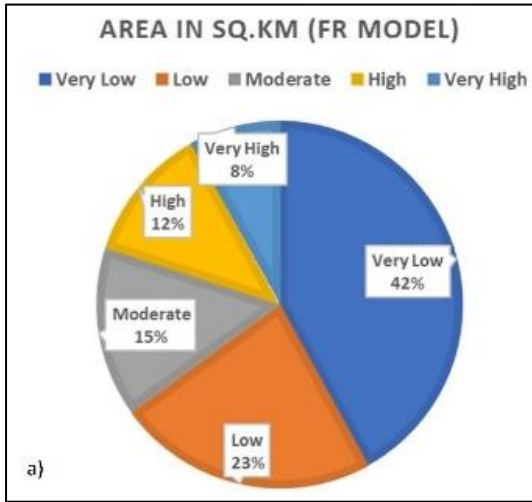


Fig. 8 a) Percentage distribution of landslide susceptibility zonation using FR and b) Relationship between percentage of areas of landslide and susceptibility level.

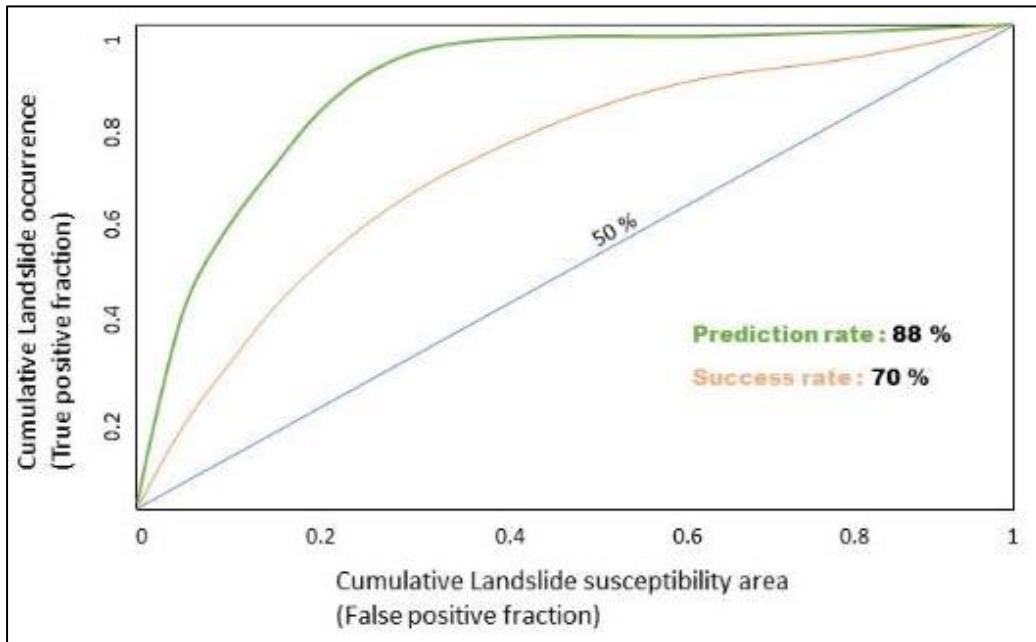


Fig. 9 Analysis of ROC curve for the landslide susceptibility map.

criteria and weightage to each factor is shown in Figure 7, which indicates that the distance to road and distance to streams are the dominant factors

affecting the stability of slope. The pie chart (Fig. 8a) describes the area of different classes in percentage in which the landslide susceptible zone

for very high and high classes are 8 and 12% respectively. Most of the area falls in very low susceptible zone. The relationship between landslide occurrence and each susceptibility classes as assessed by Frequency ratio method has been

plotted and presented in Figure 8b. The receiver operative characteristic (ROC) curve for the validation of the results is shown in Figure 9.

Table 1. The Frequency Ratio (FR) values obtained for slope, Aspect, Curvature, Relief, Hill shade and Geology parameters

S. No.	Parameters	Classes	Class Pixels	% Class Pixels	Landslide Pixels	% Landslide Pixels	FR
1.	Slope	0 -10°	10665	10.644	65	5.657	0.531
		10°- 20°	13653	13.626	124	10.792	0.792
		20°- 30°	18931	18.893	238	20.714	1.096
		30°- 40°	22010	21.966	279	24.282	1.105
		40°- 50°	19099	19.061	251	21.845	1.146
		50°- 60°	11635	11.612	145	12.620	1.086
		>60°	4206	4.198	47	4.091	0.974
Total			100199		1149		6.732
2.	Aspect	North	12605	12.580	173	15.057	1.196
		Northeast	18336	18.300	267	23.238	1.269
		East	14650	14.621	184	16.014	1.095
		Southeast	10965	10.943	93	8.094	0.739
		South	10230	10.210	72	6.266	0.613
		Southwest	12263	12.239	92	8.007	0.654
		West	12371	12.346	141	12.272	0.993
		Northwest	8779	8.762	127	11.053	1.261
Total			100199		1149		7.825
3.	Curvature	Concave	17874	17.451	262	22.802	1.306
		Flat	57552	56.192	645	56.136	0.999
		Convex	26995	26.357	242	21.062	0.799
Total			102421		1149		3.104
4.	Hill shade	0-69	10352	10.419	124	10.792	1.035
		69-117	17562	17.675	197	17.145	0.970
		117-161	23139	23.289	282	24.543	1.053
		161-205	24688	24.848	245	21.323	0.858
		205-254	23617	23.770	301	26.197	1.102
Total			99358		1149		5.019
5.	Relief (m)	1198-1641	18548	18.110	289	25.152	1.388
		1641-2084	24012	23.444	161	14.012	0.597
		2084-2528	22726	22.189	126	10.966	0.494
		2528-2971	23234	22.685	106	9.225	0.406
		2971-3415	13901	13.572	467	40.644	2.994
Total			102421		1149		5.882
6.	Geology	Kaplas Granite	44821	43.760	449	39.077	0.893
		Salkhala fm.	27363	26.715	353	30.722	1.15
		Vaikrita Grp.	30241	29.525	347	30.200	1.022
Total			102425		1149		3.065
7.	Distance to Streams (m)	0-100	10876	2.91	142	12.53	4.306
		100-200	15401	4.12	249	21.98	5.332
		200-500	23722	6.35	258	22.77	3.587
		500-800	25467	6.81	122	10.77	1.580
		800-9806	29827	79.81	362	31.95	0.400
Total			373744		1133		15.208
8.	LULC	Bare Ground	35875	1.00	13	1.13	1.136
		Built Area	32708	9.08	155	13.49	1.486
		Crops	52486	0.00	4	0.35	0
		Snow/Ice	60201	16.70	306	26.63	1.594
		Trees	1465	0.00	79	6.88	0
		Water	21142	58.66	592	51.52	0.878
Total			202412		1149		5.095
9.	Distance to Road (m)	0-150	20420	5.831	1116	99.288	17.026
		150-200	14468	4.131	8	0.711	0.172
		200-500	17096	4.882	0.00	0.00	0
		500-800	23669	6.759	0.00	0.00	0
		800-9928	27452	78.395	0.00	0.00	0
Total			350175		1124		17.198

Table 2. Table showing the percentage of area covered by each class by using landslide susceptibility zonation map

Class	Pixel Count	Area (in sq. km)	% age of area covered
Very Low	14764	44.19	42
Low	17319	24.66	23
Mode rate	20519	14.94	15
High	26292	11.52	12
Very High	20464	8.1	8
Total	99358	103.41	100

CONCLUSIONS

The Landslide Susceptibility Index was calculated in the current study using a GIS environment and nine conditioning parameters (slope, slope aspect, slope curvature, relief, hill shade, lithology, distance to river, distance to stream, and LULC). The model employed in this research will reasonably estimate the landslide susceptibility along the Baderwah- Bani Road stretch. The main

FUNDING

This work did not receive any external funding.

CONFLICT OF INTEREST

The authors declare no conflict of interest.

REFERENCES

- Aleotti, P. and Chowdhury, R. (1999). Landslide hazard assessment: summary review and new perspectives. *Bulletin of Engineering Geology and the environment*, v. 58, pp. 21-44.
- Bhat, G.M., Pandita, S.K., Dhar, B.L., Sahni, A.K. and Haq, I.U. (2002). Preliminary geotechnical investigation of slope failures along Jammu-Srinagar national highway between Batote and Banihal. *Aspects of Geology Environment of the Himalaya*, pp. 275-288.
- Bonham-Carter, G. (1994). *Geographic information systems for geoscientists: modelling with GIS* (No. 13). Elsevier.
- Brabb, E.E., Colgan, J. and Best, T.C. (1999). Map showing inventory and regional susceptibility for Holocene debris flows and related fast moving landslides in the conterminous United States. U.S. Geological Survey Publication, Series number 2329.
- Buckley, A. (2010). Understanding curvature rasters, in imagery, mapping, mapping center lead. *ArcGIS Block*.
- Carrara, A., Cardinali, M., Detti, R., Guzzetti, F., Pasqui, V. and Reichenbach, P. (1991). GIS techniques and statistical models in evaluating landslide hazard. *Earth Surface Processes and Landforms*, v. 16(5), pp. 427-445.
- Cevik, E. and Topal, T. (2003). GIS-based landslide susceptibility mapping for a problematic segment of the natural gas pipeline, Hendek (Turkey). *Environmental Geology*, v. 44, pp. 949-962.
- Choudhary, J.B. (2006). Geotechnical and Structural evaluation of Tectonostratigraphic Units along Head Race Tunnel, Sewa Hydroelectric Project. Stage-II, Kathua District. Unpublished Ph.d thesis. University of Jammu, Jammu, India.

factors influencing the frequency of landslides have been identified as human activities, including an increase in built-up areas (roads and buildings) and agricultural practices having the greatest influence on steep slopes. Due to the burden of the expanding population, people have been compelled to concentrate their enterprises on high mountain slopes. In order to safeguard people and property against landslides, the susceptibility maps may be used as key instruments in the planning and management of upcoming development projects in this area. While the low susceptibility zones are often safe for the construction of infrastructure, the high and very high susceptibility zones require extra engineering, geological, and geotechnical considerations.

ACKNOWLEDGEMENTS

We are grateful to the Department of Geology at the University of Jammu for their support, and the reviewers for their valuable comments, which helped to improve our presentation.

- Dai, F.C., Lee, C.F., Li, J. X.Z.W. and Xu, Z.W. (2001). Assessment of landslide susceptibility on the natural terrain of Lantau Island, Hong Kong. *Environmental Geology*, v. 40, pp. 381-391.
- Fuchs, G. (1975). Contributions to the Geology of the North-Western Himalayas. *Abhandlungen der Geologischen Bundesanstalt*, 66 Figures and 5 Plates, v. 32, pp. 1-65.
- Gansser, A. (1981). The geodynamic history of the Himalaya. *Zagros Hindu Kush Himalaya Geodynamic Evolution*, v. 3, pp. 111-121.
- Girma, F., Raghuvanshi, T.K., Ayenew, T. and Hailemariam, T. (2015). Landslide hazard zonation in Ada Berga district, central Ethiopia – A GIS based statistical approach. *Journal of Geomatics*, 9(1), pp. 25-38.
- Guzzetti, F., Reichenbach, P., Cardinali, M., Ardizzone, F. and Galli, M. (2003). The impact of landslides in the Umbria region, central Italy. *Natural Hazards and Earth System Sciences*, v. 3(5), pp. 469-486.
- Guzzetti, F., Reichenbach, P., Cardinali, M., Galli, M. and Ardizzone, F. (2005). Probabilistic landslide hazard assessment at the basin scale. *Geomorphology*, v. 72(1-4), pp. 272-299.
- Lee, S. A.R.O. (2005). Application of logistic regression model and its validation for landslide susceptibility mapping using GIS and remote sensing data. *International Journal of Remote Sensing*, v. 26(7), pp. 1477-1491.
- Lee, S. and Pradhan, B. (2006). Probabilistic landslide hazards and risk mapping on Penang Island, Malaysia. *Journal of Earth System Science*, v. 115, pp. 661-672.
- Lee, S. and Pradhan, B. (2007). Landslide hazard mapping at Selangor, Malaysia using frequency ratio and logistic regression models. *Landslides*, v. 4(1), pp. 33-41.
- Lee, S. and Talib, J.A. (2005). Probabilistic landslide susceptibility and factor effect analysis. *Environmental Geology*, v. 47, pp. 982-990.
- McMohan, C.A. (1885). Some further notes on the geology of parts of Chamba. *Records Geological Survey of India*, v. 18, pp. 35-78.
- Petley, D.N. (2008). The global occurrence of fatal landslides in 2007. In *Geophysical Research Abstracts*, vol. 10, pp. 3.
- Pham, B.T., Tien Bui, D. and Prakash, I. (2018). Application of classification and regression trees for spatial prediction of rainfall-induced shallow landslides in the Uttarakhand area (India) using GIS. *Climate Change, Extreme Events and Disaster Risk Reduction: Towards Sustainable Development Goals*, pp. 159-170.
- Poudel, K. and Regmi, A.D. (2016). Landslide susceptibility mapping along Tulsipur-Kapurkot road section and its surrounding region using bivariate statistical model. *Journal of Nepal Geological Society*, v. 50(1), pp. 83-93.
- Siddle, H.J., Jones, D.B. and Payne, H.R. (1991). Development of a methodology for landslide potential mapping in the Rhondda Valley. In *Slope stability engineering developments and applications: Proceedings of the international conference on slope stability organized by the Institution of Civil Engineers and held on the Isle of Wight on 15–18 April 1991*. Thomas Telford Publishing, pp. 137-142.
- Singh, Y. and Bhat, G.M. (2010). Role of basin morphometric parameters in landslides along the national highway-1A between Udhampur and Batote, Jammu and Kashmir, India: a case Study. *Himalayan Geology*, v. 31(1), pp. 43-50.
- Singh, Y. and Bhat, G.M. (2011). Landslide investigations: Morphometric and Geotechnical Approach - a case study from Northwest Himalaya, India. LAP Lambert Academic Publications. P. 112, ISBN-10: 9783844301502.
- Singh, Y., Bhat, G. M., Sharma, V., Pandita, S. K. and Thakur, K.K. (2012). Reservoir induced landslide at Assar, Jammu and Kashmir: a case study. *Journal of the Geological Society of India*, v. 80, pp. 435-439.
- Singh, Y., Sharma, V., Pandita, S.K., Bhat, G.M., Thakur, K.K. and Kotwal, S.S. (2014). Investigation of landslide at Sangaldan near tunnel-47, on Katra-Qazigund railway track, Jammu and Kashmir. *Journal of the Geological Society of India*, v. 84, pp. 686-692.
- Soeters, R. and Van Westen, C.J. (1996). Slope instability recognition, analysis and zonation. *Landslides: Investigation and Mitigation*, v. 247, pp. 129-177
- Thakur, V.C. (1981). Regional framework and geodynamic evolution of the Indus-Tsangpo suture zone in the Ladakh Himalayas. *Earth and Environmental Science Transactions of The Royal Society of Edinburgh*, v. 72(2), pp. 89-97.
- Van Westen, C.J., Van Asch, T.W. and Soeters, R. (2006). Landslide hazard and risk zonation—why is it still so difficult? *Bulletin of Engineering geology and the Environment*, v. 65, pp. 167-184.
- van Westen, C.J., Castellanos, E. and Kuriakose, S.L. (2008). Spatial data for landslide susceptibility, hazard, and vulnerability assessment: An overview. *Engineering Geology*, v. 102(3-4), pp. 112-131.
- Varnes, D.J. (1984). Landslide hazard zonation: a review of principles and practice (No. 3).

Heavy metal toxicity and its human health assessment: A preliminary study from the Perumal Lake sediments, Tamil Nadu, India

Baranidharan Sathyanarayanan and Vasudevan Sivaprakasam*

Department of Earth Sciences, Annamalai University, Annamalai Nagar - 608002, Chidambaram, Tamil Nadu, India

*E-mail address: devansiva@gmail.com

ABSTRACT

The current investigation manifests the heavy metal toxicity and its human health assessment to appraise the environmental deterioration of the sediments within the Perumal Lake, Tamil Nadu, India. Five surface samples were collected from the Perumal Lake in 2023, which undergoes the selective perception of the granulometric analysis, implying supremacy of the clay content and limited sand and silt contents. The organic matter indicates the higher input of waste disposal, and the CaCO₃ illustrates the existence of shell fragments in the lake environments. Noteworthy results of the heavy metal concentration as arranged in the devaluation order as Zn > Cu > Fe > Cr > Ni > Mn > Pb > Co > Cd. Followed by the heavy metal concentration, the environmental contamination indices such as I_{geo} denote that except for Cd metal, other heavy metals indicate moderate to extreme pollution status. The Enrichment Factor (Ef) illustrates Fe, Co, Cd, Zn, Cu, Ni, and Pb, highlighting no metal enrichment. In contrast, Mn and Cr reveal low metal enrichments, and the Cf reveals all the heavy metals, which argues for low to high contamination ranges. The C_d and the mC_d are categorized as very high, and PERI underscores the low-risk category. The Hazard Index (HI) of the non-carcinogenic category and carcinogenic demonstrates that children and adults are primarily at risk of ingestion. At the same time, the dermal pathway indicates low jeopardy to children and adults and no risk to humans. The Heavy Metal Toxicity Load (HMTL) poses the sample location three registers a significant accumulation of toxic contagion proposed to remove from the sediments. Realm of heavy metal toxicity and its human health assessment underscores for researchers in environmental quality determination, and the strategies discussed such as phytoremediation, in-situ capping, and biotechnological techniques, may be helpful in evaluation and implement remediation methods of pollution in aquatic environments.

KEYWORDS: Environmental indices, Non-carcinogenic, Carcinogenic assessment, Hazard Index, Lake sediments.

INTRODUCTION

Encyclopedically, the heavy metals in the aquatic environments were derived from the weathering of geogenic materials and anthropogenic inputs (Armstrong-Altrin et al., 2021 and 2022; Singh et al., 2022). Nonetheless, the heightened contamination of the heavy metals in the lake environs reveals tremendous inputs of anthropogenic sources (Gao et al., 2016; Zhang et al., 2018). Nuanced observation illustrates the sediments were palpable as an imperative parameter for transporting heavy metals from the river to the lake environment. Elaborate studies handled by the Tamil Nadu Pollution Control Board show that almost 80% of the water is drained into the rivers as polluted industrial waste. As a result, elevated polluted inputs limelight, environmental deterioration, and human hazards. An immense accumulation of heavy metals in the sediments specifies the aquatic environment is polluted. Heavy metal toxicity in sediments and lake water unveils the hazardous impacts on humans, fishes, vertebrates, and invertebrates. This could lead to bioaccumulation and persistence in the aquatic environments, posing non-carcinogenic

and carcinogenic risks to human beings once they intrude into the food web (Ouyang et al., 2018; Ali and Khan, 2018). The assertive clustering of heavy metals in sediments debilitated by approaching water mixed with the food cycle, argues for health issues for the habitants who regularly consume in the surrounding environments (Qing et al., 2015). Admittance of the heavy metals into the lake environs expedites the fine and clay particles in the sediments, constraining the heavy metals to assemble undesirable biological effects (Bibi et al., 2007). Peculiar researchers who studied heavy metal toxicity conceded grains in the sediments play a vital role in the variation in the heavy metal concentrations, and intriguingly, the heavy metals heightened with a concurrent decrease in the dimension of the grains in the aquatic environments (Tansel and Rafiuddin, 2016). Heavy metal enrichments in the provenance unveiled adequate dissemination typically through motorcycle exhausts, mining, boat and ship transportation, industrialization, fertilizers, pesticides, atmospheric airborne deposits and paints, and rapid urbanization activities (Islam et al., 2017).

A geochemical study of heavy metals such as Fe, Mn, Cu, Cr, Co, Ni, Zn, Cd, and Pb unveiled a framework for evaluating the sediments' origin, fate, and metals inputs (Arakel and Hongjun, 1992). Anthropogenic metals employ an intricate interplay of the heavy metals and the sediments disclosed with the fine particles. Fe-Mn oxides' interplay with the organic matter implies the ion exchange process, complexation, and chemical adsorption, which demonstrate environmental deterioration compared with natural sources (Palma et al., 2015). A comprehensive study of the heavy metal concentration data alone cannot offer nuanced data on sediment toxicity and the quality of adverse environmental pollution. A variety of environmental pollution indices, such as Geoaccumulation index, Enrichment factor, Contamination factor, Degree of contamination, and Potential Ecological Risk Index, have been developed and employed to study the toxicity aspects of aquatic environments (Gupta et al., 2014; Sivakumar et al., 2016).

Bonnail et al. (2019), while studying the Ganga River sediments to address the enrichment of heavy metals such as Cs, Co, Hg, Ni, Pb, and Zn content, and this could be a result of higher anthropogenic and natural activities illustrates the hazards circumstance for environments and the human beings. Nuanced observation implies that hospital effluents are an essential contributor to the heavy metal accumulation in the encompassing aquatic environment in the Cauvery river (Devarajan et al., 2015). Suresh et al. (2012) studied the Veeranam lake sediments to address the Cadmium (Cd) metal concentration, which infers a higher ecological risk, leading to adverse health risks and environmental contamination impacts. Ramanathan et al. (1999) investigated the Pichavaram mangroves to establish heavy metal dissemination. However, the study elaborated that the metal concentration of the sediments suggests the environment is unpolluted by the chemical incursions. Lake sediments of Pykara reported heavy metals such as Co, Cr, Cd, Ni, Zn, Cu, Pb, and As argues the elevated pollution status of the aquatic environs (Singh and Vasudevan, 2023). The record of dual exposure routes, such as the Carcinogenic and Non-carcinogenic categories, illustrates rigorous exploration of Human health risk assessment. This could be due to ingestion, inhalation, and dermal pathways. Regarding health hazards, the International Agency for Research on Cancer (IARC, 2012) demonstrates that the inhabitants' exposure to heavy metals such

as Cd, Cr, Pb, and As represents carcinogens. In contrast, Cu, Zn, Fe, Ni, Mn, and Co admit the non-carcinogenic risks.

Rapid industrialization and urbanization possess the accessibility of heavy metals in the socio-environment, along with imprudent annihilation practices, illustrating the potent contamination of aquatic regions, which are responsible for human health hazards and other organisms. In recent decades, monitoring the water bodies has been considered as important to ensure and safeguard the environment from heavy metal pollution. In this scrutiny, careful examination of broad evaluation aims to address the environmental pollution and human health assessment in the sediments of Perumal lake, Tamil Nadu. Heavy metal toxicity has various appraisal indexes such as I_{geo} , EF, CF, C_d , and mC_d , and PERI to monitor the environmental contaminations. Based on these indices, we evaluated the level of heavy metal contamination in the Perumal Lake sediments. The outcome of this research will provide a baseline information on the quality and health hazards to the local community.

STUDY AREA

The present study examines the Perumal Lake in the Cuddalore district, Tamil Nadu, India. The Perumal Lake is considered a unanimous prominent tank in the Cuddalore district of Tamil Nadu. The study area covers a total surface area of 13.24 sq. km between the latitudes $11^{\circ} 30'$ to $11^{\circ} 45'$ N and longitudes $79^{\circ} 30'$ to $79^{\circ} 47'$ E and placed in the SOI Toposheets no. 58 M/10 (Fig. 1).

Mean Sea Level (MSL) of the lake is situated at an altitude of 80 feet in the Neyveli tertiary uplands. The dynamic flow of the rivers, such as the Gadilam and Ponnaiyar rivers in the

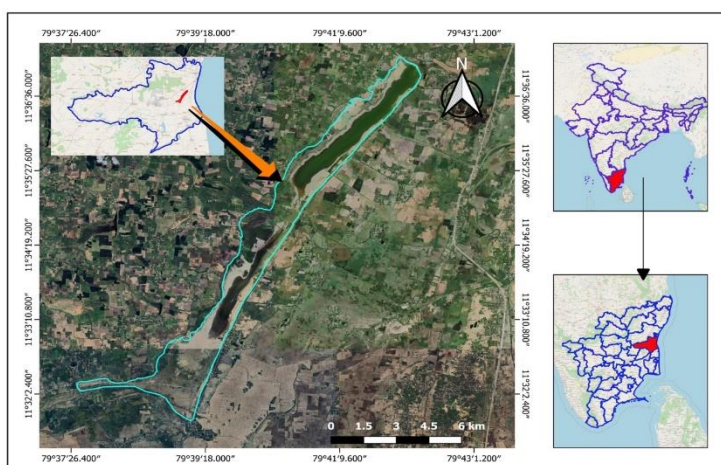


Figure 1 Dimension of the present investigation demonstrates in Google Earth View to demarcate the shape of the Perumal Lake

north and the Vellar and Coleroon rivers in the south, drains to the lake. An insightful understanding argues the rivers flow from west to

east in a sub-parallel pattern in the interplay between the lakes. The land pattern of the study unveils the geological age represented from the Mio-Pliocene to recent sediments. Furthermore, the morphometric characteristic of the lake underscores invaluable insights of length and width covers as 11.5 km and 2.07 km with a mean depth of about 3.10 m. The average rainfall of the Cuddalore districts exhibits 1,116.32 mm.

MATERIALS AND METHODS

In March 2023, a total of five surface sediment samples were collected during the summer season in the Perumal Lake at a depth of 0 to 10 cm using a Van Veen Surface Sampler (Fig. 2). The geo-coordinates of the respective samples were recognized by the GPS (Garmin, eTrex) (Table 1). To avoid the contaminations, the

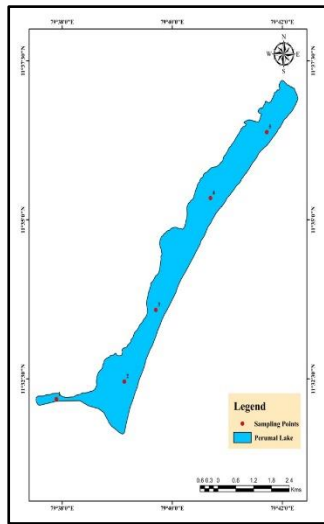


Figure 2 Location map of the surface sediments obtained from the present investigating area

collected sediments were perfectly packed within the pre-cleaned zip lock plastic bags and transported to the laboratory for preliminary process.

To remove the humid content from the sediments, the samples were dried in a hot air oven at 60°C. The Garmin GPS Map 178 (Chartplotter / Sounder) has identified the lake's morphometric parameter. The physicochemical

characteristics of sediments include granulometric analysis, organic matter, calcium carbonate, and

heavy metals. 100g of sediment samples were taken from the bulk samples using the cone and quartering method to determine the grain size characteristics. The sediment samples were dissolved with Hydrogen peroxide (H₂O₂) to remove the Organic matter from the sediments (Gee and Bauder, 1986). Afterward, the sediments were distinguished using sieve shaking methods (using ASTM sieves ranging from 2mm to 0.063mm for 15 minutes) and particle size analysis. The fractionated sediments were retained in the sieve stacks to identify the phi value of the sediments to reckon the appropriate sand, silt, and clay percentage using the ternary textural classification of hydrodynamic subdivisions (Flemming, 2000). Insightful analysis has underscores to appraise the organic matter and calcium carbonate of the sediments employed in the muffle furnace at the temperature of 550°C for 4 hours, followed by burning at 925°C for 2 hours (Bacardit and Camarero, 2010).

The sediments were pulverized in the agate mortar and stored in a glass bottle at 4°C until the chemical analysis section was carried out (Türkmen and Akbulut, 2015). To estimate the metal fractions in the sediments, the samples' clones of 0.05g were mixed with the 10 ml of associated acid as a 7:3:1 ratio of HF, HNO₃, and HClO₄ for the dilution. After digestion of the sediments, the retained solution is computed with the 250ml of double distilled water and stored in polythene bottles for Inductive Coupled Plasma – Mass Spectrometry (ICP-MS) analysis were carried out at National Geophysical Research Institute (NGRI), Hyderabad, India in Perkin Elmer SCIEX ELAN @ DRC-II to demonstrate the heavy metal content of Fe, Mn, Cu, Co, Zn, Cr, Ni, Pb, and Cd (Al-Qadasy, 2017).

ECOLOGICAL RISK ASSESSMENT METHODS

GEOACCUMULATION INDEX (I_{geo})

The I_{geo} implies an extent of heavy metal contamination in the studies sediments respecting the average shale concentration of the metals (Guo et al., 2015). The algorithm to enumerate the I_{geo} is adopted as (Muller, 1969)

$$I_{geo} = \frac{\log_2 C_n}{1.5 B_n} \quad \text{Eq. (A.1)}$$

C_n represents the concentration of the sediments, 1.5 is the factor value adopted as presumed lithogenic variation (Taylor, 1964), and B_n represents the Background value of the metals proposed by Turekian and

TABLE 1. Coordinates of sample locations, textural characteristics, organic matter, and calcium carbonate content in the Perumal Lake surface sediments

S. No	Latitude	Longitude	Sand	Silt	Clay	Organic Matter (%)	Calcium Carbonate (%)
1	11°32'11.02"	79°37'53.65"	2.7	4.3	93	3.12	0.69
2	11°32'27.50"	79°39'7.79"	1.8	1.2	97	2.48	0.66
3	11°33'35.09"	79°39'42.07"	4.6	2.4	93	1.67	0.58
4	11°35'20.61"	79°40'41.62"	4.2	0.8	95	2.08	0.77
5	11°36'22.73"	79°41'43.09"	0.7	3.2	96.1	2.88	0.89
Min			0.7	0.8	93	1.67	0.58
Max			4.6	4.3	97	3.12	0.89
Avg			2.76	2.43	94.9	0.02	0.72

Wedepohl (1961). The Igeo is classified as seven on the basic pollution level in the sediments. The classification states as 0-unpolluted, 0-1 states unpolluted to moderately polluted, 1 – 2 represents moderately polluted, 2 – 3 indicates moderately polluted to strongly polluted, 3 – 4 infers strongly polluted, 4 – 5 stands for strongly polluted to highly polluted, and > 5 shows extremely polluted.

CONTAMINATION FACTOR (CF)

The pivotal role played by the heavy metals intruding into the sediments due to the human effects is evaluated by the Cf (Ahmed et al., 2016). The CF is accessed based on the equation,

$$CF = \frac{C_n}{B_n} \quad \text{Eq. (A.2)}$$

Where C_n indicates the concentration of the metals accessed from the sediments, B_n poses the Background value of the heavy metals. The Contamination factor of the sediments is categorized into four classes such as $CF < 1$ represents low contamination factor, $1 \leq CF \leq 3$ states moderate contamination factor, $3 \leq CF \leq 6$ shows considerable contamination factor, and $CF > 6$ means very high contamination factor (Taylor, 1964).

ENRICHMENT FACTOR (EF)

Nuance assessment poses the intense heightened of heavy metals and it explains the degree of anthropogenic inputs in the aquatic environments, which is studied by the enrichment factor indices (Sakan et al., 2009). The formula to compute the EF is denoted as,

$$EF = \frac{(C_n/C_{fe})}{(B_n/B_{Fe})} \quad \text{Eq. (A.3)}$$

In this study, Fe was adopted as the reference element for the standardization as a result of the association of Fe with fine-grained sediments and metal fractionation and behavior are examined as similar to abounding heavy metals, followed by Fe, which is mainly derived from the geogenic process in most of the environments tends to be uniform (Bhuiyan et al., 2010). The formula states that C_{fe} represents Fe concentration in the sediments, and B_{fe} indicates Background geochemical concentration. The enrichment factors are classified in the following order: $EF < 2$ shows low metal enrichment, $2 \leq EF \leq 5$ presents moderate enrichment, $5 \leq EF \leq 20$ displays high enrichment, $20 \leq EF \leq 40$ accounts for very high contamination, and followed by $EF > 40$ infers extremely high contamination (Pekey, 2006).

DEGREE OF CONTAMINATION

The C_d examined the synergy of the CF for the analogous samples. To derive the C_d assessment as a consequence of the equation stated as

$$C_d = \sum_{i=1}^{n-1} Cf \quad \text{Eq. (A.4)}$$

In this case, C_d is posed as the contamination degree, n is noted as number of elements in samples, and CF reflects the contamination factor of the sediments. The C_d is classified into 4 categories: $C_d < 6$, which is designated a low contamination degree; $6 \leq C_d < 12$ represents a moderate contamination degree; $12 \leq C_d < 24$ stands for a considerable contamination degree; and $C_d \geq 24$ indicates a very high contamination degree.

The mC_d demonstrates the omnipresent contamination suggests the synergy response to multi-metals / organic matter in the sediments. The Formulae to attain the mC_d are determined by,

$$mC_d = \frac{\sum_{i=1}^{n-1} Cf}{n} \quad \text{Eq. (A.5)}$$

This could deal with the parameters such as n affirms the no. of elements and CF states Contamination Factor. Noxious classification of mC_d categorized as $mC_d < 1.5$ represents nil to very low, $1.5 \leq mC_d < 2$ denotes low degree, $2 \leq mC_d < 4$ infers moderate degree, $4 \leq mC_d < 8$ shows high degree, $8 \leq mC_d < 16$ stands for very high, $16 \leq mC_d < 32$ indicates extremely high, and $mC_d \leq 32$ means ultra-high (Abraham and Parker, 2008).

POTENTIAL ECOLOGICAL RISK INDEX (PERI)

The synergy of the PERI desires to pervasively estimate the severity of the metal contamination in sediments by contemplating the toxicity of the metals and ecological antiphon of the environment (Weber et al., 2013). The formulae examine the PERI as

$$E_r^i = T_r^i \times C_B^i \quad \text{Eq. (A.6)}$$

$$RI = \sum_{i=1}^m E_r^i \quad \text{Eq. (A.7)}$$

Where the RI is the ubiquitous of the potential individual heavy elements, E_r^i represents the potential risk of individual heavy elements, T_r^i infers toxicity response factor for metals $Pb=Cu=Ni=5$, $Zn=1$, $Cr=1$, and C_B^i indicates the Background level of the heavy metal concentrations.

HEALTH RISK ASSESSMENT

The comprehensive study of the health risks in sediments from India falls into the carcinogenic and non-carcinogenic prospects of

Table 2. Units used for the calculation of non-carcinogenic and carcinogenic risk human health risk assessments (Source: Alghamdi et al., 2018 and Vinod Kumar et al., 2020)

IR	Ingestion Rate	0.2 g/d for child and 0.1 g/d for adult
ER	Exposure Frequency	365 d / yr for both adult and children
ED	Exposure duration	6 yr for child and 30 yr for adult
SA	Skin Surface area existing	1600 cm ² / event for child and 4350 cm ² / event for adult
AF	Sediments to skin adherence Factor	0.2 mg/cm ² for child and 0.7 mg / cm ² for adult
ABS	Absorption Factor	0.001 for child and 0.01 for adult
CR	Conversion Factor	10 ⁻⁶ (Kg/mg)
BW	Body weight	15 kg for child and 70 Kg for adult
AT	Average Time	2190 days for child and 10,950 days for adult
RfD _i	Reference dose for ingestion pathway	Fe (0.3), Cu (0.04), Co (0.0003), Mn (0.014), Cd (0.5), Zn (0.3), Ni (0.002), Pb (0.0035), As (0.3), and Cr (1.5) mg/kg/day
RfD _d	Reference dose for dermal pathway	Fe (4.50E-02), Cu (12), Co (0.06), Mn (1.84E-03), Cd (0.005), Zn (60), Ni (5.4), Pb (0.42), As (0.123), and Cr (0.015)

habitats through two vulnerability routes: the average daily dose (ADD) of ingestion and dermal contact. The human risk underscores the nuanced observation of exposure, tolerance level, lifestyle, body weight, and individual habits (Swarnalatha et al., 2015). The health risk assessment profound insights were carried out on children and adults. The ADD (ingestion and Dermal Pathways) were meticulously observed with the formulae adopted as

$$ADD_i = (M \times IR \times ER \times ED / BW \times AT) \times 10^{-6} \quad \text{Eq. (A.8)}$$

$$ADD_d = (M \times SA \times AF \times ABS \times ER \times ED / BW \times AT) \times 10^{-6} \quad \text{Eq. (A.9)}$$

Where, M is the metal concentration of Fe, Mn, Cu, Cr, Zn, Pb, Ni, and Co in the sediments. The other abbreviations can be explained in Table 2. The Non-carcinogenic risk of the heavy metals study was conducted in the sediments to decode the HQ (Hazard Quotient) and HI (Hazard Index) (USEPA 2015). To assess the Hazard Quotient, the peculiar heavy metal in the sediments and the HI enumerate the comprehensive synergy of the HQ,

$$HQ = \left(\frac{ADD_{ing}}{RfD_{ing}} \right) \quad \text{Eq. (A.10)}$$

$$HQ = \left(\frac{ADD_{derm}}{RfD_{derm}} \right) \quad \text{Eq. (A.11)}$$

$$HI = HQ_{ing} + HQ_{derm} \quad \text{Eq. (A.12)}$$

Where ADD is the Average Daily Dose, RfD states the Reference dose of the metals.

LCR enumerates the carcinogenic risk that plays a pivotal role in any cancer disease whose entire life is liable to carcinogenic vulnerability (Li et al., 2014). The LCR is calculated using the formula adopted by Kusin et al. (2018):

$$LCR = (ADD_{ing} \times SF) + (ADD_{derm} \times SF) \quad \text{Eq. (A.13)}$$

Where SF is denoted as Slope Factor, SF affirms that heavy metals cause cancer to human beings.

HEAVY METAL TOXICITY LEVEL (HMTL)

Saha and Paul (2018) proposed that heavy metal toxicity load analysis yields profound insights into the environment's heavy metal accumulation. However, the study deals into the HMTL and detachably removes a percentage of elevated heavy metals in the environment. The algorithm to evaluate the HMTL reveals the quantification assessments as,

$$HMTL_i = C_i \times HIS \quad \text{Eq. (A.14)}$$

where Ci is the concentration of the metal i in sediments and HIS is the hazard intensity score obtained from (ATSDR 2019).

RESULTS AND DISCUSSION

PHYSIOCHEMICAL CHARACTERISTICS OF THE LAKE SEDIMENTS

The synergy of the textural parameters and heavy metal concentration analysis yields profound insights into heavy metal toxicity, ecological risk assessment indices, Human health Hazards, and Heavy Metal Toxicity Load intricacies. The comprehensive research systematically delves into the heavy metal toxicity and human health assessments of Perumal lake sediments. Sediment's physiochemical properties, including granulometric analysis, organic matter, and calcium carbonate content, reveals significant trends. The sediment composition is characterized by a sand-silt-clay ratio, with sand ranging from 0.7 to 4.6 % (average 2.76), silt from 0.8 to 4.3 % (average 2.43), and clay from 93 to 97 % (average 95). Ternary classification of textural characteristics suggests predominant clay matrices in the surface sediments, indicating relatively high clay content. The ternary classification of the hydrodynamic textural characteristics urges the surface sediments mostly implanted in the E-VI category, which implies

predominantly clay matrixes (Fig. 3). These noteworthy findings could affirm that the sediments comprised relatively soarer content of

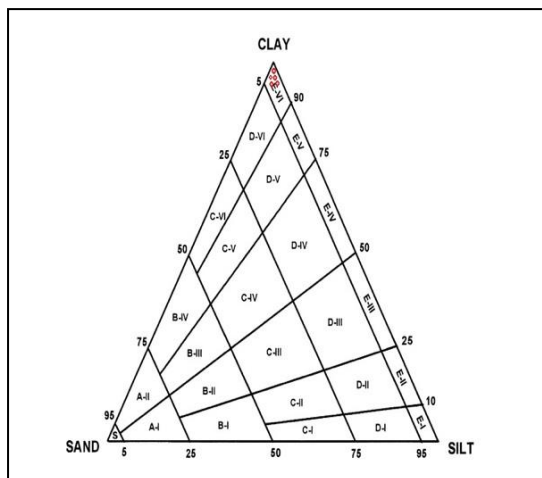


Figure 3 Ternary diagram of hydrodynamic nomenclature of the surface sediments of the present investigating area

clay sediments.

Moreover, the presence of organic matter (OM) in sediments ranges from 1.67 to 3.12% (average 2.43%), while calcium carbonate (CaCO₃) levels indicate values from 0.58 to 0.89% (average 0.72%). The abundance of clay sediments suggests that lake water is highly unstable and susceptible to wave erosion (Wildi et al., 2004). Additionally, the presence of organic matter in sediments points to the discharge of agricultural runoff and untreated urban and industrial waste from the surrounding areas (Goher et al., 2014). The profound interplay of these CaCO₃ not only defines the weathering of calcareous rock (limestone or metamorphosed limestone rocks) but also accentuates the exquisite intricacies of the calcareous microorganisms, offering an elevation of the anthropogenic inputs to the sediments (Saravanan et al., 2018).

S.No	Fe	Mn	Cr	Cu	Co	Ni	Zn	Pb	Cd
1	203	148	90.3	329	4.95	210	630	85.1	5.1
2	248	152	53.2	143	6.69	101	311	65.1	4.9
3	271	144	582	551	15.5	334	296	46.9	4.7
4	428	152	562	468	22.4	282	250	60.2	4.9
5	271	144	47.5	174	7.5	112	148	48.6	4.6
Min	203	144	47.5	143	5.0	101	148	46.9	4.6
Max	428	152	582	551	22.4	334	630	85.1	5.1
Average	293	148	281	337	12.1	210	345	62.6	4.8

LAKE MORPHOMETRIC CHARACTERISTICS

According to Håkanson (1981), the morphometric parameters encompass the lake's area, length, width, and depth. Meticulous observation of the morphometric characteristics implies the area is 13.24 sq. km, Maximum length states 11.54 km, maximum width indicates 2.07 km, and followed by mean depth implies 3.1 m of the lake.

DISSEMINATION OF HEAVY METAL CONCENTRATION AND ITS IMPLICATIONS

The spatial diffusion of heavy metal concentration urges profound insights of sediments from lake are Fe (203 – 428 ppm), Mn (144 – 152), Cr (47.49 to 581 ppm), Cu (143 – 551 ppm), Co (4.95 – 22.42 ppm), Ni (101 – 334 ppm), Zn (148 – 629.6 ppm), Pb (46.9 – 85.1 ppm), and Cd (4.6 – 5.1 ppm), respectively (Table 3). As per the original research presumptions, the Perumal lake sediments implies the heavy metal concentration were predominately formulated in the recession form as Zn > Cu > Fe > Cr > Ni > Mn > Pb > Co > Cd. As arbitrary to the average shale sedimentary concentration, the heavy metals such as Cr, Cu, Co, Ni, Zn, Pb, and Cd are enumerated as heightened value, whereas the Fe and Mn metals represent the minimal concentration, respectively (Turekian and Wedepohl, 1961). From the presumption urges, Fe, Mn, and Co metals were amplified in sample location 4, Cr, Cu, and Ni metals significantly enriched in sample location 3, and followed by Zn, Pb, and Cd elevated their concentration in the sample location 1 (Fig. 4). Textural analysis helps to figure out the influences on the heavy metal concentration of the Lake sediments. The realm of the clay sediments reveals the larger surface area to absorb the heavy metal scavenging phases such as Fe/Mn hydrolysates (Bradl, 2004).

A comprehensive analysis of the preceding studies enumerates the elevated Fe and Mn metal concentrations in the lake sediments to trivially ensure metal on the earth's crust (Singh and Vasudevan, 2023). Suresh et al. (2012) analyzed the heavy metal concentration of Veeranam lake sediments i.e. Cd (0.81 µg g⁻¹), Cu (94.12 µg g⁻¹), Pb (30.06 µg g⁻¹), Ni (63.61 µg g⁻¹), Zn (180.08 µg g⁻¹), and Cr (88.20 µg g⁻¹). Some other studies examine that Fe, Mn, Cu, Cr, Co, Ni, Pb, and Zn concentrations are higher than the Average Shale Sedimentary Concentration (Arulpoomalai Ayyanar, 2020). The magnitude of the heavy metal contagion in the sediments states as a sink drains from various sources

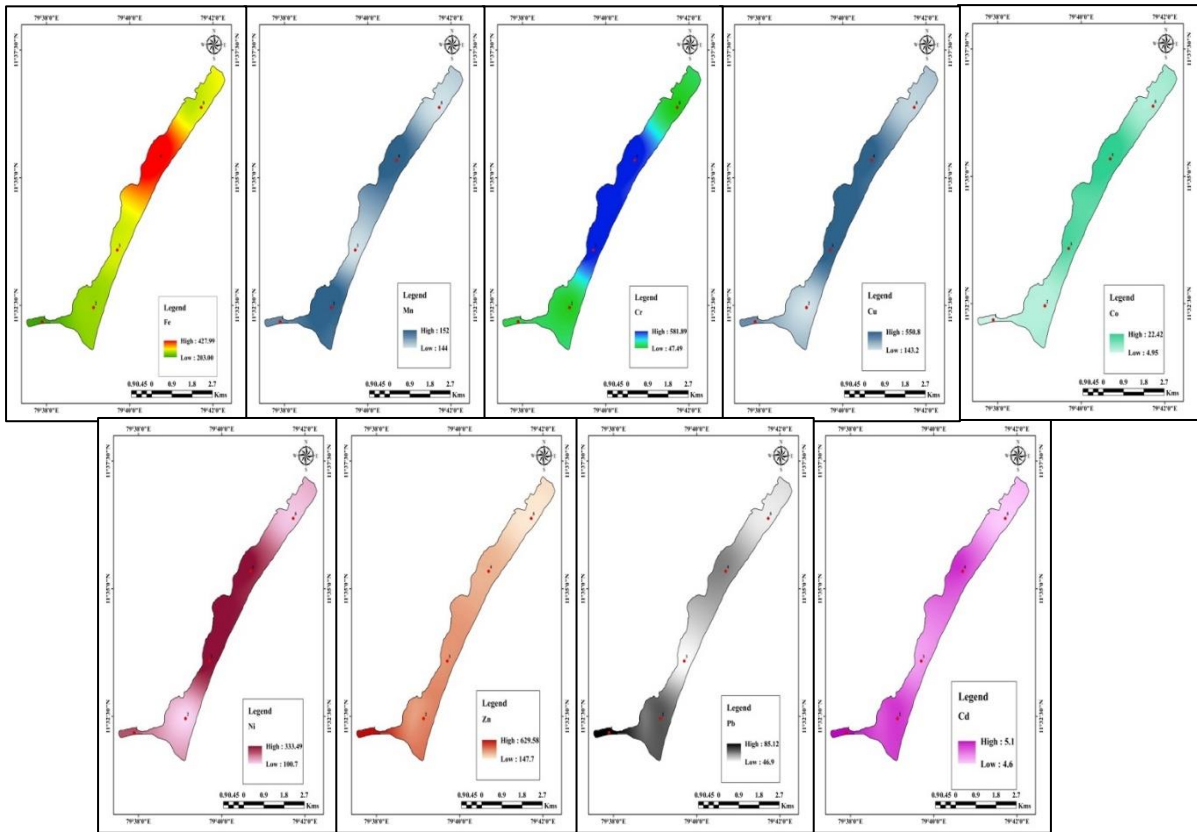


Figure 4 Heavy Metal Concentration of the surface sediments argues to inspect the metal enrichments in the sample location of the present investigating area.

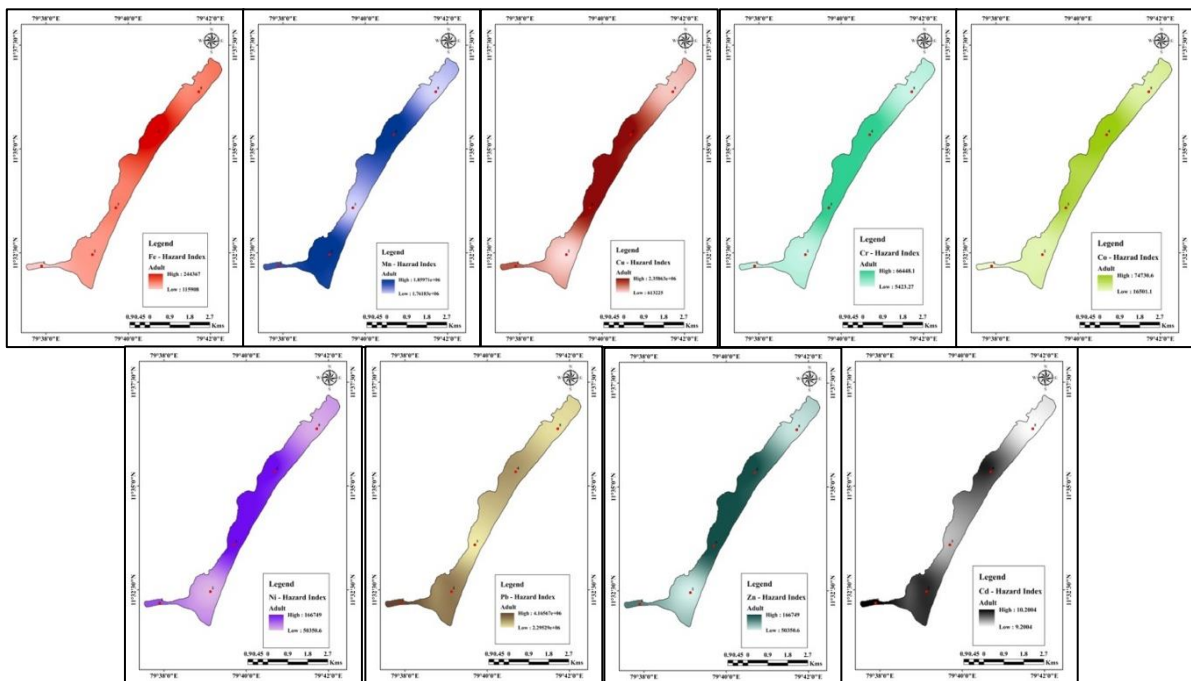


Figure 5 Human Health Assessment poses Hazard index of the heavy metals in the surface sediments inspect the non-carcinogenic jeopardy for the adults of the present investigating area.

such as bioaccumulation and biomagnification, which are deleterious to the environment (Bastami et al., 2014).

PEARSON CORRELATION

The statistical analysis of the Pearson correlation strategic approach allows us to generate a robust and realistic analysis regarding heavy

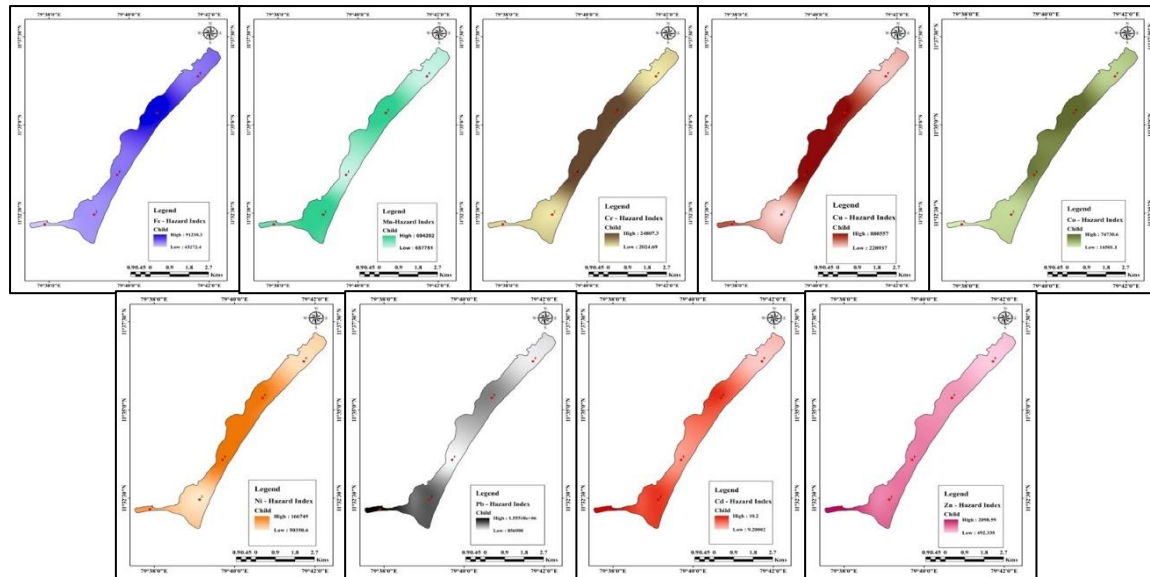


Figure 6 Human Health Assessment poses Hazard index of the heavy metals in the surface sediments inspect the non-carcinogenic jeopardy for the child of the present investigating area.

metal concentration, textural characteristics, and OM and CaCO_3 of the sediments, affording insight of utmost relevance. The Pearson correlation is presented in Table 4.

Fe metal exhibits significant correlations with Chromium (Cr) and Cobalt (Co) and moderate correlations with Copper (Cu) and sand content while showing negative correlations with Zinc (Zn), Lead (Pb), Cadmium (Cd), silt, and OM. Manganese (Mn) concentration notably correlates with Pb, Cd, and clay but lacks correlations with Cr, Cu, Ni, silt, and CaCO_3 . Chromium content is significantly associated with Cu, Co, Ni, and sand but negatively correlated with other metals. Copper concentration strongly correlates with Co, Ni, and sand but negatively correlates with other metals. Similarly, Co concentration correlates with Ni and sand, with negative associations with other metals. Nickel concentration is adversely correlated with sand and negatively associated with other parameters. Zinc content is significantly correlated with Pb, Cd, and sand but negatively correlated with clay and CaCO_3 . Lead content significantly correlates with Cd and OM but is negatively associated with sand, clay, and CaCO_3 . Cadmium exhibits weak associations with other metals, while sand is negatively associated with silt, clay, OM, and CaCO_3 . Silt content is positively associated with OM, Clay is positively associated with CaCO_3 , and OM is correlated with CaCO_3 . These Pb metals, predominantly related to organic matter, play a vital role in the toxicity index. To state that the Cu, Ni, Zn, and Cr were observed indicates the same sources and transport pathways of these contaminants (Haller et al., 2009; Pote et al., 2008). Heavy metals such as Cr, Cu, Ni, Zn, Pb, and Co possess the influences of extensive anthropogenic activities, including the heavy discharge of

untreated urban and industrial effluents into the lakes (Sivalingam et al., 2020).

ENVIRONMENTAL TOXICITY INDICES OF THE LAKE SEDIMENTS

To predict the I_{geo} of the heavy metals in the sediments unveils that Fe, Mn, and Co were elevated at sample location 4, which presumes in the moderately to extremely polluted category, and Cr, Cu, Ni signifies the strongly polluted categories, which peculiarly at the sample location 3, and followed by Zn, Pb, and Cd accounted significantly in the sample location 1. In contrast, the Zn and Pb urge moderately to highly polluted zones. However, Cd was observed as unpolluted. In the Perumal Lake, the Zn and Pb enrichments demonstrate the discharges of industrial disposal and fertilizers to the sediments (Yang et al., 2018). Besides, the Cu, Co, and Ni metals pose the metal melting factory emission may be the reason for the enrichment (Wang et al., 2018).

Consequently, Mn and Fe contaminations are contributed to the sake of sewage sludge and boat repairing processes due to the unpolluted action of the Cd, which does not play a vital role in the sediments (Soliman et al., 2019). The EF of the lake sediments is notably suggested as no metal enrichment, except Cu and Zn, which are classified as low metal enrichments. On sample location, the study urges the Cr and Cu to be elevated in the locations 3 and 4. In contrast, Ni and Zn increased in locations 1, 2, and 3, confess the low metal enrichment to moderate enrichment (Fig. 6). The EF affirms the origin of these heavy metals in the Perumal Lake sediments, which is mainly related to the geogenic background and deposited due to natural weathering process (runoff and erosion) (Zhang and Liu, 2002).

Table 4. Pearson correlation analysis for the heavy metal concentrations, textural parameters, OM and CaCO₃ of the Perumal Lake sediments

Parameters	Fe	Mn	Cr	Cu	Co	Ni	Zn	Pb	Cd	Sand	Silt	Clay	OM	CaCO ₃
Fe	1.000													
Mn	0.394	1.000												
Cr	0.666	-0.013	1.000											
Cu	0.427	-0.159	0.929	1.000										
Co	0.909	0.210	0.917	0.746	1.000									
Ni	0.400	-0.153	0.918	0.999	0.726	1.000								
Zn	-0.525	0.161	-0.213	0.103	-0.402	0.137	1.000							
Pb	-0.358	0.482	-0.413	-0.190	-0.424	-0.162	0.892	1.000						
Cd	-0.145	0.641	-0.149	0.024	-0.161	0.052	0.854	0.949	1.000					
Sand	0.450	0.107	0.920	0.952	0.757	0.956	0.169	-0.070	0.197	1.000				
Silt	-0.720	-0.627	-0.453	-0.121	-0.647	-0.106	0.553	0.365	0.120	-0.311	1.000			
Clay	0.166	0.401	-0.469	-0.762	-0.168	-0.779	-0.592	-0.227	-0.273	-0.655	-0.515	1.000		
OM	-0.521	0.004	-0.876	-0.709	-0.774	-0.699	0.418	0.614	0.349	-0.763	0.644	0.177	1.000	
CaCO ₃	0.285	-0.085	-0.370	-0.467	-0.060	-0.495	-0.448	-0.157	-0.322	-0.620	0.105	0.476	0.513	1.000

A proximate inquiry of the CF shows that the Fe and Mn metals accounted for low contamination factors. Cr, Cu, Co, Ni, Zn, and Pb indicate considerable contamination factors. Consequently, Cd exhibits high contamination factor in the lake sediments. Notable findings indicate that the considerable contamination of Cr, Cu, Co, Ni, Zn, and Pb in the sediments could be attributable to anthropogenic and geogenic sources. This could exhibit the anthropogenic influences of the sediments due to point pollution sources and non-point pollution sources linked to vehicle sources, agricultural runoff, sewage and waste discharges, electroplating, and clothing industries. The accumulation of Pb from the contamination factor inferences reveals vehicle emission deposits from the nearby roadways (Yang and Rose, 2005; Gupta et al., 2013; Njenga et al., 2009).

Research suggests that the abnormal enrichment of Cd in sediments is due to the disposal of batteries, electroplating, pigments, and metal manufacturing (Jain et al., 2010). Furthermore, the sources of Zn in the sediments are due to the wear and tear of tires and brake lining (Singh and Kumar, 2017), followed by Cu enrichments poses the metal plating, antifouling, and brake lining wears (Duodu et al., 2016). The ambiguous result of the C_d and mC_d examines the accretion of heavy metals and urges a very high contamination degree and a high degree of contamination in the sediments, as shown in Table 5. Based on the comprehensive forecast of the PERI was calculated for each sampling location, 1 (11.36), 2 (6.24), 3 (14.34), 4 (13.34), and 5 (4.43) urges a low risk (PERI < 150) to the local biological communities.

HEALTH RISK ASSESSMENT OF HEAVY METALS IN SEDIMENTS

The conspicuous observation of heavy metals embellishment urges the non-carcinogenic

and carcinogenic threat analysis in surface sediments to affirm the ingestion and dermal pathway for adults and children, listed in Tables 6 and 7. The valuable insight of the average daily dose computed in mg/kg/day unit was forecast for the heavy metals, such as Fe, Mn, Cr, Cu, Co, Ni, Zn, Pb, and Cd. The result found that the examined ADD_{ing} value of the heavy metals is potentially adverse than the RfD_{ing} delves the ingestion route probably causes harmful effects on humans in the environment. The intriguing findings underscore the nuanced interplay of ADD_{ing} value for heavy metals such as Fe, Mn, Cr, Cu, Co, Ni, Zn, Pb, and Cd values, unveiling the ADD_{derm} route's influential characteristics for adults and children. Remarkably, an insightful examination of ADD illuminates an oral intake through the accidental contact of the sediments in the hand-to-mouth aspects.

The Non-carcinogenic health risks coupled with exposure to heavy metals such as Fe, Mn, Cr, Cu, Co, Ni, Zn, Pb, and Cd for the adult and child contemporary in the surrounding lakes (Table 5). To address these non-carcinogenic risks, we evaluated the Hazard Quotient of ingestion (HQ_{ing}) and Hazard Quotient of dermal (HQ_{derm}) to affirm the health risks to the habitants. The HQ value is less than 1.0, denoted as safe conditions, and has no harmful effects, whereas the HQ value greater than 1.0 indicates harmful effects (Qu et al., 2012; USEPA, 2015).

It is worth noting that this assessment shows the HQ_{ing} of the heavy metals such as Fe, Mn, Cr, Cu, Co, Ni, Zn, Pb, and Cd values predominately higher than 1.0, it would be harmful to the adult and child. In contrast, the HQ_{derm} showed no detrimental effects on human health due to less than 1.0. Rigorous investigation implies the heavy metals in the sediments due to the rapid urbanization, growing population, industrialization, and agricultural inputs (Alghamdi et al., 2018).

Consequently, the HI of the sediments plays a pivotal role in enumerating the high-end

Table 5. Environmental toxicity Indices such as I_{geo}, EF, CR, C_d and mC_d, and PERI for the Perumal Lake sediments

	Geoaccumulation index			Results	Enrichment factor			Results	Contamination Factor			Results	Cd	mCd	PERI	
	Min	Max	Avg		Min	Max	Avg		Min	Max	Avg					
Fe	6.81	7.13	6.95	Extremely polluted				No metal enrichment	0.00	0.01	0.01	Low contamination Factor	Min	25.92	2.88	4.43
Mn	4.91	4.94	4.92	Highly Polluted	0.64	0.27	0.45	No metal enrichment	0.17	0.18	0.17	Low contamination Factor	Max	45.73	5.08	14.34
Cr	3.45	4.54	3.97	Strongly polluted	0.82	1.15	0.14	No metal enrichment	0.53	6.47	3.12	Considerable contamination Factor	Avg	36.54	4.06	9.78
Cu	3.63	4.22	3.94	Strongly polluted	0.42	1.03	0.19	No metal enrichment	3.18	12.24	7.49	High Contamination Factor	Results	Very High Contamination Degree	High degree contamination	Low Risk
Co	1.80	2.45	2.10	Moderately polluted	0.98	0.94	0.96	No metal enrichment	0.26	1.18	0.63	Low contamination Factor				
Ni	3.66	4.18	3.92	Strongly polluted	0.59	0.23	0.25	No metal enrichment	1.48	4.90	3.09	Considerable contamination Factor				
Zn	3.97	4.60	4.27	Highly Polluted	0.45	2.10	0.32	No metal enrichment	1.55	6.63	3.63	Considerable contamination Factor				
Pb	2.80	3.05	2.91	Moderately polluted	0.86	0.58	0.77	No metal enrichment	2.35	4.26	3.13	Considerable contamination Factor				
Cd	0.04	0.01	0.01	Un polluted	0.99	0.97	0.98	No metal enrichment	15.33	17.00	16.14	High Contamination Factor				

Table 6 Pervasive Study of the Non-Carcinogenic for the Adult and Child in the study area

	ADULT					CHILD				
	ADDi	ADDd	HQi	HQd	HI	ADDi	ADDd	HQi	HQd	HI
Fe	48680.42	0.000123627	162268.05	0.002747267	162268.05	18174.02	6.06293E-06	60580.07	0.000134732	60580.07
Mn	25350.81	0.00006438	1810772.45	0.03498913	1810772.48	9464.30	3.15733E-06	676021.71	0.001715942	676021.72
Cr	45715.05	0.000116096	30476.70	0.007739752	30476.71	17066.95	5.69361E-06	11377.97	0.000379574	11377.97
Cu	57049.61	0.000144881	1426240.24	1.20734E-05	1426240.24	21298.52	7.10528E-06	532463.02	5.92107E-07	532463.02
Co	1952.36	4.95813E-06	37993.33	8.26355E-05	37993.33	728.88	2.43157E-07	37993.33	4.05262E-06	37993.33
Ni	35552.80	9.02886E-05	103780.00	1.67201E-05	103780.00	13273.05	4.42795E-06	103780.00	8.1999E-07	103780.00
Zn	55987.62	0.000142184	1089.53	2.36974E-06	1089.53	20902.04	6.97301E-06	1089.53	1.16217E-07	1089.53
Pb	10478.11	2.66098E-05	2993745.20	6.33567E-05	2993745.20	3911.83	1.305E-06	1117664.87	3.10715E-06	1117664.87
Cd	829.04	2.1054E-06	9.68	0.00042108	9.68	309.51	1.03253E-07	9.68	2.06507E-05	9.68

	ADULT					CHILD				
	ADDi	SFi	ADDd	SFd	LCR	ADDi	SFi	ADDd	SFd	LCR
Cr	45715.05	22857.527	0.000116096	0.002321926	0.02285753	17066.95	8533.477	5.694E-06	0.000113872	0.0085335
Cu	57049.61	96984.336	0.000144881	0.006157447	0.096984342	21298.52	36207.49	7.105E-06	0.000301974	0.0362075
Ni	35552.8	20913.414	9.02886E-05	0.003837266	0.020913418	13273.05	7807.675	4.428E-06	0.000188188	0.0078077
Pb	10478.11	89.06392	2.66098E-05		8.90639E-05	3911.827	33.25053	1.305E-06		3.325E-05

S.No	Cr	HMTL-Cr	Removal	Cu	HMTL-Cu	Removal	Ni	HMTL-Ni	Removal	Zn	HMTL-Zn	Removal
1	90.33	75786.87	6.77%	328.9	264764.5	19.75%	210.2	208728.6	20.25%	629.6	574824.8	38.52%
2	53.22	44651.58	3.99%	143.2	115276	8.60%	100.7	99995.1	9.70%	310.7	283669.1	19.01%
3	581.9	488214.1	43.61%	550.8	443394	33.08%	333.5	331165.5	32.14%	296.4	270613.2	18.14%
4	561.5	471098.5	42.08%	468.4	377062	28.13%	281.8	279827.4	27.15%	249.9	228158.7	15.29%
5	47.49	39844.11	3.56%	174	140070	10.45%	111.6	110818.8	10.75%	147.7	134850.1	9.04%
HIS	893			805			993			913		
Permissible Load	80370			36225			67524			86735		
Permissible Limit (mg/kg)	90			45			68			95		

risk of heavy metals attributed based on the summation of HQ_{ing} and HQ_{derm} of the sediments. The HI value attributes, as the value is less than 1.0 and greater than 1.0, imply no risk and high risk to adults and children (Qing et al., 2015). This could lead to the result observed for HI of adult and child states that the sediments were highly considerable as risk categories indicate chronic non-carcinogenic effects play a significant role of oral exposure through the food contagion consumed from sediments as presented in Tables 6 and 7.

LCR represents a value is lesser than 1×10^{-6} and denotes no risk/effects to humans, whereas an LCR greater than 1×10^{-6} urges a high risk of cancer to human beings and followed by a range of 1×10^{-6} to 1×10^{-4} illustrates that it undergoes tolerable risk of heavy metals to habitants (USEPA, 2011; Karunanidhi et al., 2022). In these present inferences, the LCR value for heavy metals such as Cr, Cu, Ni, and Pb illustrates the sediments of the Perumal Lake accounting as the values are inferior to 1×10^{-6} registered as unworthy sediments to cause cancer to adult and child in the surrounding regions (Table 7). On pioneering innovation research illuminates the assorted heavy metals in sediments emerges as the premise for several cancers. Cr and Ni were associated with diseases such as lung, paranasal sinuses, and nasal cavity cancer (Cancer-Causing Substances in the Environment – NCI).

HEAVY METAL TOXICITY LOAD

Employing the heavy metal toxicity load evaluation demonstrates the glut of heavy metals load in the Lake environments. It unveils a noteworthy picture for adequate removal of metal loads taken in monitoring the environments. The HMTL examines the heavy metal values, permissible limits, and percentage removal of toxic loads (Table 8). The allowable limit of heavy metals toxicity is accounted for by hazard intensity scores (HIS) proposed by ATSDR (2019). The HMTL value of sediments resulted in the average shale concentration of sediments (Turekian and Wedepohl, 1961). The meticulous observation of the percentage of HMTL removal of the heavy metals such as Cr (3.56% - 43.61%; avg. 20%), Cu (8.60 - 33.08%; avg. 20.24%), Ni (9.70 - 32.14%; avg. 20.26%), and Zn (4 - 38.52%, avg. 21.08%), respectively (Table 8). In the study area, sample location 3 registers a significant accumulation of toxic contagion proposed to be removed from the sediments, except Zn, which is higher in location 1.

CONCLUSION

An extensive investigation into heavy metal concentrations in Perumal Lake sediment, Cuddalore district, Tamil Nadu, yields significant insights. Key findings include the prevalence of clay content in surface sediments, with minimal

contributions from organic matter (OM) and calcium carbonate ($CaCO_3$) in heavy metal association. Metal gradation follows $Zn > Cu > Fe > Cr > Ni > Mn > Pb > Co > Cd$, with low Fe and Mn values, possibly due to limited geogenic input. Anthropogenic sources, including urban and industrial effluents, agricultural runoff, and vehicle emissions, contribute significantly to Cu, Cr, Co, Ni, Zn, and Pb accumulation through unprocessed urban and industrial effluents, agricultural runoff and vehicles emission may leads to aquatic toxicity.

The correlation analysis suggests that heavy metals do not bind significantly with textural, OM, and $CaCO_3$ components, thus limiting their impact on sediment dispersion. Anthropogenic influences, such as agrochemicals, vehicle emissions, untreated waste discharge, and rapid urbanization, contribute extensively to heavy metal accumulation in sediments. Exploration of environmental toxicity indices, including I_{geo} , EF, CF, Cd, mCd, and PERI, reveals moderate to extreme pollution levels for most heavy metals except for Cd.

Non-carcinogenic assessments reveal potential risks to children and adults from ingesting sediments, while dermal exposure poses no significant risk. Combined HQ values underscore the chronic non-carcinogenic effects of oral exposure to foods sourced from the lake surroundings, particularly affecting adults and children. Furthermore, the assessment of LCR for heavy metals suggesting that the sediments pose negligible risk of causing cancer to adults and children in the surrounding areas. Notably, this finding underscores the effectiveness of potential remediation techniques in addressing heavy metal toxicity in sediments. Various remediation strategies, including phytoremediation, in-situ capping, and biotechnological approaches, offer promising avenues for mitigating heavy metal contamination.

ACKNOWLEDGEMENT

The authors would like to thank Annamalai University for their valuable support in providing access to use research equipments. The assistance and resources provided by Annamalai University have been instrumental in the successful completion of this study. We extend our heartfelt gratitude to the Editor of the Journal Indian Association of Sedimentologists Dr. John S. Armstrong-Altrin and the two reviewers for their suggestions and guidance, which improved the quality of our presentation.

CONFLICT OF INTEREST

The authors declare that they have no known competing interests.

ABBREVIATION

I_{geo} - Geoaccumulation Index; Ef - Enrichment Factor; Cf - Contamination Factor; C_d and the mC_d - Degree of Contamination and Modified Degree of Contamination; PERI - Potential Ecological Risk Index; ADD - Average Daily Dose; HI - Hazard Index; LCR - Lifetime Carcinogenic Risk; HMTL - Heavy Metal Toxicity Load; HQ - Hazard Quotation

REFERENCES

- Abraham, G.M.S. and Parker, R.J. (2008). Assessment of heavy metal enrichment factors and the Degree of contamination in marine sediments from Tamaki Estuary, Auckland, New Zealand. *Environmental Monitoring and Assessment*, v. 136, pp. 227-238.
- Ahmed, K.M., Baki, M.A., Kundu, G.K., Saiful Islam, M., Monirul Islam, M. and Muzammel Hossain, M. (2016). Human health risks from heavy metals in fish of Buriganga river, Bangladesh. *SpringerPlus*, v. 5, pp. 1-12.
- Al-Qadasy, M.K.O., Babaqi, A.S., Al-Abyadh, M.M. and Al-kaf, A.G.A. (2017). Investigation of toxic metals pollution in water, sediment and fish at Aden coast, Gulf of Aden, Yemen. *University Journal Pharm Research*, v. 2, pp. 42-49.
- Ali, H. and Khan, E. (2018). Bioaccumulation of non-essential hazardous heavy metals and metalloids in freshwater fish. Risk to human health. *Environmental Chemistry Letters*, v. 16(3), pp. 903-917.
- Alghamdi, B.A., El Mannoubi, I. and Zabin, S.A. (2019). Heavy metals' contamination in sediments of Wadi Al-Aqiq water reservoir dam at Al-Baha region, KSA: Their identification and assessment. Human and ecological risk assessment: An International Journal, v. 25(4), pp. 793-818.
- Arakel, A.V. and Hongjun, T. (1992). Heavy metal geochemistry and dispersion pattern in coastal sediments, soil, and water of Kedron Brook floodplain area, Brisbane, Australia. *Environmental Geology and Water Sciences*, v. 20(3), pp. 219-231.
- Armstrong-Altrin, J.S., Madhavaraju, J., Vega-Bautista, F., Ramos-Vázquez, M.A., Pérez-Alvarado, B.Y., Kasper-Zubillaga, J.J. and Bessa, A.Z.E. (2021). Mineralogy and geochemistry of Tecolutla and Coatzacoalcos beach sediments, SW Gulf of Mexico. *Applied Geochemistry*, v. 134, p. 105103.
- Armstrong-Altrin, J.S., Ramos-Vázquez, M.A., Madhavaraju, J., Marca-Castillo, M.E., Machain-Castillo, M.L. and Márquez-García, A.Z. (2022). Geochemistry of marine sediments adjacent to the Los Tuxtlas Volcanic Complex, Gulf of Mexico: constraints on weathering and provenance. *Applied Geochemistry*, v. 141, p. 105321.
- ATSDR (2019). Substance priority list | ATSDR [Internet]. accessed October 30, 2022. <https://www.atsdr.cdc.gov/spl/index.html>
- Ayyanar, A. and Thatikonda, S. (2020). Distribution and ecological risks of heavy metals in Lake Hussain Sagar, India. *Acta Geochimica*, v. 39(2), pp. 255-270.
- Bastami, K.D., Bagheri, H., Kheirabadi, V., Zaferani, G.G., Teymori, M.B., Hamzehpoor, A., Soltani, F., Haghparast, S., Harami, S.R.M., Ghorghani, N.F. and Ganji, S. (2014). Distribution and ecological risk assessment of heavy metals in surface sediments along southeast coast of the Caspian Sea. *Marine Pollution Bulletin*, v. 81(1), pp.262-267.
- Bacardit, M. and Camarero, L. (2010). Atmospherically deposited major and trace elements in the winter snowpack along a gradient of altitude in the Central Pyrenees: the seasonal record of long-range fluxes over SW Europe. *Atmospheric Environment*, v. 44(4), pp. 582-595.
- Bibi, M.H., Ahmed, F. and Ishiga, H. (2007). Assessment of metal concentrations in lake sediments of southwest Japan based on sediment quality guidelines. *Environmental Geology*, v. 52, pp. 625-639.
- Bhuiyan, M.A., Parvez, L., Islam, M.A., Dampare, S.B. and Suzuki, S. (2010). Heavy metal pollution of coal mine-affected agricultural soils in the northern part of Bangladesh. *Journal of Hazardous Materials*, v. 173(1-3), pp. 384-392.
- Bonnail, E., Antón-Martín, R., Riba, I. and DelValls, T.Á. (2019). Metal distribution and short-time variability in recent sediments from the Ganges River towards the Bay of Bengal (India). *Geosciences*, v. 9(6), p. 260.
- Bradl, H.B. (2004). Adsorption of heavy metal ions on soils and soils constituents. *Journal of Colloid and Interface Science*, v. 277(1), pp. 1-18.
- Cancer-causing substances in the environment - NCI. Accessed October 31, 2022. <https://www.cancer.gov/about-cancer/causes-prevention/risk/substances>
- Devarajan, N., Laffite, A., Ngelikoto, P., Elango, V., Prabakar, K., Mubedi, J.I., Piana, P.T., Wildi, W. and Poté, J. (2015). Hospital and urban effluent waters as a source of accumulation of toxic metals in the sediment receiving system of the Cauvery River, Tiruchirappalli, Tamil Nadu, India. *Environmental Science and Pollution Research*, v. 22, pp. 12941-12950.
- Duodu, G.O., Goonetilleke, A. and Ayoko, G.A. (2016). Comparison of pollution indices for the assessment of heavy metal in Brisbane River sediment. *Environmental Pollution*, v. 219, pp. 1077-1091.
- Flemming, B.W. (2000). A revised textural classification of gravel-free muddy sediments on the basis of ternary diagrams. *Continental Shelf Research*, v. 20(10-11), pp. 1125-1137.

- Gao, L., Wang, Z., Shan, J., Chen, J., Tang, C., Yi, M. and Zhao, X. (2016). Distribution characteristics and sources of trace metals in sediment cores from a trans-boundary watercourse: an example from the Shima River, Pearl River Delta. *Ecotoxicology and Environmental Safety*, v. 134, pp. 186-195.
- Gee, G.W. and Bauder, J.W., (1986). Particle-size analysis. *Methods of soil analysis: Part 1 Physical and Mineralogical Methods*, v. 5, pp. 383-411.
- Goher, M.E., Farhat, H.I., Abdo, M.H. and Salem, S.G., (2014). Metal pollution assessment in the surface sediment of Lake Nasser, Egypt. *The Egyptian Journal of Aquatic Research*, v. 40(3), pp. 213-224.
- Gupta, B., Kumar, R. and Rani, M. (2013). Speciation of heavy metals in water and sediments of an urban lake system. *Journal of Environmental Science and Health, Part A*, v. 48(10), pp. 1231-1242.
- Gupta, S., Jena, V., Matic, N., Kapralova, V. and Solanki, J.S. (2014). Assessment of geo-accumulation indexes of heavy metal and source of contamination by multivariate factor analysis. *International Journal of Hazard Matter*, v. 2 (2), pp. 18-22.
- Guo, W., Huo, S., Xi, B., Zhang, J. and Wu, F. (2015). Heavy metal contamination in sediments from typical lakes in the five geographic regions of China: Distribution, bioavailability, and risk. *Ecological Engineering*, v. 81, pp. 243-255.
- Hakanson, L. (1981). *A manual of lake morphometry*. Springer Science & Business Media.
- Haller, L., Poté, J., Loizeau, J.L. and Wildi, W. (2009). Distribution and survival of faecal indicator bacteria in the sediments of the Bay of Vidy, Lake Geneva, Switzerland. *Ecological Indicators*, v. 9(3), pp. 540-547.
- IARC (2012). *IARC Monographs on the Identification of Carcinogenic Hazards to Humans*. The International Agency for Research on Cancer, France (Last update January 2020).
- Islam, M.S., Ahmed, M.K., Raknuzzaman, M., Habibullah-Al-Mamun, M. and Kundu, G.K. (2017). Heavy metals in the industrial sludge and their ecological risk: A case study for a developing country. *Journal of Geochemical Exploration*, v. 172, pp. 41-49.
- Jain, C.K., Gurunadha Rao, V.V.S., Prakash, B.A., Mahesh Kumar, K. and Yoshida, M., (2010). Metal fractionation study on bed sediments of Hussainsagar Lake, Hyderabad, India. *Environmental Monitoring and Assessment*, v. 166, pp. 57-67.
- Karunanidhi, D., Aravinthasamy, P., Subramani, T., Chandrajith, R., Raju, N.J. and Antunes, I.M.H.R., (2022). Provincial and seasonal influences on heavy metals in the Noyyal River of South India and their human health hazards. *Environmental Research*, v. 204, p. 111998.
- Kusin, F.M., Azani, N.N.M., Hasan, S.N.M.S. and Sulong, N.A. (2018). Distribution of heavy metals and metalloid in surface sediments of heavily-mined area for bauxite ore in Pengerang, Malaysia and associated risk assessment. *Catena*, v. 165, pp. 454-464.
- Li, Q., Zhou, J.L., Wang, Y., Li, H., Huang, B. and Pan, X.J. (2013). Effects of sediment dredging on heavy metal removal in Dianchi lake, China. *Advanced Materials Research*, v. 726, pp. 1654-1658.
- Li, Z., Ma, Z., van der Kuijp, T.J., Yuan, Z. and Huang, L. (2014). A review of soil heavy metal pollution from mines in China: pollution and health risk assessment. *Science of the total environment*, v. 468, pp. 843-853.
- Muller, G.M. (1969). Index of geoaccumulation in sediments of the Rhine River. *Geo Journal*, v. 2, pp. 108-118.
- Njenga, J.W., Ramanathan, A.L. and Subramanian, V. (2009). Partitioning of heavy metals in the sediments of Lake Naivasha, Kenya. *Chemical Speciation & Bioavailability*, v. 21(1), pp. 41-48.
- Ouyang, W., Wang, Y., Lin, C., He, M., Hao, F., Liu, H. and Zhu, W. (2018). Heavy metal loss from agricultural watershed to aquatic system: A Scientometrics Review. *Science of the Total Environment*, v. 637, pp. 208-220.
- Palma, P., Ledo, L. and Alvarenga, P., (2015). Assessment of trace element pollution and its environmental risk to freshwater sediments influenced by anthropogenic contributions: The case study of Alqueva Reservoir (Guadiana Basin). *Catena*, v. 128, pp. 174-184.
- Pekey, H., (2006). Heavy metal pollution assessment in sediments of the Izmit Bay, Turkey. *Environmental Monitoring and Assessment*, v. 123, pp. 219-231.
- Poté, J., Haller, L., Loizeau, J.L., Bravo, A.G., Sastre, V. and Wildi, W. (2008). Effects of a sewage treatment plant outlet pipe extension on the distribution of contaminants in the sediments of the Bay of Vidy, Lake Geneva, Switzerland. *Bioresource Technology*, v. 99(15), pp. 7122-7131.
- Qing, X., Yutong, Z. and Shenggao, L., (2015). Assessment of heavy metal pollution and human health risk in urban soils of steel industrial city (Anshan), Liaoning, Northeast China. *Ecotoxicology and Environmental Safety*, v. 120, pp. 377-385.
- Qu, C., Sun, K., Wang, S., Huang, L. and Bi, J., (2012). Monte Carlo simulation-based health risk assessment of heavy metal soil pollution: A case study in the Qixia mining area, China. *Human and Ecological Risk Assessment: An International Journal*, v. 18(4), pp. 733-750.
- Ramanathan, A.L., Subramanian, V., Ramesh, R., Chidambaram, S. and James, A. (1999). *Environmental geochemistry of the Pichavaram mangrove ecosystem (tropical), southeast coast*

- of India. *Environmental Geology*, v. 37, pp. 223-233.
- Saha, P. and Paul, B. (2018). Assessment of heavy metal toxicity related with human health risk in the surface water of an industrialized area by a novel technique. *Human and Ecological Risk Assessment: An International Journal*.
- Sakan, S.M., Đorđević, D.S., Manojlović, D.D. and Predrag, P.S. (2009). Assessment of heavy metal pollutants accumulation in the Tisza river sediments. *Journal of Environmental Management*, v. 90(11), pp. 3382-3390.
- Saravanan, P., Krishnakumar, S., Pradhap, D., Silva, J.D., Arumugam, K., Magesh, N.S. and Srinivasalu, S. (2018). Elemental concentration based potential ecological risk (PER) status of the surface sediments, Pulicat lagoon, Southeast coast of India. *Marine Pollution Bulletin*, v. 133, pp. 107-116.
- Singh, K.K. and Vasudevan, S. (2022). Source and ecological risk assessment of trace metal contamination in Lake Pykara sediments, Southern India. *Arabian Journal of Geosciences*, v. 15(15), pp.1310.
- Singh, K.K. and Vasudevan, S. (2023). Evaluation of trace metal contamination history during 1910–2019 AD by ²¹⁰Pb dating from Lake Pykara sediments, India. *Arabian Journal of Geosciences*, v. 16(4), pp. 236.
- Singh, U.K. and Kumar, B. (2017). Pathways of heavy metals contamination and associated human health risk in Ajay River basin, India. *Chemosphere*, v. 174, pp. 183-199.
- Sivakumar, S., Chandrasekaran, A., Balaji, G. and Ravisankar, R. (2016). Assessment of heavy metal enrichment and the Degree of contamination in coastal sediment from South East Coast of Tamilnadu, India. *Journal of Heavy Metal Toxicity and Diseases*, v. 1(2), pp.1-8.
- Sivalingam, P., Al Salah, D.M.M. and Poté, J. (2020). Sediment heavy metal contents, ostracod toxicity and risk assessment in tropical freshwater lakes, Tamil Nadu, India. *Soil and Sediment Contamination: An International Journal*, v. 30(2), pp. 231-252.
- Soliman, N.F., Younis, A.M. and Elkady, E.M. (2019). An insight into fractionation, toxicity, mobility and source apportionment of metals in sediments from El Tamsah Lake, Suez Canal. *Chemosphere*, v. 222, pp. 165-174.
- Suresh, G., Sutharsan, P., Ramasamy, V. and Venkatachalapathy, R. (2012). Assessment of spatial distribution and potential ecological risk of the heavy metals in relation to granulometric contents of Veeranam lake sediments, India. *Ecotoxicology and Environmental Safety*, v. 84, pp. 117-124.
- Swarnalatha, K., Letha, J., Ayoob, S. and Nair, A.G. (2015). Risk assessment of heavy metal contamination in sediments of a tropical lake. *Environmental Monitoring and Assessment*, v. 187, pp. 1-14.
- Tansel, B. and Rafiuddin, S. (2016). Heavy metal content in relation to particle size and organic content of surficial sediments in Miami River and transport potential. *International Journal of Sediment Research*, v. 31(4), pp. 324-329.
- Taylor, S.R. (1964). Abundance of chemical elements in the continental crust: a new table. *Geochimica et Cosmochimica Acta*, v. 28(8), pp. 1273-1285.
- Türkmen, A., Türkmen, M., Tepe, Y. and Akyurt, İ. (2015). Heavy metals in three commercially valuable fish species from Iskenderun Bay, Northern East Mediterranean Sea, Turkey. *Food Chemistry*, v. 91(1), pp. 167-172.
- Turekian, K.K. and Wedepohl, K.H. (1961). Distribution of the elements in some major units of the earth's crust. *Geological Society of America Bulletin*, v. 72(2), pp. 175-192.
- USEPA. 2011. Exposure factors handbook 2011 edition (final report) | risk assessment Portal| USEPA. accessed September 2, 2022. <https://cfpub.epa.gov/ncea/risk/recordisplay.cfm?deid=236252>
- U. S. Environmental Protection Agency (USEPA) (2015). Risk based screening table generic, summary table. United States Environmental Protection Agency. URL <http://www.epa.gov/risk/riskbased-screening-table-generic-tables> (Accessed 31 January 2016)
- Wang, G., Hu, X., Zhu, Y., Jiang, H. and Wang, H. (2018). Historical accumulation and ecological risk assessment of heavy metals in sediments of a drinking water lake. *Environmental Science and Pollution Research*, v. 25, pp. 24882-24894.
- Weber, P., Behr, E.R., Knorr, C.D.L., Vendruscolo, D.S., Flores, E.M., Dressler, V.L. and Baldissarotto, B. (2013). Metals in the water, sediment, and tissues of two fish species from different trophic levels in a subtropical Brazilian river. *Microchemical Journal*, v. 106, pp. 61-66.
- Wildi, W., Dominik, J., Loizeau, J.L., Thomas, R.L., Favarger, P.Y., Haller, L., Perroud, A. and Peytremann, C. (2004). River, reservoir and lake sediment contamination by heavy metals downstream from urban areas of Switzerland. *Lakes & Reservoirs: Research & Management*, v. 9(1), pp. 75-87.
- Yang, Y., Song, W., Lin, H., Wang, W., Du, L. and Xing, W. (2018). Antibiotics and antibiotic resistance genes in global lakes: a review and meta-analysis. *Environment International*, v. 116, pp. 60-73.
- Yang, H. and Rose, N. (2005). Trace element pollution records in some UK lake sediments, their history, influence factors and regional differences. *Environment International*, v. 31(1), pp. 63-75.
- Zhang, J. and Liu, C.L. (2002). Riverine composition and estuarine geochemistry of particulate metals in China—weathering features, anthropogenic

- impact and chemical fluxes. *Estuarine, Coastal and Shelf Sciences*, v. 54(6), pp. 1051-1070.
- Zhang, Z., Lu, Y., Li, H., Tu, Y., Liu, B. and Yang, Z. (2018). Assessment of heavy metal contamination, distribution and source identification in the sediments from the Zijiang River, China. *Science of the Total Environment*, v. 645, pp. 235-243.

Provenance of sediments and environmental risk assessment of heavy metals in the “Mis Amores” beach, Veracruz, Gulf of Mexico, Mexico

Mayla A. Ramos-Vázquez^{1,*}, John S. Armstrong-Altrin^{2,3}, Gloria D. Fernández-Guevara⁴, Jayagopal Madhavaraju⁵, Sanjeet K. Verma¹, and Rathinam Arthur James³

¹ División de Geociencias Aplicadas, Instituto Potosino de Investigación Científica y Tecnológica (IPICYT), Camino a la Presa San José 2055, San Luis Potosí 78216, México

² Universidad Nacional Autónoma de México, Instituto de Ciencias del Mar y Limnología, Unidad de Procesos Oceánicos y Costeros, Ciudad Universitaria, Ciudad de México 04510, Mexico

³ Department of Marine Sciences, Bharathidasan University, Tiruchirappalli, 620024, Tamil Nadu, India

⁴ Posgrado en Ciencias del Mar y Limnología, Universidad Nacional Autónoma de México, Ciudad Universitaria, 04510 Mexico City, CDMX, Mexico.

⁵ Estación Regional del Noroeste, Instituto de Geología, Universidad Nacional Autónoma de México, E-mail address: mayla.ramos@ipicyt.edu.mx

ABSTRACT

In this study, grain-size, mineralogy, and geochemistry of Mis Amores (MA) beach sediments, Tuxpan, Veracruz State, Gulf of Mexico are analyzed. The textural parameters reveal that the sediments are fine-grained and vary from well-sorted to very well-sorted nature. The SEM-EDS analysis reveal that the sediments are abundant in minerals such as quartz, alkali feldspars, zircon, ilmenite, and pyroxene. Geochemically, the sediments are classified as sub-arkose type. The Chondrite normalized rare earth elements (REE) pattern suggest that the source area is dominated by felsic and intermediate igneous rocks ($Eu/Eu^* = 0.90 - 1.19$, number of samples $n = 16$). The provenance discrimination diagrams indicated that the MA sediments were derived by the weathering of felsic igneous rocks, probably from the Trans Mexican Volcanic Belt. The results of this study reveal that the Tuxpan River played an important role in delivering sediments to the MA beach area.

The environmental indices suggest that the sediments are moderately contaminated by Zn and moderate to extremely contaminated by Cu and As. The Cu (> 84%) and Zn (> 82%) concentrations are predominantly associated with the exchangeable fraction, which are readily bioavailable. Cu, As, and Zn in the MA sediments were derived from the agricultural activities and waste water discharges from the sanitary network of the Tuxpan town and port.

Keywords: Environmental pollution, provenance, clastic sediments, heavy metals, tectonic setting

INTRODUCTION

Coastal or transitional environment constitutes the limit between continental and marine environments, which are active due to tides, rivers, wave and wind actions (Martínez et al., 2007; Davis and Fitzgerald, 2020). Many studies during the last decade have focused on the characterization of coastal sediments (Bela et al., 2023; Ramos-Vázquez et al., 2022). These studies discussed the provenance changes due to coastal processes (erosion and accretion), precipitation, river and coastal runoff, compositional variations and, biological and anthropogenic factors due to industrial and agricultural activities.

The detrital sediments are the products of weathering, erosion, and transport. Geochemical

properties of clastic sediments may be modified during alteration and metamorphism; however, the immobile trace and REE concentrations can be utilized to infer provenance (Tawfik et al., 2018; Nikunj et al., 2023; Paul et al., 2023). The mineralogical components and heavy mineral assemblages in sediments are useful to determine their provenance (Resmi and Achyuthan, 2018; Jiang et al., 2022). The chemical behavior of REE and their resistance to chemical mobilization in sediments have been used as provenance indicators (Ramos-Vázquez et al., 2018). In addition, provenance of sediments can be inferred through textural, mineralogical, chemical, and geochronological variations (Wang et al., 2018). There are studies focused on the mineralogical

and geochemical characteristics of beach sediments along the Gulf of Mexico (Campeche to Tamaulipas) (Tapia-Fernández et al., 2017; Armstrong-Altrin et al., 2018, 2021; Armstrong-Altrin, 2020; Ramos-Vázquez and Armstrong-Altrin, 2019, 2021). These studies also interpreted the possible contamination by heavy metals as well as the sediment provenance.

The trace metals originated due to natural (erosion and weathering) and anthropogenic (industrial and mining activities) sources can easily transfer into the marine environment, via municipal and industrial discharges (Nagarajan et al., 2019; Gülşen-Rothmund et al., 2023). Several chemical indices were utilized in various studies to calculate the enrichment of heavy metals in sediments and to differentiate the natural and anthropogenic origin of metals in sediment (Yang et al., 2021; Cai et al., 2023).

In this study, we analyzed the texture, mineralogy, and geochemical composition of sediments collected in the Mis Amores (MA) beach near Tuxpan, Veracruz State, Gulf of Mexico. The objective of this study is to infer the provenance characteristics of sediments. In addition, we utilized the chemical indices such as Enrichment Factor (EF; Zoller et al., 1974), Geoaccumulation Index (I_{geo} ; Müller, 1969), Adverse Effect Index (AEI; Long et al., 1995), and Pollution Load Index (PLI; Tomlinson et al., 1980) to identify the possible source of contaminants.

Study Area

Gulf of Mexico is a region with enormous maritime and oil exploration activities. In the southern region of the Veracruz State, pollution has increased due to the operation of petrochemical industries in the Coatzacoalcos region (Aquino-Gaspar et al., 2021). MA beach is located near the mouth of the Tuxpan River, Veracruz State, western Gulf of Mexico (Fig. 1). The Tuxpan River Basin is located in the eastern portion of Mexico, covering an area of 5837 km² of the Veracruz (72.1%), Puebla (15.2%), and Hidalgo (12.7%) States (INEGI, 2016). The tributary rivers are Pantepec, Vinazco, Buenavista, Tuxpan, and Tecomate stream (INECC, 2018).

Winds in the Gulf of Mexico have important seasonal influences. During winter, the Gulf is influenced by cold air masses coming from the north, which cause strong cold fronts (Zavala et al., 2014). During summer, the currents in the Tamaulipas and Veracruz states flow north, while in the fall and winter seasons the current flows

south until it reaches the Bay of Campeche, where it meets an opposing current that runs along the coast (Zavala et al., 2003).

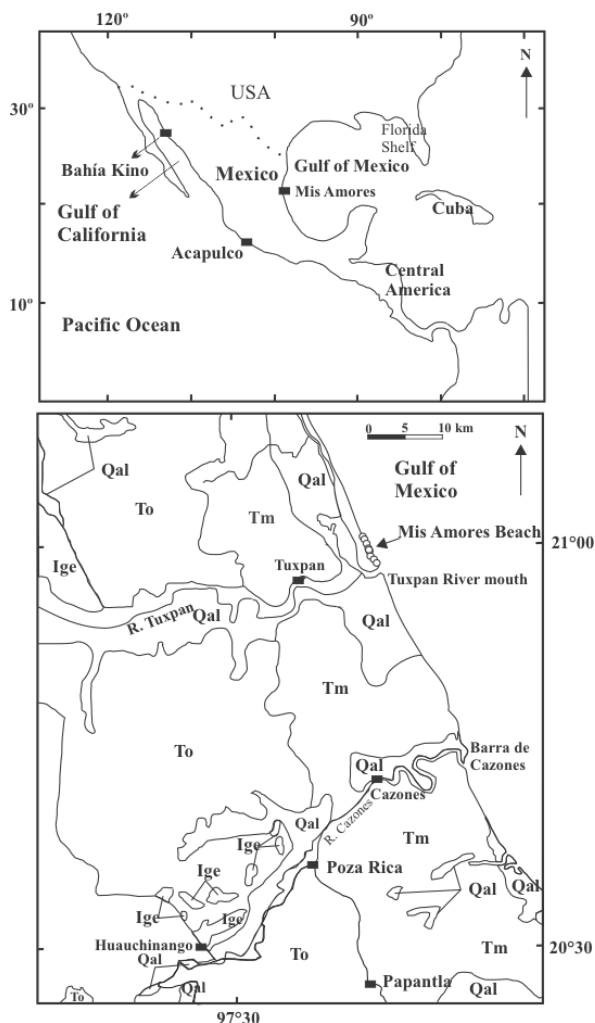


Fig. 1 Map showing sample locations in the Mis Amores beach, Veracruz State, Gulf of Mexico. Map modified after Armstrong-Altrin (2009). Volcanic and sedimentary units are: Ig = intrusive igneous rocks; Ige = extrusive igneous rocks (andesite); Jss = sedimentary rocks (lower Jurassic); Mi = intrusive rocks (Mesozoic); Pz = metamorphic rocks (Proterozoic); Qal = alluvium (Quaternary); Tiv = volcanic rocks (lower Tertiary); Tivc = volcanoclastic rocks (lower Tertiary); Tm = marine rocks (Tertiary; sandstone, mudstone); To = sandstone and limestone (Oligocene); Tsc = clastic rocks (upper Tertiary).

METHODOLOGY

Totally, 16 sediment samples, approximately 2 kg were collected in the swash zone of the “Mis Amores” beach. Granulometric analysis was carried out by the Ro-Tap Sieve Shaker located at Institute of Marine Sciences and Limnology (ICML), Mexico City. All 20 samples were air-dried and sieved through ASTM sieves for 20 minutes (No. 12, 14, 16, 20, 35, 60, 80, 100, 12, 140, 170, 200, and 230 μm).

SEM-EDS

Five selected samples were analyzed by a JEOL JXA-8900R electron microprobe, which is housed in the Institute of Geophysics, UNAM, Mexico City. Peak counting times were 40 s for each element, except for Na and K with counting time 10s.

GEOCHEMISTRY

Sixteen sediment samples were powdered by an agate mortar ($< 75 \mu\text{m}$) and their major element concentrations were determined using a Thermo Scientific Niton FXL 950 X-ray Fluorescence (XRF). Accuracy of major element analysis was monitored by an international standard JGB1 (GSJ). Loss on ignition was obtained by weighing after combustion 1 h at 1000°C . Concentrations of trace and rare earth elements were determined by a digestion method using aqua regia leach at 95°C , 0.5 g sample was digested in a microprocessor-controlled digestion block, then analyzed by the ICP-MS using a Perkin Elmer Sciex Elan 9000. The operation procedure to measure trace element concentrations was similar as detailed in Jarvis (1988). The United States Geological Survey Standard BCR-2 (Basalt, Columbia River) was used and the analytical precision of trace elements was less than 5%. Eu and Ce anomalies are calculated as $\text{Eu}/\text{Eu}^* = \text{Eu}_{\text{CN}}/[(\text{Sm}_{\text{CN}})(\text{Gd}_{\text{CN}})]^{1/2}$ and $\text{Ce}/\text{Ce}^* = \text{Ce}_{\text{CN}}/[(\text{La}_{\text{CN}})(\text{Pr}_{\text{CN}})]^{1/2}$, respectively (CN chondrite normalized values are from Taylor and McLennan 1985).

STATISTICAL ANALYSIS

Pearson’s correlation analysis was performed using Microsoft Excel 2010.

RESULTS

GRAIN SIZE ANALYSIS

The sediments are associated predominately with medium to fine-grained sand. The textural parameters like sorting, skewness, and kurtosis, reveal that the sediments are

moderately sorted, near symmetrical, and leptokurtic, respectively (Table 1).

Sample	Mz (θ)	Sorting (θ)	Skewness	Kurtosis
MA1	2.76	0.29	-0.08	1.19
MA3	2.74	0.33	-0.30	1.18
MA5	2.78	0.40	-1.26	1.06
MA7	2.75	0.32	-0.23	1.23
MA9	2.72	0.33	-0.15	0.94
MA11	2.69	0.40	-0.24	1.09
MA13	2.76	0.30	-0.13	1.03
MA15	2.73	0.37	-0.23	1.31
MA17	2.85	0.23	-0.01	0.91
MA19	2.82	0.25	-0.08	0.93
MA21	2.86	0.25	-0.04	1.05
MA23	2.83	0.24	-0.1	1.00
MA25	2.88	0.26	-0.1	1.04
MA27	2.88	0.23	-0.04	0.98
MA29	2.80	0.25	-0.07	1.02
MA31	2.88	0.24	-0.05	1.36
Mean	2.80	0.29	-0.19	1.08
SD	0.06	0.06	0.30	0.13

SEM-EDS

The mineral composition in samples MA5, MA15, MA17, and MA23 are detected by SEM-EDS. The sediments are dominated SiO_2

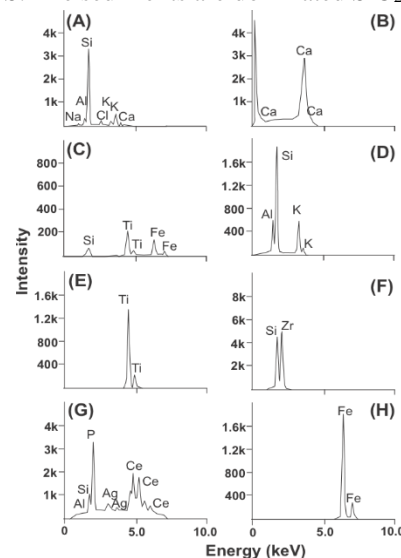


Fig. 2 SEM-EDS compositional data for the Mis Amores beach sediments, Gulf of Mexico. A) quartz and k-feldspar, B) calcite, C) ilmenite, D) k-feldspar, E) calcium sulfate, F) zircon, G) apatite, H) magnetite or hematite, and I) rutile.

content (~ 66-80%), which reveals the abundance of quartz grains (Fig. 2A). The CaO content (~ 3-11%) reveal the presence of calcite and shell fragments in sediments. In sample MA17, Al₂O₃ and K₂O concentrations vary between ~ 3% - 7% and ~ 0.8% - 2.8%, respectively, suggesting the abundance of k- feldspar. Similarly, the TiO₂ and Fe₂O₃ contents vary between 0.7% - 0.24% and 1.11% - 1.84%, respectively. Other mineral phases detected are pyroxene, monzonite, and zircon (Fig. 2 A, F and G). Peaks for sulfur and calcium are detected in samples MA5 and MA17.

GEOCHEMISTRY

The concentrations of major, trace, and rare earth elements are listed in Tables 2, 3, and 4, respectively. The sediments are enriched in SiO₂ content (~ 72.3 wt.% - 85.4 wt.%), which is followed by Al₂O₃ (mean = 5.65 wt.%) and CaO (mean = 5.26 wt.%) contents. The major element concentrations are normalized with respect to the average Upper Continental Crust (UCC) values (Fig. 3; McLennan, 2001).

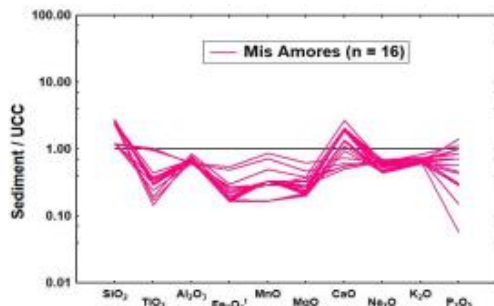


Fig. 3 Diagram showing major element concentrations normalized against average upper continental crust (UCC) values for the Mis Amores beach sediments. Average UCC values are from McLennan (2001).

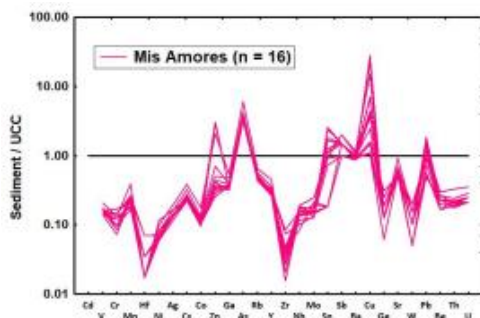


Fig. 4 Upper continental crust (UCC) normalized trace element diagram for the Mis Amores beach sediments. The average UCC values are from McLennan (2001).

The trace element concentrations are also normalized with respect to average UCC values (Fig. 4; McLennan, 2001). Relative to UCC the MA sediments are higher in Zn, As, and Cu contents, and lower in B, Sn, Sb, and B contents, suggesting a lithogenic origin (Armstrong-Altrin et al., 2019). The REE concentrations are normalized with respect to the average Chondrite values (Fig. 5; McLennan, 2001). The Chondrite normalized REE patterns consist slightly negative and positive europium anomalies, and are depleted with respect to UCC (Fig. 5).

ENVIRONMENTAL INDICES

The environmental indices such as EF (Zoller et al., 1974), I_{geo} (Müller, 1969), AEI (Long et al., 1995), and PLI (Tomlinson et al., 1980) were utilized in various studies to assess the pollution level of marine and lake sediments (Ramos-Vázquez et al., 2017; Madadi et al., 2023). In this study, we utilized these environmental indices to infer the variations in elemental concentrations, toxicity, and ecological

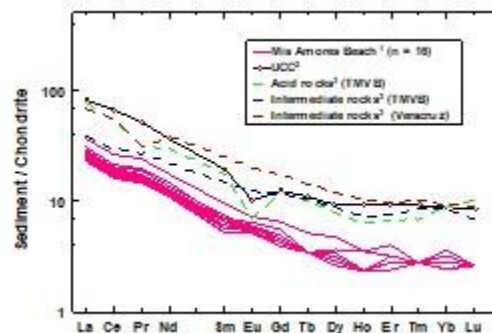


Fig. 5 Chondrite-normalized REE patterns for the Mis Amores beach sediments. Average composition of source rocks: ¹ This study, ² The average UCC values are from McLennan (2001), ³ Verma (2015)

state. According to the obtained values, in Table 5, we assigned different colors to identify the level of contamination, i.e. yellow corresponds to slight enrichment, orange indicates moderate enrichment, and red indicates strong to extreme enrichment.

The EF values vary from 1.21 to 1.57 for Cd (in all samples), 1.27 to 1.43 for Ba (in all samples), and 1.11 to 2.52 for Pb (only in 11 samples). The values with extreme enrichment are in elements Cu (1.49 - 41.47), As (7.19 - 4.86), and Zn (0.37 - 4.28). However, an enrichment is not identified for the elements Cr, Ni, Co and V.

On the other hand, I_{geo} indicated a possible contamination for Zn, Cu, and As with different degrees, i.e. moderate contamination for

Zn and As. However, Cu indicates contamination in 11 samples with a range between moderate to extreme (average $I_{geo} = 2.2$). The adverse effect index calculated based on the NOAA reference Tables (with respect to ERL) indicates potentially toxic effects to organisms by Cu in 13 samples (Fig. 6), which is consistent with the I_{geo} results. The PLI reveal that there is a higher pollutant load in a few samples. Based on the environmental indices the trace metals contamination can be ranked in decreasing order: Cu > As > Zn > Cd > Ba.

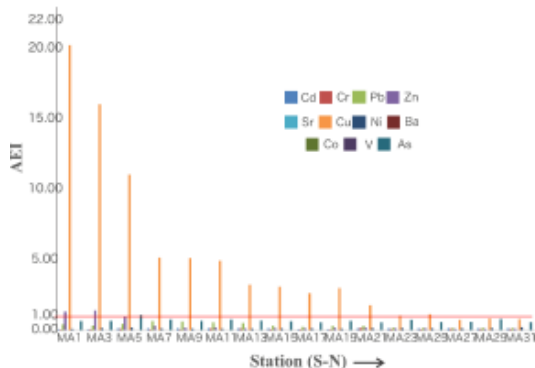


Fig. 6 Adverse Effect Index (AEI) in the Mis Amores beach sediments, Veracruz State, Gulf of Mexico.

DISCUSSION

The grain size variations can provide information on the origin and paleoenvironment. Some authors documented that poorly sorted

sediments with positive skewness values are indicators of aeolian transport (Xiong et al., 2010; Jian-Wu et al., 2013). The fine-grained sediments in the MA beach indicate a constant reworking of sediments in the foreshore region due to wind and wave actions. About 16 samples in the MA beach are well-classified, which is probably due to the oscillatory movement of water in the break zone that tends to separate suspended particles (fine-grained) from coarse-grained particles (transported as bed load). On the other hand, the combination of well-classified and very well-classified in samples MA5 and MA11 represent the high influence of wind action. 5 samples are categorized as leptokurtic and 11 as mesokurtic, suggesting long transport of sediments and long distance between the source area and the coast.

The SEM-EDS analysis suggests the abundance of minerals like quartz, calcite,

ilmenite, magnetite, titanite, pyroxene, feldspar-K, apatite, and zircon in sediments (Fig. 2A-G). These minerals are detected due to the elevated concentrations of elements like Fe_2O_3 , MnO, TiO_2 , SiO_2 , CaO, (Ce, La, Pr, Nd, Th, and Y), PO_4 , and $ZrSiO_4$. Enrichment of some rare earth elements is probably due to the abundance of apatite in sediments.

The SiO_2 content shows negative correlation with elements like Al_2O_3 , MgO, K_2O , TiO_2 , V, Sr, Rb, REEs, Yb, and Th, which indicates that SiO_2 is controlled by quartz (Ekoa Bessa et al., 2021a). Relative to UCC the MA sediments are enriched in SiO_2 and CaO contents and depleted in remaining elements. The Al_2O_3/TiO_2 ratio values vary from ~ 30.6 to 104.5 and are > 28, which suggests that the sediments

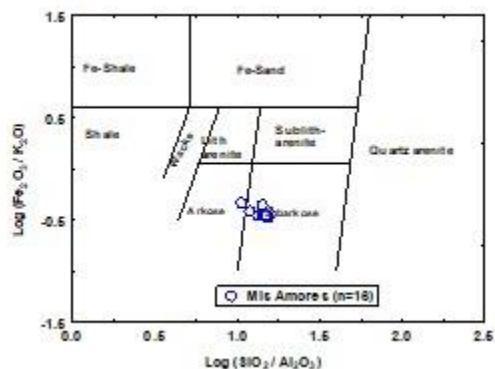


Fig. 7 Geochemical classification of sediments based on $\log(SiO_2/Al_2O_3)$ and $\log(Fe_2O_3/K_2O)$ ratios (Herron, 1988).

were derived from felsic rocks (Girty et al., 1996). Based on the geochemical classification of Herron (1988), the sediments are classified as subarkose (Fig. 7), suggesting that the sediments are geochemically mature and consistent with the high SiO_2 content (> 75%). A modified weathering index Chemical Index of Weathering ($CIW = 80.2 - 86.3$) demonstrates a highly weathered sediments derived from a distance source.

The positive correlation of Ba versus K_2O ($r = 0.95$; $n = 16$) and Al_2O_3 versus K_2O (0.98 ; $n = 16$) reveals their association with k-feldspars (Armstrong-Altrin et al., 2021, 2022). In addition, the positive correlation of Ca against Sr, Rb, and Ba ($r = 0.89$, $r = 0.61$, $r = 0.59$; respectively; $n = 16$) suggests metal exchange among minerals.

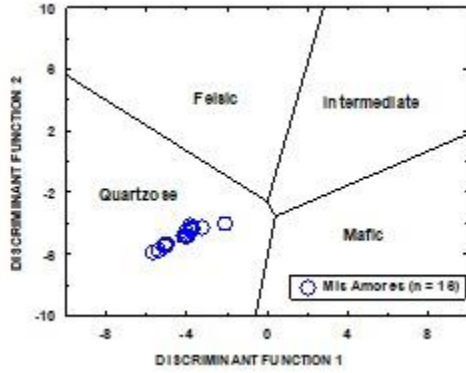


Fig. 8 Provenance discriminant function diagram of Roser and Korsch (1988). The discriminant functions are: Discriminant Function 1 = $(-1.773 \times \text{TiO}_2) + (0.607 \times \text{Al}_2\text{O}_3) + (0.760 \times \text{Fe}_2\text{O}_3) + (-1.500 \times \text{MgO}) + (0.616 \times \text{CaO}) + (0.509 \times \text{Na}_2\text{O}) + (-1.224 \times \text{K}_2\text{O}) + (-9.090)$; Discriminant Function 2 = $(0.445 \times \text{TiO}_2) + (0.070 \times \text{Al}_2\text{O}_3) + (-0.250 \times \text{Fe}_2\text{O}_3) + (-1.142 \times \text{MgO}) + (0.438 \times \text{CaO}) + (1.475 \times \text{Na}_2\text{O}) + (1.426 \times \text{K}_2\text{O}) + (-6.861)$.

TiO₂, Fe₂O₃, MnO, and MgO in sediments represent mafic minerals such as magnetite, ilmenite, and rutile (Mohanty et al., 2023). Similarly, enrichment of Ba, Cu, and Zn contents is characteristics of felsic igneous rocks (Tiju et al., 2018). On the provenance discrimination diagram of Roser and Korsch (1986) (Fig. 8), the sediments are classified as felsic igneous and quartzose sedimentary provenances.

Trace element concentrations in clastic sediments are highly useful tool to infer their origin, because incompatible trace elements (Th, U, Pb, Rb, Sr, and Ba) are enriched in sediments derived from felsic igneous rocks, while compatible elements (Ni and Cr) are enriched in mafic igneous rocks (Cullers and Podkovyrov, 2000; Ramos-Vázquez and Armstrong-Altrin,

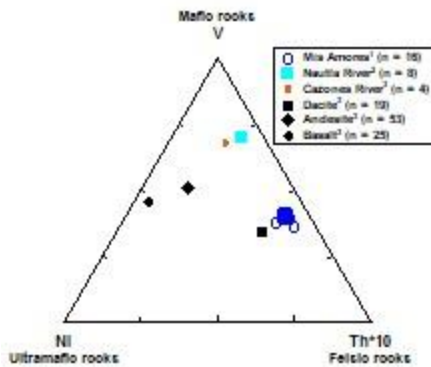


Fig. 9 Ni-Th*10-V ternary diagram for the Mis Amores beach sediments (after Bracciali et al., 2007). Average composition of source rocks: ¹ This study, ² Armstrong-Altrin et al. (2021); ³ Armstrong-Altrin (2009)

2021). The ternary diagram based on trace elements like Ni, Th, and V (Bracciali et al., 2007) reveals a felsic source rock, similar to dacite for the MA beach sediments (Fig. 9). For comparison, on the Ni-Th*10-V ternary diagram the trace element contents of the nearby Nautla and Cazonas River samples and source rocks adjacent to the study area are also included (Armstrong-Altrin, 2009) (Fig. 9). The Ni-Th*10-V ternary diagram reveals that the sediments were possibly derived from felsic igneous rocks. This interpretation is consistent with the geology of the Gulf of Mexico coastal area. According to the obtained results, we infer that the source of sediments is dacites and rhyolites in the Trans-

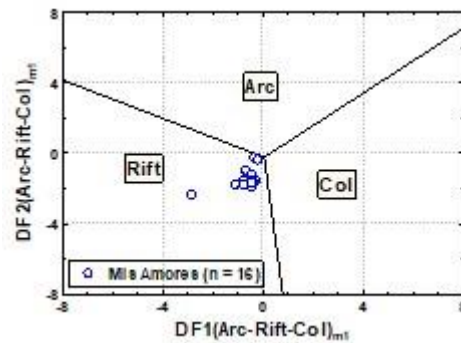


Fig. 10 Tectonic discrimination diagram for the high-silica clastic sediments ($\text{SiO}_2 > 63$ wt. %; Verma and Armstrong-Altrin, 2013). The subscript m1 in DF1 and DF2 represents the high-silica diagram based on log_e-ratios of major elements. The discriminant function equations are: $\text{DF1}_{(\text{Arc-Rift-Col})_{\text{m1}}} = (-0.263 \times \ln(\text{TiO}_2/\text{SiO}_2)_{\text{adj}}) + (0.604 \times \ln(\text{Al}_2\text{O}_3/\text{SiO}_2)_{\text{adj}}) + (-1.725 \times \ln(\text{Fe}_2\text{O}_3/\text{SiO}_2)_{\text{adj}}) + (0.660 \times \ln(\text{MnO}/\text{SiO}_2)_{\text{adj}}) + (2.191 \times \ln(\text{MgO}/\text{SiO}_2)_{\text{adj}}) + (0.144 \times \ln(\text{CaO}/\text{SiO}_2)_{\text{adj}}) + (-1.304 \times \ln(\text{Na}_2\text{O}/\text{SiO}_2)_{\text{adj}}) + (0.054 \times \ln(\text{K}_2\text{O}/\text{SiO}_2)_{\text{adj}}) + (-0.330 \times \ln(\text{P}_2\text{O}_5/\text{SiO}_2)_{\text{adj}}) + 1.588$

$$\text{DF2}_{(\text{Arc-Rift-Col})_{\text{m1}}} = (-1.196 \times \ln(\text{TiO}_2/\text{SiO}_2)_{\text{adj}}) + (1.604 \times \ln(\text{Al}_2\text{O}_3/\text{SiO}_2)_{\text{adj}}) + (0.303 \times \ln(\text{Fe}_2\text{O}_3/\text{SiO}_2)_{\text{adj}}) + (0.436 \times \ln(\text{MnO}/\text{SiO}_2)_{\text{adj}}) + (0.838 \times \ln(\text{MgO}/\text{SiO}_2)_{\text{adj}}) + (-0.407 \times \ln(\text{CaO}/\text{SiO}_2)_{\text{adj}}) + (1.021 \times \ln(\text{Na}_2\text{O}/\text{SiO}_2)_{\text{adj}}) + (-1.706 \times \ln(\text{K}_2\text{O}/\text{SiO}_2)_{\text{adj}}) + (-0.126 \times \ln(\text{P}_2\text{O}_5/\text{SiO}_2)_{\text{adj}}) - 1.068.$$

Mexican Volcanic Belt and were transported to the beach by the Nautla and Cazonas Rivers.

The REE contents of the analyzed sediments are reported in Table 4. The chondrite normalized REE patterns show fractionated LREE with negative europium anomaly (Fig. 5). The europium anomaly is dominated with a weak negative Eu anomaly ($\text{Eu}/\text{Eu}^* = \sim 0.9$ to 1.19), which signify the domination of felsic source rock with little contribution by andesites. Also, in Figure 5, we compared the REE patterns of Mis Amores sediments with felsic and intermediate rocks from the nearby Trans Mexican

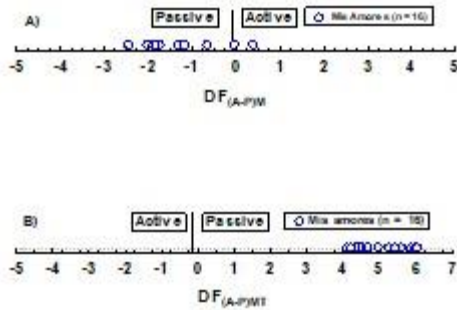


Fig. 11 A) Major element (M)-based multidimensional tectonic discriminant function diagram for the discrimination of active (A) and passive (P) margin settings (Verma and Armstrong-Altrin, 2016). The function ($DF_{(A-P)M}$) is to be calculated from the equation $DF_{(A-P)M} = (3.0005 * ilr1_{TiM}) + (-2.8243 * ilr2_{AlM}) + (-1.0596 * ilr3_{FeM}) + (-0.7056 * ilr4_{MnM}) + (-0.3044 * ilr5_{MgM}) + (0.6277 * ilr6_{CaM}) + (-1.1838 * ilr7_{NaM}) + (1.5915 * ilr8_{KM}) + (0.1526 * ilr9_{PM}) - 5.9948$

B) Major and trace elements (MT) based diagram. The function ($DF_{(A-P)MT}$) is to be calculated from equation: $DF_{(A-P)MT} = (3.2683 * ilr1_{TiMT}) + (5.3873 * ilr2_{AlMT}) + (1.5546 * ilr3_{FeMT}) + (3.2166 * ilr4_{MnMT}) + (4.7542 * ilr5_{MgMT}) + (2.0390 * ilr6_{CaMT}) + (4.0490 * ilr7_{NaMT}) + (3.1505 * ilr8_{KMT}) + (2.3688 * ilr9_{PMT}) + (2.8354 * ilr10_{CrMT}) + (0.9011 * ilr11_{NbMT}) + (1.9128 * ilr12_{NiMT}) + (2.9094 * ilr13_{VMT}) + (4.1507 * ilr14_{YMT}) + (3.4871 * ilr15_{ZrMT}) - 3.2088$. Ilr = isometric log-ratio transformation.

Belt (Verma, 2015). The similarity among REE patterns supports for a felsic provenance. The Σ REE content show a positive correlation with Al_2O_3 ($r = 0.92$; $p < 0.05$; $n = 16$), Fe_2O_3 ($r = 0.98$; $p < 0.05$), MnO ($r = 0.63$; $p < 0.05$), MgO ($r = 0.92$; $p < 0.05$) Th ($r = 0.96$; $p < 0.05$), Ba ($r = 0.83$; $p < 0.05$), Sr ($r = 0.90$; $p < 0.05$), and V ($r = 0.97$; $p < 0.05$), suggesting a similar source for these elements (Madhavaraju et al., 2021).

Furthermore, the major and trace element concentrations in clastic sediments has been widely applied to infer the tectonic setting of an unknown sedimentary basin (Bhatia, 1983; Roser and Korsch, 1986; Verma and Armstrong-Altrin, 2013, 2016). In this study, we utilized the tectonic discrimination diagrams of Verma and Armstrong-Altrin (2013, 2016) (Figs. 10 and 11A and B). On these tectonic discrimination diagrams the Mis Amores sediments plot in the rift and passive margin fields, which suggest a passive margin setting for the Gulf of Mexico sediments. This interpretation is consistent with the tectonic history of the Gulf of Mexico.

The heavy metal concentrations in beach sediments were analyzed in various studies from different parts of the world to infer the level of contamination (Ayala-Pérez et al., 2021; Ekoa Bessa et al., 2021 b). In this study, we attempt to evaluate the level of trace metal pollution in the

MA beach sediments, because we believe that the level of pollutants is increased recently due to the industrialization and uncontrolled urbanization in the coastal regions of the Gulf of Mexico. The trace element patterns normalized with respect to UCC show a notable enrichment of As, Cu, and Zn and these elements are considered as best environmental indicators (Villanueva and Botello, 1998; Velandia-Aquino et al., 2023).

The environmental indices such as EF, I_{geo} , AEI, and PLI reveal a moderate to severe enrichment for As, Zn, and Cu contents, suggesting an anthropogenic source. Sadiq (1992) and Reimann and Caritat (1998) reported that the use of pesticides, herbicides, and fungicides for agricultural activities is responsible for the enrichment of these metals in sediments. Also, an extensive occupation of land along the Tuxpan River basin for agricultural activities (43%) is increased recently. The concentration of metals Cu, As, and Zn in sediments is a potential danger to the local environment (Table 5). The tourist and urban activities in the MA beach area may be responsible for the accumulation of heavy metals in sediments. The concentration of Cu (~ 26 ppm - 690 ppm), also imply its derivation due to industrial, tourism, and recreational activities. In addition, Cu and Zn are related to wastewater discharges that may originate from the nearby Tuxpan City. Zn can be also attributed to activities in the Tuxpan port, because Zn is commonly used in the port infrastructures to prevent the corrosion by seawater (Reimann and Caritat, 1998; Zhou et al., 2024). Similarly, source of As is primarily attributed to agricultural and aqua cultural activities in the coastal area (Gustafsson and Jacks, 1995; Sun et al., 2025). Cu and Zn in sediments may derive from the anti-corrosion coatings, discarded batteries, and printing. However, evidence of contamination attributed to activities associated with oil industry is not observed in this study.

CONCLUSIONS

The Mis Amores beach sediments are very well-sorted and mineralogically mature. The textural parameters reveal a high energy beach environment. The geochemistry data reveal that the sediments were derived from the felsic igneous rocks in the Trans-Mexican Volcanic Belt and transported to the beach by the Tuxpan and Nautla Rivers. The tectonic discrimination diagrams indicated a passive margin setting, which is consistent with the general geology of the southern Gulf of Mexico.

Moderate to severe contamination of Cu, As, and Zn in sediments reflects an intense use of fertilizer and pesticides in the nearby agricultural areas. The enrichment of Zn and As are also

associated with the Tuxpan port infrastructure activities. We did not find any contamination in sediments due to oil exploration activity, although is common in the Gulf of Mexico. This study

Table 5. Comparison of trace metal concentrations in the Mis Amores beach sediments, Gulf of Mexico with environmental indices

Sample	Metal	EF	Igeo	AEI	PLI	Sample	EF	Igeo	AEI	PLI	Sample	EF	Igeo	AEI	PLI	Sample	EF	Igeo	AEI	PLI
MA1	Cd	1.53	-0.56	0.08	0.64	MA9	1.43	-0.56	0.15	0.52	MA17	1.57	-0.56	0.08	0.44	MA25	1.51	-0.56	0.15	0.40
	Cr	0.11	-4.38	0.07			0.12	-4.15	0.09			0.15	-3.96	0.10			0.14	-3.96	0.10	
	Pb	1.82	-0.31	0.44			2.47	0.23	0.64			1.11	-1.05	0.26			0.75	-1.57	0.18	
	Zn	4.30	0.93	1.35			0.53	-1.99	0.18			0.53	-2.11	0.16			0.53	-2.06	0.17	
	Sr	0.91	-1.32	N/A			0.87	-1.27	N/A			0.90	-1.35	N/A			0.75	-1.57	N/A	
	Cu	41.48	4.20	20.29			9.84	2.22	5.15			5.56	1.27	2.66			2.32	0.07	1.16	
	Ni	0.09	-4.67	0.12			0.09	-4.56	0.13			0.11	-4.37	0.15			0.11	-4.37	0.15	
	Ba	1.32	-0.77	N/A			1.39	-0.60	N/A			1.34	-0.78	N/A			1.36	-0.70	N/A	
	Co	0.14	-3.99	N/A			0.17	-3.67	N/A			0.15	-3.91	N/A			0.16	-3.82	N/A	
	V	0.21	-3.42	N/A			0.22	-3.24	N/A			0.23	-3.33	N/A			0.22	-3.33	N/A	
As	5.51	1.29	0.67	5.25	1.32	0.68	4.92	1.09	0.59	4.92	1.15	0.61								
MA3	Cd	1.31	-0.56	0.08	0.71	MA11	1.41	-0.56	0.15	0.56	MA19	1.49	-0.56	0.08	0.47	MA27	1.46	-0.56	0.15	0.38
	Cr	0.12	-3.96	0.10			0.20	-3.38	0.15			0.12	-4.15	0.09			0.19	-3.50	0.14	
	Pb	1.27	-0.59	0.36			2.19	0.08	0.58			1.31	-0.74	0.33			0.72	-1.58	0.18	
	Zn	3.88	1.01	1.43			0.70	-1.57	0.24			0.60	-1.86	0.20			0.37	-2.55	0.12	
	Sr	0.89	-1.11	N/A			0.90	-1.20	N/A			0.87	-1.33	N/A			0.75	-1.51	N/A	
	Cu	28.06	3.87	16.09			9.34	2.17	4.97			6.01	1.46	3.03			1.49	-0.52	0.77	
	Ni	0.10	-4.20	0.17			0.09	-4.56	0.13			0.10	-4.51	0.14			0.10	-4.37	0.15	
	Ba	1.38	-0.47	N/A			1.32	-0.65	N/A			1.27	-0.79	N/A			1.35	-0.67	N/A	
	Co	0.17	-3.47	N/A			0.17	-3.60	N/A			0.16	-3.75	N/A			0.14	-3.91	N/A	
	V	0.23	-3.08	N/A			0.22	-3.24	N/A			0.25	-3.16	N/A			0.21	-3.33	N/A	
As	4.79	1.32	0.68	5.89	1.51	0.78	5.45	1.32	0.68	4.86	1.18	0.62								
MA5	Cd	1.21	-0.56	0.15	0.80	MA13	1.49	-0.56	0.15	0.50	MA21	1.48	-0.56	0.15	0.47	MA29	1.49	-0.56	0.15	0.41
	Cr	0.16	-3.50	0.14			0.21	-3.38	0.15			0.24	-3.15	0.17			0.18	-3.64	0.12	
	Pb	1.56	-0.19	0.48			2.14	-0.04	0.53			1.31	-0.73	0.33			0.75	-1.55	0.19	
	Zn	2.46	0.46	0.98			0.46	-2.25	0.15			0.63	-1.79	0.21			0.41	-2.43	0.13	
	Sr	1.08	-0.71	N/A			0.91	-1.27	N/A			0.79	-1.47	N/A			0.93	-1.24	N/A	
	Cu	17.88	3.33	11.09			6.50	1.57	3.26			3.56	0.71	1.80			1.72	-0.36	0.86	
	Ni	0.12	-3.94	0.21			0.10	-4.51	0.14			0.12	-4.20	0.17			0.12	-4.20	0.17	
	Ba	1.37	-0.38	N/A			1.43	-0.62	N/A			1.38	-0.66	N/A			1.43	-0.62	N/A	
	Co	0.21	-3.09	N/A			0.16	-3.75	N/A			0.15	-3.82	N/A			0.16	-3.82	N/A	
	V	0.24	-2.87	N/A			0.22	-3.33	N/A			0.23	-3.24	N/A			0.22	-3.33	N/A	
As	7.19	2.02	1.11	5.66	1.37	0.71	4.64	1.09	0.59	6.54	1.57	0.82								
MA7	Cd	1.40	-0.56	0.15	0.57	MA15	1.48	-0.56	0.15	0.47	MA23	1.55	-0.56	0.15	0.40	MA31	1.51	-0.56	0.15	0.39
	Cr	0.12	-4.15	0.09			0.14	-3.96	0.10			0.18	-3.64	0.12			0.18	-3.64	0.12	
	Pb	2.52	0.29	0.67			1.38	-0.65	0.35			0.86	-1.41	0.21			0.71	-1.64	0.18	
	Zn	0.97	-1.09	0.33			0.53	-2.05	0.17			0.51	-2.17	0.16			0.43	-2.38	0.14	
	Sr	0.89	-1.22	N/A			0.91	-1.25	N/A			0.83	-1.46	N/A			0.77	-1.52	N/A	
	Cu	9.66	2.23	5.18			6.14	1.50	3.12			2.20	-0.04	1.07			1.63	-0.44	0.81	
	Ni	0.10	-4.41	0.15			0.10	-4.41	0.15			0.12	-4.24	0.17			0.17	-3.69	0.24	
	Ba	1.38	-0.58	N/A			1.36	-0.67	N/A			1.31	-0.79	N/A			1.32	-0.75	N/A	
	Co	0.17	-3.60	N/A			0.17	-3.67	N/A			0.15	-3.91	N/A			0.16	-3.82	N/A	
	V	0.23	-3.16	N/A			0.22	-3.33	N/A			0.21	-3.42	N/A			0.22	-3.33	N/A	
As	5.85	1.51	0.78	5.22	1.26	0.66	6.36	1.49	0.77	4.84	1.12	0.60								

Yellow = slight enrichment; orange = moderate enrichment; red = strong to extreme enrichment

reveals the importance of sediment geochemistry to infer the provenance as well as to understand the level of heavy metal contamination in beach sediments.

CREDIT AUTHORSHIP CONTRIBUTION STATEMENT

Mayla A. Ramos-Vázquez: Writing – review and editing, Investigation, Logistic fieldwork, Data curation, Methodology, Validation. **John S. Armstrong-Altrin:** Writing - review and editing, Formal analysis, Resources, Funding acquisition. **Gloria D. Fernández-Guevara:** logistic fieldwork, data curation, methodology, formal analysis, analysis. **Jayagopal Madhavaraju:** Methodology, Formal Analysis, Editing. **Sanjeet K. Verma:** Methodology, Formal Analysis, Review and Editing. **Rathinam Arthur James:** Data curation,

Methodology, Formal analysis. All authors contributed equally in writing.

DECLARATION OF COMPETING INTEREST

The authors declare that they have no known competing financial interests or personal relationship that could have appeared to influence the work reported in this paper.

ACKNOWLEDGEMENT

Ramos-Vázquez extends her gratitude to CONAHCyT for the postdoctoral fellowship (CVU: 595593). Armstrong-Altrin acknowledge the financial support extended by the CONAHCyT (no: A1-S-21287) and PAPIIT (IN-104824) projects. We are grateful to Carlos Linares López, Laura E. Gómez Lizárraga, and Arturo Ronquillo Arvizu for their laboratory

assistance during the course of this study. This work was initiated during the sabbatical period of John S. Armstrong-Altrin (2023), which was approved by DGAPA (PASPA), UNAM.

REFERENCES

- Aquino-Gaspar, H.M., Díaz-Ovalle, Ch.O., López-Molina, A., Conde-Mejía, C. and Valenzuela-Gómez, L.M. (2021). Incident analysis of the “Pajaritos” petrochemical complex. *Journal of Loss Prevention in the Process Industries*, v. 70, no. 104404.
- Armstrong-Altrin, J.S. (2009). Provenance of sands from Cazonos, Acapulco, and Bahía Kino beaches, Mexico. *Revista Mexicana de Ciencias Geológicas*, v. 26(3), pp. 764-782.
- Armstrong-Altrin, J.S. (2020). Detrital zircon U-Pb geochronology and geochemistry of the Riachuelos and Palma Sola beach sediments, Veracruz State, Gulf of Mexico: a new insight on palaeoenvironment. *Journal of Palaeogeography*, v. 9 (4), pp. 28.
- Armstrong-Altrin, J.S., Lee, Y.I., Kasper-Zubillaga, J.J., Carranza-Edwards, A., Garcia, D., Eby, N., Balaram, V. and Cruz-Ortiz, N.L. (2012). Geochemistry of beach sands along the Western Gulf of Mexico, Mexico: Implication for provenance. *Chemie der Erde Geochemistry*, v. 72, pp. 345-362.
- Armstrong-Altrin, J.S., Madhavaraju, J., Vega-Bautista, F., Ramos-Vázquez, M.A., PérezAlvarado, B.Y., Kasper-Zubillaga, J.J. and Ekoa Bessa, A.Z. (2021). Mineralogy and geochemistry of Tecolutla and Coatzacoalcos beach sediments, SW Gulf of Mexico. *Applied Geochemistry*, v. 134, no.105103.
- Armstrong-Altrin, J.S., Ramos-Vázquez, M.A., Hermenegildo-Ruiz, N.Y. and Madhavaraju, J. (2021). Microtexture and U-Pb geochronology of detrital zircon grains in the Chachalacas beach, Veracruz State, Gulf of Mexico. *Geological Journal*, v. 56(5), pp. 2418-2438.
- Armstrong-Altrin, J.S., Ramos-Vázquez, M.A., Madhavaraju, J., Marca-Castillo, M.E., Machain-Castillo, M.L. and Márquez-García, A.Z. (2022). Geochemistry of marine sediments adjacent to the Los Tuxtlas Volcanic Complex, Gulf of Mexico: Constraints on weathering and provenance. *Applied Geochemistry*, v. 141, no. 105321.
- Armstrong-Altrin, J.S., Ramos-Vázquez, M.A., Zavala-Léon, A.C. and Montiel-García, P.C. (2018). Provenance discrimination between Atasta and Alvarado beach sands, western Gulf of Mexico, Mexico: constraints from detrital zircon chemistry and U-Pb geochronology. *Geological Journal*, v. 53(6), pp. 2824-2848.
- Ayala-Pérez, M.P., Armstrong-Altrin, J.S. and Machain-Castillo, M.L. (2021). Heavy metal contamination and provenance of sediments recovered at the Grijalva River delta, southern Gulf of Mexico. *Journal of Earth System Science*, v. 130, article no. 88
- Bela, V.A., Bessa, A.Z.E., Armstrong-Altrin, J.S., Kamani, F.A., Nya, E.D.B. and Ngueutchoua, G. (2023). Provenance of clastic sediments: A case study from Cameroon, Central Africa. *Solid Earth Sciences*, v. 8(2), pp. 105-122.
- Bhatia, M.R. (1983). Plate tectonics and geochemical composition of sandstones. *Journal of Geology*, v. 91, pp. 611-627.
- Botello, A.V., Ponce-Vélez, G., Armstrong-Altrin, J.S., Fragoso, S.V. and Velandia-Aquino, L.B. (2023). Concentration of polycyclic aromatic hydrocarbons (PAHs) in sediments from the Tampamachoco lagoon, Tuxpan River mouth, Gulf of Mexico. *Arabian Journal of Geosciences*, v. 16, no. 556.
- Bracciali, L., Marroni, M., Pandolfi, L. and Rocchi, S. (2007). Geochemistry and petrography of Western Tethys Cretaceous sedimentary covers (Corsica and Northern Apennines): from source areas to configuration of margins. In: Arribas, J., Critelli, S., Johnsson, M. J. (Eds.), *Sedimentary Provenance and Petrogenesis: Perspectives from Petrography and Geochemistry Geological Society of America Special Paper*, vol. 420, pp. 73-93.
- Cai, P., Cai, G., Yang, J., Li, X., Lin, J., Li, S. and Zhao, L. (2023). Distribution, risk assessment, and quantitative source apportionment of heavy metals in surface sediments from the shelf of the northern South China Sea. *Marine Pollution Bulletin*, v. 187, n. 114589.
- Cullers, R. and Podkovyrov, V. (2000). Geochemistry of the Mesoproterozoic Lakhanda shales in southeastern Yakutia, Russia: implications for mineralogical and provenance control, and recycling. *Precambrian Research*, v. 104, pp. 77-93.
- Davis, R.A. and Fitzgerald, D.M. (2020). *Beaches and Coasts*. Wiley. 2nd edition.
- Ekoa Bessa, A.Z., Nguetchoua, G., Janpou, A. K., El-Amier, Y.A., Nguetnga, O.N.N.M., Kayou, U.R., Bisse, S. B., Mapuna, E.C.N. and Armstrong-Altrin, J.S. (2021a). Heavy metal contamination and its ecological risks in the beach sediments along the Atlantic Ocean (Limbe coastal fringes, Cameroon). *Earth Systems and Environment*, v. 5, pp. 433-444.
- Ekoa Bessa, A. Z., Paul-Désiré, N., Fuh, G.C., Armstrong-Altrin, J.S. and Betsi, T.B. (2021b). Mineralogy and geochemistry of the Ossa lake Complex sediments, Southern Cameroon:

- Implications for paleoweathering and provenance. *Arabian Journal of Geosciences*, v. 14, Article no. 322.
- Folk, R.L. and Ward, W.C. (1957). Brazos River Bar: A study in the significance of grain size parameters. *Journal of Sedimentary Petrology*, v. 27, pp. 3-26.
- Girty, G., Ridge, D., Knaack, C., Johnson, D. and Al-Riyami, R. (1996). Provenance and depositional setting of Paleozoic Chert and Argillite, Sierra Nevada, California. *Journal of Sedimentary Research*, v. 66, pp. 107-118.
- Gülşen-Rothmund, H.I., Arslan, Ş., Kurtuluş, B., Tunca, E., Avşar, U. and Avşar, Ö. (2023). Assessment of trace metal pollution in the coastal sediments of Fethiye-Göcek Bay (SW Turkey) and evaluation of pollution sources. *Marine Pollution Bulletin*, v. 186, no. 114387.
- Gustafsson, J.P. and Jacks, G. (1995). Arsenic geochemistry in forested soil profiles as revealed by solid-phase studies. *Applied Geochemistry*, v. 10, pp. 307-315.
- Herron, M. (1988). Geochemical classification of terrigenous sands and shales from core or log data. *Journal of Sedimentary Petrology*, v. 58, pp. 820-829.
- Instituto Nacional de Estadística y Geografía (2016). Estudio de información integrada de la Cuenca del Río Tuxpan. INEGI, 99.
- Instituto Nacional de Ecología y Cambio Climático (2018). Plan de Acción para el Manejo Integral de Cuencas Hídricas (PAMIC): Cuenca del Río Tuxpan. INECC, 109.
- Jarvis, K.E. (1988). Inductively coupled plasma mass spectrometry: A new technique for the rapid or ultra level determination of the rare-earth elements in geological materials. *Chemical Geology*, v. 68, pp. 31-39.
- Jian-Wu, L., Wei, Y., Gan-Lin, Z., Li-Dong, Z., Yong-Jian, J. and Zi-Tong, G. (2013). Grain Size Evidence of Multiple Origins of Red Clays in the Jinhua-Quzhou Basin, South China. *Pedosphere*, v. 23(5), pp. 686-695.
- Jiang, Ch., Li, Y., Li, Ch., Zheng, L. and Zheng, L. (2022). Distribution, source and behavior of rare earth elements in surface water and sediments in a subtropical freshwater lake influenced by human activities. *Environmental Pollution*, v. 313, no.
- Long, E.R., Macdonald, D.D., Smith, S.L. and Calder, F.D. (1995). Incidence of adverse biological effects within ranges of chemical concentrations in marine and estuarine sediments. *Environmental Management*, v. 19, pp. 81-97.
- Madadi, R., Mejjad, N. and De-la-Torre, G.E. (2023). Geochemical speciation, ecological risk, and source identification of heavy metal(loid)s in sediments and waters from Musa Estuary, Persian Gulf. *Marine Pollution Bulletin*, v. 190, no. 114836.
- Madhavaraju, J., Armstrong-Altrin, J.S., Pillai, R.B. and Pi-Puig, T. (2021). Geochemistry of sands from the Huatabampo and Altata beaches. Gulf of California, Mexico. *Geological Journal*, v. 56, pp. 2398-2417.
- Martínez, M.L., Intralawan, A., Vázquez, G., Pérez-Maqueo, O., Sutton, P. and Landgrave, R. (2007). The coasts of our world: ecological, economic and social importance. *Ecological Economics*, v. 63(2-3), pp. 254-272.
- McLennan, S.M. (2001). Relationship between the trace element composition of sedimentary rocks and upper continental crust. *Geochemistry Geophysics Geosystems*, v. 2(4).
- Mohanty, S., Adikaram, M., Sengupta, D., Madhubashini, N., Wijesiri, Ch., Adak, S., Bera, B. (2023). Geochemical, mineralogical and textural nature of beach placers, north-east Sri Lanka: Implications for provenance and potential resource. *International Journal of Sediment Research*, v. 38(2), pp. 279-293.
- Müller, G. (1969). Index of geoaccumulation in sediments of the Rhine River. *Geological Journal*, v. 2, pp. 109-118.
- Nagarajan, R., Anandkumar, A., Hussain, S.M., Jonathan, M.P., Ramkumar, Mu, Eswaramoorthi, S., Saptoru, A. and Chua, H.B. (2019). Geochemical characterization of beach sediments of the NW Borneo, SE Asia: implications on provenance, weathering intensity and assessment of coastal environmental status. In: Ramkumar, Mu, Arthur James, R., Menier, D., Kumaraswamy, K. (Eds.), *Coastal Zone Management: Global Perspectives, Regional Processes, Local Issues*. Elsevier, pp. 279-330.
- Nikunj, K., Shivam, M., Chandrakant, G. and Laxman, M. (2023). Texture and major element geochemistry of channel sediments in the Orsang and Hiren River Basins, Gujarat, India: Implications for provenance and weathering. *Journal of the Indian Association of Sedimentologists*, v. 40 (II), pp. 57-67.
- Paul, A.Q., Dar, S.A., Singh, B.P., Kumar, H. and Ahmad, M. (2023). Geochemistry of recent sediments of the Kurheri basin, Son River, Madhya Pradesh, Central India: implications for source area weathering, sediment provenance, maturity, and sorting. *International Journal of Earth Sciences (Geol Rundsch)*, v. 112, pp. 1803-1821.

- Reimann, C. and Caritat, P. (1998). Chemical elements in the environment: fact sheets for the geochemist and environmental scientist. Berlin: Springer.
- Ramos-Vázquez, M.A. and Armstrong-Altrin, J.S. (2019). Sediment chemistry and detrital zircon record in the Bosque and Paseo del Mar coastal areas from the southwestern Gulf of Mexico. *Marine and Petroleum Geology*, v. 110, pp. 650-675.
- Ramos-Vázquez, M.A. and Armstrong-Altrin, J.S. (2021). Provenance of sediments from Barra del Tordo and Tesoro beaches, Tamaulipas State, northwestern Gulf of Mexico. *Journal of Palaeogeography*, v. 10(20), pp. 1-17.
- Ramos-Vázquez, M.A., Armstrong-Altrin, J.S., Machain-Castillo, M.L. and Gío-Argáez, F.R. (2018). Foraminiferal assemblages, ¹⁴C ages, and compositional variations in two sediment cores in the western Gulf of Mexico. *Journal of South American Earth Sciences*, v. 88, pp. 480-496.
- Ramos-Vázquez, M.A., Armstrong-Altrin, J.S., Rosales-Hoz, L., Machain-Castillo, M.L. and Carranza-Edwards, A. (2017). Geochemistry of deep-sea sediments in two cores retrieved at the mouth of the Coatzacoalcos river delta, Western Gulf of Mexico, Mexico. *Arabian Journal of Geosciences*, v. 10, pp. 148.
- Ramos-Vázquez, M.A., Armstrong-Altrin, J.S., Madhavaraju, J., Gracia, A., Salas-de-León, D.A. (2022). Mineralogy and geochemistry of marine sediments in the Northeastern Gulf of Mexico. In: Armstrong-Altrin JA, Pandarinath K, Verma S. (Eds.), *Geochemical Treasures and Petrogenetic Processes*. pp. 153-183.
- Resmi, M.R. and Achyuthan, H. (2018). Lower Palar River Sediments, Southern Peninsular, India: Geochemistry, Source-Area Weathering, Provenance and Tectonic Setting. *Journal of the Geological Society of India*, v. 92, pp. 83-91.
- Roser, B. and Korsch (1986). Determination of tectonic setting of sandstone-mudstone suites using SiO₂ content and K₂O/Na₂O ratio. *Journal of Geology*, v. 94, pp. 635-650.
- Roser, B.P. and Korsch, R.J. (1988). Provenance signatures of sandstone-mudstone suites determined using discrimination function analysis of major element data. *Chemical Geology*, v. 67, pp. 119-39.
- Sadiq, M. (1992). Toxic metal chemistry in marine environments. New York: Marcel Dekker.
- Sun, Y., Zhang, X., Peng, H., Zhou, W., Jiang, A., Zhou, F., Wang, H. and Zhan, W. (2025). Development of a coupled model to simulate and assess arsenic contamination and impact factors in the Jinsha River Basin, China. *Journal of Environmental Science*, v. 147, pp. 50-61.
- Tapia-Fernandez, H.J., Armstrong-Altrin, J.S. and Selvaraj, K. (2017). Geochemistry and U-Pb geochronology of detrital zircons in the Brujas beach sands, Campeche, Southwestern Gulf of Mexico, Mexico. *Journal South American Earth Sciences*, v. 76, pp. 346-361.
- Tawfik, H.A., Salah, M.K., Maejima, W., Armstrong-Altrin, J.S., Abdel-Hameed, A-M.T. and Ghandour M.M.E. (2018). Petrography and geochemistry of the Lower Miocene Moghra sandstones, Qattara Depression, north Western Desert, Egypt. *Geological Journal*, v. 53, pp. 1938-1953.
- Taylor, S.R. and McLennan, S.M. (1985). *The Continental Crust: Its Composition and Evolution*. Blackwell Publishing, Oxford, UK, p. 312
- Tiju, I.V., Prakash, T.N., Nagendra, R. and Nagarajan, R. (2018). Sediment geochemistry of coastal environments, southern Kerala, India: implication for provenance. *Arabian Journal of Geosciences*, v. 11(61).
- Tomlinson, D.L., Wilson, J.G., Harris, C.R. and Jeffrey, D.W. (1980). Problems in the assessment of heavy metal level in estuaries and the formation of pollution index. *Helgoland Marine Research*, v. 33, pp. 566-575.
- Velandia-Aquino, L.B., Botello, A.V., Ponce-Vélez, G., Namihira-Santillán, P.E., Villanueva-Fragoso, S. (2023). Vertical Distribution of Potentially Toxic Metals and PAHs in the Alvarado Lagoon, Veracruz in the Southern Gulf of Mexico. *Estuaries and Coasts*. <https://doi.org/10.1007/s12237-023-01307-6>.
- Verma, S.P. (2015). Origin, evolution, and tectonic setting of the eastern part of the Mexican Volcanic Belt and comparison with the central American volcanic arc from conventional multielement normalized and new multidimensional discrimination diagrams and discordancy and significance tests. *Turkish Journal of Earth Sciences*, v. 24, pp. 111-164.
- Verma, S.P. and Armstrong-Altrin, J.S. (2013). New multi-dimensional diagrams for tectonic discrimination of siliciclastic sediments and their application to Precambrian basins. *Chemical Geology*, 355, pp. 117-133.
- Verma, S.P. and Armstrong-Altrin, J.S. (2016). Geochemical discrimination of siliciclastic sediments from active and passive margin settings. *Sedimentary Geology*, v. 332, pp. 1-12.
- Villanueva, F.S. and Botello, A.V. (1998). Metal Pollution in Coastal Areas of Mexico. In: Ware, G.W. (eds.) *Reviews of Environmental Contamination and Toxicology*. Reviews of

- Environmental Contamination and Toxicology, vol 157. Springer, New York, NY.
- Wang, Z., Wang, J., Fu, X., Zhan, W., Armstrong-Altrin, J.S., Yu, F., Feng, X., Song, C. and Zeng, S. (2018). Geochemistry of the Upper Triassic black mudstones in the Qiangtang Basin, Tibet: Implications for paleoenvironment, provenance, and tectonic setting. *Journal of Asian Earth Sciences*, v. 160, pp. 118-135.
- Xiong, S., Ding, Z., Zhu, Y., Zhou, R. and Lu, H. (2010). A ~ 6 Ma chemical weathering history, the grain size dependence of chemical weathering intensity, and its implications for provenance change of the Chinese loess-red clay deposit. *Quaternary Science Reviews*, v. 29(15-16), pp. 1911-1922.
- Yang, L., Ma, X., Luan, Z. and Yan, J. (2021). The spatial-temporal evolution of heavy metal accumulation in the offshore sediments along the Shandong Peninsula over the last 100 years: Anthropogenic and natural impacts. *Environmental Pollution*, v. 15(289), no. 117894.
- Zavala, J. and Morey, O'Brien (2003). Seasonal circulation on the western shelf of the Gulf of Mexico using a high-resolution numerical model. *Journal of Geophysical Research*, v. 108(C12), no. 3389.
- Zavala, J., Romero, R., Mateos, A. and Morey, S. (2014). The response of the Gulf of Mexico to wind and heat flux forcing: What has been learned in recent years? *Atmósfera*, v. 27(3), pp. 317-334.
- Zhou, Y., Du, S., Liu, Y., Yang, T., Liu, Y., Li, Y. and Zhang, L. (2024). Source identification and risk assessment of trace metals in surface sediment of China Sea by combining APCA-MLR receptor model and lead isotope analysis. *Journal of Hazardous Materials*, v. 465, no. 133310.
- Zoller, W.H., Gladney, E.S. and Duce, R.A. (1974). Atmospheric concentrations and sources of trace metals at the South Pole. *Science*, v. 183, pp. 198-200.

Depositional sequences and sea level changes during Bathonian-Oxfordian, Kutch (Kachchh) Basin, Gujarat, India

Diwakar Mishra

Department of Geology, College of Earth Sciences and Engineering, University of Dodoma, P.O Box 11090, Dodoma, Tanzania

E-mail: mishradiwakar988@gmail.com

ABSTRACT

The Kutch sedimentary basin is situated at extreme west of Indian Peninsula is an excellent example of cyclic sedimentation in Mesozoic shallow marine regime. The Bathonian to Santonian shallow marine rocks crops out in the Kutch Mainland extending for ~ 193 km from Habo in the east to Lakhpat in the west. Based on detail field studies in the Jhura dome, Kutch Mainland and laboratory investigations of 43 carbonate rock samples, the 370 m succession of carbonate-dominated rocks is stacked into three depositional sequences of regional importance. The 84 m Transgressive sequence-I of Bathonian age consisting of four microfacies assemblages represents an upward deepening facies succession. The 130 m regressive sequence of Callovian age composed of five microfacies assemblages showing upward shoaling facies succession. It was deposited during stillstand period followed by gradual increase in sediment supply. The 155 m transgressive sequence II of Early Oxfordian age consists of four microfacies assemblages that deposited during highstand of sea level in the basin together with episodic and less sediment supply. The relative sea level curves indicate high-order sea level variation during whole sequence before to major drop in sea level at the end of the transgressive sequence-II. The microfacies study reveals that these high order sequences are regionally comparable and might have been controlled by an active tectonic mechanism together with global sea level change.

Keywords: Microfacies, Depositional sequences, Sea level curve, Bathonian-Oxfordian succession, Kachchh basin.

INTRODUCTION

Geoscientific study of Kutch basin has an applied aspect (e.g., Lohani et al., 2022; Shaikh et al., 2020, 2022; Dhawale et al., 2023) to comment on hydrocarbon prospect of the terrain. The Kutch basin is located on the prime hydrocarbon belt of the western part of Indian subcontinent and it has been classified as category-II based on the degree of hydrocarbon perspectivity (Dwivedi, 2016). Following the geodynamic classification of Indian sedimentary basins, Kutch basin is a pericratonic rift basin (Biswas et al., 1993). Mesozoic shallow marine rocks of Kutch basin have been continuous focus of Oil and Natural Gas Corporation Ltd (ONGC) of India since its inception in the mid-1950. Recent hydrocarbon discoveries in the offshore and onshore of Kutch basin have presumed greater importance (Patil et al., 213). In this context is here delineated high order depositional sequences (transgressive-regressive facies) that can help to map the distribution of source and reservoir rocks in sequence stratigraphic framework. Occurrence of hydrocarbon is well known in Cenozoic high order sequences in Gulf of Mexico and Niger Delta (Amodu et al., 2022; Rassi, 2002). The distribution and heterogeneity of source rocks are well connected to various orders of depositional cycles identified in Paleozoic to Mesozoic successions (van Buchem et al., 2005).

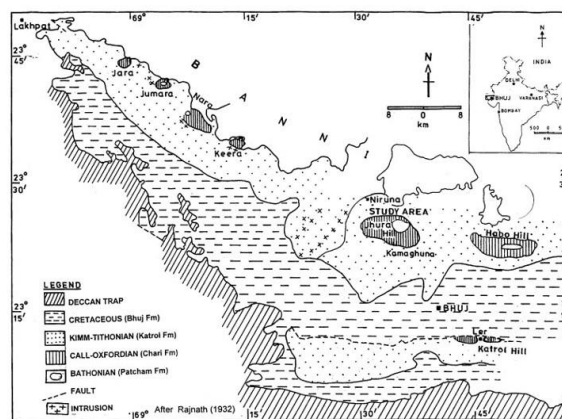


Figure. 1 Geological map of Mainland along with location of the studied section. Map modified after Rajnath (1932).

Middle Jurassic to Upper Cretaceous sedimentary successions of Kutch basin are exposed extensively in the Kutch Mainland, Wagad, the 'Islands' of Pachcham, Bela and Khadir, and the Chorar hills. The Mesozoic sedimentary successions of Kutch basin were divided into four 'Groups' namely Patcham, Chari, Katrol and Umia in ascending order by Stoliczka (Waagen, 1873), and Jhurio, Jumara, Jhuran and Bhuj formations in Mainland by Biswas (1971, 1977). Continuous succession from Bathonian to Santonian is exposed in various outcrops of Kutch Mainland. The succession is composed of most

conspicuous ridge extending for about 193 km from Habo in the east to Lakhapat in the west. Geological map of Mainland along with location of studied section is shown in Figure 1 (Rajnath, 1932) and lithostratigraphic framework of Middle Jurassic rocks of Kutch mainland in Table 1.

Table 1. Lithostratigraphic framework of Middle Jurassic rocks of the Kutch/Kachchh Mainland.			
Age	After (Krishna, 2002 integrated to Stoliczka (In Waagen 1873)		After Biswas (1977)
	Formation	Member	Formation
Callovian – Middle Oxfordian	Chari Oolite	Dhosa	Jumara
Bathonian	Patcham		Jhurio

The review of the previous literature (Biswas, 1981, 2016) reveals two distinct megacycles (second order cycles) in the Kutch basin: a transgressive cycle comprises Jhurio and Jumara formations (Patcham and Chari formations of Stoliczka, 1873) followed by a regressive cycle (Jhuran and Bhuj formations). These two lower order cycles include several high orders fluctuations of sea level. Bajocian to Oxfordian was a period of major sea level rise in Kutch graben (Krishna et al., 1983), followed by major drop in sea level till Neocomian.

Present investigation includes Patcham and Chari formations deposited during major rise in sea level and it would help in developing high order sequences in well resolve time frame (Bathonian to Early Oxfordian) which reflect regional relative sea level fluctuations. Identification of high-order tectonic sequences based on vertical facies change is a major criterion for regional correlation (Abbott and Sweet, 2000). The sequences of < 3 Ma duration are found throughout Phanerozoic would be globally correctable (Haq et al., 1988). There are four scales of sequence development in stratigraphic record related to range of time. The third order cycle varies from < 1 to ~ 10 Ma (Vail et al., 1977a). Most of the geologists assume the time durations between 0.5 and 3-5 Ma for the third order eustatic cycles. By knowing the pattern of third order depositional sequences through lithofacies analysis along with existing biostratigraphic data is providing finer stratigraphic details that recognizable across the basin. These 3rd order sequences are helpful in formulation of outcrop-based sequence stratigraphic model for Patcham and Chari formations and hydrocarbon exploration (van Buchem et al., 2002).

Previous geological studies did not distinguish microfacies in well resolve time frame of the carbonate dominated Patcham and Chari formations of Mainland of the Kutch basin. There is much scope for developing high order depositional sequences with support of biostratigraphic and genetic

sedimentological principles. Existing lower order (2nd order) Transgressive – Regressive model in the basins can be improved by considering microfacies analysis of carbonate-dominated succession. The study also attempts to document the fine stratigraphic details by establishing high order Transgressive-Regressive sequences during Bathonian to Early Oxfordian.

METHODOLOGY

This study includes detailed field and lab investigations of a single section (Badi section) of the Jhura hill. I present a stratigraphic column that shows all sedimentary features (Fig. 2). Around 43 rock samples were collected according to change in lithology. Petrographic characters of all the rocks were observed and examined under a polarizing microscope. Additionally, modal percentage of different allochems, orthochems and associated detritals were identified and counted using point counter, which helped in their classification of facies. In order to know the mineral composition of mudrocks, three samples were examined by x-ray diffraction available in the laboratory of Oil and Natural Gas Corporation Ltd. (ONGC) Dehradun, India.

RESULTS MICROFACIES DESCRIPTION OF GRAINSTONES (A):

This is the most abundant and frequently occurring lithofacies in the Patcham Formation and is interbedded with calcareous mudstone and well observed in Badi section. It is characterized by grain-supported fabric and on the basis of types of allochems, orthochems and their relative abundances Dunham (1962), this lithofacies has been divided into four microfacies which are described below:

Oolitic fossiliferous grainstone (A₁):

It is very thickly bedded and contains well preserved fossils and ooids. Fossils are mostly mollusks and foraminifera. These fossils are commonly coated with ferruginous material. Good preservation of few mega fossils has also been noticed. Spherical to elliptical shaped ooids having 0.2 to 0.4 mm diameters are commonly present. Few ooids with quartz nucleus are well preserved. (Plate 1A). Fossils and ooids are cemented by spiritric materials. Modal analysis of this microfacies was carried out to identify the precise percentage of framework grains. The result is as follows: fossils – 64.9%, ooids – 10.8%, intraclasts – 3.8 %, peloids – 1.5 %, spars 17.8 % and terrigenous clasts – 1.3% (Table 2).

Intraclastic grainstone (A₂):

The main components of this microfacies are micritic intraclasts and larger foraminifers. Bioturbations are frequently observed. Micritic

Table 2. Modal Composition of grainstones (% by vol.)										
S.No	Sample No.	Allochems					Orthochems		Total	Dunhm's nomenclature
		Ooid	Fossil	Intraclast	Peloid	Sand	Micrite	Spar		
1	S-99/124	11.3	64.5	3.4	1.5	1.8	-	17.5	100	Oolitic Fossiliferous Grainstone (A ₁)
2	S-99/143	10.2	62.7	4.0	3.0	1.0	-	19.1	100	
3	S-99/144	10.8	67.5	4.5	0.0	1.4	-	16.8	100	
	Average	10.8	64.9	3.8	1.5	1.3	-	17.8	100	
4	S-99/104	-	7.1	45.0	-	1	-	46.7	100	Intraclastic Grainstone (A ₂)
5	S-99/105	-	6.5	45.7	-	-	-	47.6	100	
6	S-99/111	-	7.0	46.5	-	-	-	46.0	100	
	Average		6.82	45.7	-	1.28		46.16	99.72	
7	S-99/150	2.5	20.0	4.2	-	40.7	-	35.6	100	Bioclastic Grainstone (A ₃)
8	S-99/149	6.0	32.4	10.5	-	9.0	-	42.1	100	
9	S-99/148	4.5	27.3	8.4	-	8.5	-	47.3	100	
	Average	4.3	26.5	7.7		19.4		41.6	99.9	
10	S-99/116	2.5	65.7	4.2	1.5	5.5	-	20.6	100	Fossiliferous Grainstone (A ₄)
11	S-99/126	19.5	51.0	2.0	1.0	7.0	-	19.5	100	
12	S-99/137	1.5	67.5	4.8	5.5	2.0	-	18.9	100	
13	S-99/142	0.3	68.2	9.8	3.1	1.5	-	17	100	
	Average	5.9	63.1	5.2	2.7	4.0		19	100	

intraclasts are (sub)spherical. These allochems are bounded by microsparitic orthochems (Plate 1B). Modal analysis of this microfacies is as follows: 6.82 % fossils, 45.7 % intraclasts, 1.2% sand and 46.16% spar (Table 2).

Bioclastic grainstone (A₃):

It is characterized by mostly shell fragments and terrigenous materials and few percentages of ooids (Plate 1C). These fragments are cemented by coarsely crystalline carbonate materials. Fossil fragments are mostly mollusks and echinoids. Modal analysis exhibits fossil fragments – 26.5 %, sand – 19.4%, intraclasts – 7.7%, ooids- 4.3% and spars – 41.6 % (Table 2).

Fossiliferous grainstone (A₄):

It is thinly bedded, moderately bioturbated and contains well preserved megafossils (mollusks and echinoids) and coarser clastic materials of 0.5 cm to 2 cm diameter (Plate 1D). Few clastic materials of 2 to 5 cm diameter are present. However, well rounded pebbles are commonly noticed. Modal analysis reveals the percentages of the following: fossils - 63.1%, intraclasts - 5.2%, ooids - 5.9%, peloids - 2.7%, sand - 4% and spar - 19.0% (Table 2).

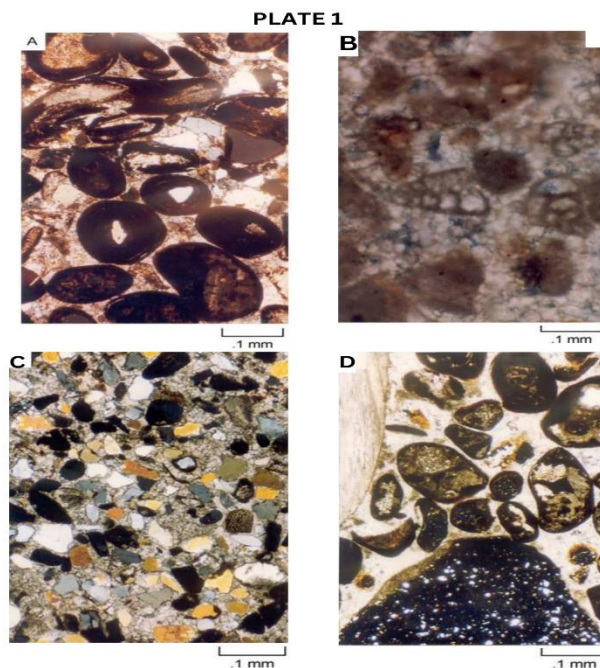


Plate 1. Photomicrograph showing petrographic types of grainstones: A - Oolitic fossiliferous grainstone, B - Intraclastic grainstone, C - Bioclastic grainstone, D- Fossiliferous grainstone.

S/N	Sample No	Allochems				Sand	Orthochems		Total	Dunham's nomenclature
		Ooid	Fossil	Int	Pel		Micrite	Sp.		
1	S-99/65A	53.65	-	-	-	-	46.34	-	100	Oolitic Packstone: (B₁)
2	S-99/65B	53.95	3.8	-	-	1.3	40	-	100	
3	S-99/67	46.95	1.0	-	-	6.4	45.5	-	100	
	Average	51.46	1.6	0	0	2.5	43.9		100	
4	S-99/68	33.9	11.9	-	-	8.7	45.4	-	100	Bioclastic Oolitic Packstone: (B₂)
5	S-99/70	44.6	9.1	-	-	11.2	37.1	-	100	
6	S-99/161A	32.5	9.2	-	-	9.2	47.27	-	100	
	Average	36.98	10.1			9.7	43.25		100	
7	S-99/76	1.0	24.9	-	-	19.0	55	-	100	Fossiliferous Packstone: (B₃)
8	S-99/79	2.2	37.4	-	-	10.3	50	-	100	
9	S-99/81	1.0	30.5	-	-	13.4	55	-	100	
	Average	1.4	30.9			17.6	53.3		100	
10	S-99/96	-	69.5	-	-	-	32.4	-	100	Bioclastic Packstone: (B₄)
11	S-99/97	-	66.5	-	-	-	33.4	-	100	
12	S-99/98	0.5	65.5	-	-	-	33.7	-	100	
13	S-99/99	7.5	38.8	-	-	4.3	49.2	-	100	
14	S-99/101A	4.6	44.3	-	-	4.9	45.8	-	100	
15	S-99/101B	3.5	45.5	-	-	3.5	47	-	100	
16	S-99/101C	7.5	42.0	-	-	3.3	47.2	-	100	
	Average	3.08	53.15			2.9	41.2		100	

oids-51.46%, micrite- 43.9%, fossil fragments-1.6%, terrigenous constituents-2.54% (Table 3).

MICROFACIES DESCRIPTION OF PACKSTONES (B):

This lithofacies are mainly confined to the upper part of the Chari Formation and normally interbedded with siltstone. It is distinguished by grain-supported textures and contains ~ 60-65% allochems consisting of ooids, shell fragments and terrigenous clasts of various size grade embedded in micritic matrix. Based on the present allochems and orthochems and their relative abundances (Dunham, 1962), this lithofacies has been divided into four microfacies as follows.

Oolitic packstone (B₁):

This microfacies is very thin and observed in the uppermost bed of Dhosa Oolite member exposed in Kutch Mainland. It contains boulders, cobbles and pebbles within the fine-grained calcareous sandstone/siltstone, mudstone and ironstone. These fragments are subangular to subrounded and embedded in an oolitic micritic matrix. This microfacies is composed of mostly allochems consisting of ooids and few shell fragments. On the basis of occurrence of various allochems, the rock can be named as oolitic packstone. The size of ooids varies from 0.25 to 1.0 mm and are mostly ellipsoidal. Ooids are highly ferruginised and their color varies from deep brown to light yellow. These are concentric and have heterogeneous nucleus. Shell fragments include mollusks, echinoderms, brachiopods and coated with iron oxide. Modal analysis reveals the presence of

Bioclastic oolitic packstone (B₂):

It is the most abundant and frequently occurring microfacies in the Dhosa Oolite Member. The Bioclastic oolitic packstone is hard and compact, generally of light yellow / yellowish brown in colour containing deep brown ooids. This microfacies shows rhythmic alternations with soft beds of siltstone (C₁). These are present just below the oolitic packstone microfacies in the Badi section. The Bioclastic oolitic packstone contains significant amount of shell fragments and sand size clastics and differs from normal oolitic packstone. It is a grain-supported oolitic carbonate rock and is made up of monocrystalline quartz, feldspars and ooids embedded in a microcrystalline carbonate matrix (Plate 2A). Modal analysis of bioclastic oolitic packstone was carried out to know the percentage distribution of various constituents. The study reveals the presence of ooids 36.98 %, micrite-43.25%, sand – 9.7% and shell fragments – 10.06 % (Table 3).

Fossiliferous packstone (B₃):

This microfacies is typically developed in the lower part of Dhosa Oolite member and interbedded with gypsiferous mudstone (C3). The Fossiliferous packstone contains appreciable number of well-preserved fossils and sand size clastics. Besides, ooids are also observed in few slides but their percentage is very less. The allochems are embedded in micritic matrix (Plate 2B). Modal analysis of sandy fossiliferous packstone reveals the presence of fossils-

30.9%, sand (quartz and feldspar) – 17.6 %, micrite- 53.33% and ooids – 1.4% (Table 3).

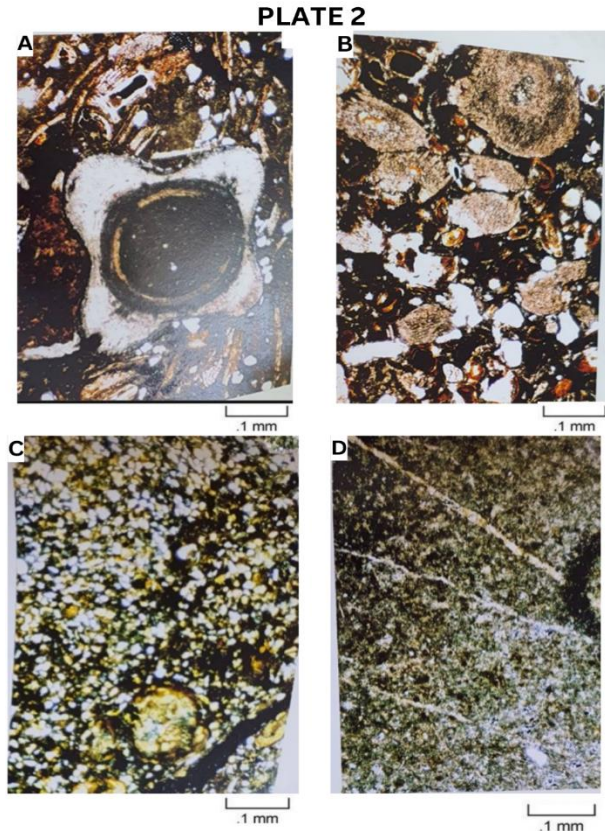


Plate 2. Photomicrographs exhibit packstone and mudrock types: A - Bioclastic oolitic packstone, B - Fossiliferous packstone, C - Siltstone, D - Calcareous mudstone.

Bioclastic packstone (B₄):

It is one of the significant microfacies of Dhosa Oolite member and interbedded with siltstone (C₁). Shell fragments and subspherical to elliptical, subrounded pebbles of ironstone, calcareous mudstone with ferruginous coating form the framework of the rock which are cemented by fericite. Thin section study shows that this rock is rich in shell fragments, mostly of bivalves. Internal fabric of shell fragments is partially preserved and consists of micrite or microsparite. Thin section study of bioclastic packstone reveals the presence of fossil fragments- 53.15%, ooids- 3.08%, micrite – 41.2% and terrigenous clastics like quartz, feldspars- 2.28% (Table 3).

MICROFACIES DESCRIPTION OF MUDROCKS (C):

It is most abundant lithofacies in the Patcham and Chari Formations and occurs in association with different types of limestone and sandstone microfacies. This lithofacies is generally bioturbated

except in the case of gypsiferous mudstone which are thinly bedded to laminated and nodular/concretionary in nature. Murdock's are mostly fragile weathered fine grained moderately compact to soft and variable in color e.g., earthy / yellowish brown / light and dark grey. In the present study classification of argillaceous rock proposed by Blatt et al. (1980) has been followed. The result of x-ray diffraction (XRD) shows that chlorite and illite-mica are dominant in siltstone and comparatively low in gypsiferous mudstone. Montmorillonite is present mainly in calcareous mudstone and as a minor constituent in siltstone. Identified minerals with their respective peak values obtained from the analysis are shown in Table 4. This lithofacies is divided compositionally into following three microfacies. The microfacies are described below:

Siltstone (C₁):

It is thinly bedded to laminated in lower part of the sequence and highly disrupted by biological reworking in the upper part. Siltstone is brown moderately compact weathered and contains calcareous nodules at places. The siltstones are fine-grained clastics dominating over clay and show moderate to poor sorting. Fine clastic materials are floated in clayey matrix. Muscovite is the common mica present in the rock (Plate 2C). Mineralogically it is composed of 65 to 70% silt-sized detritals like quartz, feldspars and some limestone clasts. Clay mineral (illite- mica, chlorite and montmorillonite) from 25 to 30%. Other accessories like iron oxide, shell fragments and heavy minerals constitute < 5% of the rock.

Calcareous mudstone (C₂):

This microfacies is bioturbated, greenish grey color, rich in micro- fossils and contains marly concretions. The calcareous materials are predominant over argillaceous materials. Micritic and pelletic material are homogeneously distributed in the microfacies. Some fragments can also be observed (Plate 2D). Mineralogically, calcareous mudstone is composed of mainly calcite and little montmorillonite.

Gypsiferous mudstone (C₃):

This microfacies is yellowish brown to grey, massive and at places parallel laminated. Field observation reveals the interlayering of thinly bedded to laminated mudstone and gypsum. In Badi section, ~ 1 cm thick gypsum layer and ~ 7 cm laminated mudstone are distinctly observed in nala cutting. Gypsiferous mudstones at times contain calcareous and ferruginous nodules of various shape and sizes. Mineralogical composition of this microfacies indicates gypsum as the dominant constituent besides

Table 4. X-ray diffraction analysis of mudrocks (C)							
Microfacies	Sample Number	Montmorillonite	chlorite	Illite-Mica	Calcite	Quartz	Gypsum
Siltstone (C ₁)	S-99/99	15.09 (885)	7.008 (733) 3.55 (648)	9.92 (584) 4.92 (474) 4.42 (467)	3.01 (518)	3.31 (496) 4.16 (496)	
Calcareous mudstone (C ₂)	S- 99/105	14.92 (448)			3.02 (1796) 3.82 (302)	3.32 (783) 422 (308)	
Gypsiferous mudstone (C ₃)	S- 99/77B		7.04 (372) 3.54 (334)	4.42(346)		3.32 (1264) 4.24 (815)	7.47 (1726) 3.04 (720) 3.75 (524) 2.85 (400) 2.66 (435) 2.77 (258)

chlorite and illite- mica. The character of detritals is similar as in the siltstone. Only the occurrence of subhedral grains of gypsum and abundance of argillaceous matrix distinguishes this rock from siltstone. Gypsum is distinctly observed and its percentage is quite high. Ferruginised carbonate pellets are uniformly distributed in the rock (Plate 3A).

MICROFACIES DESCRIPTION OF SANDSTONES (D):

The sandstones are interbedded with siliceous mudrocks and occur in the Chari Formation. This lithofacies is thickly to thinly bedded, coarse to fine grained, hard and compact but at times highly weathered and fragile. The regular increase in thickness of the bed can be observed in the section. The petrographic description of various microfacies types is given below:

Medium to coarse grained sandstone (D₁):

This microfacies is thickly to thinly bedded, medium to coarse grained, hard and compact and exhibit a range of colors from dirty yellow to reddish brown and grey. Calcareous variety of sandstones predominate over argillaceous and siliceous. Fossil fragments are commonly present in the sandstones. Microscopic examination reveals that the dominant constituents of the sandstones are quartz, feldspars, rock fragments, mica, and shell fragments lithified by calcareous, argillaceous and ferruginous cementing material (Plate-3B). Thin section study reveals the presence of quartz 79.95%, feldspars 14.57% and rock fragments 5.30% (Table 5).

Fine-grained sandstone (D₂):

This microfacies is thinly bedded and mostly fine grained. The grains are moderately to poorly sorted except few samples which show well sorting. The detritals are mostly floating in the calcareous cement. In some of the samples, the cementing material is coarsely crystallized calcium

carbonate (sparite). The dominant constituents of the sandstones are quartz, feldspars, rock fragments, mica, and shell fragments lithified by calcareous, argillaceous and ferruginous cementing material (Plate 3C).

Pebbly cherty calcilithite (D₃):

This sandstone is thinly bedded, pebbly to very coarse grained and showing reverse grading. Among the rock fragments, chert, phyllite, quartzite, granite, limestone, dolerite and basalt are common

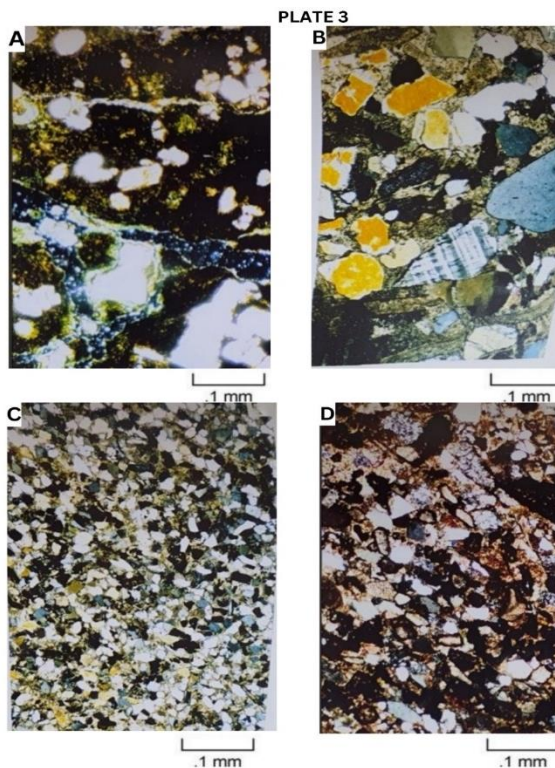


Plate-3 Photomicrographs: A - Gypsiferous mudstone and sandstone types: B - Medium to coarse-grained sandstone, C - Fine-grained sandstone, D - Pebbly cherty calcilithite.

(Plate 3D). The size of igneous and metamorphic fragments varies from 0.8 to 2.5 mm whereas the average size of sedimentary rock fragments (limestone and chert) is 0.5 mm. The rock fragments are mostly subangular and subrounded. Modal analysis reveals the presence of quartz 28.05%, feldspars 10.55% and rock fragments 61.25% (Table 5).

MICROFACIES ASSEMBLAGE:

On the basis of detailed field studies in Jhura dome, Kutch Mainland and lab investigation, the 370 m succession of rocks is stacked in to various microfacies assemblages that refers to the architecture of vertical succession of depositional sequences (fig.2). The total of 13 microfacies assemblages were identified: The lower 84 m consisting of four microfacies assemblages:

- (i) oolitic fossiliferous grainstone - bioclastic grainstone (A₁-A₃),
- (ii) oolitic fossiliferous grainstone - calcareous mudstone (A₁-C₂),
- (iii) fossiliferous grainstone - calcareous mudstone(A₄-C₂),
- (iv) intraclastic grainstone - calcareous mudstone (A₂-C₂). The middle 130 m composed of five microfacies assemblages: (i) fine grained sandstone - siltstone (D₂ – C₁), (ii) bioclastic packstone – siltstone (B₄-C₁), (iii) pebbly cherty calcilithite microfacies (D₃), (iv) gypsiferous mudstone - fine grained sandstone (D₂ – C₃), (v) medium to coarse grained sandstone microfacies (D₁) and the upper 155 m consists of four microfacies assemblages: (i) gypsiferous mudstone-medium to fine grained sandstone (D₂-C₃), (ii) fossiliferous packstone - gypsiferous mudstone (B₃-C₃), (iii) bioclastic oolitic packstone – siltstone (B₂ –C₁), (iv) oolitic packstone microfacies (B₁).

DISCUSSIONS

Depositional Sequences and Relative Sea level changes

On the basis of detailed field studies, lab investigations, the succession of present area is stacked into three third order depositional sequences. The stacking pattern of microfacies assemblages comprises to the architecture of a vertical succession of depositional sequences. Transgressive sequence- I, Regressive sequence and Transgressive sequence-II stacking patterns can be recognized (Fig.2). In Transgressive sequence-I, the microfacies assemblage become more distal upward or representing an

upward-deepening facies succession. In Regressive sequence, the microfacies assemblage become more proximal upward to or showing an upward-shoaling facies succession and in Transgressive sequence-II, the facies showing upward deepening facies

Table 5. Modal composition of sandstones (excluding cement, micas and accessories) (% by vol) (D₁)

S/No	Sample No.	quartz	feldspar	Rock Fragments	Total	Maturity Index
1	S- 99/82	80.3	15.5	4.1	99.9	4.09
2	S-99/84	82.3	13.8	3.7	99.8	4.70
3	S-99/85	77.5	18.0	4.0	99.5	3.52
4	S-99/87	85.8	11.2	2.9	99.9	6.08
5	S-99/89	83.9	10.3	5.7	99.9	5.24
6	S-99/90	86.0	9.3	4.5	99.8	6.23
7	S-99/91	75.6	20.3	4.0	99.9	3.11
8	S-99/162	69.8	17.8	12.3	99.9	2.31
9	S-989168	78.4	15.0	6.5	99.9	3.60
Average		79.95	14.57	5.30	99.9	4.32

Pebbly cherty calcilithite (D₃)

1	S-99/93	30.7	12.8	56.4	99.9	0.44
2	S-99/94	25.4	8.3	66.1	99.8	0.34
Average		28.05	10.55	61.25	99.85	0.39

succession. Based on lithofacies analysis together with existing biostratigraphic data, the local sea level curve derived in present investigation has been compared with global standard. Departure from global standard during regressive interval reveal local tectonic disturbances (Jacquie and de Graciansky, 1998) which may be considerable importance in regional correlation, however, transgressive intervals showing similar trend with global standard. This kind of global synchronization of these sequences suggests they have great potential as events having chronostratigraphic value. These transgressive and regressive sequences correlate reasonably well with ‘anoxic’ and ‘oxic’ events during which ‘organic rich’ and ‘organic poor’ facies may have been deposited (Miall, 1984; van Buchem et al., 2002; Soua and Chihi, 2014). The main source rocks for hydrocarbon in North African basins, West European and Russian platform basins are associated with short lived oceanic anoxic events that occurred during transgressive phases in Jurassic time (e.g., review in Soua, 2014; Mattioli et al., 2004). The Transgressive intervals (TS-I and TS-II) in present investigation may correspond to horizons of principal source rocks of hydrocarbons. Transgressive successions are commonly fine grained, thinly bedded and low permeability intervals that can act as seal rocks (Olsen, 1998). The interpretation of transgressive-regressive sequences is integrated with the existing biostratigraphic data available to make it regionally comparable. The description and

interpretation of each sequence are given as follows (Fig.2).

TRANSGRESSIVE SEQUENCE-I (TS-I)

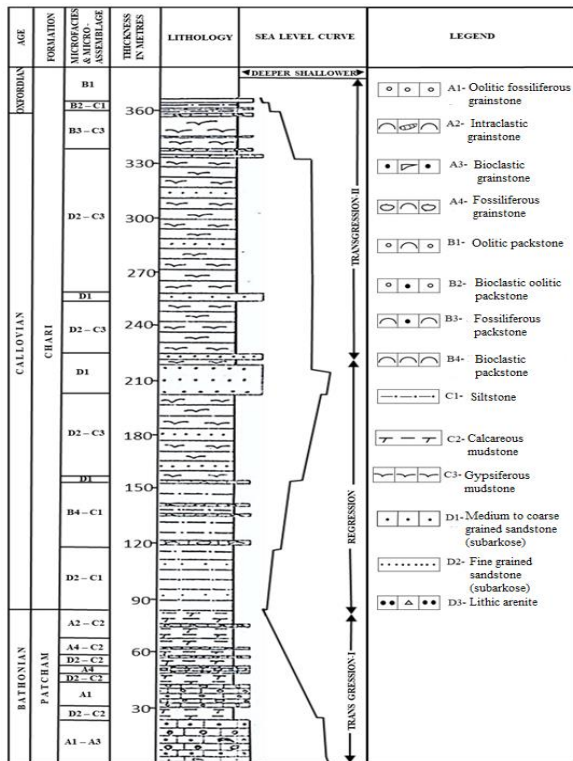


Figure 2. Litho-column showing sequences of microfacies assemblages, sea level curve and depositional sequences during the Bathonian to Oxfordian, Jhura dome, Kutch/Kachchh Mainland (modified after Mishra 2002).

(BATHONIAN):

The total thickness of TS-I is 84.34 m. It is composed of dominantly carbonate rocks and bounded below by coarse grained carbonate rocks and upper boundaries is conformable and characterized by change in lithofacies from nonclastic to clastic. TS-I of Bathonian age (Rajnath, 1932; Stoliczka, 1873) composed of mostly calcareous mudstone microfacies (C₂) and subordinately grainstone lithofacies (A). From bottom to top the sequence of four microfacies assemblage occurs in the following order: (i) oolitic fossiliferous grainstone – bioclastic grainstone (A₁-A₃). (ii) oolitic fossiliferous grainstone – calcareous mudstone (A₁ – C₂), (iii) fossiliferous grainstone – calcareous mudstone (A₄- C₂), (iv) intraclastic grainstone- calcareous mudstone (A₂-C₂). There is general increase in the percentage of calcareous mudstone and decrease in coarse grained grainstone in upward direction. Each assemblage showing irregular contacts and varying number of clastic constituents occur as separate layers mixed with carbonate rocks.

Interpretation

An initial rise in sea level (Bajocian/Bathonian time) is marked by basal layer of coarse-grained carbonate grading upward into bioturbated, fine-grained calcareous mudstone with abundance of microfossils. These carbonate deposits are explained as transgressive deposits on a gently sloping carbonate shelf. Alternating calcareous mudstone and grainstone may indicate deposition from storms and fair-weather settling during net sea level rise (Mishra and Tiwari, 2006). These transgressive deposits are related to initial transgression phase in the basin and may contain organic rich anoxic facies. Most of the source rock intervals of the Tunisian basins North Africa are accompanied with initial transgression phase that occurred in early to middle Jurassic time (e.g., review in Soua, 2014). The regular fining upward stacking pattern of microfacies suggests that rise in sea level was continuous and comparable with the global rise of relative sea-level during Bathonian time (Vail et al., 1977b), but the rate of relative rise of sea level was slow as revealed by regular decrease in thickness of grainstone microfacies (A). Frequent tectonic episode is revealed by varying number of terrigenous materials occur as discrete layers admixed with carbonate beds together with irregular contacts between the microfacies.

REGRESSIVE SEQUENCE (RS) (CALLOVIAN):

The preserved thickness of Regressive Sequence is 130 m. This sequence of Callovian age (Krishna and Ojha, 1996) is dominantly siliciclastic and consists of mostly mudrocks (gypsiferous mudstone microfacies and siltstone microfacies) subordinately with varying proportion of sandstone and carbonate microfacies (i.e. mudrock microfacies > sandstone microfacies > carbonate microfacies). Its lower and upper sequence boundaries are conformable and characterized by microfacies change. The lower boundary is marked by change in microfacies from nonclastic to fine grained clastic and upper is distinguished by very thickly bedded medium to coarse-grained clastics (D₁). From base to top, the sequence of five microfacies assemblage occurs in the following order: (i) fine grained sandstone (subarkose) – siltstone (D₂ – C₁), (ii) bioclastic packstone – siltstone (B₄-C₁), (iii) pebbly cherty calcilithite ‘D₃’ microfacies, (iv) gypsiferous mudstone - fine grained sandstone (D₂ – C₃), (v) medium to coarse grained sandstone (D₁). The basal part of this sequence is marked by predominance of siltstone and fine-grained sandstone microfacies assemblage (D₂ – C₁), followed by siltstone - bioclastic packstone microfacies assemblage (B₄-C₁). The middle and upper strata are characterized by gypsiferous mudstone (C₃) interbedded with medium to coarse grained sandstones microfacies (D₁). There is general increase in bed

thickness of clastic microfacies (D₂ – C₃) and (D₁) in upward direction.

Interpretation

Abundance of fine grained clastic (D₂ – C₁ assemblage) at the base of this sequence are interpreted to have been deposited in a relatively deep-water environment, possibly indicating a standstill or a relative lowering of sea level. Preservation of pebbly cherty calcilithite microfacies 'D₃' (storm unit) indicate a shallowing upward trend during deposition of B₄-C₁ assemblage and is interpreted as low stand, relatively shallower water deposits as supported by coarse grained clastics and abundance of eroded rock fragments. Extensive erosion suggests a relative drop in sea level. (D₂ – C₃) assemblage is believed to have been deposited within standing body of water environment during maximum fall in sea level. (D₁) is a shallowest deposit and deposited during maximum sand supply in Middle Callovian. Upward stacking pattern of microfacies assemblage in the study area indicate regressive deposits and overall shallowing of the sea that is regionally correlative but not comparable with the global trend of relative sea-level rise during Middle Jurassic time (Vail et al., 1977b).

TRANSGRESSIVE SEQUENCE – II (TS-II) (EARLY OXFORDIAN):

The total thickness of this sequence is 155.8 m. Its basal boundary is marked by microfacies change from coarse grained clastic to fine grained clastic and upper boundary is characterized by conglomeratic horizon indicating condensed marine facies (hardground) of Oxfordian age and by basin- wide occurrence of condensation phenomena (Fursich et al., 1992). Transgressive sequence II of Early Oxfordian age (Krishna, 1990; Krishna et al., 1998) consists of four microfacies assemblages and occur from base to top in following order: (i) gypsiferous mudstone-fine grained sandstone (D₂-C₃), (ii) fossiliferous packstone - gypsiferous mudstone (B₃-C₃), (iii) bioclastic oolitic packstone – siltstone (B₂ –C₁), (iv) oolitic packstone microfacies (B₁). There is general increase in bed thickness of carbonate microfacies (B₃-C₃), (B₂ –C₁) and (B₁) in upward direction. Appreciable percentage of terrigenous materials like sand and gravel are admixed with carbonate beds, however varying number of carbonate rocks are present in clastic rocks (siltstone). All the carbonate assemblages exhibit erosional surfaces.

Interpretation

Initial rise in relative sea level is indicated by preservation of fossiliferous packstone microfacies (B₃) in the lower part of this sequence. Microfacies assemblages B₃-C₃ and B₂-C₁ has been regionally correlated and deposited during slow sea level rise as

explained by abrupt change in detrital grain size, mixing of two lithology, plenty of siliciclastic in each microfacies, whereas oolitic packstone microfacies (B₁) exhibit its deposition during rapid sea level rise as supported by reduced thickness, erosive to irregular contact and presence of intraformational conglomeratic materials (Tiwari and Mishra, 2007). It is also justified by upward thickening of packstone microfacies. Upward stacking pattern of microfacies assemblage reveals transgressive deposits and overall deepening of the sea that is comparable with the global rise of relative sea-level during Early Oxfordian time (Vail et al., 1977b). It is maximum transgression in the basin covering large geographic area that results from combined effect of 2nd and 3rd order sea level variations. These transgressive maxima (B₂-C₁ assemblage and B₁ microfacies) may be associated with horizons of major accumulation of organic matter (van Buchem et al., 2002). Main European source rocks of petroleum are well related to transgressive maxima of Jurassic time (Cojan and Renard, 2002). Frequent tectonism is marked by erosional contacts between the microfacies assemblages and abundance of conglomeratic materials that characterizes the microfacies.

These 3rd order depositional sequences described above TS-I, Regressive and TS-II corresponding to Bathonian, Callovian and Early Oxfordian respectively are attributed to both regional tectonic mechanism and global sea level change Cloetingh (1986, 1988), Kauffman (1984), and (Yunbo et al., 2014). Shift in source area and transport direction from north-northwest to east -northeast during studied interval may have contributed significant influx of immature clastics (Mishra and Tiwari, 2005) that indicate short transport or tectonic instability condition or both. Alternate and mixed deposition of low to high energy siliciclastics and carbonates as reflected in each microfacies indicating different phases of tectonics.

CONCLUSIONS

Bathonian to Early Oxfordian succession having total thickness of 370 m is stacked in to three third-order depositional sequences. The 84 m Transgressive sequence-I, 130 m. Regressive sequence and 155 m. Transgressive sequence-II have been recognized. The stacking pattern of 13 microfacies assemblages refer to the architecture of vertical succession of depositional sequences. From the present study, it is inferred that the Transgressive Sequence-I was deposited during relative sea level rise and less sediment supply in Bathonian. Regressive Sequences was deposited during stillstand period followed by relatively high rate of sediment supply in Middle Callovian and Transgressive Sequence – II was deposited during highstand of sea level along with

frequent and extremely low rate of sediment supply in Early Oxfordian. The relative sea level curves reveal sea level fluctuations during the deposition of whole sequence prior to major drop in sea level at the end of Transgressive Sequence- II. These high order sequences are regionally comparable and might have been generated due to regional tectonic mechanism together with global sea level change.

ACKNOWLEDGEMENT:

The author wishes to thank the Head of the Department of Geology, University of Dodoma, Tanzania for providing necessary support in the preparation of the manuscript and thankful to Prof. R. N. Tiwari, Former Head of the Department of Geology, Banaras Hindu University, India for providing necessary laboratory facilities. I express my gratitude to the Chief Editor Dr. John S. Armstrong-Altrin and reviewer Prof. Soumyajit Mukherjee (IIT, Bombay) for providing comments on the earlier version of this manuscript.

REFERENCES

Abbott, S.T. and Sweet, I.P. (2000). Tectonic control on third-order sequences in a siliciclastic ramp-style basin; an example from the Roper Superbasin (Mesoproterozoic), northern Australia. *Australian Journal of Earth Sciences*, v. 47 (3), pp. 637-657.

Amodu, A., Oyetade, O.P., Fadiya, S.L. and Fowora, O. (2022). Sequence stratigraphic analysis and hydrocarbon prospectivity of AMO Field, deep offshore Niger Delta, Nigeria. *Energy Geoscience*, v. 3, pp. 80-93.

Biswas, S.K. (2016). Mesozoic and tertiary stratigraphy of Kutch (Kachchh): A review. *In: Conference GSI*, pp. 1-24.

Biswas, S.K. (1971) Note on the geology of Kutch. *Quart. Jour. Geol. Min. Metal. Soc. India*, v. 43, pp. 223-236.

Biswas, S.K. (1977). Mesozoic rock stratigraphy of Kutch, Gujarat. *Quart. Jour. Geol. Min. Metal. Soc. India*, v. 49, pp. 1-52.

Biswas, S.K. (1981). Basin framework, palaeoenvironment and depositional history of Mesozoic sediments of Kutch basin Western India. *Quart. Jour. Geol. Min. Metal. Soc. India*, v. 83, pp. 56-85.

Biswas, S.K., Basin, A.I. and Ram, J. (1993). Classification of Indian Sedimentary Basins in the framework of plate tectonics. *Proc. Second seminar on Petroliferous Basins of India*, Indian Petroleum Pub. Dehradun1, pp. 1-46.

Blatt, H., Middleton, G.V. and Murray, R.C. (1980). *Origin of Sedimentary Rocks*. 2nd Ed., Prentice-Hall, New Jersey, p. 634.

Cloetingh, S. (1986). Intraplate stresses: A new tectonic mechanism for fluctuations of relative sea level. *Geology*, v. 14, pp. 617-620.

Cloetingh, S. (1988). Intraplate stresses: a tectonic cause for third order cycles in apparent sea level? in C. Wilgus (ed.), *Sea Level Changes: an integrated approach*, SEPM Special Publication, v. 42, pp. 19-29.

Cojan, I. and Renard, M. (2002). *Sedimentology*. 1st edition, Oxford and IBH Publishing Co. Pvt. Ltd, New Delhi, India, p. 483.

Dwivedi, A.K. (2016). Petroleum exploration in India - a perspective and endeavors. *Proc. India Nat. Sci. Acad.* v. 82, pp. 881-903.

Dhawale, M.S., Mukherjee, S. and Biswas M. (2023). Morphotectonics and paleo stress analyses of Kutch area, Gujarat, India. *Results in Earth Sciences* 1, 100002.

Dunham, R.J. (1962). Classification of carbonate rocks according to depositional textures. in: Ham, W.E. (Ed.), *Classification of Carbonate Rocks*. Am. Assoc. Petrol. Geol. Mem, v. 1, pp. 108-121.

Fursich, F.T., Oschmann, W., Singh, I.B. and Jaitly, A.K. (1992). Hardground, reworked concretion levels and condensed horizon in the Jurassic of Western India: their significance for basin analysis. *Jour. Geol. Soc. London*, v. 149, pp. 313-331.

Haq, B.U., Hardenbol, J. and Vail, P. R. (1988). Mesozoic and Cenozoic stratigraphy and cycle of sea level change, In *Sea Level changes, an integrated approach*. Wilgus, C.K. (ed.), S.E.P.M. Sp. Pub. v. 42, pp. 71-108.

Jacquin, T. and de Graciansky, P.C. (1998). Transgressive/regressive (second order) facies cycles: the effect of tectono-eustasy. In: de Graciansky, P.C. et al. (Eds.), *Mesozoic and Cenozoic Sequence Stratigraphy of European Basins*. S.E.P.M. Spec. Publ. v. 60, pp. 31-42

Kauffman, E.G. (1984). Palaeogeography and evolutionary response dynamic in the Cretaceous Western Interior sea-way of North America. *Geol. Ass. Canada. Sp. Pap.* v. 27, pp. 273-30.

Krishna, J. (1990). A comment on the paper 'Dhosa Oolite' Transgressive Condensation Horizon of Oxfordian of Kachchh, Western India, By I.B. Singh, (Published in *Jour. Geol. Soc. of India*, v.34, (2),1989). *Jour. Geol. Soc. India*. v. 36 (2), pp. 204-205.

Krishna, J. (2002). Mesozoic microstratigraphy, DST sponsored contact programme on 'structure, tectonics and Mesozoic stratigraphy of Kachchh, 14-20th January, organized by M.S. University of Baroda (course director S.K. Biswas), Lecture Notes, pp. 98-121.

Krishna, J. and Ojha, J.R. (1996). The Callovian Ammonoid Chronology in Kachchh (India), *Geo Research Forum*, v.1-2, pp. 151-166. Transact Publications, Switzerland.

Depositional sequences and sea level changes during Bathonian-Oxfordian, Kutch (Kachchh) Basin, Gujarat, India

- Krishna, J., Pathak, D.B. and Pandey, B. (1998). Development of Oxfordian (early Upper Jurassic) in the most proximally exposed part of Kachchh basin at Wagad, outside the Kachchh Mainland. *Jour. Geol. Soc of India*, v. 52, pp. 513-522.
- Krishna, J, Singh, I.B., Howard, J.D. and Jafer. S.A. (1983). Implication of new data on Mesozoic rocks of Kachchh, Western India. *Nature*, v. 305 (5937), pp. 790-792.
- Lohani, N., Mukherjee, S., Singh, S., Pawar, A. and Shaikh, M. (2022). Structural geological field guide: Bhuj area (Gujarat, India). In: Mukherjee, S. (Ed.) *Structural Geology and Tectonics Field Guidebook*—v. 2. Springer. pp. 227-250.
- Mishra, D. and Tiwari, R.N. (2005). Provenance Study of Siliciclastic Sediments, Jhura Dome, Kachchh, Gujarat. *Jour. Geol. Soc. of India*, v. 65, pp. 703-714.
- Mishra, D. and Tiwari, R.N. (2006). Lithofacies and depositional dynamics of golden Oolite (Bathonian), Kachchh Mainland, Gujarat (India). *Jour. Asian Earth Sciences*. v. 26, pp. 449-460.
- Mattioli, E., Pittet, B., Palliani, R., Röhl, H. J., Schmid-Röhl, A. and Morettini, E. (2004). Phytoplankton evidence for the timing and correlation of palaeo-oceanographical changes during the early Toarcian oceanic anoxic event (Early Jurassic). *Journal of the Geological Society*, v. 161, no. 4, pp. 685-693.
- Miall, A.D. (1984). *Principles of Sedimentary Basin Analysis*, Springer Verlag, P. 490.
- Mishra, D. (2002). Lithofacies and paleo environmental studies of Jurassic rocks of Jhura Dome, Kachchh Mainland, Gujarat. Ph.D. Thesis, Banaras Hindu University, India, P. 126.
- Patil, D.J., Mani, D., Madhavi, T., Sudarshan, V., Srikarni, C., Kalpana, M.S. and Dayal, A.M. (2013). Near surface hydrocarbon prospecting in Mesozoic Kutch sedimentary basin, Gujarat, Western India—A reconnaissance study using geochemical and isotopic approach. *Journal of Petroleum Science and Engineering*, v. 108, pp. 393-403.
- Olsen, T.R. (1998). High-resolution sequence stratigraphy of pro-grading shoreface systems—a comparison between the Ran-noch/Etve Formations, Tampen Spur area, northern North Sea and the Point Lookout Formation, Mancos Canyon, southwest Colorado. In: Gradstein, F.M., Sandvik, K.O., Milton, N. J. (Eds.), *Sequence Stratigraphy—Concepts and Application*. Norwegian Petroleum Society Special Publication, v. 8, pp. 355-372
- Rajnath (1932). A contribution to the stratigraphy of Cutch. *Q. J. Geol. Min. Met. Soc. India*. IV, pp. 161-174.
- Rassi, C. (2002). Assessment of production predictability of fourth order systems tracts in the Miocene offshore Louisiana Gulf Coast. *Association of Geological Societies*, v. 52.
- Shaikh, M., Maurya, D.M., Mukherjee, S., Vanik, N., Padmalal, A. and Chamyal, L. (2020). Tectonic evolution of the intra-uplift Vigodi-Gugriana-Khirastra-Netra Fault System in the seismically active Kachchh Rift Basin, India: Implications for the western continental margin of the Indian plate. *Journal of Structural Geology*, v. 140, pp. 104-124.
- Shaikh, M.A., Patidar, A.K., Maurya, D.M., Vanik, N.P., Padmalal, A., Tiwari, P., Mukherjee, S. and Chamyal, L.S. (2022). Building tectonic framework of a blind active fault zone using field and ground-penetrating radar data. *Journal of Structural Geology*, v. 155, no. 104526.
- Soua, M. and Chihi, H. (2014). Optimizing exploration procedure using Oceanic Anoxic Events as new tool for hydrocarbon strategy in Tunisia. In Gaci S., Hachay O. (Eds.), *Advances in data, methods, models and their applications in Oil/Gas exploration*, Cambridge Scholars Publishing (C.S.P.) Edition, p. 55.
- Soua, M. (2014). A review of Jurassic oceanic anoxic events as recorded in the northern margin of Africa, Tunisia. *Journal of Geosciences and Geomatics*, v. 2, no. 3, pp. 94-106.
- Tiwari, R.N. and Mishra, D. (2007) Microfacies Analysis of Transgressive Condensed Sequence: A study from the Oxfordian of Kachchh Basin, Gujarat. *Jour. Geol. Soc. India*, v. 70, pp. 923-932.
- Vail, R.P., Mitchum, R.M., Jr. and Thompson III S. (1977a). Seismic stratigraphy and global changes in sea level, part four: global cycle of relative changes of sea level. *A.A.P.G. Mem.*, v. 26. pp. 83-98.
- Vail, P., Mitchum Jr., R. and Thompson III, S. (1977b). Seismic stratigraphy and global changes of sea level: Part 4. Global cycles of relative changes of sea level: Section 2. Application of seismic reflection configuration to stratigraphic interpretation. *A.A.P.G. Special* v. 165, pp. 83-97.
- Van Buchem, F.S.P., Razin, P., Homewood, P.W., Oterdoom, W.H. and Philip, J. (2002). Stratigraphic organization of carbonate ramps and organic-rich intrashelf basins: Natih Formation (middle Cretaceous) of northern Oman: *A.A.P.G. Bulletin*, v. 86, pp. 21-54.
- Van Buchem, F.S.P., Huc, A.Y., Pradier, B. and Stefani, M. (2005). Stratigraphic patterns in carbonate source rock distribution: 2th to 4th order control and sediment flux, In: Harris, N.B., Pradier, B. (Eds.) *The deposition of organic rich sediments, models, mechanisms and consequences*, S.E.P.M. Special Publication no. 82, pp. 191-223.

Waagen, W. (1873). Jurassic fauna of Kutch: The Cephalopoda. Palaeont. Indica, v. 9, pp. 1-247.

Yunbo, Z., Zongju, Z., Genhou, W., Zaixing, Jiang, Mingjian, W., Min, Z. and Shibei, Z. (2014) Type

Diwakar Mishra
division and controlling factor analysis of 3rd order sequences in marine carbonate rocks. Geoscience Frontiers, v. 5 (2), pp. 289-298.

Stability assessment and mitigation of vulnerable slopes utilizing kinematic analysis and slope mass rating approach along Basohli-Bani Road, Kathua District, Jammu and Kashmir

Shifali Chib* and Yudhbir Singh

Department of Geology, University of Jammu, Jammu-180006 (India)

Email Address: Shifali.chib@jammuuniversity.ac.in

ABSTRACT

Slope instability issues have a significant impact on the community's and surrounding area's socio-economic development. The current study examined the stability of sensitive rock-cut slopes in the Basohli-Bani region of Kathua district using geotechnical investigations. The study region is located in the Outer and Lesser Himalayan tectonic zones in the northwestern Himalaya. The current study's purpose was to determine the slope's stability status so that rapid mitigating measures could be recommended to avoid population losses and inconveniences. The stability assessment was conducted using rock mass characterization techniques for slope stability evaluation, such as Slope Mass Rating (SMR) classification system. Kinematic analysis was also employed to look at the various mechanisms of structurally controlled failures in jointed rock masses. The input data for the slope stability assessment was gathered through extensive fieldwork and stereonet plotting. The wedge mode of failure is the most prevalent mode, as demonstrated by kinematic analysis of the structural discontinuities. A total of thirty-two land sliding locations were considered for the cut slope stability evaluations. The SMR results show that sixteen of the thirty-two vulnerable locations are unstable, seven are completely unstable, eight are partially stable, one is stable, and none is completely stable. Site-specific mitigation strategies have been recommended for rock cut slopes that are partially stable, unstable, or completely unstable. These measures also help to mitigate the socio-economic repercussions. This study will aid ministry of road transport and highways even more because numerous civil engineering projects are now ongoing and several new ones are in the planning phases in the study area.

Keywords: Stability assessment, RMR, SMR, kinematic analysis, mitigation.

INTRODUCTION

The Himalayan orogeny is the consequence of the collision of Indian and Eurasian plates, and it is the greatest field laboratory on the planet for studying rock mechanics, geology, and geo hazards (Singh and Goel, 2002). Natural disasters have become far more common in recent decades. Natural disasters such as hurricanes, earthquakes, erosion, tsunamis, and landslides inflict significant loss of life and property damage to national and local governments. Landslides are a prevalent natural hazard that affects hilly locations all over the world; they have a significant impact on human lives and infrastructure. During the 1990s, landslides accounted for around 9% of all natural catastrophes globally. According to Schuster (1996), this tendency is anticipated to continue in the next decades as a result of increasing urbanization and development, ongoing deforestation, and higher regional precipitation in landslide-prone regions as a result of shifting climatic patterns. According to the Government Disaster Management Plan Report, the majority of the locations in Ladakh and J&K are very susceptible to landslides (SDMP, 2017). The frequency of landslides is growing drastically

(Singh and Goel, 2002) as a result of unorganized development of different civil infrastructural works such as buildings, roads, rail network, and so on. Because of the dynamic character of the slopes, geomorphology, snowfall, intense and continuous rainfall, and continuing neotectonic activity, the hill slopes of the Lesser Himalayas are well recognized for their instability. This obviously implies that any development activity carried out in the Himalayan region requires an extensive and meticulous assessment in all aspects, otherwise it will cause major disruption and tremendous damage in terms of life, property, and the environment. The best practice in any civil engineering construction is to obtain extensive geological and geotechnical knowledge in advance in order to determine the severity of connected difficulties and, consequently, to execute mitigation measures to limit risks. Proper investigations and slope characterization are necessary for safer construction and less slope failures. The cost-benefit ratio of landslide mitigation techniques is particularly high in mountainous places across the world. These early geological and geotechnical studies on diverse rock/slope mass attributes, general geology,

hydrology, and climate of the region are critical in solving such complicated geo-engineering challenges.

Slope instability in hilly places, particularly along recently cut road cuttings, has been a major concern among geoscientific groups in recent years (Sah et al., 2018; Siddique et al., 2017; Vishal et al., 2015, 2017; and Singh et al., 2010). Hoek and Bray (1981) observed that road bends, particularly in rough terrains, had a significant impact on the strength of the rock slope. In recent years, increasing anthropogenic activities appear to be a contributing cause to the instability of Himalayan slopes. According to Pantelidis (2009), the problems of instability along certain roadways are caused by inconsistencies in rock mass conditions as well as the effect of a number of external factors (environmental factors, seismic activity, anthropogenic activity, and water in the form of rainfall on slopes). In recent years, the geoscientific community has achieved remarkable progress in the field of engineering geology, and several categorization methods, such as rock mass rating 'RMR' (Bieniawski, 1973; 1979; 1984; 1989 and 1993), slope mass rating 'SMR' (Romana, 1985; Romana et al., 2003), Chinese slope mass rating 'CSMR' (Chen, 1995), continuous slope mass rating 'CoSMR' (Tomás et al., 2007) and graphical slope mass rating (Tomás et al., 2012). Numerous researchers have used these classification approaches extensively for evaluating the stability of slopes (Dhiman and Thakur, 2022; Pandey et al., 2022; Jaiswal et al., 2023; Kainthola et al., 2023). These categorization systems are regarded as the backbone of major civil engineering projects and serve as a significant tool in the design sector (Duran and Douglas, 2000). As a result, it is evident that understanding the geological as well as engineering features of slope materials (rocks/soils) is critical in combating the threat of slope instabilities. The current study additionally employs a kinematic analysis approach to determine the general mechanism of failures of rock/slope mass and their trajectories (Hoek and Bray, 1981). Numerous researchers throughout the world have widely employed the kinematic approach in conjunction with RMR and SMR for slope stability study (Sharma et al., 2010).

STUDY AREA

The research region covers parts of the Basohli (latitudes 32°30'12" N and longitudes 75°48'55" E) and Bani (latitudes 32°42'18" N and longitudes 75°48'33" E) areas in the Kathua district

of Jammu and Kashmir Union Territory (Fig. 1). The research area encompasses 85 square km along the major road. The research region is identified by several key structural characteristics and water-sensitive lithologies. From north to south, the Panjal Thrust, Shali Thrust, Murree Thrust, and Main Boundary Thrust are the major structural units falling in the study area as shown in Table 1 (Choudhary, 2006; Jamwal et al., 2020). The Panjal Thrust separates the Salkhala Formation and the Punera Granite Gneiss in the research region. The Shali Thrust separates the strata of the Baila Formation and the Gamir Formation in the area under examination (Choudhary, 2006). The Murree Thrust separates the Murree Group from the Souni Volcanics. The Upper Siwalik Group is separated from the Murree Group by the Main Boundary Thrust, which is located in the southern section of the study region. The Sewa River, a tributary of the Ravi River, drains the study area, which is located between 460 and 1280 metres above mean sea level. The research region receives an average of 1672mm of rain per year, with summer temperatures averaging 18-45°C and winter temperatures averaging 2.05-20.76°C.

METHODOLOGY

The purpose of this slope stability analysis was to determine places impacted by landslides, as well as their current and future vulnerability to landslides, and to characterize the rock mass along the road. The study region is characterized by the occurrence of several discontinuities (Fig. 2). Field investigations were conducted at thirty-two different locations (Table 2) to investigate slope stability and rock mass characteristics. The values of rock mass parameters were recorded for slope stability analysis using Romana's slope mass rating (SMR) classification system and kinematic analysis. Slope mass characterization is required for geotechnical investigations, which are based on several parameters of rock/rock mass and aim to categorize a terrain into distinct types of slope classes as well as their susceptibility to landslides, in order to offer relevant support measures.

a) BASIC ROCK MASS RATING (RMR_{basic}):

To use Bieniawski's basic rock mass rating system (RMR_{basic}), a particular site was divided into a number of geological structural units, with each type of rock mass represented by a separate geological structural unit. The five fundamental rock mass rating parameters used for each structural unit are as follows:

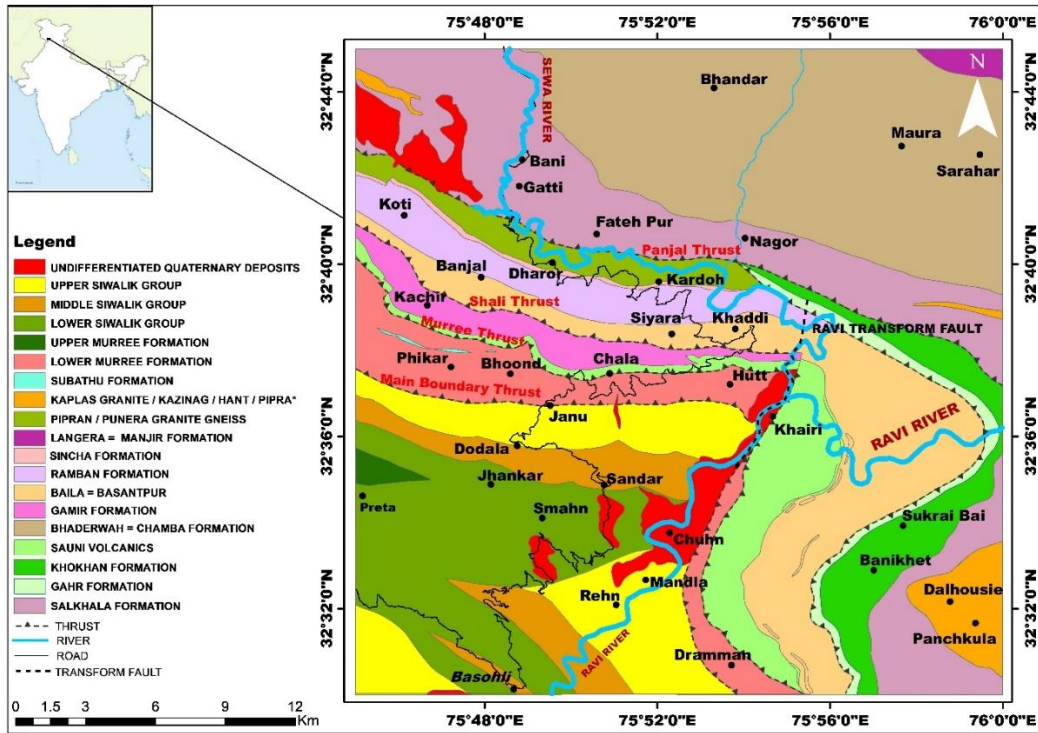


Fig. 1: Geological map of the study area.

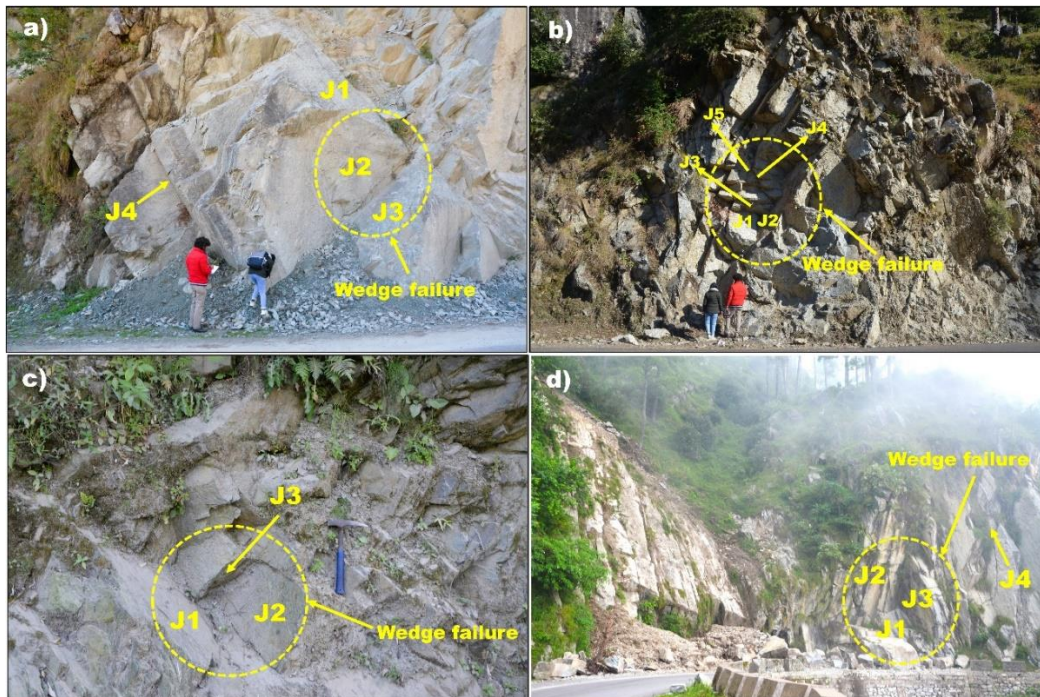


Fig. 2: Field photographs showing the presence of different structural discontinuities in the study area.

Table 1. Tectonostratigraphic setup of the study area from north to south (modified after Choudhary et al., 2006).

Subgroup/Formation	Lithology	Age
Siwalik	Sandstone, siltstone, conglomerate and clay beds	Mid Miocene to Early Pleistocene
	-----Main Boundary Thrust (Mundan Thrust) -----	
Murree	Sandstones, shales and mudstones	Miocene
	-----Murree Thrust-----	
Souni Volcanics	Green meta basalt with shale, slate and quartzite	Paleoproterozoic/Neoproterozoic??
Gamir	Bands of purple shale and limestone, bands of conglomerates and cherty shales, quartzites	Neoproterozoic
	-----Shali Thrust (= Sudh Mahadev Thrust) -----	
Baila	Carbonaceous slates, calcareous shale, nodular and lenticles of limestone	Neoproterozoic
Ramban	Bluish grey phyllitic slates, grey to dark grey shales/slates with bands of grey quartzites	Neoproterozoic
Sincha	Pinkish grey limestone and sandy dolomites	Neoproterozoic
Punera Granite Gneiss	Granite and augen gneiss	? Palaeozoic
	-----Panjal Thrust (= Jutogh Thrust) -----	
Salkhala	Carbonaceous phyllite, schist, limestone and quartzite	Undifferentiated Proterozoic
Bhaderwah	Carbonaceous slate, phyllite and quartzite	Neoproterozoic

- 1. Uniaxial compressive strength/Point Load Index (PLI):** Standard size rock samples have been taken from 32 locations, and values were acquired using a point load instrument. The equation used for calculating PLI is given below-

$$I_{L(50)} = P / (D.W)^{0.75} \sqrt{D_{50}}$$

where $I_{L(50)}$ = Point load lump strength (MPa); P = Peak load at failure in N; D = distance between point loads (mm); W = Mean width of lump (mm); and D_{50} = Standard size of lump (50mm).

- 2. Rock quality designation (RQD):** Palmstrom (2005) equation was used to analyse RQD-

$$RQD = 110 - 2.5 (J_v)$$

where, J_v is a total number of joints per cubic meter and is computed from the equation given below (Palmstrom, 1982; 1996)-

$$J_v = [(1/S_1) + (1/S_2) + (1/S_3) \dots + (N_r/5)]$$

where, S_1, S_2, S_3 are the joint set spacing and N_r is the number of random joints.

- 3. Discontinuity spacing:** The term discontinuity covers joints, beddings or foliations, shear zones,

minor faults, or other surfaces of weakness. For each set of discontinuities, the linear distance between two adjacent discontinuities should be measured and the ratings for the most critical discontinuities are obtained.

- 4. Discontinuity condition:** This parameter includes-roughness of discontinuity surfaces, their separation, length or persistence, weathering of the wall rock or the planes of weakness and infilling (gouge) material.

- 5. Ground water condition:** A general condition can be described as completely dry, damp, wet, dripping, and flowing. The ratings of all these parameters are given in table 3.

Table 2. Table showing different locations under investigation.

Landslide site No.	Latitude	Longitude	Type of slide	Angle of reach	Formation involved in landslide
LS -1	32°35'10" N	75°50'32" E	Rock slide	70°-75°	Middle Siwalik
LS- 2	32°37'05" N	75°49'56" E	Complex slide	68°-73°	Lower Murree
LS- 3	32°37'15" N	75°50'57" E	Debris slide	64°-78°	Lower Murree
LS- 4	32°37'15" N	75°51'36" E	Rock fall	60°-65°	Lower Murree
LS- 5	32°37'47" N	75°53'22" E	Rock fall	58°-63°	Souni volcanics
LS- 6	32°37'51" N	75°53'39" E	Rock fall	70°-75°	Souni volcanics
LS- 7	32°38'30" N	75°54'10" E	Rock fall	82°-86°	Baila Formation
LS- 8	32°39'23" N	75°52'47" E	Rock fall	65°-75°	Ramban Formation
LS- 9	32°39'19" N	75°52'27" E	Rock fall	65°-68°	Ramban Formation
LS- 10	32°39'41" N	75°51'29" E	Rock fall	70°-72°	Punera Granite Gneiss
LS -11	32°39'51" N	75°51'14" E	Rock topple	75°-77°	Punera Granite Gneiss
LS- 12	32°39'48" N	75°50'37" E	Rock fall	69°-72°	Punera Granite Gneiss
LS- 13	32°39'40" N	75°50'29" E	Rock fall	76°-79°	Sincha Formation
LS- 14	32°39'41" N	75°50'05" E	Rock fall	70°-72°	Sincha Formation

LS- 15	32°39'40" N	75°49'43" E	Rock fall	62°-65°	Ramban Formation
LS- 16	32°39'41" N	75°49'42" E	Rock fall	51°-56°	Ramban Formation
LS- 17	32°39'59" N	75°49'06" E	Rock fall	82°-85°	Punera Granite Gneiss
LS- 18	32°40'07" N	75°49'04" E	Rock topple	57°-60°	Punera Granite Gneiss
LS- 19	32°40'34" N	75°48'51" E	Rock fall	58°-62°	Punera Granite Gneiss
LS- 20	32°40'34" N	75°48'44" E	Rock fall	58°-60°	Punera Granite Gneiss
LS- 21	32°40'37" N	75°48'46" E	Rock fall	65°-67°	Punera Granite Gneiss
LS- 22	32°40'39" N	75°48'46" E	Debris slide	65°-67°	Punera Granite Gneiss
LS- 23	32°40'55" N	75°48'34" E	Rock fall	59°-63°	Punera Granite Gneiss
LS- 24	32°41'08" N	75°48'39" E	Rock slide	52°-54°	Punera Granite Gneiss
LS- 25	32°40'58" N	75°48'45" E	Rock fall	68°-70°	Salkhala Formation
LS- 26	32°41'02" N	75°48'48" E	Rock fall	68°-70°	Salkhala Formation
LS- 27	32°41'53" N	75°48'28" E	Rock fall	70°-72°	Salkhala Formation
LS- 28	32°41'55" N	75°48'36" E	Rock fall	50°-53°	Salkhala Formation
LS- 29	32°41'59" N	75°48'36" E	Rock fall	55°-60°	Salkhala Formation
LS- 30	32°42'13" N	75°48'29" E	Rock fall	68°-70°	Salkhala Formation
LS- 31	32°42'17" N	75°48'30" E	Rock fall	68°-73°	Salkhala Formation
LS- 32	32°42'19" N	75°48'32" E	Rock fall	70°-72°	Salkhala Formation

b) KINEMATIC ANALYSIS:

Markland (1972) coined the term 'kinematic analysis' and Goodman (1989) uses the term "Kinematics" to describe the movement of bodies without mentioning the forces that cause them to move. It is a useful approach for determining the likely mode of failure (plane, wedge, and topple failure) in unfavorably oriented jointed rock masses (Kumsar et al., 2000; Um and Kulatilake, 2001; Yoon et al., 2002).

c) SLOPE MASS RATING (SMR):

Romana (1985) first suggested the Slope Mass Rating (SMR) technique for assessing rock slope stability. It is calculated by adding the ratings of four adjustment factors (F1, F2, F3) for the joint-slope relationship and factor (F4) depending on the type of excavation from Bieniawski's (1989) basic rock mass rating (RMR_{basic}) scheme. In this study, Romana's (1985; 1993) slope mass classification system has been used. The following equation is the generic formulation used to determine the SMR findings in the region under inquiry.

$$SMR = RMR_{basic} + (F1 \times F2 \times F3) + F4$$

Where RMR_{basic} is the basic RMR index derived from Bieniawski's (1989) rock mass categorization and may be obtained by combining the five fundamental parameters listed above for RMR_{basic}; F1 is determined by the parallelism of strikes of joint and slope face; F2 is the joint dip angle; F3 shows the connection between slope face and joint's dips; and F4 is determined by the excavation process.

RESULTS AND DISCUSSION

The RMR_{basic} values found for all 32 sites varies from 48 to 84, reflecting three rock mass classes, namely Class I-very good, Class II-good, and Class III-fair (Table 3). The lowest rating value of 48 has been obtained at LS-29, while the highest rating value of 84 was obtained at LS-12. The

aggregate basic rock mass rating values for every factor indicated that of the total chosen sites, twenty-seven sites fall into the good category, accounting for 84.375% of the sites, and four fall into the fair category, accounting for 12.5% of the sites. However, just one site (site-12) comes into the very good category, accounting for 3.125% of the sites. The study also concludes that a few locations that fall into the marginal good and very close to fair categories require a closer look in terms of preventive measures to avoid becoming more vulnerable in the near future. The findings of kinematics analysis obtained by stereographic projections for 32 sites utilizing Rocscience Dip software clearly indicate the likelihood of wedge, planar, and toppling failure modes as main structural instability on slopes in the research region (Table 4). The analysis also finds that wedge mode of failure is the most common, accounting for about 63.36% of failure probability, while planar mode of failure accounts for 23.76% of failure probability and toppling mode accounts for 12.87% of failure probability in the studied region (Fig. 3). The SMR values obtained from the research region (Table 5) show that sixteen sites out of thirty-six falls into the unstable group, accounting for 50% of the analyzed sites. In contrast, seven sites (21.875% of the examined sites) are classified as completely unstable. eight of the remaining nine sites are classified as partially stable, accounting for 25% of the evaluated sites. The remaining one site is classified as stable, accounting for 3.125% of the studied locations. Figure 4 and 5 below depicts the slope stability map created for the research region. A comparison of the RMR_{basic} results with the SMR index (Fig. 6) revealed that the majority of the sites falling under the good, very good and fair category under RMR_{basic} fall in the unstable (LS-1, LS-2, LS-4, LS-5, LS-8, LS-12, LS-13, LS-14, LS-15, LS-16, LS-19, LS-20, LS-22, LS-24, LS-25, and LS-32), completely unstable (LS-6, LS-17, LS-23, LS-26, LS-27, LS-29 and LS-31) as well as partially stable category (LS-3, LS-7, LS-9, LS-10, LS-11, LS-21,

LS-28 and LS-30) under the SMR scheme. This shows that although the rock masses of the study area fall mostly in good condition but the parallelism between the orientation of joint sets and slope is so

strong that this parallelism is one of the triggering factors which is affecting the stability of the slope in the study area.

Table 3. The basic rock mass rating values (RMR_{basic}) calculated from the study area (Bieniawski, 1979).

Landslide site no.	Point load index	RQD from Jv	Ratings of rock mass		Ground water condition	RMR _b value	Roc k clas s	Rock mass quality
			Discontinuit y spacing	Discontinuit y condition				
LS-1	20	20	10	10	15	75	II	Good
LS-2	17	17	10	20	10	74	II	Good
LS-3	13	13	10	20	15	71	II	Good
LS-4	17	17	10	20	15	79	II	Good
LS-5	17	17	10	10	15	69	II	Good
LS-6	13	13	8	20	15	69	II	Good
LS-7	13	13	8	20	15	69	II	Good
LS-8	17	17	8	10	15	63	II	Good
LS-9	17	17	10	20	7	71	II	Good
LS-10	20	20	15	10	15	80	II	Good
LS-11	8	8	8	20	15	59	III	Fair
LS-12	17	17	10	25	15	84	I	Very Good
LS-13	17	17	10	10	15	69	II	Good
LS-14	17	17	10	10	15	69	II	Good
LS-15	13	13	8	20	10	64	II	Good
LS-16	17	17	10	10	15	69	II	Good
LS-17	13	13	8	25	15	74	II	Good
LS-18	17	17	10	10	15	69	II	Good
LS-19	17	17	10	10	15	69	II	Good
LS-20	17	17	10	10	15	69	II	Good
LS-21	13	13	8	10	15	59	III	Fair
LS-22	17	17	10	10	15	69	II	Good
LS-23	17	17	10	10	10	64	II	Good
LS-24	17	17	15	10	15	74	II	Good
LS-25	13	13	10	10	15	61	II	Good
LS-26	13	13	8	20	15	69	II	Good
LS-27	17	17	10	20	15	79	II	Good
LS-28	8	8	8	10	15	49	III	Fair
LS-29	13	13	8	10	4	48	III	Fair
LS-30	17	17	15	10	15	74	II	Good
LS-31	17	17	10	10	15	69	II	Good
LS-32	20	20	10	20	15	75	II	Good

Result: Very good = 1, Good = 27, Fair = 4, Poor = 0 and Very Poor = 0

Table 4. Data on joint–slope orientation and probable mode of failures of the study area.

Landslide site no.	Slope orientation DD/DA	Joints orientation					Probability of failure Planar - P; Flexural Toppling - FT; Direct toppling - DT; Oblique toppling - OT; Wedge – W.
		J1 DD/DA	J2 DD/DA	J3 DD/DA	J4 DD/DA	J5 DD/DA	
LS-1	105/72	117/69	046/77	323/42	308/56	-	P-J1; W-J1 & J2; J1 & J3
LS-2	200/70	060/35	155/45	120/70	190/52	-	P-J4; W-J2 & J3; J2 & J4; J3 & J4
LS-3	076/59	085/48	180/40	282/36	042/64	-	P-J1; W-J1 & J2; J1 & J4
LS-4	210/63	215/56	062/33	145/69	040/61	-	P-J1; W-J1 & J2; J1 & J3; J1 & J4
LS-5	165/60	184/35	123/78	050/36	-	-	P-J1; W-J1 & J2; J1 & J3
LS-6	155/73	175/63	355/25	110/64	245/86	-	P-J1; DT-J2 & J4; W-J1 & J3; J1 & J4; J3 & J4
LS-7	229/85	032/50	168/46	253/60	243/33	-	FT-J1; W-J2 & J3
LS-8	045/75	350/50	055/86	125/75	030/70	-	P-J4; W-J3 & J4
LS-9	265/68	235/52	185/15	045/33	285/65	-	P-J4; W-J1 & J4
LS-10	099/72	049/52	210/52	152/81	235/12	-	W-J1 & J3
LS-11	325/77	115/65	031/64	158/46	217/68	-	DT-J1 & J4; J3 & J4; OT-J1 & J2
LS-12	246/72	238/43	320/41	156/74	035/57	-	P-J1; DT-J3 & J4; W-J1 & J2; J1 & J3
LS-13	271/79	284/43	337/44	133/18	-	-	P-J1; W-J1 & J2
LS-14	350/72	009/62	205/15	294/86	035/75	-	P-J1; W-J1 & J3; J1 & J4
LS-15	115/73	096/70	180/86	295/38	-	-	P-J1; W-J1 & J2
LS-16	130/59	124/56	195/63	105/14	-	-	P-J1; W-J1 & J2
LS-17	345/83	355/79	280/72	190/78	285/40	025/64	P-J1; W-J1 & J2; J1 & J3; J1 & J4; J2 & J5; J3 & J4; J4 & J5

LS- 18	090/60	103/67	206/73	349/57	083/82	-	DT-J2 & J3; W-J1 & J3
LS- 19	350/60	010/55	240/74	268/60	200/78	-	P-J1; OT-J2 & J4; W-J1 & J2; J1 & J3
LS- 20	125/60	135/58	310/45	110/61	-	-	P-J1; W-J1 & J3
LS- 21	120/67	040/65	320/83	020/33	-	-	FT-J2
LS- 22	043/67	035/65	180/70	084/59	-	-	P-J1; W-J1 & J2; J1 & J3
LS- 23	070/63	130/63	077/58	040/49	019/72	-	P-J2; W-J1 & J2; J1 & J3; J1 & J4; J2 & J3; J2 & J4
LS- 24	033/54	073/51	021/64	351/41	226/24	-	W-J1&J3
LS- 25	350/70	305/45	210/80	300/85	010/35	240/15	P-J4; OT-J2 & J3; W-J1 & J2; J3 & J4
LS- 26	320/70	360/75	235/38	325/60	270/75	-	P-J3; W-J1 & J3; J1 & J4; J2 & J3; J3 & J4
LS- 27	236/72	241/46	205/84	043/66	166/74	-	P-J1; FT-J3; OT-J2 & J3; W-J1 & J2; J1 & J3; J1 & J4
LS- 28	135/53	205/68	270/53	310/12	275/86	-	W-J1 & J2
LS- 29	241/60	345/60	260/55	295/33	-	-	P-J2
LS- 30	250/70	305/35	210/80	280/70	310/85	-	W-J1 & J2; J3 & J4
LS- 31	250/73	310/45	260/55	200/65	356/85	-	P-J2; W-J1 & J2; J1 & J3; J1 & J4; J2 & J3; J2 & J4; J3 & J4
LS- 32	240/72	270/75	225/55	010/60	-	-	P-J2; OT-J1 & J3; W-J1 & J2; J2 & J3

Result: P = 24, FT = 3, DT = 5, OT = 5 and W = 64.

Table 5. Results of SMR obtained from the study area (Romana, 1985) where P= planar failure, W= wedge failure; FT= flexural toppling; DT= direct toppling and OT= oblique toppling.

Landslide site no.	RMR basic	Failure	F1×F2×F3	F4	SMR value	Classes No.	Rock mass description	Stability of particular type of failure	Probability of each type of failure	Overall Stability and probability of failure
LS-1	75	P ₁	-35	0	40	IV	Bad	Unstable	0.6	Unstable, 0.6
		W ₁₂	-50		25	IV	Bad	Unstable	0.6	
		W ₁₃	-1.35		73	II	Good	Stable	0.2	
LS-2	74	P ₄	-17.5	0	56	III	Normal	Partially stable	0.4	Unstable, 0.6
		W ₂₃	-43.35		30	IV	Bad	Unstable	0.6	
		W ₂₄	-7.65		66	II	Good	Stable	0.2	
		W ₃₄	-42		32	IV	Bad	Unstable	0.6	
LS-3	71	P ₁	-21.25	0	49	III	Normal	Partially stable	0.4	Partially stable, 0.4
		W ₁₂	-6.3		64	II	Good	Stable	0.2	
		W ₁₄	-24		47	III	Normal	Partially stable	0.4	
LS-4	79	P ₁	-42.5	0	36	IV	Bad	Unstable	0.6	Unstable, 0.6
		W ₁₂	-1.35		77	II	Good	Stable	0.2	
		W ₁₃	-35		44	III	Normal	Partially stable	0.4	
		W ₁₄	-1.35		77	II	Good	Stable	0.2	
LS-5	69	P ₁	-29.4	0	39	IV	Bad	Unstable	0.6	Unstable, 0.6
		W ₁₂	-6.3		62	II	Good	Stable	0.2	
LS-6	69	P ₁	-35	0	34	IV	Bad	Unstable	0.6	Completely unstable, 0.9
		W ₁₃	-42		27	IV	Bad	Unstable	0.6	
		W ₁₄	-51		18	V	Very Bad	Completely unstable	0.9	
		W ₃₄	-51		18	V	Very Bad	Completely unstable	0.9	
LS-7	69	DT ₂₄	0		69	II	Good	Stable	0.2	Partially stable, 0.4
		W ₂₃	-7.65	0	61	II	Good	Stable	0.2	
		FT ₁	-17.5		51	III	Normal	Partially stable	0.4	
LS-8	63	P ₄	-35	0	28	IV	Bad	Unstable	0.6	Unstable, 0.6
		W ₃₄	-24		39	IV	Bad	Unstable	0.6	
LS-9	71	P ₄	-20	0	51	III	Normal	Partially stable	0.4	Partially stable, 0.4
		W ₁₄	-9		62	II	Good	Stable	0.2	
LS-10	80	W ₁₃	-24	0	56	III	Normal	Partially stable	0.4	Partially stable, 0.4
LS-11	59	DT ₁₄	-3.75	0	55	III	Normal	Partially stable	0.4	Partially stable, 0.4
		DT ₃₄	-0.9		58	III	Normal	Partially stable	0.4	
		OT ₁₂	-3.75		55	III	Normal	Partially stable	0.4	
LS-12	84	P ₁	-43.35	0	40	IV	Bad	Unstable	0.6	Unstable, 0.6
		W ₁₂	-6.3		77	II	Good	Stable	0.2	
		W ₁₃	-35.7		48	III	Normal	Partially stable	0.4	
		DT ₃₄	-4.2		79	II	Good	Stable	0.2	
LS-13	69	P ₁	-35.7	0	33	IV	Bad	Unstable	0.6	Unstable, 0.6
		W ₁₂	-7.65		61	II	Good	Stable	0.2	
LS-14	69	P ₁	-35	0	34	IV	Bad	Unstable	0.6	Unstable, 0.6
		W ₁₃	-24		45	III	Normal	Partially stable	0.4	
		W ₁₄	-24		45	III	Normal	Partially stable	0.4	
LS-15	64	P ₁	-35	0	29	IV	Bad	Unstable	0.6	Unstable, 0.6
		W ₁₂	-35		29	IV	Bad	Unstable	0.6	

Table 5 contd. Results of SMR obtained from the study area (Romana, 1985; 1993) where P= Plane failure, W= wedge failure; FT= flexural toppling; DT= direct toppling and OT= oblique toppling.

Landslide site no.	RMR basic	Failure	F1×F2×F3	F	SMR value	Class No.	Rock mass description	Stability of particular type of failure	Probability of each type of failure	Overall Stability and probability of failure
LS-16	69	P ₁	-42.5	0	26	IV	Bad	Unstable	0.6	Unstable,0.6
		W ₁₂	-35		34	IV	Bad	Unstable	0.6	
LS-17	74	P ₁	-35	0	39	IV	Bad	Unstable	0.6	Completely unstable,
		W ₁₂	-9		65	II	Good	Stable	0.2	0.9
		W ₁₃	-6.3		67	II	Good	Stable	0.2	
		W ₁₄	-7.65		66	II	Good	Stable	0.2	
		W ₂₅	-60		14	V	Very Bad	Completely unstable	0.9	
		W ₃₄	-7.65		66	II	Good	Stable	0.2	
		W ₄₅	-20.4		53	III	Normal	Partially stable	0.4	
LS-18	69	W ₁₃	-7.65	0	61	II	Good	Stable	0.2	Stable, 0.2
		DT ₂₃	0		69	II	Good	Stable	0.2	
LS-19	69	P ₁	-35	0	34	IV	Bad	Unstable	0.6	Unstable, 0.6
		W ₁₂	-7.65		61	II	Good	Stable	0.2	
		W ₁₃	-20.4		48	III	Normal	Partially stable	0.4	
		OT ₂₄	-3.75		65	II	Good	Stable	0.2	
LS-20	69	P ₁	-35	0	34	IV	Bad	Unstable	0.6	Unstable, 0.6
		W ₁₃	-35		34	IV	Bad	Unstable	0.6	
LS-21	59	FT ₂	-10	0	49	III	Normal	Partially stable	0.4	Partially stable, 0.4
LS-22	69	P ₁	-42.5	0	26	IV	Bad	Unstable	0.6	Unstable, 0.6
		W ₁₂	-6.3		62	II	Good	Stable	0.2	
		W ₁₃	-7.5		61	II	Good	Stable	0.2	
LS-23	64	P ₂	-42.5	0	21	IV	Bad	Unstable	0.6	Completely unstable,
		W ₁₂	-20		44	III	Normal	Partially stable	0.4	0.9
		W ₁₃	-51		13	V	Very Bad	Completely Unstable	0.9	
		W ₁₄	-35		29	IV	Bad	Unstable	0.6	
		W ₂₃	-9		55	III	Normal	Partially stable	0.4	
		W ₂₄	-42.5		21	IV	Bad	Unstable	0.6	
LS-24	74	W ₁₃	-35.7	0	38	IV	Bad	Unstable	0.6	Unstable, 0.6
LS-25	61	P ₄	-29.4	0	31	IV	Bad	Unstable	0.6	Unstable, 0.6
		W ₁₂	-7.65		53	III	Normal	Partially stable	0.4	
		W ₃₄	-6.3		54	III	Normal	Partially stable	0.4	
		OT ₂₃	-3.75		57	III	Normal	Partially stable	0.4	
LS-26	69	P ₃	-51	0	18	V	Very Bad	Completely unstable	0.9	Completely unstable,
		W ₁₃	-24		45	III	Normal	Partially stable	0.4	0.9
		W ₁₄	-42.5		26	IV	Bad	Unstable	0.6	
		W ₂₃	-7.65		61	II	Good	Stable	0.2	
		W ₃₄	-42		27	IV	Bad	Unstable	0.6	
LS-27	79	P ₁	-51	0	28	IV	Bad	Unstable	0.6	Completely unstable,
		W ₁₂	-6.3		72	II	Good	Stable	0.2	0.9
		W ₁₃	-1.35		77	II	Good	Stable	0.2	
		W ₁₄	-60		19	V	Very Bad	Completely Unstable	0.9	
		FT ₃	-17.5		61	II	Good	Stable	0.2	
		OT ₂₄	-3.75		75	II	Good	Stable	0.2	
LS-28	49	W ₁₂	-7.5	0	42	III	Normal	Partially stable	0.4	Partially stable, 0.4
LS-29	48	P ₂	-35	0	13	V	Very Bad	Completely Unstable	0.9	Completely unstable,
										0.9
LS-30	74	W ₁₂	-6.3	0	67	II	Good	Stable	0.2	Partially stable, 0.4
		W ₃₄	-24		50	III	Normal	Partially stable	0.4	
LS-31	69	P ₂	-42	0	27	IV	Bad	Unstable	0.6	Completely unstable,
		W ₁₂	-7.65		61	II	Good	Stable	0.2	0.9
		W ₁₃	-35.7		33	IV	Bad	Unstable	0.6	
		W ₁₄	-35.7		33	IV	Bad	Unstable	0.6	
		W ₂₃	-60		9	V	Very Bad	Completely Unstable	0.9	
		W ₂₄	-24		45	III	Normal	Partially stable	0.4	
		W ₃₄	-35.7		33	IV	Bad	Unstable	0.6	
LS-32	75	P ₂	-42	0	33	IV	Bad	Unstable	0.6	Unstable, 0.6
		W ₁₂	-9	0	66	II	Good	Stable	0.2	
		W ₂₃	-3.6	0	71	II	Good	Stable	0.2	
		OT ₁₃	-3.75	0	71	II	Good	Stable	0.2	

Result: Completely unstable = 7, Unstable = 16, Partially stable = 8, Stable = 1 and completely stable = 0

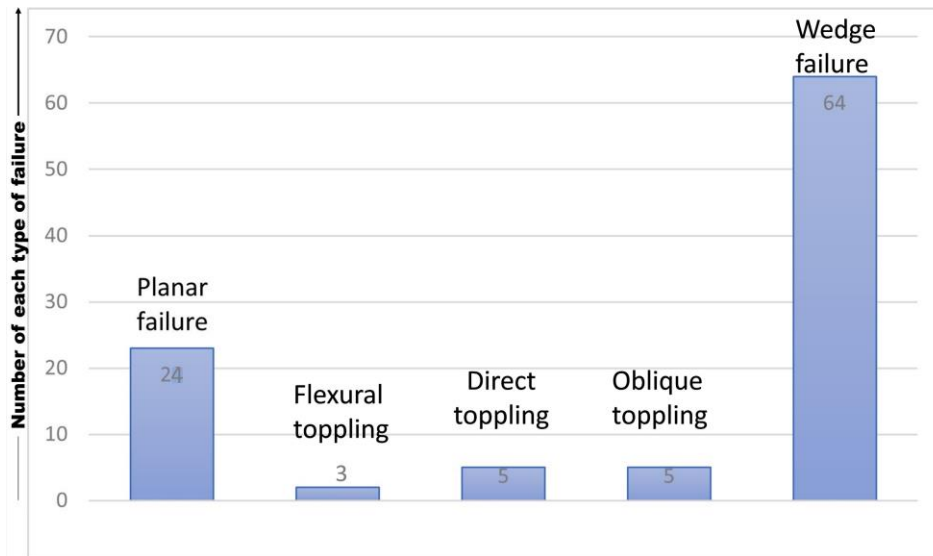


Fig. 3: Different types of failure modes in the study area.

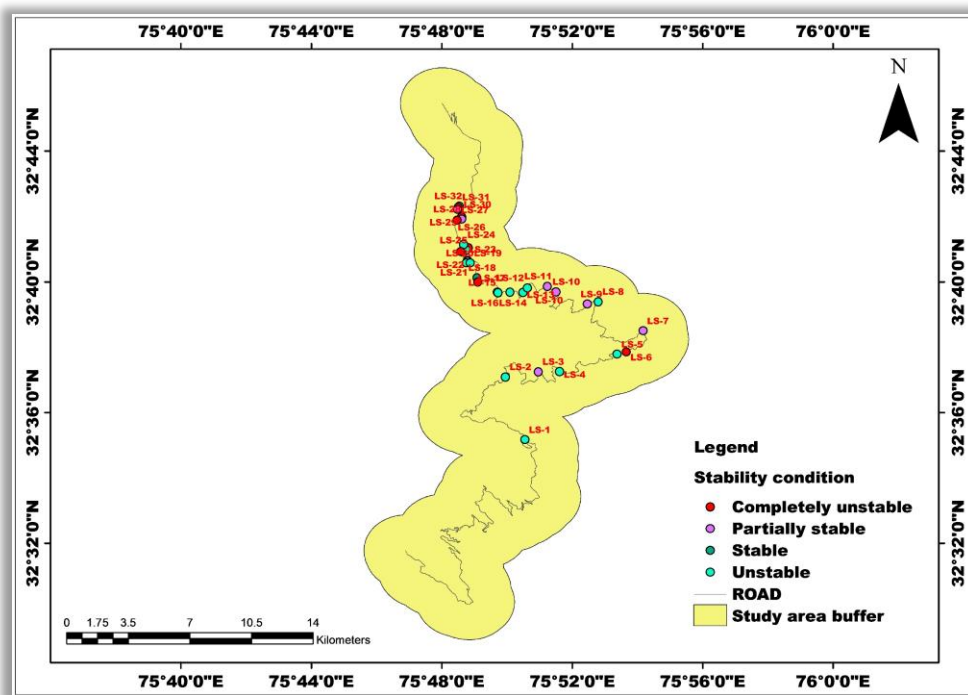


Fig. 4: Slope stability map of the study area.

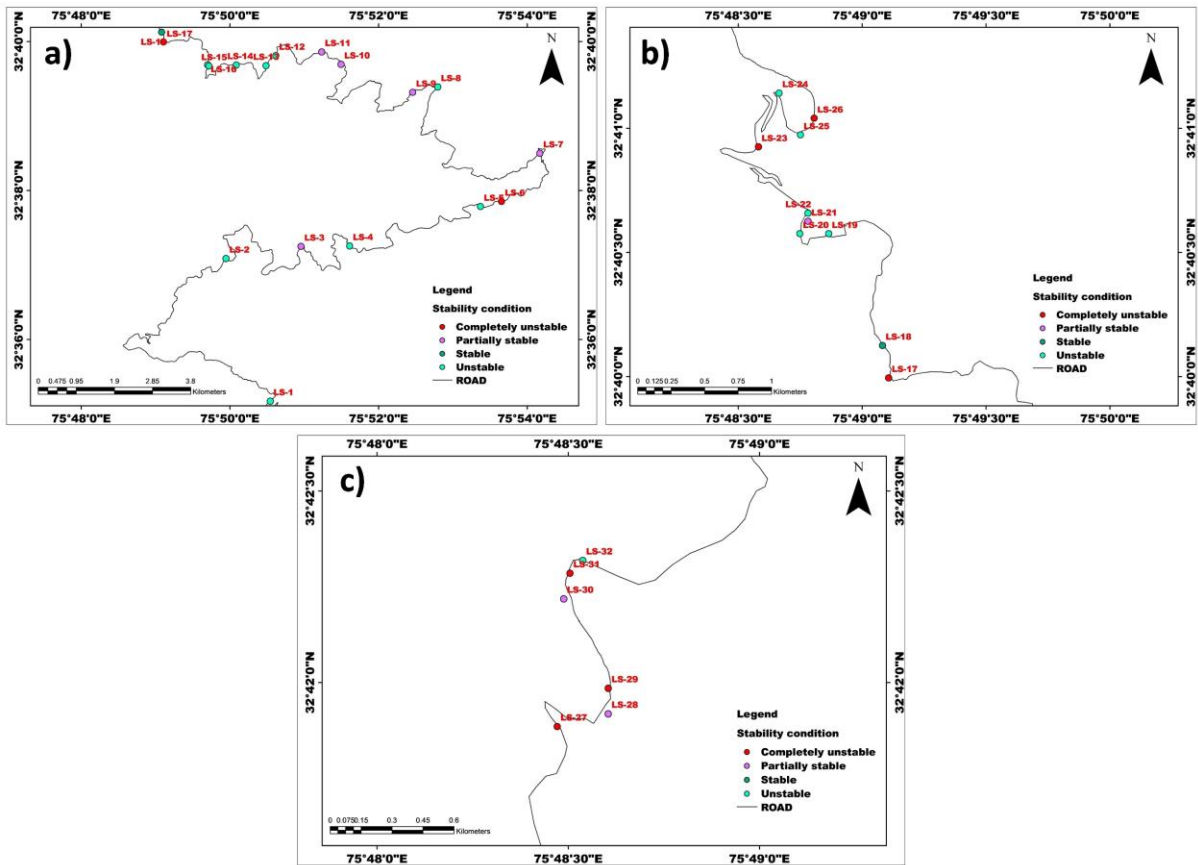


Fig. 5 a, b and c) Wider view of slope stability maps showing road and the stability condition of each land sliding site along the road.

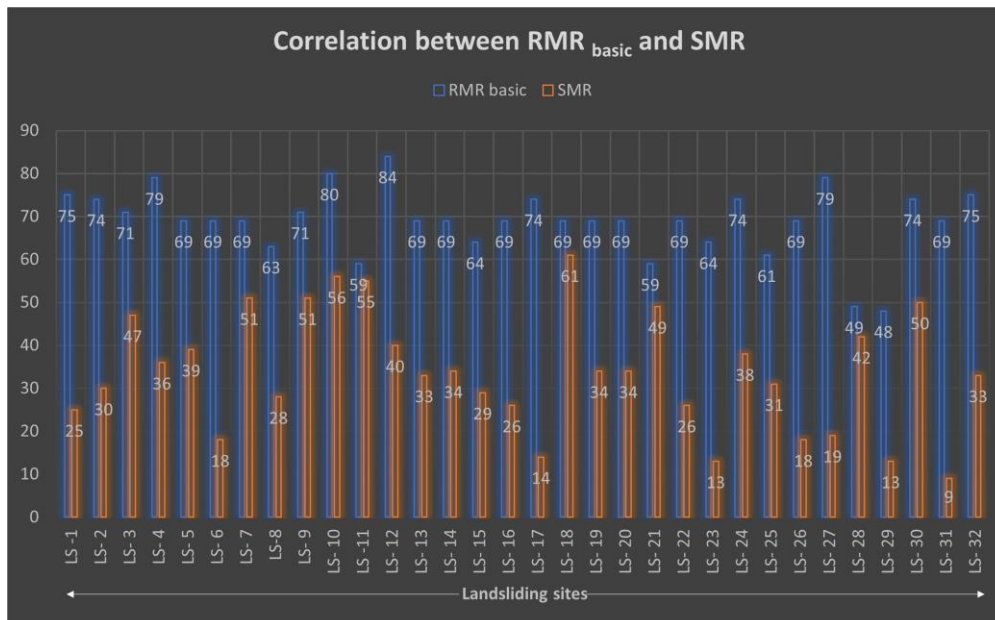


Fig. 6: The contrasting results evaluated through implementation of RMR_{basic} and SMR.

CAUSES OF FAILURE:

The study revealed that the occurrence of andslides in the study region was the cumulative effect of several factors. According to the research’s

key findings, the main causes that are reducing the stability of the slopes in the study area are wide and open apertures of the structural discontinuities, systematic toe cutting, weak lithology, high slope

Table 6. Mitigation measures suggested for each land sliding site (Romana, 1985)

Site No.	Suggested mitigation measures
LS -1	Spot bolting, toe wall and/or concrete, well developed deep drainage system
LS- 2	Anchors, systematic shotcrete, toe wall and/or concrete, well developed deep drainage system
LS- 3	Toe ditch and/or nets, systematic bolting/anchors, systematic shotcrete, toe wall and/or dental concrete, drainage
LS- 4	Systematic bolting, wire mesh, toe wall and/or concrete, well developed drainage system
LS- 5	Systematic bolting, wire mesh, toe wall and/or concrete, well developed drainage system
LS- 6	Gravity or anchored wall or systematic bolts, wire mesh, toe wall and/or concrete, drainage
LS- 7	Spot or systematic bolting, spot shotcrete, drainage
LS- 8	Anchors, systematic shotcrete/bolting, toe wall and/or concrete, well developed drainage system
LS- 9	Spot or systematic bolting, spot shotcrete, drainage
LS- 10	Toe ditch and/or nets, spot or systematic bolting, spot shotcrete, drainage
LS -11	Spot or systematic bolting, spot shotcrete, drainage
LS- 12	Toe ditch and/or wire meshes, systematic bolting/anchors, systematic shotcrete, toe wall and/or dental concrete, drainage
LS- 13	Anchors, systematic shotcrete, toe wall and/or concrete, well developed drainage system
LS- 14	Anchors, systematic shotcrete, toe wall and/or concrete, well developed drainage system
LS- 15	Systematic reinforced shotcrete/systematic bolting, wire mesh, toe wall and/or concrete, well developed deep drainage system
LS- 16	Systematic reinforced shotcrete/systematic bolting, wire mesh, toe wall and/or concrete, well developed deep drainage system
LS- 17	Gravity or anchored wall, toe wall and/or concrete, deep drainage
LS- 18	Toe ditch or fence nets, spot or systematic bolting, drainage
LS- 19	Anchors, systematic shotcrete, toe wall and/or concrete, well developed drainage system
LS- 20	Anchors, systematic shotcrete, toe wall and/or concrete, well developed drainage system
LS- 21	Toe ditch and/or wire meshes, systematic bolting/anchors, systematic shotcrete, toe wall and/or dental concrete, drainage
LS- 22	Systematic reinforced shotcrete/systematic bolting, wire mesh, toe wall and/or concrete, well developed deep drainage system
LS- 23	Gravity or anchored wall, toe wall and/or concrete, deep drainage
LS- 24	Anchors, systematic shotcrete, toe wall and/or concrete, well developed drainage system
LS- 25	Anchors, systematic shotcrete, toe wall and/or concrete, well developed drainage system
LS- 26	Gravity or anchored wall, toe wall and/or concrete, deep drainage
LS- 27	Gravity or anchored wall, toe wall and/or concrete, deep drainage
LS- 28	Toe ditch and/or nets, systematic bolting/anchors, systematic shotcrete, toe wall and/or dental concrete, drainage
LS- 29	Gravity or anchored wall, toe wall and/or concrete, deep drainage
LS- 30	Toe ditch and/or nets, systematic bolting/anchors, systematic shotcrete, toe wall and/or dental concrete, drainage
LS- 31	Gravity/anchored wall or systematic bolts with wire meshes, toe wall and/or concrete, deep drainage
LS- 32	Anchors, systematic shotcrete, toe wall and/or concrete, well developed drainage system

gradient, anthropogenic activities, shear zones, absence of drainage system and highly stressed regime due to the proximity to various faults.

SUGGESTED MITIGATION MEASURES:

The recommended mitigation measures for each location are shown in table 6.

CONCLUSION:

Two significant empirical methodologies-SMR, and kinematic analysis, were used in this work to provide adequate conclusions on slope stability circumstances. The primary goal of using these methodologies in the research region was to gain a better understanding of the rock quality, slope stability, and likely modes and orientations of failure. SMR aided in assessing slope stability; and kinematic analysis aided in predicting the direction and mode of failures. SMR data show that the majority of the sites are in the unstable group, and kinematic analysis suggests that the wedge mode of failure is the most dominant form of failure in the study area. The variance in comparison studies of RMR_{basic} and SMR values suggests that the interaction between structurally oriented discontinuities and the slope is one of the

significant factors which is controlling slope instability in the study area.

ACKNOWLEDGEMENTS:

We are highly grateful to the Department of Geology, University of Jammu for their continuous assistance and for providing the facilities needed to conduct this study.

CONFLICT OF INTEREST:

The authors declare no conflict of interest.

REFERENCES:

- Bieniawski, Z. T. (1973). Engineering classification of jointed rock masses. *Civil Engineering= Siviele Ingenieurswese*, 1973(12), 335-343.
- Bieniawski, Z. T. (1979). The geomechanics classification in rock engineering applications. In *ISRM Congress* (pp. ISRM-4CONGRESS). ISRM.
- Bieniawski, Z. T. (1984). Rock mechanics design in mining and tunneling, *Balkema, Rotterdam, Boston*, 55-95.
- Bieniawski, Z. T. (1989). Engineering rock mass classifications: a complete manual for engineers and geologists in mining, civil, and petroleum engineering. *John Wiley & Sons*.

- Bieniawski, Z. T. (1993). Classification of rock masses for engineering: the RMR system and future trends. In *Rock testing and site characterization* (pp. 553-573). Pergamon.
- Chen, Z. (1995). Recent developments in slope stability analysis. In *ISRM Congress* (pp. ISRM-8CONGRESS). ISRM.
- Choudhary, J. B. (2006). Geotechnical and Structural evaluation of Tectonostratigraphic Units along Head Race Tunnel, Sewa Hydroelectric Project. Stage-II, Kathua District. *Unpublished Ph. d thesis. University of Jammu, Jammu.*
- Dhiman, R. K., and Thakur, M. (2022). Slope Mass Rating (SMR) charts for onsite classification of rock slopes. *Authorea Preprints.*
- Duran, A., and Douglas, K. (2000). Experience with empirical rock slope design. In *ISRM International Symposium* (pp. ISRM-IS). ISRM.
- Goodman, R. E. (1991). Introduction to rock mechanics. *John Wiley & Sons, New York, 562.*
- Hoek, E., and Bray, J. D. (1981). Rock slope engineering. *CRC press.*
- Jaiswal, A., Verma, A. K., and Singh, T. N. (2023). Evaluation of slope stability through rock mass classification and kinematic analysis of some major slopes along NH-1A from Ramban to Banihal, North Western Himalayas. *Journal of Rock Mechanics and Geotechnical Engineering.*
- Jamwal, M., Pandita, S. K., Sharma, M., and Bhat, G. M. (2020). Petrography, Provenance and Diagenesis of Murree Group Exposed along Basohli-Bani Road, Kathua District, Jammu and Kashmir. *Journal of the Indian Association of Sedimentologists, 37(2), 15-26.*
- Kainthola, A., Pandey, V. H. R., Singh, P. K., and Singh, T. N. (2023). Stability Assessment of Markundi Hills Using Q-slope, SMR and Simulation Tools. In *Landslides: Detection, Prediction and Monitoring: Technological Developments* (pp. 87-107). Cham: Springer International Publishing.
- Kumsar, H., Aydan, Ö., and Ulusay, R. (2000). Dynamic and static stability assessment of rock slopes against wedge failures. *Rock Mechanics and Rock Engineering, 33, 31-51.*
- Markland, J. T. (1972). A useful technique for estimating the stability of rock slopes when the rigid wedge slide type of failure is expected. *Interdepartmental Rock Mechanics Project, Imperial College of Science and Technology.*
- Palmstrom, A. (1982). The volumetric joint count—a useful and simple measure of the degree of rock mass jointing. In *International Association of Engineering Geology. International congress. 4* (pp. 221-228).
- Palmström, A. (1996). The weighted joint density method leads to improved characterization of jointing. In *Conference on recent advances in tunnelling technology, New Delhi.*
- Palmstrom, A. (2005). Measurements of and correlations between block size and rock quality designation (RQD). *Tunnelling and Underground Space Technology, 20(4), 362-377.*
- Pandey, V. H. R., Kainthola, A., Sharma, V., Srivastav, A., Jayal, T., and Singh, T. N. (2022). Deep learning models for large-scale slope instability examination in Western Uttarakhand, India. *Environmental Earth Sciences, 81(20), 487.*
- Pantelidis, L. (2009). Rock slope stability assessment through rock mass classification systems. *International Journal of Rock Mechanics and Mining Sciences, 46(2), 315-325.*
- Romana, M. (1985). New adjustment ratings for application of Bieniawski classification to slopes. In *Proceedings of the international symposium on role of rock mechanics, Zacatecas, Mexico* (pp. 49-53).
- Romana, M., Serón, J. B., and Montalar, E. (2003). SMR geomechanics classification: application, experience and validation. In *ISRM Congress* (pp. ISRM-10CONGRESS). ISRM.
- Sah, N., Kumar, M., Upadhyay, R., and Dutt, S. (2018). Hill slope instability of Nainital City, Kumaun Lesser Himalaya, Uttarakhand, India. *Journal of rock mechanics and geotechnical engineering, 10(2), 280-289.*
- Schuster, R. L. (1996). Socioeconomic significance of landslides. *Landslides: Investigation and mitigation, 247, 12-35.*
- SDMP. (2017) State Disaster Management Plan. India: Department of Disaster Management, Relief, Rehabilitation and Construction, Government of Jammu and Kashmir.
- Sharma, V., Bhat, G. M., Choudhary, J. B., and Singh, Y. (2010). Stability Assessment of rock slopes using RMR, modified SMR Technique and Kinematic analysis around Barrage site of Chutak Hydroelectric Power Project. *Himalayan Geology, 31(1), 35-4.*
- Siddique, T., Pradhan, S. P., Vishal, V., Mondal, M. E. A., and Singh, T. N. (2017). Stability assessment of Himalayan Road cut slopes along National Highway 58, India. *Environmental Earth Sciences, 76, 1-18.*
- Singh, B., and Goel, R. K. (2002). Software for engineering control of landslide and tunnelling hazards. *CRC Press.*
- Singh, T. N., Verma, A. K., and Sarkar, K. (2010). Static and dynamic analysis of a landslide. *Geomatics, Natural Hazards and Risk, 1(4), 323-338.*
- Tomás, R., Delgado, J., and Serón, J. B. (2007). Modification of slope mass rating (SMR) by continuous functions. *International journal of rock mechanics and mining sciences, 44(7), 1062-1069.*

- Tomás, R., Cuenca, A., Cano, M., and García-Barba, J. (2012). A graphical approach for slope mass rating (SMR). *Engineering Geology*, 124, 67-76.
- Um, J. G., and Kulatilake, P. H. (2001). Kinematic and block theory analyses for shiplock slopes of the Three Gorges Dam Site in China. *Geotechnical & Geological Engineering*, 19, 21-42.
- Vishal, V., Pradhan, S. P., and Singh, T. N. (2015). Analysis of stability of slopes in Himalayan terrane along National Highway: 109, India. In *Engineering Geology for Society and Territory-Volume 1: Climate Change and Engineering Geology* (pp. 511-515). Springer International Publishing.
- Vishal, V., Siddique, T., Purohit, R., Phophliya, M. K., and Pradhan, S. P. (2017). Hazard assessment in rockfall-prone Himalayan slopes along National Highway-58, India: rating and simulation. *Natural Hazards*, 85, 487-503.
- Yoon, W. S., Jeong, U. J., and Kim, J. H. (2002). Kinematic analysis for sliding failure of multi-faced rock slopes. *Engineering Geology*, 67(1-2), 51-61.

A Detailed Report on

39th

CONVENTION OF INDIAN ASSOCIATION OF SEDIMENTOLOGISTS

Dec. 06th to 08th, 2023

Tamil Nadu, INDIA

International Conference on

**Voyage of Sedimentology from the Mountains
to the Oceans: An Innovative Trajectory**



IAS@AU - 2023



DEPARTMENT OF EARTH
SCIENCES

ANNAMALAI
UNIVERSITY



39th Convention of Indian Association of Sedimentologists

&

International Conference

on

Voyage of Sedimentology from the Mountains to the Oceans: An Innovative Trajectory

Organised By

Department of Earth Sciences Annamalai University, Annamalai
Nagar, Chidambaram, Tamil Nadu, India

Convener

Dr. S Vasudevan, Associate Professor

Advisor

Prof. T. Ramkumar

Organizing Secretaries

Dr. M.V. Mukesh, Associate Professor

Dr. P. Anandhan, Assistant Professor

Dr. G. Ramesh, Assistant Professor

Venue

Tech-Park - Auditorium
Kumararajah Muthiah Chettiar Building
Annamalai University Annamalai Nagar
Chidambaram - 608 002, Tamil Nadu, India



IAS Governing Council

- President** : **Prof. G. N. Nayak, Goa University, Goa**
- Vice Presidents** : **Prof. G. M. Bhat, Jammu University**
Prof. S. Banerjee, IIT Bombay, Mumbai
- General Secretary** : **Prof. M E A Mondal, AMU, Aligarh, UP**
Prof. A.V.Joshi, M.S. Baroda University
- Joint Secretary** : **Prof. Subir Sarkar, Jadavpur University, Kolkata**
Prof. B.P. Singh, BHU, Varanasi, UP
- Treasurer** : **Prof. Abdullah Khan, AMU, Aligarh, UP**
- Joint Treasurer** : **Dr. S.H. Alvi, AMU, Aligarh, UP**
- Editor /Joint Editor** : **Prof. R. Nagendra, Bangalore, Karnataka**
Dr. Bashir Ahmad Lone, Jammu University

Members:

- Dr. S.R. Singara Subramanian, Professor of Earth Sciences, AU**
- Dr. R.S. Kumar, Professor of Earth Sciences, AU**
- Dr. R. Prabhakaran, Associate Professor of Earth Sciences, AU**
- Dr. S. Aravindan, Associate Professor of Earth Sciences, AU**
- Dr. T. Jeyavel Rajakumar, Associate Professor of Earth Sciences, AU**
- Dr. B. Selvaraj, Associate Professor of Earth Sciences, AU**
- Dr. N. Ganesh, Assistant Professor of Earth Sciences, AU**
- Dr. K. Sujatha, Assistant Professor of Earth Sciences, AU**

Supporting Researchers:

- Dr. P. Balamurugan, Dr. R. Selvaganapathi, Dr. G. Sathiyamoorthy**
Mr. S. Baranidharan, Mr. J. Vigneshwar, Mr. P. Sivaranjan, and
Mr. S. Pravinraj

The 39th Annual Convention of the Indian Association of Sedimentologists (IAS) and the International Conference on "**Voyage of Sedimentology from the Mountains to the Oceans: An Innovative Trajectory**" took place from December 6th to 8th, 2023, at the Department of Earth Sciences, Annamalai University. This event was organized under the auspices of the IAS and held in anticipation of the impending centenary year of Annamalai University and the Azadi Ka Amrit Mahotsav.

The conference was meticulously conceptualized to showcase various aspects of sedimentary processes, environments, and resources, aligning with the overarching themes of the approaching centenaries. It aimed to bring together experts, researchers, academicians, and professionals in sedimentology to share their groundbreaking research, ideas, and experiences related to sedimentary processes, environments, and resources. As a multidisciplinary field, Sedimentology plays a pivotal role in elucidating Earth's history, managing energy and mineral resources, addressing environmental concerns, mitigating geological hazards, studying climate change, and supporting civil engineering and construction projects. The significance of sedimentology lies in its ability to provide invaluable insights into the processes and environments shaping our planet, contributing to various practical applications with profound societal, economic, and environmental implications.

With a comprehensive agenda, the conference featured the International Association of Sedimentologists Lecture series, keynote speeches, invited talks, oral and poster presentations, and Workshops centered on identified themes. Additionally, post-conference field excursions were organized to enhance participants' understanding and exploration of sedimentological concepts in practical settings.

Considering the expansive range of research topics and their credibility within the field of sedimentology, we have identified ten overarching scientific themes. These themes span various disciplines and employ multidisciplinary approaches, reflecting the diverse and dynamic nature of sedimentological research. The ten major scientific themes are as follows:

1. Ancient Earth : Unveiling the Climate & Environment of Deep Time
2. Forces Beneath : Exploring Tectonics & Volcano Sedimentology
3. Life Through Layers : Understanding Biological Processes in Sedimentation

4. From Land to Sea : Decoding Continental Depositional Systems
5. Oceanic Mysteries : Unraveling Marine Depositional Systems
6. Shaping the Present : Modern Sedimentary Processes Unveiled
7. Treasures of the Earth: Unlocking Resources through Sedimentology
8. Earth's Vulnerability : Investigating Environmental & Hazard Sedimentology
9. Chemical Clues : Insights into Sedimentary Geochemistry
10. Cutting-Edge Sedimentology : Exploring New Technologies in the Field

In facilitating a post-conference field excursion, the intention was to acquaint young researchers with the intricacies of field-based sedimentology in the Coastal Geomorphology (Explore the unique mangrove forests of Pichavaram and the picturesque Pondicherry Beach). The participants were exposed to the activities of Lignite Opencast Mining, Neyveli (Gain firsthand experience of lignite mining and power generation by visiting Neyveli, home to NLC India Limited).

Synopsis View of the Conference Content:		
S. No.	Details	No.
1	Convention Address	1
2	International Association of Sedimentologists Lecture Series Talk	3
3	Invited Key Note Address	12
4	Distinguished Lectures	12
5	Paper Presentation - Oral (32), Virtual (11) and Poster (24)	67
6	Young Sedimentologists Award Presentations	3
7	Workshops	2
8	Post-Conference Field Visit	2
9	Total Abstracts	172

The opening session of the **39th Convention of the Indian Association of Sedimentologists (IAS)** and the International Conference on "**Voyage of Sedimentology from the Mountains to the Oceans: An Innovative Trajectory**" took place at the Tech Park Auditorium of Annamalai University. Professor RM Kathiresan, Vice-Chancellor of Annamalai University, delivered the inaugural address. He spoke on the sediments' importance, characteristics, and influence on agricultural activities. Enhanced Soil and sediments are the life to the river, plants, and living organisms, which is the propulsive vitality for the country's socio-economic growth.



Professor Ganapathy Shanmugam, University of Texas at Arlington, USA, gave the convention address. At the same time, Professor Daniel Ariztegui from the University of Geneva, Switzerland, served as the Guest of Honour. Professor G.N. Nayak, President of the Indian Association of Sedimentologists, delivered a special address. Professor R.S. Kumar, Head of the Department, warmly welcomed the attendees. Professor T. Ramkumar, the Advisor, provided detailed insights into the conference, and Dr. S. Vasudevan, the Convener, expressed gratitude in the form of a vote of thanks during the inaugural function of the convention and International conference. Afterward, an abstract volume was released during the inauguration.

CONVENTION ADDRESS:

Distinguished Annamalai University alumnus **Professor Ganapathy Shanmugam**, currently affiliated with the University of Texas at Arlington, USA, delivered an enlightening discourse on the challenges within sedimentological research. His insightful presentation not only elucidated the intricacies of this field but also underscored the tremendous opportunities it presents. Drawing upon his illustrious 40-year career, Professor Shanmugam generously shared his wealth of experience with the conference delegates, inspiring them to strive for success. During this event, he delivered a captivating address titled "My Scientific Journey from Annamalai University to America and Beyond (1962 – 2023): Process Sedimentology, Appalachian Tectonics, Physical Oceanography, Fossil Fuels, Climate Change, and J. Robert Oppenheimer."



Professor Shanmugam recounted his rich experiences, highlighting an impressive portfolio of almost 150 completed projects and over 380 publications in esteemed Indian and international journals. Noteworthy is his role as a principal investigator for various scientific projects, including fan delta and braid deltas, estuarine sedimentation, hyperpycnal flows, submarine fans, MTD (Mass Transport Deposits), and more. His invaluable contributions in diverse scientific domains reflect the depth of his expertise and the breadth of his impact. Professor Shanmugam's address served as a beacon for aspiring researchers, providing profound insights into the complexities of sedimentological research while exemplifying the potential for exploration and achievement in this dynamic field.

INTERNATIONAL ASSOCIATION OF SEDIMENTOLOGISTS LECTURE SERIES:

Renowned scholar **Professor Daniel Ariztegui**, former President of the International Association of Sedimentologists and affiliated with the University of Geneva, Switzerland, delivered a compelling discourse that propelled the advancement of global sedimentological research. Professor Ariztegui's presentation, titled "Biotic and Abiotic Signatures in Lacustrine Carbonates and Their Application to the Earth and Planetary Fossil Record," delved into the fascinating realm of lacustrine carbonates and their significance in deciphering the Earth and planetary fossil record. Emphasizing the crucial role of microbialites, he underscored their importance in geological evidence of the planet's ecosystem.



Professor Ariztegui also shared insights from his research conducted in the challenging habitats of Argentinean and Chilean Patagonia. The examination focused on unraveling the characteristics of microbialites through a meticulous analysis of fabric, mineralogy, and geochemistry attributes. The research findings elucidated the intricate coupling of microbiological and mineralogical activities, offering valuable insights into bio-mineralization processes. Highlighting the significance of microbial carbonates, Professor Ariztegui emphasized their pivotal role in enhancing the reconstruction of environmental conditions. The

research outcomes contribute crucial data that enhances our understanding of the Earth's history and provides valuable perspectives for future exploration and scientific inquiry. Professor Ariztegui's comprehensive presentation illuminated the profound interplay between microbiology and mineralogy in sedimentological research.

Esteemed international speaker **Professor Matthieu J.B. Cartigny** from the University of Durham, United Kingdom, delivered an enlightening presentation on the intriguing subject, "Demystifying Turbidity Currents through Ocean Floor Observation." Profoundly sharing his expertise, he shed light on the dynamics of sediment density flows and how turbidity currents instigate transformative alterations in the ocean floor.



Professor Cartigny's research not only unraveled the significance of turbidity currents but also accentuated their role in sediment fluxes, emphasizing their connection to the carbon cycle. He articulated how these currents play a vital role in sustaining ecological communities on the deep ocean bed, contributing to the intricate web of marine life.

Through rigorous exploration, Professor Cartigny underscored the hazards of turbidity currents to submarine infrastructures, making a compelling case for a comprehensive understanding of these phenomena. The insights shared by Professor Cartigny deepen our knowledge of turbidity currents and bring attention to their far-reaching ecological implications and potential risks to underwater structures. His presentation, anchored in ocean floor observations, is valuable to sedimentological research and underscores the interconnectedness of marine processes with broader ecological systems.

Esteemed international speaker **Professor Tracy D. Frank** from the University of Connecticut, USA, delivered a thought-provoking presentation on the intricate topic, "Pace, Magnitude, and Nature of Terrestrial Climate Change through the End-Permian Extinction in Southeastern Gondwana." Her research delved into

the critical aspects of rapid climate change and environmental shifts, focusing on their significant role in extinction at the end of the Permian period.



Professor Frank's study, centered on eastern Australia's Bowen and Sydney basins, presented a stratigraphically complete upper Permian to middle Triassic succession. This accumulation occurred in coastal alluvial plains within retro-arc foreland basin settings. The research offered valuable insights into the End-Permian extinction horizon, revealing the abrupt disappearance of coal-forming forest communities. The inference drawn from Professor Frank's meticulous study illuminated the profound impact of acidification on the persistence of moisture-loving terrestrial flora. The immediate extinction observed was coupled with the constant moisture nature, which facilitated the formation of coal-forming vegetation in the Mid-Triassic period.

This presentation contributes significantly to our understanding of the End-Permian extinction event and underscores the intricate interplay between climate change, environmental shifts, and terrestrial ecosystems. Professor Frank's research enriches the scientific discourse on paleoclimatology and extinction events, emphasizing the importance of studying geological records for insights into our planet's dynamic environmental history.

KEYNOTE ADDRESS:

The 12 keynote addresses delivered during the conference served as a collective powerhouse of knowledge, seamlessly merging diverse perspectives and cultivating a profound understanding of sedimentological research across various domains. Each keynote speaker contributed unique insights, enriching the conference with their expertise. The comprehensive range of topics covered during these addresses facilitated a holistic exploration of sedimentology, bringing together



Prof. G.N. NAYAK



Prof. A.V. JOSHI



Dr. R.K. SINGHAL



Prof. M. E. A. MONDAL

scholars, researchers, and professionals from different disciplines. The wealth of knowledge shared through these keynotes elevated the conference and laid the foundation for continued advancements and discoveries in the dynamic field of sedimentology.

President of the Indian Association of Sedimentologists, Professor G.N. Nayak from Goa University, delivered a compelling keynote address that delved into the theme, "Weathering and Climate Fluctuations during the Last ~6000 Years: An Investigation through a Sediment Core, off Mahanadi River Mouth, Western Bay of Bengal." His presentation captivated the audience, shedding light on the intricate interactions between weathering processes and climate variations over the past millennia.

In his keynote address, **Professor A.V. Joshi**, from the Department of Earth Sciences at M.S. University of Baroda, Vadodara, delivered a comprehensive overview under the title "Lower Tapti Basin of Gujarat – Example of Quaternary Fluvial Sedimentation and Neo-Tectonism." This illuminating presentation provided valuable insights into the intricate processes at play in the Lower Tapti Basin. It offered a profound understanding of the dynamics of Quaternary fluvial sedimentation and neo-tectonism in the region.

Dr. Rakesh Kumar Singhal, Former Head of the Analytical Chemistry Division at Bhabha Atomic Research Center, Mumbai, delivered an insightful address on "Application of Radioisotope in Assessment of Potential Ecological Risk due to

Sedimentation and Accumulation of Trace Metals." Dr. Singhal's presentation highlighted the complexities of these environmental processes and underscored the importance of employing advanced analytical techniques for a comprehensive understanding of ecological dynamics.

Professor M. E. A. Mondal, General Secretary of the Indian Association of Sedimentologists at Aligarh Muslim University (AMU), Aligarh, delved into "Clastic Sediment Geochemistry – A Tool for Enhancing Provenance Understanding." He has showcased the critical importance of geochemical analyses in unraveling sediment provenance, contributing to a more nuanced comprehension of geological processes and environmental dynamics.

In his keynote address, **Dr. Rajat Mazumder**, from the Department of Applied Geosciences at the German University of Technology in Oman, delved into "Precambrian Terrestrial Sedimentation on the Singhbhum Craton, India." With a focus on this ancient geological formation, Mr. Mazumder provided a compelling glimpse into Earth's terrestrial history during the Precambrian era. His presentation shed light on the intricate processes that shaped the terrestrial sedimentation on the Singhbhum Craton, contributing valuable insights to our understanding of the geological evolution of this significant region.

Professor S.M. Ramasamy, Professor of Eminence in the Department of Remote Sensing at Bharathidasan University, Tiruchirappalli, shared his profound expertise in a keynote address titled



Dr. RAJAT MAZUMDER



Prof. S.M. RAMASAMY



Prof. D. PADMALAL



Dr. D. GNANASUNDAR &
Prof. SM USSAIN

"Earth Systems and The Depositional Dynamics." Through his presentation, Professor Ramasamy provided a holistic perspective highlighting Earth's systems' interconnectedness and elucidated the intricate dynamics governing deposition processes. His address showcased his eminence in the field and contributed valuable insights into the complex interplay between Earth's systems and the resulting depositional phenomena.

Professor D. Padmalal, Scientist G and Group Head of the Hydrology Group (HyG) at the National Centre for Earth Science Studies in Thiruvananthapuram, Kerala, delivered a keynote address titled "Late Quaternary Coastal Evolution of Kerala, Southwest India: Selected Case Studies Using Multiproxy Analysis." In his presentation, Professor Padmalal presented compelling case studies that utilized multiproxy analysis to unravel the intricate details of the late Quaternary coastal evolution in Kerala. His address not only showcased his leadership as a scientist but also demonstrated the application of advanced analytical techniques in understanding the geological history of the region.

Dr. D. Gnanasundar, Senior Joint Commissioner-III at the National Hydrology Project, Ministry of Jal Shakti, India, delved into the intricacies of "Decoding Sequential Stratification (Sediment Stratigraphy) of Coastal Aquifers to Understand Aquifer Hydraulics for Decisive Management of Coastal Aquifers." Dr. Gnanasundar provided valuable insights into the dynamic world of aquifer stratigraphy and hydraulics through his exploration. His presentation demonstrated his leadership in the field and contributed significant

knowledge to the understanding and managing of coastal aquifers.

Prof. Shaik Mohammad Hussain, from the Department of Geology at the University of Madras, provided a comprehensive address on "Sediment-Ostracoda Relationship In Freshwater, Brackish Water, And Marine Environments Of Tamil Nadu: Implications On The Siltation And Paleoenvironment." Prof. Hussain unveiled the intriguing relationship between sediment and ostracoda in diverse aquatic environments in his presentation. This exploration demonstrated his expertise and illuminated the implications of this relationship on siltation patterns and paleoenvironmental reconstructions.

In her keynote address, **Dr. Binita Phartiyal**, Scientist-F at the Birbal Sahni Institute of Palaeosciences in Lucknow, U.P., shed light on "Landscape Evolution, Sediment Characterization, and Climatic Record of Northwest Trans-Himalaya during Late Quaternary." Through her comprehensive presentation, Dr. Phartiyal provided valuable insights into the dynamic processes of landscape evolution, sediment characterization, and climatic records in the Northwest Trans-Himalayan region during the Late Quaternary period.

In his keynote address, **Dr. Himanshu Bali**, from the Department of Geology at the Central University of Tamil Nadu, delved into the intriguing topic of "Decoding Tectonic History and Related Paleooceanographic Shifts through Biogenous Sediments: Exploring the Applications of Foraminifera." His presentation gave unique

perspective on utilizing foraminifera to decode geological and paleoceanographic shifts. His expertise and exploration of this microscopic marine life enriched the symposium by providing valuable insights into the historical changes in Earth's tectonic activity and paleoceanographic conditions.

DISTINGUISHED LECTURES

The conference featured a series of distinguished lectures, each offering valuable insights into various aspects of sedimentological research. Here is an enhanced description of the distinguished lectures:



Glimpses of Distinguished Lectures

- **Dr. Ananya Chutia** delivered an illuminating lecture on the "Paleocene-Eocene Thermal Maximum Event – In Search of Its Evidence from Eastern Himalaya, Arunachal Pradesh," providing a comprehensive exploration of the geological evidence of this significant climatic event.
- **Dr. Arvind Kumar Singh's** lecture on "Shales: An Essential User Guide to Understand Sediment Dynamics, Operative Processes, and Ancient Environments" offers a detailed guide to deciphering sediment dynamics and ancient environments through studying shales.
- **Dr. Santanu Banerjee** presented insights on "Reverse Weathering through Geological Time and Its Implications," unraveling the geological processes of reverse weathering and its broader implications.
- **Dr. Sandip Kumar Roy** explored the topic of "In Quest of Big Hydrocarbon Discoveries from Indian Sedimentary Basins," shedding light on the search for significant hydrocarbon reserves in Indian sedimentary basins.
- **Dr. S.K Srivastava** discussed "Cenozoic Sedimentation in Parts of Inner Fold Belt, Nagaland, India: Changes Through Time," providing a temporal perspective on sedimentation dynamics in the Inner Fold Belt of Nagaland.
- **Dr. Suchana Taral** shared insights on "Trace Fossils as a Proxy for Recognizing Depositional Environment in Stratigraphic Record: A Case Study from the Siwalik Succession of the Eastern Himalaya, Arunachal Pradesh," highlighting the utility of trace fossils in understanding depositional environments.
- **Dr. Seema Singh's** lecture on "Palaeosol Micromorphology as a Tool in Geological Investigations: Indian Context" explored the application of palaeosol micromorphology as a valuable tool in geological studies within the Indian context.
- **Dr. Priyabrata Das** provided insights into "Rhythmic Stratifications in the Martian Rock Records," offering a fascinating perspective on the rhythmic stratifications observed in the rock records of Mars.
- **Dr. Pratima M. Kessarkar** delved into the question, "Are the Himalayas a Major Source of Sediments to the Bay of Bengal during the Recent Past?" examining the role of the Himalayas in contributing sediments to the Bay of Bengal in recent geological history.
- **Dr. Adrita Choudhuri's** lecture on "Evolution of a Confined Gravelly River to a Braided- Meandering River in the Lake Cretaceous Khasi Group, Southern Shillong Plateau, NE India," traced the evolutionary path of a river system in the Lake Cretaceous Khasi Group.
- **Dr. Rasikh Barkat** explored "Continental Sedimentation Preceding the Emergence of Terrestrial Plants: An Example from Neoproterozoic Banganapalle Formation, Kurnool Group, India," shedding light on continental sedimentation patterns before the emergence of terrestrial plants during the Neoproterozoic era.

Each distinguished lecture added depth and breadth to the symposium, contributing valuable perspectives to the field of sedimentology

ORAL, VIRTUAL and POSTER PRESENTATION

The conference features an array of captivating presentations spanning sedimentology, with a particular focus on diverse topics such as:

- Unveiling the Provenance and Geochemical Traits of Argillaceous Sedimentary Rocks within the Paleoproterozoic Formations of the Cuddapah Basin, India.
- Exploring Sedimentological Signatures of Ramp-Rimmed Carbonate Platform Settings within the Palaeoproterozoic Vempalle Formation, Papaghani Group, Cuddapah Basin.
- Analyzing Microfacies and Diagenetic Processes in the Limestones of the Middle-Jurassic Fort Member, Jaisalmer Formation, Western Rajasthan, India, and their Implications for Depositional Environments and Reservoir Quality.
- Investigating Floral Diversity and Depositional Environments of Early Permian Sequences in the Chirimiri Coalfield, Son Basin, India.



Glimpses of Delegates Presentation

- Unraveling the Geochemical Makeup of Siliciclastic Sedimentary Rocks in the Paleoproterozoic Bijawar Basin, Bundelkhand Craton, Central India, and its Insights into Provenance, Paleoweathering, and Geodynamics.
- Architectural Analysis of Late Miocene Middle Siwalik Fluvial Sequences in the Himalayan Foreland Basin, India.
- Deciphering the Sedimentation History of the Deformed and Metamorphosed Paleoproterozoic Parsoi Formation within the Mahakoshal Group, Central India Tectonic Zone, for Insights into Paleoproterozoic Back-Arc Rift Basin Sedimentation Patterns.
- Shedding Light on the Origin of Ooids through Insights from the Hamira Member, Jaisalmer, India.
- Exploring the Environmental Significance of Seismites and Tsunamites as Key Signatures for Sedimentary Environments and Tectonics in the Proterozoic Vindhyan Basin, India.
- Investigating Seismicity Forcing in an Immature Passive Margin Basin through a Case Study from the Lower to Middle Member of the Jhuran Formation, Kutch, India.
- Understanding Seismic-Induced Basin Subsidence across Siliciclastic to Carbonate Transitions in the Early-Middle Jurassic Succession of Jaisalmer, Rajasthan.



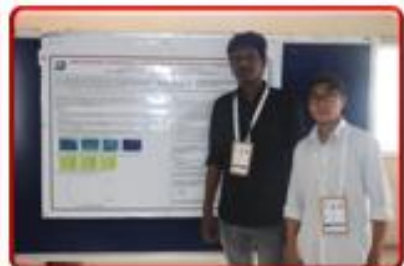
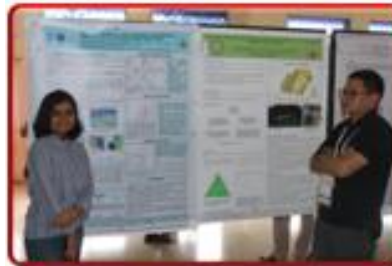
Best Paper Presentation:

**1st Prize Awarded to Mr. Kumil Ahmad, BSIP, Lucknow, and
2nd Prize to Ms. Concy Gomes, CSIR-NIO Goa**

India, and their Interpretation as Benthic Seaweeds.

- Documenting a New Record of Ediacaran Complex Acanthomorphic Palynoflora (ECAP) from the Mahi Formation of the Krol Belt, Lesser Himalaya, India.
- Establishing the Chronostratigraphic Status of the Bilara Carbonate within the Marwar Supergroup, Western India.
- Investigating Body Size-Ornamentation Covariation in Pisotrigonia from Kutch, Western India, and its Ecological and Evolutionary Implications.
- Developing a Depositional Model and Sequence Stratigraphic Framework for the Paleoproterozoic to Mesoproterozoic Lokapur Subgroup of the Bagalkot Group, Kaladgi Basin, Karnataka.
- Tracing Sediment Provenance and Dispersal Patterns from the Bay of Bengal to Antarctica.
- Analyzing Changes in Arabian Sea Denitrification Intensity off Goa through Inferences from a Sediment Core.
- Conducting X-ray diffraction Studies of Minerals and Sediment Textures of Saltpan Core from Mahabalipuram, Tamil Nadu, India.

- Tracing the Transition from Estuarine to Fluvial Environments through Records from the Middle Part of the Bhuj Formation, Kutch Mainland, India.
- Analyzing Architectural Elements of the Upper Part of the Bhuj Formation, Gadhsisa, Western Kutch, India.
- Field Identification of Paleosol with Continental Ichnofabric: A Case Study from the Early Miocene KhariNadi Formation in the Kutch (Kachchh) Basin, Gujarat.
- Exploring Exceptionally Preserved Macroscopic Carbonaceous Compression Fossils from the Early Mesoproterozoic Singhora Group, Chhattisgarh Supergroup,



Glimpses of Delegates Poster Presentation

- Investigating Petrographic and Granulometric Properties of Rocks from the Motur Formation (Middle Permian) around Imlikheda Area, Betul District, Madhya Pradesh.
- Unveiling Modern Sedimentary Processes through Research on the Source of Chemical Ions and Recharge Estimation in the Groundwater of Kandi Belt, Jammu District, Jammu and Kashmir, India.

This list captures the essence of each presentation with clarity and coherence, enhancing its overall appeal and comprehension for conference attendees.



YOUNG SEDIMENTOLOGISTS AWARD PRESENTATION



Young Sedimentologists Award Competitors Acknowledged for Their Efforts: Congratulations to Mr. Baranidaran, Annamalai University and Ms. Pratiksha P. Bagul, Savitribai Phule Pune University



**Best Poster Paper Presentation:
1st Prize Awarded to Mr. Gursewak Singh, BSIP, Lucknow, and
2nd Prize to Ms. Samhabana Lenka, CSIR-NIO, Goa**



Young Sedimentologists Award presented to Ms. Shifali Chip, Jammu University

WORKSHOPS



Prof. T. RAMKUMAR, from the Annamalai University, Tamil Nadu, India, led a comprehensive workshop titled "Chemical Clues: Coastal Sediment Geochemistry." During this workshop, he delved into the critical aspects of sedimentology, emphasizing the significance of geochemical factors, metal accumulation in sediments, bioavailability, partitioning, sequential extractions, and their implications for environmental management and risk assessments. Prof. Ramkumar's insightful session gave attendees valuable insights into the intricate interplay between chemical clues and coastal sediment dynamics, paving the way for informed decision-making and sustainable environmental practices.

Dr. ALEXANDER BRAISER, from the University of Aberdeen, King's College, Scotland, UK, hosted an enlightening workshop titled "Navigating the Publishing Process in Sedimentology." In the workshop, Dr. Braiser provided invaluable insights into the expectations of sedimentological editors, debunked myths surrounding the peer-review process, and underscored the importance of publication ethics. His engaging session empowered researchers with the knowledge and tools to navigate manuscript preparation and submission, guiding them toward successful publication in internationally renowned sedimentology journals.

CULTURAL PROGRAM



As a highlight of the conference, an enchanting cultural program titled "Bharathanatyam" dance was graced on the evening of December 6th, 2024. The captivating performance featured the students of the Department of Music at Annamalai University. Choreographer, Dr. A. Esther Pradeeba, an Associate Professor of Music, orchestrated the intricate movements and expressions, adding depth and finesse to the display of this classical dance form.

POST-CONFERENCE FIELD VISITS

A captivating two-day field excursion (9 and 10 December 2023) unfolded with a diverse itinerary to immerse participants in the rich tapestry of natural landscapes and human activities.

On the first day, participants embarked on a journey to Kodyampallyam and Pudahupalayam beaches, where they were treated to a firsthand exploration of coastal geomorphology. Amidst the picturesque beach environments, attendees witnessed the fascinating formations of groins, dunes, small cliffs, and the telltale imprints of longitudinal drift currents. The highlight of the day was an enchanting voyage into the heart of the unique mangrove forest of Pichavaram, expertly guided by boat through the labyrinthine waterways that wind their way through this remarkable ecosystem.





VALEDICTORY OF THE CONFERENCE AND GENERAL BODY MEETING OF THE INDIAN ASSOCIATION OF SEDIMENTOLOGISTS

The valedictory function of the 39th Annual Convention of the Indian Association of Sedimentologists (IAS) and the International Conference on "Voyage of Sedimentology from the Mountains to the Oceans: An Innovative Trajectory" marked the culmination of a stimulating and insightful event that brought together experts, researchers, and enthusiasts from around the world to explore the dynamic field of sedimentology.

Under the leadership of Prof. G. N. NAYAK, President, and Prof. M.E.A. MONDAL,

The second day of the excursion took participants to the heart of lignite opencast mining. From a panoramic viewpoint, attendees gained insight into the scale and scope of mining activities. Participants were granted access inside the mines, providing a rare opportunity to witness firsthand the intricacies of extraction processes. Moreover, the expedition ventured into the afforestation regions, offering a glimpse into efforts to restore and preserve the ecological balance amidst the mining landscape.



General Secretary of the Indian Association of Sedimentology, the activities and reports of the Association spanning from 2022 to 2023 were presented to the esteemed General Body and unanimously approved by its members. This reaffirmed the Association's commitment to advancing sedimentological knowledge and fostering collaboration within the community.

Dr. M. V. MUKESH, Organizing Secretary-1, warmly welcomed all attendees, expressing heartfelt gratitude for their invaluable contributions to the conference's success. Following this, **Dr. P. ANANDHAN**, Organizing Secretary-2, provided a concise overview of the conference's key themes and highlights, showcasing the diverse array of topics explored and the depth of discussions undertaken. The presidential address, delivered by **Dr. R.S. KUMAR**, Professor and Head of the Department of Earth Sciences, set the tone for the ceremony, highlighting the significance of the conference and the promising future of sedimentology research.

Distinguished speakers and experts were then invited to share their reflections on the conference and offer insights into the future directions of sedimentological studies, emphasizing emerging trends, technological advancements, and interdisciplinary collaborations.

Dr. A. RAGUPATHY, Director of DARE at Annamalai University, delivered a compelling valedictory address, encapsulating the essence of the conference and stressing the importance of sustained collaboration and knowledge exchange in propelling sedimentology forward. **Prof. SM. RAMASAMY**, Professor of Eminence at Bharathidasan University, Tamil Nadu, echoed these sentiments, underlining the significance of interdisciplinary approaches and innovative methodologies in addressing contemporary challenges in sedimentary processes.

During the ceremony, distinguished recognition was bestowed upon exemplary contributors and achievers in sedimentology research. Achievement Awards were presented to those who exhibited outstanding dedication and impact through their exceptional work, thereby acknowledging their significant contributions to the advancement of the field.

During the ceremony, recognition was bestowed upon outstanding contributors to sedimentology research. **Dr. G. RAMESH**, Organizing Secretary-3, lauded the exemplary achievements of **Prof. T.**



RAMKUMAR, Advisor at the Department of Earth Sciences, Annamalai University, before presenting him with the esteemed Special Achievement Award. This accolade honored Prof. RAMKUMAR's unwavering dedication and profound impact on the field of sedimentology.



Decoding Clastic Sedimentary Systems: Report Iftikhar Ahmad^{1*}, M.E.A. Mondal^{1#}, Kr. Farahim Khan¹ and P.P. Chakraborty²

¹Department of Geology, Aligarh Muslim University, Aligarh 202002

²Department of Geology, University of Delhi, Delhi 110007

E-mail Address: *iftikhar.gl@amu.ac.in, #erfan.mondal@gmail.com

Sedimentology plays a key role in hydrocarbon exploration as it helps in identifying and interpreting sedimentary environments, which in turn helps in locating potential hydrocarbon reservoirs. Also, for a better understanding of the surface processes of the earth, interdisciplinary study of allied branches of geosciences is necessary.

The Department of Geology, Aligarh Muslim University, Aligarh (India) under the aegis of the Indian Association of Sedimentologists organized Training-cum-Field Workshop on “Decoding Clastic Sedimentary Systems” during February 20-25, 2024.

Here, we present a detailed report of The Training-cum-Field Workshop. The workshop aimed to impart training to students, research scholars, early career researchers and industry professionals on

various aspects of clastic sedimentary systems including sequence stratigraphy, basin analysis, prospect evaluation, exploration of unconventional resources, depositional environment and paleocurrent analysis of siliciclastic rocks, etc. The workshop included classroom lectures covering wide ranging topics in sedimentology to enhance the knowledge of clastic sedimentary systems of the young students and experienced professionals. It also comprised tutorials and hands-on exercises on sequence stratigraphy, paleocurrent analysis, thin section study of siliciclastic rocks and drone-based topographic change detection exercise. A two-day dedicated field training was conducted in nearby sedimentary basins as part of the workshop.

110 participants from different institutions across India attended the workshop. Outstation

participants included students from MS University of Baroda, Kumaun University (Nainital), University of Calicut, Birbal Sahni Institute of Paleosciences (Lucknow), IISER Kolkata, University of Kerala, University of Lucknow, Indian Institute of Petroleum and Engineering (Visakhapatnam), KJ Somaiya College of Science



Figure 1: View of the dais during the Inaugural Function of the Training-cum-Field Workshop “Decoding Clastic Sedimentary Systems” on February 20, 2024. (L-R): Prof. Rashid Umar (AMU), Prof. Kr. Farahim Khan (Chairperson, Department of Geology, AMU, Aligarh), Prof. Q.H. Ansari (Dean, Faculty of Science, AMU, Aligarh), Chief Guest - Dr. Kalachand Sain (Director, Wadia Institute of Himalayan Geology, Dehradun), Guest of Honour - Prof. Partha Pratim Chakraborty (University of Delhi) and Prof. M.E.A. Mondal (Convenor, AMU).

and Commerce (Mumbai), Central University of Kerala, University of Delhi, IISER Mohali, ONGC and Aligarh Muslim University. Due to limited logistic resources in the Bayana town of Rajasthan, only 45 early bird registered participants (first come-first serve) out of the 110 participants, were selected for the fieldwork program. Remaining participants attended the lecture series and the dedicated workshop on sequence stratigraphy.

Eight renowned experts of sedimentology and allied fields rendered their services as resource persons for the workshop. The experts included **Dr. Kalachand Sain** (Director, Wadia Institute of Himalayan Geology, Dehradun), **Prof. Partha Pratim Chakraborty** (University of Delhi), **Dr. Sandip Kr. Roy** (Retired Petroleum Geoscience Expert from Petronas, Malaysia), **Mr. Riyasat Husain** (Retired

TPL Specialist 1 Geology from Kuwait Oil Company), **Prof. Uma Kant Shukla** (Banaras Hindu University), **Prof. M. Masroor Alam** (ZHCET, AMU), **Dr. Arvind Kumar Singh** (Birbal Sahni Institute of Paleosciences, Lucknow) and **Dr. Yunus Ali P.** (IISER Mohali). The workshop received fundings/sponsorships from industry, alumni and individuals that include Oil and Natural Gas Corporation Limited (ONGC), Council of Scientific & Industrial Research (CSIR), M/s Syed Akhtar Ali Group, Owais Metal and Mineral Processing Ltd (OMMPL), Rawbare, Techno Consultant, Mr Rizwan Ahmad and Mr. Syed Sifat Ali.



Figure 2: Audience during the Inaugural Function of the Training-cum-Field Workshop “Decoding Clastic Sedimentary Systems” on February 20, 2024.

The inaugural function of the workshop was held on February 20, 2024 which was followed by three lengthy but productive technical sessions highlighting important aspects of sedimentology, field geology and use of remote sensing/technology in geosciences. Dr. Kalachand Sain, a renowned geophysicist and Director of the Wadia Institute of Himalayan Geology (Dehradun) and Prof. Partha Pratim Chakraborty of the University of Delhi (Delhi) served as the Chief Guest and Guest of Honour, respectively, of the inaugural session on February 20, 2024.

Dr. Kalachand Sain delivered a plenary talk on “Energy Resources and Energy Security in India”. Addressing the gathering, Dr. Sain said that energy is the main driver for socio-economic development of any country. He further added “As the world grapples with the carbon footprint in the current climate change scenario, efforts are being made to find alternatives to fossil fuels”. He highlighted that despite the potential of renewable/green energy sectors such as solar, wind, ocean current or wave or tidal, geothermal, hydrogen, hydro, biofuels, and waste-to-energy, no significant advancement has been made and currently 80% of the global energy requirement is met by fossil fuels – a trend that is likely to continue for a few more decades.

Dr. Sain also emphasised that to meet the United Nations' target of carbon neutrality by 2050 and net zero carbon emission by 2070, research on Carbon Capture, Utilisation and Sequestration (CCUS) needs to be strengthened. He remarked that India produces only 30% of its energy requirement indigenously with no major oil/gas fields discovered in recent decades. Therefore, venturing into difficult terrains such as the fold thrust belts or foreland of the Himalaya, sub-volcanic regions in central-western India, and offshore, deep and ultra-deep

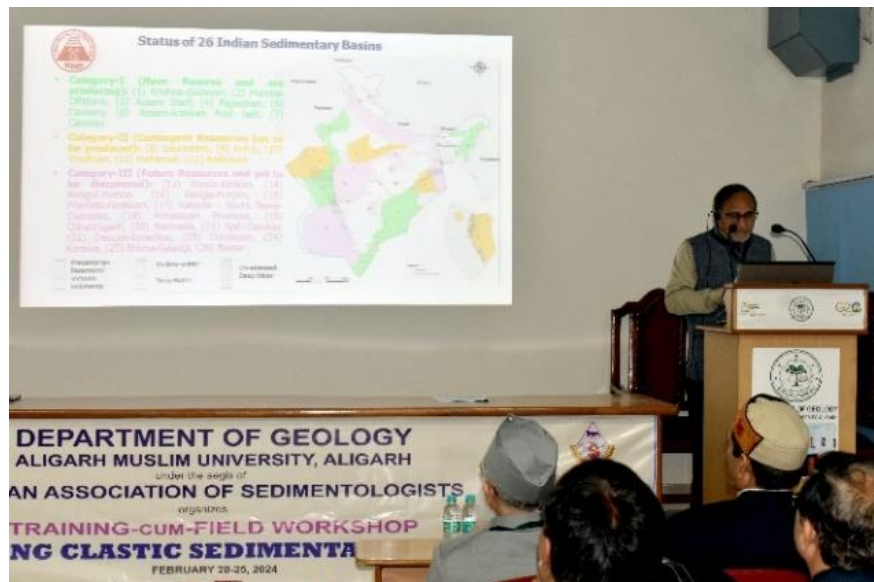


Figure 3: Dr. Kalachand Sain (Director, Wadia Institute of Himalayan Geology, Dehradun), Chief Guest of the inaugural function of the Training-cum-Field Workshop, delivering plenary talk on “Energy Resources and Energy Security in India”.

waters for exploration is the need of the hour. He also said that the unconventional energy resources like submarine gas-hydrates, shale gas/oil, and coal bed methane (CBM) have great potential in India.

Dr. Kalachand Sain said that science-technology-innovation interface is crucial to tap these resources in an economically affordable and environmentally safe manner.



Figure 4: Prof. Partha Pratim Chakraborty (University of Delhi), Guest of Honour of the inaugural function of the Training-cum-Field Workshop, delivering keynote talk on “Siliciclastic depositional systems: Processes and Products (with special emphasis on rock record)”.

Prof. Partha Pratim Chakraborty, the Guest of Honour, stated that it is a unique form of training/workshop that includes fieldwork along with classroom-based lectures and tutorials. Prof. Chakraborty took five lectures (including two practical exercises) including “Siliciclastic depositional systems: Processes and Products (with special emphasis on rock record)”, “Thin section study of quartz arenite, feldspathic arenite, arkose, lith arenite, etc.” and “An introduction to Sequence Stratigraphy: A state-of-the art technique for Basin Analysis”. He explained the nuances of sequence stratigraphy and its importance in petroleum industry. He said that sequence stratigraphy provides a comprehensive understanding of the depositional history of sedimentary basins and plays a pivotal role in the petroleum industry, particularly in the exploration and production of hydrocarbons. Throwing light on the history of sequence stratigraphy, he said it was proposed by the Exxon Group as a branch of stratigraphy that peeps into a sedimentary succession in spatio-temporal framework. Prof. Chakraborty said “sequence stratigraphy helps in identifying the depositional environments that are most likely to contain hydrocarbons. It allows us to understand the distribution and connectivity of reservoirs, which is crucial for efficient extraction”. He explained that it also aids in the prediction of reservoir quality and emphasised that by understanding the sequence of events that led to the formation of a particular sedimentary layer, we can predict the porosity and permeability of potential reservoirs. He further added “sequence stratigraphy provides valuable insights into the migration paths of hydrocarbons and this knowledge is essential for locating traps and seals, which are key elements in the accumulation of hydrocarbons”.

Prof. Chakraborty, in his concluding remark, highlighted that sequence stratigraphy is an indispensable

tool in petroleum industry which not only enhances our understanding of sedimentary basins but also guides us in efficient exploration and production of hydrocarbons. He also conducted practical exercises on paleocurrent analysis and fundamentals of sequence stratigraphy.

Mr. Riyasat Husain (Petroleum Geoscience Consultant & Former TPL Specialist 1 Geology, Kuwait Oil Company) delivered a talk on “Basin analysis to prospect evaluation - Protocol for hydrocarbon exploration” explaining that the protocol for hydrocarbon exploration involves a systematic process starting from basin analysis, moving to prospect evaluation, and finally employing an integrated approach for a comprehensive evaluation. He said that this process helps in identifying potentially prospective hydrocarbon provinces and specific plays within them and that the ultimate goal is to locate and extract hydrocarbons in the most efficient and

environmentally friendly manner. He also gave another talk on “Exploration of unconventional resources” in which he explained that exploration of unconventional resources involves a wide-ranging approach that includes understanding the geologic and petrophysical aspects, engaging advanced recovery methods, and leveraging the latest technologies for enhanced field development planning.

Another leading sedimentologist of the country, Prof. Uma Kant Shukla (Banaras Hindu University) presented an eye-catching talk on “Validation of Fluvial Models in the Himalayan Foreland Basin, India”. He explained that validation of fluvial models in the Himalayan Foreland Basin involves a comprehensive approach that includes understanding gravel progradation, conducting sedimentary facies analysis, and employing other sedimentological models. He clarified that such process helps in understanding the complex interplay between tectonics, climate, and fluvial processes in shaping the basin.

Dr. Yunus Ali P. (IISER Mohali) gave a scintillating presentation on “Remote Sensing of fluvial systems, especially on the rapid river incision and sediment budget in Rishiganga following a major ice-rock avalanche” and practically demonstrated “drone-based topographic change detection” using a highly sophisticated drone camera.

Mudstones are important component of sedimentary record, preserving information about paleo-environmental conditions, paleoclimate and evolution of life on Earth. Dr. Arvind Kumar Singh (Birbal Sahni Institute of Paleosciences, Lucknow) gave a stimulating talk on “Mud and Mudstones: a repository of information on low energy environment and its processes” in which he explained that mud and mudstones serve as a significant repository of information on low energy environments and their processes. He highlighted that the fine-grained

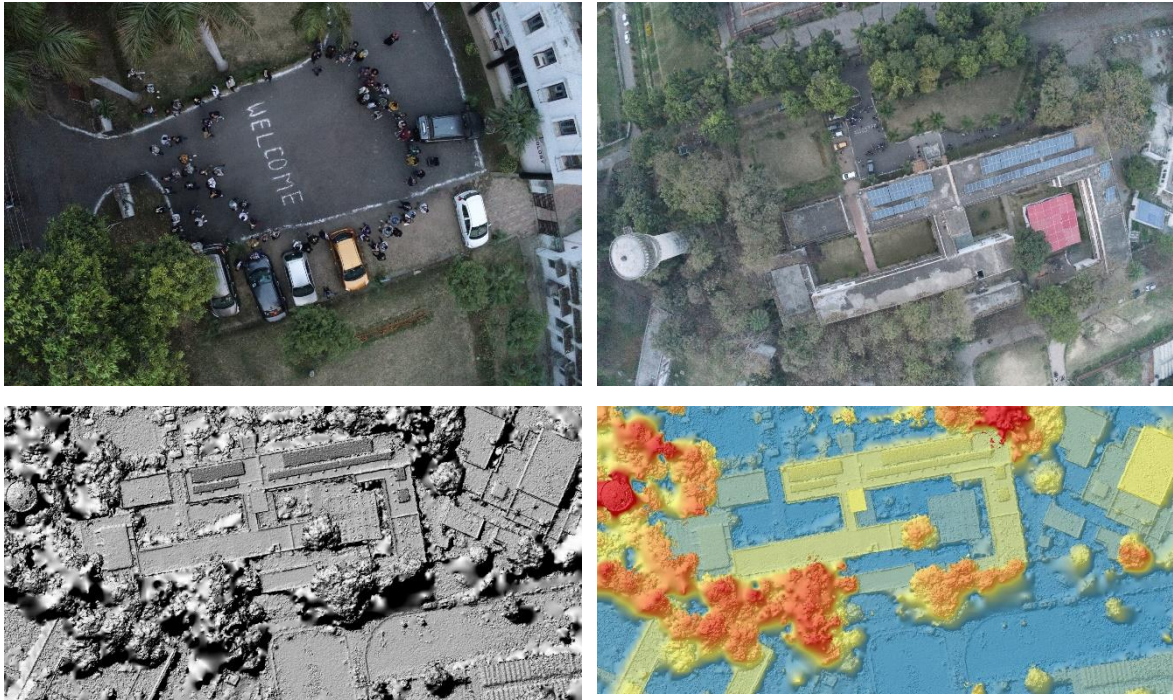


Figure 5: Demonstration of “drone-based topographic change detection” by Dr. Yunus Ali P. (IISER Mohali) during the Training-cum-Field Workshop on February 20, 2024. The photographs were captured using a high-quality camera mounted on a highly sophisticated drone. The bottom photographs are processed images.



Figure 6: Prof. Partha Pratim Chakraborty, Prof. Uma Kant Shukla and Dr. Arvind Kumar Singh leading from the front and explaining the nuances of conducting fieldwork in sedimentary basins to the participants during the Training-cum-Field Workshop on February 21-22, 2024.

nature of mudstones allows it to capture and preserve detailed sedimentary structures and microfossils, making it a valuable record for geologists studying Earth’s geological history. Later, he conducted hands-on practical exercises on sedimentary rock classification.

The field training was led by Prof. Partha Pratim Chakraborty (University of Delhi), Prof. Uma Kant Shukla (Banaras Hindu University) and Dr. Arvind Kumar Singh (BSIP, Lucknow) alongside Prof. M.E.A. Mondal (AMU; Convenor) and Dr. Ifikhar Ahmad (AMU; Organizing Secretary). This fieldwork provided participants with hands-on experience and a deeper understanding of clastic sedimentary systems. It aimed at studying the geological features of the area and

understanding their formation and significance in the context of clastic sedimentary systems.

Considering the continuous stress due to exhaustive technical sessions and fieldwork, and understanding the significance of mental health of the participants, the 4th Day of the Training-cum-Field Workshop (i.e., February 23, 2024) commenced with a brief tour of the Aligarh Muslim University campus during the pre-lunch session. The participants were overwhelmed on seeing the architectural and cultural heritage of the campus. The campus excursion was followed by a technical session encompassing lectures on sequence stratigraphy, clastic geochemistry, and ge-engineering during the post-lunch session



Figure 7: Group photograph of field party at a sedimentary outcrop of Bayana Basin (Delhi Supergroup) near Bayana Town in Bharatpur (Rajasthan).



Figure 8: Glimpses of the participants enjoying the museums, architectural and cultural heritages of the Aligarh Muslim University, Aligarh during the campus excursion on February 23, 2024 as part of the Training-cum-Field Workshop.



Figure 9: Lectures, practical exercises and interactive sessions on sequence stratigraphy conducted by Dr. Sandip Kr. Roy during the dedicated 2-day workshop on sequence stratigraphy on February 24-25, 2024 as part of the Training-cum-Field Workshop “Decoding Clastic Sedimentary Systems”.

Sequence stratigraphy is a method developed to support geoscientists in the geologic interpretation of subsurface data. During the last leg of the 6-day event, the

Training-cum-Field Workshop on “Decoding Clastic Sedimentary Systems” also featured a two-day (February 24-25, 2024) dedicated workshop on sequence stratigraphy by a renowned specialist of the subject, Dr. Sandip Kr. Roy. The workshop covered the basic terminologies of surfaces, systems tracts, sequence sets, and stratigraphic hierarchy, and their definitions. The method was described and applied in training sketches and datasets to later be used to interpret subsurface data in non-marine, shallow marine, and deep marine depositional settings.

The 6-day workshop came to conclusion with a valedictory session on the evening of February 25, 2024 (Sunday). The Chief Guest of the session, Dr. Sandip K. Roy, said he is overwhelmed on the active participation from the students during the workshop on sequence stratigraphy. He said that this workshop was a unique one which encompassed almost all fields and aspects of clastic sedimentology. He congratulated the Department of Geology, AMU, Aligarh for successfully and flawlessly organizing the workshop. Prof. Kr. Farahim Khan (Chairperson, Department of Geology, AMU) said such workshops that includes classroom teaching coupled with field training are rare and is the need of the hour to inculcate basic understandings of the subject of geology. He congratulated the organizing committee and the volunteers for their meticulous effort and making the workshop a grand success. Prof. M.E.A. Mondal, Convener of Training-cum-Field



Figure 10: Few glimpses from the valedictory session. (Row 1; L to R): Dr. Sandip K. Roy (Chief Guest of the session) expressing his views about the workshop; and Prof. Kr. Farahim Khan (Chairperson, Department of Geology, AMU) speaking on the efforts of the organizing committee and thanking the resource persons, sponsors, participants, etc. for making the workshop a grand success.

Workshop, said that the workshop provided the participants with an opportunity to apply theoretical knowledge to practical scenarios, thereby enhancing their skills and understanding in these areas. Dr. Iftikhar Ahmad, Organizing Secretary of the Training-cum-Field Workshop, presented a detailed report during the valedictory session and said that the workshop served as a platform for the participants to gain a comprehensive understanding of clastic sedimentary systems and sequence stratigraphy. He further added that the event was

successful in fostering a collaborative learning environment and promoting the exchange of ideas among the participants. Participants also shared their feedback and thanked the Department of Geology, AMU and Indian Association of Sedimentologists for giving them opportunity where they learned theoretical as well as practical aspects of clastic sedimentology. The valedictory session concluded with certificate distribution followed by a group photograph.



Figure 11: Few glimpses from the valedictory session (Row 1; L to R): Dr. Iftikhar Ahmad (AMU, Organizing Secretary) presenting a brief report of the workshop; and audience during the session. (Row 2; L to R): Prof. M. Masroor Alam (ZHCET, AMU) and Ms. Vedashree Athalye (KJ Somaiya College of Science and Commerce, Mumbai) sharing their experience with the audience. (Row 3; L to R): Mr. Abhinav Jain (BSIP) and Ms. Dilisha Saboor Kidwai (AMU) sharing their feedback.



Figure 12: Few glimpses of certificate distribution to the participants by Dr. Sandip K. Roy (Chief Guest of the Valedictory Session) and Prof. Kr. Farahim Khan (Chairperson, Department of Geology, AMU). (Row 1; L to R): Mr. Abhinav Jain (BSIP), Ms. Vedashree Athalye (KJ Somaiya College of Science and Commerce, Mumbai) and Mr. Kumail Ahmad (BSIP). (Row 2; L to R): Mr. Rohit Gupta (AMU), Ms. Sidrah Iram (Indian Institute of Petroleum and Energy) and Mr. Muhammad Fayez Rizvi (AMU). (Row 3; L to R): Ms. Sneha Saraswat (AMU), Ms. Dilisha Saboor Kidwai (AMU) and Mr. Pranav Vidhushekharan (KJ Somaiya College of Science and Commerce, Mumbai).



Figure 13: Group photograph post-valedictory session.